MOLECULAR MECHANISMS OF HEXAVALENT CHROMIUM-INDUCED PREMATURE OVARIAN FAILURE

A Dissertation

by

KIRTHIRAM KRISHNAVENI SIVAKUMAR

Submitted to the Office of Graduate and Professional Studies of
Texas A&M University
in partial fulfillment of the requirements for the degree of

DOCTOR OF PHILOSOPHY

Chair of Committee,	Sakhila K. Banu
Committee Members,	Robert C. Burghardt
	Qinglei Li
	Charles R. Long
	Joe A. Arosh
Head of the Department,	Ivan Rusyn

August 2018

Major Subject: Toxicology

ABSTRACT

Environmental exposure to endocrine-disrupting chemicals (EDCs) is one of the causes of premature ovarian failure (POF). Hexavalent chromium (CrVI) is a heavy metal EDC widely used in more than 50 industries, including chrome plating, welding, wood processing, and tanneries. The US is one of the world's leading producers of chromium compounds. Recent data from USEPA indicate increased levels of Cr in drinking water from several American cities, which potentially predispose residents to various health problems. Women working in dichromate manufacturing industries and tanneries and living around Cr-contaminated areas experience several gynecological illnesses such as premature abortion, postnatal hemorrhage, birth complications, sub-fertility, and infertility. CrVI can pass through the placental barrier and cause adverse effects on the developing embryos and impair the reproductive functions in F1 offspring. Although epidemiological studies indicate that CrVI causes adverse reproductive health effects including infertility in women, the association between CrVI exposure and POF in unknown. The current study was performed to identify the molecular mechanism behind CrVI-induced POF. Results showed that prenatal exposure to CrVI in rats increased the risk of POF by increasing germ cell/oocyte apoptosis, accelerated germ cell nest (GCN) breakdown, advanced primordial follicle assembly and primary follicle transition in F1 offspring. CrVI increased germ cell apoptosis by upregulating the expression of p53, PUMA, p27, BAX, caspase-3 proteins and downregulating the expression of key cell survival proteins p-AKT, p-ERK, BCL2, BCL-XL, and XIAP. Though CrVI increased the expression of antioxidant enzyme SOD2, its antioxidant activity was diminished by Cr by increasing the translocation of p53 to mitochondria to co-localize with SOD-2. CrVI increased germ cell apoptosis by mediating p53-SIRT1-miR34a signaling network exhibited by

increased expression of acetyl-p53 and miR34a, and decreased expression of SIRT1. Inhibition of SIRT1 attenuated CrVI-induced germ cell death by upregulating pro-apoptotic proteins and downregulating anti-apoptotic proteins through p53 acetylation. While *ex vivo* treatment of ovaries with CrVI and miR34a mimetics increased germ cell apoptosis, miR34a inhibitor treatment mitigated the effect of CrVI on germ cell apoptosis. CrVI advanced GCN breakdown and increased follicle atresia in F1 female progeny by targeting X-prolyl aminopeptidase (Xpnpep) 2, a POF marker in humans. CrVI increased Xpnpep2 expression during GCN breakdown, and decreased Xpnpep2 expression during postnatal follicle development. In all the developmental stages studied, Xpnpep2 inversely regulated the expression of Collagens 1, 3, and 4. As a result of the above events, CrVI induced early reproductive senescence or POF in CrVI exposed F1 offspring.

DEDICATION

To my parents

Mr. Sivakumar Mylsamy & Mrs. Krishnaveni Sivakumar

&

My loving sister

Nivya Meenakshi

ACKNOWLEDGEMENTS

First and foremost, I would like to thank my parents, my father Mr. Sivakumar Mylsamy (Deceased) and my mother Mrs. Krishnaveni Sivakumar, for their unconditional love, blessings, inspiration, motivation, sacrifice and encouraging me to pursue my dreams. I am always thankful to them for making me an independent and positive human being. I would not be in the position right now without them. I also would like to thank my dearest sister Ms. Nivya Meenakshi Sivakumar for bringing all the happiness to me and my family.

I would like to express my heartfelt thanks to all the people who were involved in this endeavor.

I am very grateful to my advisor and committee chair, Dr. Sakhila K. Banu for giving me the opportunity to pursue doctoral degree and her guidance, support, encouragement, constructive criticisms, kindness and her trust on me.

I would like to thank my committee members, Dr. Robert C. Burghardt, Dr. Charles R. Long, Dr. Joe A. Arosh, and Dr. Qinglei Li for their guidance and support throughout the course of this research. I also express my gratitude to Dr. Joe A. Arosh, for his encouragement, advice and support throughout the course of my study.

I am deeply grateful to Dr. Rola Barhoumi Mouneimne in the Image Analysis Laboratory for her constant assistance in confocal imaging and data analyses. I would also like to acknowledge Dr. Bob Taylor for his assistance in chromium estimation.

I wish to express my deep sense of gratitude to Dr. Robert C. Burghardt for having me as his Teaching Assistant in his ‘Optical Microscopy and Live Cell Imaging’ course and supporting me. His encouragement, guidance and advice since my first year of the program were invaluable

to me. I also would like to thank him for training me in microscopy to capture high quality images and for making available the microscopy core facility throughout the course of this research.

I am deeply indebted to Dr. Jone A. Stanley, Assistant Research Scientist, SK Banu Laboratory, Veterinary Integrative Biosciences (VIBS) for being a great mentor, a good friend, and supporting me during difficult times. I would like to extend my thanks to him for being available anytime to me when in need. I also would like to acknowledge him for his assistance in animal experiments and tissue harvest, fetal whole ovarian culture, transfections, and western blots and immunoprecipitation. I also thank my colleague Mr. Jonathan C Behlen, Graduate Research Assistant, SK Banu Laboratory, VIBS for his cooperation and assistance in animal maintenance, and cell culture work.

My sincere thanks to Ms. Lin S. Bustamante and Ms. Chaitali Mukherjee in VIBS Histology Laboratory for processing the rat embryonic and fetal tissue samples, which is very challenging, and providing me with good slides for my experiments.

I am grateful to Dr. Robert C. Burghardt, Dr. Sakhila K. Banu, Dr. Joe A. Arosh, Dr. Qinglei Li, Dr. Gregory Johnson, Dr. Stephen Safe, and many other Professors with whom I had the opportunity to take interesting courses that I thoroughly enjoyed. I am also grateful for the opportunity to attend numerous stimulating seminars series, especially the Interdisciplinary Faculty of Reproductive Biology (IFRB) forum and Toxicology seminar series.

I thank Ms. Kim Daniel, Program Coordinator, Interdisciplinary Faculty of Toxicology (IFT), for all her administrative assistance; Dr. Ivan Rusyn, chair, IFT, for his inputs in Toxicology curriculum; my friends and colleagues and the department faculty and staff for making my time at Texas A&M University a great experience.

I am grateful for all the staff members in Comparative Medicine Program (CMP), in particular Andrea Moss, Ryan Byrd, Gabrielle Kapp and all other staff members for their timely help in animal training and maintenance.

Last, but by no means the least, I am indebted to my loving friends Priyaa Varshinee, Prerna Bhargava, Priya Venkat, Megha Bijalwan, Dakshnapriya Balasubbramanian, Avinash Vem, Parul Priya, Rajinesh Kakumani, Jayaveera pandian, Ashish Katiyar, Ashwanth Narayanan, Jacob Manuel, Narendra Chowdhary, Chandni Nair, Yogesh babbar, Sneha Chawla, Parvadhavardhini, Sivaram, Abishek and many other friends who travelled with me throughout this journey and shared my joy, sadness, failure and victory.

CONTRIBUTORS AND FUNDING SOURCES

Contributors

This work was supported by a dissertation committee consisting of Professors Dr. Sakhila K. Banu [advisor], Dr. Robert C. Burghardt, Dr. Qinglei Li, and Dr. Joe A. Arosh of the Department of Veterinary Integrative Biosciences, and Dr. Charles R. Long of the Department of Veterinary Physiology & Pharmacology. *In vivo* animal experimental work was partly contributed by Dr. Jone Stanley and Mr. Jonathan Behlen. Western blot and immunoprecipitation experiments; and cell culture with SIGC cells were contributed by Dr. Stanley and Mr. Behlen, respectively, as part of team project work.

Funding Sources

This work was supported by National Institute of Environmental Health Sciences (NIEHS) Grants R03ES016605-01A2, R21ES020561-01 and R01ES025234-01A1, and the Center for Translational Environmental Health Research (CTEHR, P30ES023512) to Dr. Sakhila K. Banu.

TABLE OF CONTENTS

LIST OF FIGURES

LIST OF TABLES

1. INTRODUCTION

Chromium

Chromium (Cr) is a naturally occurring metal present in the earth's crust. It is also found in rocks and soil but in smaller amounts. Cr has multiple valence states ranging from CrII to CrVI, but the thermodynamically stable forms are the elemental Cr(0), trivalent CrIII and hexavalent CrVI (1). In nature, elemental Cr(0) does not occur, and out of the three stable forms, the most stable form of Cr compounds is trivalent CrIII. It exists in CrIII state in ores such as ferrochromite or chromite [($FeCr_2O_4$] (2). The second stable form is the hexavalent CrVI which is present in small quantities in various minerals. While CrVI occurs mostly as CrO_4^{2-} or $HCrO_4$-, CrIII occurs as Cr(OH)n(3-n)+ in the environment (3). CrVI compounds have high solubility in water compared to CrIII compounds.

In humans, CrIII is an essential dietary element with a daily recommended dose of 50 to 200 μg/day for adults and is taken in various forms, such as chromium picolinate, niacin-bound chromium, chromium chloride, chromium nicotinate, and chromium-rich yeast (4-9). Its deficiency in humans is found to cause glucose intolerance, fasting hyperglycemia, glycosuria, hypoglycemia, elevated circulating insulin, decreased insulin receptor number and insulin binding, elevated body fat, increased ocular pressure, peripheral neuropathy, encephalopathy, low respiratory quotient and abnormal nitrogen metabolism (4). CrIII is essential for normal lipid, carbohydrate and protein metabolism. It acts as insulin cofactor by being part of chromodulin, an oligopeptide required to potentiate insulin action by facilitating the binding of insulin to its receptors (5). Briefly, increased glucose concentration in the blood leads to the release of insulin, binding to its receptor and activation of insulin signaling pathway in the target insulin-dependent

cells. This increase of insulin concentration in plasma leads to mobilization of chromium to insulin-dependent cells from blood. After entering the cell, four CrIII ions bind to apochromodulin, which is in the cytosol and nucleus, and produces holochromodium (i.e. Cr4-chromodulin). The newly formed holochromodium binds to insulin-stimulated receptors and enhances the insulin signaling by maintaining the receptor in its active conformation (5).

CrVI has been widely used in more than 50 industries worldwide for over 100 years (10). The main use of Cr is the production of alloys such as stainless steel because of its high strength and anti-corrosive properties. Both CrIII and CrVI forms are used in chrome plating, dye and pigment manufacturing, metallurgical, chemical, leather, refractory and textile industries, in the toner for copying machines, drilling muds, and cooling tower water treatment facilities (2). Chromium compounds from these industries are released into the environment matrices such as soil, air and water and exposing humans and animals to CrVI via inhalation, ingestion or through dermal contact. The safety limit for Cr in drinking water set by World Health Organization (WHO) is 50 μg CrVI/L (0.05 parts per million (ppm) or 50 parts per billion (ppb) and United States Environmental Protection Agency (EPA) approved safety limit for total chromium level in drinking water is 100 μg CrVI/L (0.1 ppm or 100 ppb) (11), but exceeding levels of Cr were found in surface and ground waters in the US (12). The safe level of chromium in the air set by Occupational Safety and Health Administration (OSHA) is 5μg/m^3, for an 8 hr time-weighted average. The atmospheric levels of CrVI to which general population is exposed in the US range from 1-100 ng/cm^3 but the levels can exceed the range in and around chromium manufacturing areas (12). Such environmental and occupational exposure to chromium is known to cause various health problems and increases the risk of various types of cancer in humans (13). The USEPA and International Agency for Research on Cancer (IARC) report chromium as a group “A” carcinogen

based on epidemiological and experimental studies in humans and mice (12). It has been postulated that CrIII is less toxic than CrVI. However, when mice were exposed to CrIII or CrVI, a significant increase in genotoxicity by CrIII rather than CrVI was observed due to more deletions in DNA in postnatal day 20 mice offspring (14). Thus, it is evident that CrIII is more toxic than CrVI once inside the cells.

CrVI distribution in the world

It is estimated that chromium and its compounds severely affect 300,000 people around the globe annually (12,15). On a worldwide basis, domestic waste water effluents are the major source of chromium contamination in aquatic ecosystems which account for 32.2% of the total volume of the aquatic ecosystems (2,16). Other major sources are metal manufacturing (25.6%), ocean dumping of sewage (13.2%), chemical manufacturing (9.3%), smelting and refining of nonferrous metals (8.1%), and atmospheric fallout (6.4%) (2,17). The largest contributor to the total chromium released into soil is the disposal of commercial products that contain chromium, (51%), electric utilities and other industries (33.1%), agricultural and food wastes (5.3%), animal wastes (3.9%), and atmospheric fallout (2.4%) (2,17).

Total Cr levels in drinking water sources in developing countries such as China, India, Bangladesh, and Mexico have been recorded as high as 19-50 ppm (18-20). In the Netherlands, a mean concentration of 0.7 μg/L and a maximum of 5μg/L were measured with 76% of the supplies below 1 μg/L and 98% below 2 μg/L. In India, tanning industries release about 2000-3000 tons of chromium with concentration ranging from 2000-5000 mg/L in the form of aqueous effluent to the environment (21). *In the Vellore district of Tamil Nadu state in India, which has more than 60% of Indian tanneries, it has been estimated in 2011-2012 that more than 50,000-hectare fertile lands were contaminated by CrVI with a concentration >200 mg/L, predisposing the human population*

to various ailments including cancer and infertility (22). Other places in India such as Faridabad, Vapi and Sukinda valley (chromate capital of the world) had been heavily contaminated with CrVI which disposed the population to serious ailments including dermatitis and cancers (Blacksmith Institute, 2007).

CrVI distribution in the US

In the United States (US), majority of chromium ores used for mining is imported from other countries. From 2013 to 2016, US imported Cr from South Africa (38%), Kazakhstan (10%), Russia (6%), and other countries (46%) (23). In 2017, consumption of about 6% of world chromite ore production is expected in the US in various forms of imported materials, such as chromite ore, chromium chemicals, chromium ferroalloys, chromium metal, and stainless steel (23). In the US, industries that use chromium fundamentally are the metallurgy, refractory, and chemical industries. The metallurgical industry accounts for 83.9% of the total domestic chromite consumption where chromium is used for the production of stainless steels, alloy cast irons, nonferrous alloys, and other miscellaneous materials. In the chemical industry, both CrIII and CrVI are used to make pigments (2).

Significant contamination with CrVI has been found in drinking water sources of more than 30 cities and people living in more than 7000 communities in the US. drink tap water contaminated with Cr in the US (24). According to a 2016 report from Environmental Working Group (EWG), CrVI is found to have contaminated the tap water supplies of 218 million Americans in all 50 states (25). In fresh water, dissolved chromium levels range from 10 to 500 ng/L. However, freshwater from industrial zones have levels exceeding 1 mg/L (26). It is estimated that approximately 18% of the population of the US are exposed to drinking-water levels between 2 and 60μg/L and <0.1% to levels between 60 and 120 μg/L (3). Chromium waste slag containing

potentially hazardous levels of CrVI compounds was used as land fill material in the US and is estimated that more than 90,000,000 lbs of CrVI is released into the environment from these land fill sites annually (13). In the US, total soil chromium concentrations range from 1 to 1,000 mg/kg, with an average concentration of 14 to 70 mg/kg (27).

In 2009, it is estimated in the US that chromium compounds of 30,156,862 pounds were released from 1,334 domestic manufacturing and processing facilities to soils which accounted for about 83% of the estimated total environmental releases from facilities required to report to the Toxics Release Inventory (TRI). At least 1,127 of the 1,699 hazardous waste sites in EPA National Priorities List were found to contain chromium (2). The occurrence of both individual species and total chromium in 407 water sources in the US were investigated by a Water Research Foundation-funded study. Outcome of the study states that a significant proportion of groundwater sources had total chromium concentrations, with CrVI exclusively. The database maintained by California Department of Public Health shows that CrVI has been detected in 2,310 California drinking water sources (28). Thirty percent of the drinking water sources monitored in California had detectable amounts of CrVI, out of which 86% had peak concentrations of $\leq$ 10 μg/L (29). The EPA has set the maximum contaminant level of total chromium as 100 μg/L or 0.1 ppm, but a well water from Midland, Texas was found to contain 5.28 ppm Cr. Strikingly, in one of the ground-water monitoring wells in Hinkley, California, a CrVI concentration of 5280 μg/L was reported (29,30). However, California's State Water Resources Control Board has set the maximum contamination limit (MCL) for total chromium as 50 μg/L or 0.05 ppm or 50 ppb of total chromium (31).

Toxicokinetics of chromium

Absorption

In humans, gastrointestinal absorption of chromium as estimated by many quantitative studies was less than 10% of the ingested dose (2). In the gastrointestinal tract, CrIII is absorbed very poorly after oral exposure and less than 1% of the administered dose was recovered in the urine of experimental animals (32,33). The difference in toxicity between CrVI and CrIII is almost 1000 fold due to the ability of CrVI to enter cells (34). CrVI is readily taken up by cells via anion transporters due to its structural similarity to sulfate and phosphate anions (34). It is proposed that CrIII may cross the cell membrane through pinocytosis while it has been considered that CrIII is not the substrate of anion transport system therefore it is poorly absorbed (13).

The absorption fraction of soluble CrIII, as chromium picolinate, a common form of CrIII supplement was greater than $CrCl_3$, suggesting that chromium picolinate could be toxic after its absorption and entry into the cell, and the urinary excretion was approximately 16 fold higher than $CrCl_3$ (35). In a study with rat model, when $CrCl_3$ was administered orally to adult and neonate rats (2-day old through gavage), neonates were found to absorb 10 times higher amount of chromium than the adult rats, and 35% of Cr remained in the intestine of the neonate after 1 week of gavage (36). *The high absorption of chromium in immature rats suggest that infant and children may be more susceptible to chromium toxicity than the adults.*

Distribution

The factors that determine the distribution of CrVI and CrIII containing compounds are total chromium concentration, pH, redox potential, redox reaction kinetics, the presence of oxidizing or reducing agents, and insoluble CrIII salts or CrIII complex formation (3). Based on the autopsy studies in the US, chromium concentrations were highest in liver, aorta, lung, kidney,

pancreas, spleen and heart at birth and found to decrease with age. The levels in aorta, spleen, and heart rapidly declined between the first 45 days of life and 10 years and the levels in kidney and liver declined after the second decade of life. The levels in the lung increased from midlife to old age with a decline in the early period of life (2,37). In a mice study to test the distribution of chromium to different organs, 4.4, 5.0 or 14.2 mg CrVI/kg/day as potassium dichromate or 4.8, 6.1 or 12.3 mg CrIII/kg/day as CrIII chloride was given through drinking water, and the chromium content was measured after one year in major organs like lung, heart, kidney, liver, spleen, and testes. In CrIII-treated mice, chromium was detected only in the liver whereas in CrVI treated mice chromium was accumulated in all the organs with the highest level in spleen and liver. *CrVI treated group had 40-90 times higher level of chromium accumulation compared to CrIII treated group (2,38)*. Another study showed that the levels of chromium in kidney, liver, bone, and spleen of CrVI treated rats were 9 times higher than CrIII treated rats when administered through drinking water for one year (39). Accumulation of higher levels of chromium in tissues after administration of CrVI than after CrIII reflect the higher toxicity of CrVI by reducing to CrIII after traversing plasma membrane.

Kargacin *et al*., (1993) compared the distribution of CrVI between male Fisher rats and C57BL/6j mice exposed by drinking water or by intraperitoneal injection in various organs. The concentrations of chromium accumulated in various organs (liver, kidney, spleen, femur, lung, heart, muscle, and blood) were different between rats and mice (40). A similar difference in CrVI accumulation was observed in various organs in a 2-year study by National Toxicology Program, where CrVI was administered to male and female rats and mice through drinking water (41). The results of the study showed that CrVI was carcinogenic in male and female rats and mice whereas CrIII at much higher concentrations may have been carcinogenic in male rats but was not

carcinogenic in mice or female rats. Also, Cr concentrations in the liver and glandular stomach were higher in mice, whereas kidney concentrations were higher in rats. These data suggest that any toxicological extrapolations across species need to be factored even if the routes of administration are same.

Metabolism

Once CrVI enters the cell through anion transporters, it undergoes a series of rapid metabolic reductions to intermediate species like Cr(V), Cr(IV), and is ultimately reduced to CrIII (34). CrVI reduction to CrIII occurs both extracellularly and intracellularly. The majority of the extracellular reduction of CrVI takes place in the gastrointestinal system (34,42). De Flora *et al*., (1997) reported the capacities of chromium reduction in various parts of the body through *ex vivo* data (42). CrVI from the body can be eliminated by reduction through saliva, gastric juice, intestinal bacteria, liver, blood, epithelial lining fluid, pulmonary alveolar macrophages, bronchial tree and peripheral lung parenchyma (42). For humans, overall CrVI-reducing capabilities were estimated to be 0.7-2.1 mg/ day for saliva, 8.3-12.5 mg/day for gastric juice, 11-24 mg for intestinal bacteria eliminated daily with feces, 3,300 mg/hour (h) for liver, 234 mg/h for males and 187 mg/h for females for whole blood, 128 mg/h for males and 93mg/h for females of red blood cells, 0.1-1.8 mg/h for epithelial lining fluid, 136 mg/h for pulmonary alveolar macrophages, and 260 mg/h for peripheral lung parenchyma (2).

After oral exposure of CrVI, the gastric juice in the gastric environment and ascorbate play an important role in the reduction of CrVI to CrIII constituting the first line of defense (42,43). Saliva and gastric juice readily reduce the CrVI after ingestion and is also sequestered by bacteria that are present in the intestine (42,44). Gastric juice, the main reducing agent has a high reducing capacity ranging from approximately 8 mg/L (fasting) to 31 mg/L (Fed). In the stomach,

extracellular CrVI reduction to CrIII has been considered as a protective mechanism, as about 1000-1500 ml/day (fasting) plus 800 ml/meal (Fed) of gastric juice is secreted daily which could convert CrVI to CrIII (~80 mg/day). This accounts for a low genotoxic and carcinogenic potential in animals exposed to CrVI orally through drinking water but a proportion of CrVI can escape the detoxification process by the gastrointestinal system which is evident by the presence of intracellular chromium in many tissues (34).

De Flora *et al*., (1997) reported that red blood cells accomplish the major detoxification of chromium with over half of a 100 μg dose of CrVI being sequestered or reduced by 1 ml of blood within 60 minutes (42,45). A number of enzymatic and non-enzymatic antioxidants reduce intracellular CrVI at physiological pH. For CrVI, some of the reductants are non-enzymatic antioxidants such as ascorbate, reduced glutathione, and cysteine (46,47). Both the cellular availability and reaction rate determine the primary reducing agent. In addition to non-enzymatic antioxidants, microsomal enzymes are also found to play a role in the reduction of CrVI to CrIII (48). Hepatic microsomal proteins from Sprague Dawley rat liver reduced CrVI to CrIII and the rate of reduction was found to depend on the concentration of nicotinamide adenine dinucleotide phosphate (NADPH) and the concentration of microsomal protein (48). It is suggested that the capacity to reduce CrVI is much greater in human liver compared to rat liver and the metabolism of CrVI in rodent systems may not be extrapolated to humans readily (2).

Ascorbate accounts for 80-90% of CrVI reduction *in vivo* where its concentration ranges from ~1-3 mM (34). In general, the intracellular concentration of ascorbate is very high, and levels of ~1-5 mM are present in the ovary, placenta, and brain (49,50). Extracellular reduction by ascorbate plays a protective role, where the reduced CrIII is retained and poses little or no toxic and carcinogenic activity as they cannot enter the cells (34). Intracellular reduction of CrVI to

CrIII is pro-oxidative, where after 3 h of exposure, 10 to 20 fold accumulation of CrIII, and after 24 h of exposure, 100-fold accumulation of CrIII occurs intracellularly (1). During this intracellular reduction process, transient intermediates like CrV and CrIV are produced along with a spectrum of reactive oxygen species (ie, superoxide [O2•−], hydrogen peroxide [H2O2], and hydroxyl radical [•OH]), which increase oxidative stress inside the cell (51). CrIII and the transient intermediates can cause many forms of DNA damage: binary DNA adducts, DNA double-strand breaks, DNA interstrand cross-links, oxidized bases, and DNA-protein adducts (52-54). In rats, the reduction of CrVI by microsomes can also form reactive Cr(V), which may interact with DNA and lead to cancer (55).

Excretion

Chromium which is absorbed by the body is mainly excreted by urinary tract, as about 60% of the ingested CrVI is eliminated by human kidney within 8 h in the reduced form of CrIII. While lower concentrations of chromium are excreted in sweat, hair, milk, and nails, bile excretion eliminates about 10% of ingested and absorbed chromium in the body. Also, excretion of CrIII from plasma is slower than the excretion of CrVI of the same dose which is eliminated within hours of ingestion (13,56,57). About 20-70% of the administered dose of inhaled CrVI is excreted in urine and feces. In oral exposure, Cr compounds are excreted mainly in feces due to its low absorption. Chromium is excreted in the form of complexes like CrIII-glutathione complex in urine and feces (58).

Mechanisms of chromium toxicity

The molecular mechanisms by which metals cause toxicity is not completely understood but the most important mechanism involved in the metal-induced carcinogenicity is its potential to generate reactive oxygen species (ROS) and change the cellular redox states (59,60). Fenton-type reaction is the well-known mechanism by which metal ions produce intracellular ROS during which a highly toxic ·OH is generated when a transition metal ion reacts with H_2O_2. CrIII, CrV, and CrIV can generate free radicals via the Fenton-type reaction (53). Another mechanism by which metals induce the generation of ROS is the Haber-Weiss reaction where ·OH is generated from H_2O_2 mediated by $O_2^{\cdot-}$ (61,62). CrIII, CrIV, CrV, and CrVI, can generate ROS by Haber-Weiss-type mechanism. The higher toxicity of CrVI is due to its higher redox potential. As discussed earlier, CrVI, once entering cells through anion transport system, is reduced rapidly by reductants such as ascorbate, GSH, cysteine, NADPH etc. to CrIII. During this conversion, CrVI is found to generate ·OH, $O_2^{\cdot-}$, and H_2O_2 via both Fenton and Haber-Weiss reactions (63-65). The scheme for generation of ROS, mainly ·OH by the reaction of CrVI with biological reductants are as follows (53)

CrVI + reductants → Cr(V)+H2O2→CrVI+HO^-+ ·OH

CrVI + reductants→ Cr(V) + reductants→ Cr(IV) + reductants→ CrIII + H_2O_2→ CrVI +HO^-+ ·OH

CrVI + GSH→GSSR+ $O_2^{\cdot-}$ + CrVI → Cr(V)+ O_2 + H_2O_2 → CrVI + HO^-+ ·OH

When cells are exposed to ROS chronically, the balance between the ROS levels and antioxidant system's potential to detoxify it gets disrupted and it causes oxidative stress inside the cell (66). The key metabolite involved in oxidative stress is H_2O_2 which has the capacity to freely diffuse in and out of cells, and form the most highly toxic ·OH radical (67). The potential targets of ·OH radicals are DNA, lipids and proteins (68,69). DNA damage can cause cell death induced

by pyknosis, apoptosis, and or necrosis (70-72). In mammalian cells, the most abundant adduct product by the oxidative DNA damage is 8-hydroxydeoxy guanosine (8-OHdG) which mediate transversion of G:C to T:A (73,74). During DNA replication, the 8-OHdG formation mediates transversion of A:T to C:G and is used as a biomarker for ROS induced DNA damage (75). The structural damage induced by chromium include DNA strand breaks, DNA-protein crosslinks, DNA-DNA inter-strand crosslinks, chromium-DNA adducts, and chromosomal damage (2). Functional damage includes DNA and RNA polymerase arrest, mutagenesis and changes in gene expression. Double strand breaks that occur due to Cr-DNA ternary adduct formation can lead to DNA repair errors and collapsed replication fork during DNA replication (2,76). These events caused by ROS induced oxidative DNA damage can cause cancer in humans. In human lung cells, chromium-induced chromosome instability mediated through centrosome and spindle assembly checkpoint bypass lead to lung cancer development (77-79).

In vitro, Cr-induced oxidative stress by ROS generation has been shown to result in the induction and inhibition of the transcription factors, NFkB and AP-1, p53 activation, HIF-1 (hypoxia-inducible factor 1), cell-cycle arrest, and p53-dependent apoptosis (53,80). Oral administration of mice with 5 or 10 mg/kg body weight potassium dichromate (CrVI) resulted in increased lipid peroxide (LPO) levels indicating increased oxidative stress and decreased GSH, vitamin C, SOD and catalase in the ovary(81). CrVI-induced apoptosis in Chinese hamster ovary (CHO) cells involves disruption of mitochondrial stability. Treatment with sodium chromate increased the time-dependent release of mitochondrial cytochrome *c* in cytosolic extracts of CHO cells. Co-treatment of these cells with cyclosporine A (a cytochrome c inhibitor) inhibited the release of cytochrome *c* and abrogated CrVI-induced apoptosis and DNA fragmentation (82).

Chromium exposure and risk to human

Major sources of chromium in the environment

Earth's crust has chromium and the continental dust present in the environment is the main natural source of exposure to humans. In addition, anthropogenic stationary point sources like combustion of natural gas, oil, and coal from industrial, commercial, and residential sources are the main sources of release of chromium to the atmosphere. In the US, it is estimated that about 2.7-2.9 kilotons of chromium are emitted to the atmosphere annually from anthropogenic sources, out of which *one-third of it is CrVI* (2). Chromium compounds that are present mainly as fine dust particles in the air settle down over the water and land eventually, and contaminate them. About 80-90 % of chromium from industrial processes are released as waste to different environmental compartments, while only 10-20 % of chromium actually ends up with the product. Chemical industries release approximately 82.3% of the total chromium on land, and landfilling is the most prevalent disposal method of chromium wastes from those industries. It is very important to treat the chromium-containing wastes before it is disposed to the environment. CrVI waste can be treated by reducing it to CrIII using a reducing agent and precipitating out with the use of caustic soda or lime to its hydrous oxide, which has low soil mobility, and low plant and animal availability. CrIII waste can also be disposed by converting to its hydrous oxide or converted to its oxide by incineration before disposal (2).

Environmental exposure of human population to chromium

The general population is environmentally exposed to chromium by inhaling air, drinking water from contaminated sources, or eating food or food supplements that contain chromium. It is estimated that tap water polluted with total chromium is consumed by at least 74 million people in nearly 7000 communities, and 1.7 million people in 42 communities from New Jersey, drink water

that is contaminated with CrVI in the US (83). It is estimated that adults in the US ingest approximately 60 µg/day of chromium through food (84). In most foods, total chromium levels typically range from less than 10 µg/kg to 1,300 µg/kg, and high concentrations of chromium were found on foods like fish, meat, vegetables, and fruits (3). Inhalation of cigarette smoke is also another source of chromium exposure as the mean chromium level found in US cigarettes range from 1.4 to 3.2 µg/g of dry tobacco (85) and cigarette smoke was found to contain 0.0002-0.5 µg of chromium per cigarette (86).

Occupational exposure to chromium

Occupational exposure to chromium is a major health concern due to its potential to cause adverse health effects. Exposures to families can also occur when the workers bring their contaminated shoes and contaminated clothing to their home. Exposure to chromium occurs mainly from stainless steel production, welding, chromate and chrome pigment production, chrome plating, and from working in tanning industries (87). It is estimated that professional workers in 80 industrial categories may be exposed to CrVI and are two fold more at risk compared to the general population exposure group (45). Workers from these industries are exposed to chromium mainly by inhalation exposure to chromium as dust, fumes, mist, and particles, in addition to dermal exposure. Inhalation is the main route of exposure through which occupational workers are exposed to chromium and lung is the primary target organ for inhalation exposure. Occupational exposure to chromium containing compounds causes its toxicity in various organs such as cancer in the respiratory tract, renal damage, allergy, asthma etc. Women working in Cr industries are predisposed to various gynecological disorders and infertility. Likewise, men working in Cr industries have health effects including infertility. *Please see health effects section for more details.*

Chromium exposure-epidemiological studies

Epidemiological studies in chromium exposed populations have reported health problems such as asthma, cancer, dermatitis, hypertension, back pain, bronchitis, hemoglobin changes, chromosome aberrations and DNA changes in lymphocytes (1,2,13,88,89). Blood chromium levels reported in workers from developed countries such as the USA, UK, Canada, Germany, and Spain, were lower than the values detected in the workers of developing countries such as India, China, Poland, and Pakistan. For examples, blood chromium levels detected in workers from various countries were as follows Germans: 1.5 μg/L; Spanish: 1.31 μg/L; Pakistani: 16 μg/L; Indian: 147 μg/L; Chinese: 22 μg/L (13,89-93). It is clear from the above Cr levels that workers from developing countries have much higher levels of blood Cr compared to developing countries. These workers were exposed to high level of chromium due to improper disposal of industrial waste, lack of advanced and efficient production technologies and lapse in implementing health safety regulations.

In Canada, CAREX (Carcinogen exposure) has estimated that 104,000 workers (92% male) are exposed to CrVI occupationally. Among them, the largest exposure group industries were automotive repair and maintenance; printing and support activities; sawmills and wood preservation; commercial and industry machine repair and architectural/structural metals manufacturing. The largest exposed group (n=20,000 male and n=800 female) were engaged in welding (94). In 1990, European CAREX estimated that in European Union alone about 0.8 million workers were exposed to CrVI compounds. Above 58% of these workers were in four major industrial sectors which were fabricated metal products manufacturing except machinery (n = 178,329), high-tech machinery other than electrical equipment (n = 114,452), household and personal services (n = 85,616), and transport manufacturing industries (n = 82,359) (13).

A high incidence of cancers has been reported among occupationally exposed workers through various epidemiological studies. In 1987, increased rate of mortality for lung cancer, stomach cancer, and total cancer was observed in communities with CrVI contaminated drinking water in Liaoning Province, China. Relatively high concentrations of CrVI (20 mg/L or 20 ppm) were seen in drinking water wells with noticeable yellow color in some wells (95,96). A similar increase in mortality due to stomach cancer and lung cancer was reported in the regions with CrVI contaminated drinking water in Liaoning province of China (95).

In an ecological mortality study in the Oinofita region of Greece, a significant increase in mortality due to liver cancer, lung cancer, renal cancer, and cancers of other genito-urinary organs among women was observed with the ingestion of drinking water contaminated with CrVI (97). A study in Kanpur, India reported an increase of digestive and dermatological disorders, and hematological abnormalities in a high CrVI exposed population through groundwater (∼20 mg/L) (98). The health risk of the surgical instrument manufacturing industry workers was evaluated by Junaid *et al.,* (2016) and found that chromium levels in the matrices like blood, urine, saliva, auxillary and scalp hair were significantly higher in the exposed group compared to the control group (Blood: control 5.48 µg/L; exposed 16.30 µg/L; Urine: control 4.47 µg/L; exposed 58.15 µg/L; Saliva: control 0.93 µg/L; exposed 1.25 µg/L; Auxiliary hair: control 1.20 µg/g; exposed 2.90 µg/g; and Scalp hair: control 1.38 µg/g; exposed 2.36 µg/g) (99).

Adverse health effects of CrVI exposure

Acute or accidental exposure to CrVI and severe health effects in the human and experimental animals

Human ingestion of very high doses of chromium compounds either intentionally or accidentally has caused severe hepatic, renal, respiratory, gastrointestinal, cardiovascular, hematological, dermal, immunological and lymphoreticular effects in patients who survived because of treatment or as part of the sequence ultimately leading to death (12).

Hepatic effects

Liver damage was reported in a chrome plating worker who ingested plating fluid containing chromium trioxide who exhibited toxic hepatitis, jaundice development, increase in serum lactic dehydrogenase and bilirubin levels and severe anemia (100). Female rats were more susceptible to liver damage compared to males, as only females were found to exhibit cellular histiocyte infiltration and chronic focal inflammation in the liver when exposed to chromium (101). Various mice and rat studies with different exposure periods of chromium compounds reported increased activity of alanine aminotransferase and aspartate aminotransferase, increased sinusoidal, necrosis, hepatocyte cytoplasmic vacuolization, chronic inflammation, histiocytic cellular infiltration, eosinophilic and basophilic foci, and fatty change with females showing more susceptibility to ingested chromium (2).

Renal effects

Upon analyzing the human exposure cases to chromium, acute renal failure seems to be the major cause of death in case of chromium compounds ingestion (2). Ingestion of chromium trioxide by a chrome plating worker developed tubular nephritis and acute renal failure characterized by proteinuria, anuria, and hematuria (100). Necrosis of renal tubules was observed

in three different individuals who died after ingestion of chromium (2,102-104). In rats, oral CrVI exposure increased the accumulation of lipids, phospholipids, and triglycerides, inhibition of acid phosphatase, alkaline phosphatase, lipase and glucose-6-phosphatase in the kidneys (105). Glomeruli vacuolization, degeneration of Bowman's capsule's basement membrane, and renal tubular epithelial cells are some of the changes in the histopathology of the kidneys observed in rats that were exposed to potassium chromate (2).

Respiratory effects

Two autopsy case reports revealed cardiopulmonary arrest after ingestion of sodium dichromate revealed pulmonary edema, pleural effusion, acute bronchopneumonia, severe bronchitis and lungs congested with blood-tinged bilateral pleural effusions (2).

Gastrointestinal effects

In humans, people who ingested chromium compounds were found to experience vomiting, abdominal pain, hemorrhage, and gastrointestinal burns before death; and autopsy of people who died ingesting chromium compounds revealed gastrointestinal ulceration, gastrointestinal hemorrhage, necrosis, hematemesis, nausea, and bloody diarrhea. Occupational exposure to chromium compounds was reported to cause acute gastritis, epigastric and substernal pain, and subjective symptoms of gastritis, stomach cramps, duodenal ulcers, and indigestion. Changes in the histopathology of the gastrointestinal tissues, gastrointestinal hemorrhage and irritation were observed when rats were orally exposed to CrVI compounds (2).

Cardiovascular effects

An autopsy of people who died by cardiopulmonary arrest after ingestion of sodium dichromate or potassium dichromate revealed hypoxia in the myocardium and hemorrhages in the

heart. In rats, hemorrhage in the heart, necrosis, fibrosis, and vacuolization were observed after dosing potassium dichromate for 3 weeks (2,103,106).

Hematological effects

Sublethal or lethal doses of CrVI ingestion in humans causing hematological effects were reported (2). The indicative effects of intravascular hemolysis such as decreased hemoglobin and hematocrit content, increased total WBC and reticulocyte counts, and increased free plasma hemoglobin were observed in humans after the chromium ingestion (107). Accidental swallowing of chromium trioxide by a chrome plating worker resulted in severe hemorrhage followed by anemia was reported (100).

Dermal effects

Ingestion of CrVI as potassium dichromate worsened dermatitis in 11 out of 31 individuals who are sensitive to chromium (108). Dermatitis leading to dyshidrotic lesions was observed on the hands of a building worker while administering potassium dichromate in an oral tolerance test (109).

Immunological and Lymphoreticular effects

In mice and rat studies, it was reported that exposure of CrVI as sodium dichromate through drinking water had led to histiocytic cellular infiltration, basophilic and clear cell focus, mesenteric and pancreatic lymph nodes, changes in lymphatic tissues, and hemorrhage (101).

Neurological effects

Salama *et al.,* (2016) reported acute brain injury in Albino Wistar rats when treated with potassium dichromate (110). An alteration in the locomotor activity in the brain and contents of oxidative stress biomarkers, interleukin-1β (IL-1β), phosphorylated protein kinase B (PKB), and

cyclooxygenase 2 (COX-2) were observed in Cr exposed rats (110). CrVI reduced the number of neuronal cells and affected the cholinergic and dopaminergic neuronal cells as well as the locomotor activity of drosophila (111).

Reproductive effects of chromium in male

Chromium is known to cause adverse effects on the male reproductive system contributed by various environmental, genetic, and lifestyle factors. The current understanding of the male reproductive toxicity of Cr is based on short-term exposure and/or high-dose studies from animal experiments. In general, toxins including metals may accumulate in the epididymis, prostate gland, seminal vesicle or seminal fluid and impair sperm motility. Also, the neuroendocrine axis can be affected and cause an imbalance in hormones by disrupting androgen secretion from Leydig cells or inhibin B secretion from Sertoli cells (112). All of these effects can reduce sperm motility and its ability to fertilize the oocyte causing an increase in the risk of subfertility and infertility (113).

Significant reduction in the sperm count and sperm motility with high serum follicle stimulating hormone and low levels of zinc, lactate dehydrogenase and lactate dehydrogenase C4 isoenzyme in seminal plasma were reported in male workers who were exposed to CrVI for 1-15 years occupationally in electroplating industry (114). Danadevi *et al.,* (2003) reported a 67% decrease in sperm concentration with high blood chromium level in workers from a welding plant (115). Acute and chronic exposure studies in laboratory animals show that CrVI produces adverse reproductive effects on males. In monkeys, rabbits, and rats, oral intermediate exposure to CrVI targets the male reproductive system. When Wistar rats were exposed to CrVI, testis weight was decreased, and prostate and seminal vesicles' weight were increased. An increase in serum FSH and a decrease in LH and testosterone with changes in the morphology of seminiferous tubules were also observed (116). A decrease in sperm count, sperm motility, and decreased concentration

of superoxide dismutase, catalase and reduced glutathione in seminal plasma were observed, when adult monkeys were exposed to high doses of CrVI for 6 months. These effects were reversed with the cessation of chromium treatment and simultaneous administration of vitamin-C (117). Another study reported that when monkeys were exposed to CrVI through drinking water for 180 days, decreased sperm count along with histopathological changes to the epididymis like ductal obstruction, microcanal development, accumulation of immature germ cells and multinucleate giant cells in the epididymal lumen were exhibited (118).

Reproductive effects of chromium in female

Epidemiological studies indicating reproductive toxicity of CrVI

Several reproductive problems have been reported in women living near or working in chromium industry that include: pregnancy loss, preterm labor, still-birth, spontaneous abortion, low birth rate, intrauterine growth restriction (IUGR), low birth weight offspring, infertility etc. (119-121). The placenta plays an important role in mediating fetal programming since it determines the growth, development, and health of the growing fetuses. It has been postulated that irrespective of the chromium exposure period either during or before gestation, the level of Cr in the placenta was increased. Cr accumulates during the treatment period and continues to remain in the maternal tissue compartments. The accumulated Cr can pass through the placenta to the developing fetuses during gestation and affect their growth and development (120,122).

An interesting birth cohort study was conducted among 7290 pregnant women in Hubei province, China. The study evaluated the association between preterm birth risk and maternal exposure to CrVI during pregnancy. The data indicated that higher chromium levels increased the risk of preterm birth. The association was more pronounced in male infants suggesting that Cr, apart from increasing the preterm birth risk, it's effect is also sexually dimorphic (122). A recent

study from our laboratory on the human term placenta revealed a positive correlation between Cr burden in the placenta and oxidative stress. We also observed sexual dimorphism in chromium effects, where a sex-dependent decrease in antioxidant proteins and elevated levels of apoptotic protein with an increase in Cr burden was seen (123).

Epidemiological and clinical data were analyzed recently to quantify the reproductive toxic effects of CrVI in a non-occupational population from Willits, CA. Remco Hydraulics Inc. used CrVI for chromium electroplating of hydraulic cylinders from 1963 to 1995 (124). The plant dumped toxic waste into local creeks at the top of the Eel river wastershed and contaminated ground water at four sites in and near Willits. Hexavalent chromium was the primary chemical of concern that was released. The on-site groundwater was highly contaminated with CrVI and total Cr. CrVI has been measured as high as 900 ppm and total chromium as high as 960 ppm. CrVI in on-site soil has been measured at levels up to 430 ppm and total Cr at levels up to 8,710 ppm (124). In the study, longitudinal hospital records of a newborn from 29,311-unexposed (control) and 5036-exposed (Willits population), as well as 31,444-unexposed (control) and 5558-exposed pregnant women (Willits population) were analyzed. The results indicate that CrVI adversely affected pregnancy outcomes and subsequent health of two generations, resulting in low birth rate, higher risk of pregnancy loss, and spontaneous abortion. Infants of CrVI exposed women experienced a higher rate of birth defects, perinatal jaundice, and respiratory problems. This was the first study to report the harmful reproductive effects of non-occupational CrVI exposure in women and their infants in the US (125).

Animal studies indicating reproductive toxicity of CrVI

In female Swiss albino mice, multiple reproductive effects were reported by Murthy *et al., (1996)* (126). Dose-dependent reproductive effects were observed when the mice were exposed to

different concentrations (high doses of 250, 500 and 750 ppm for 20 days and low doses of 0.05, 0.5 and 5 ppm for 90 days) of CrVI through drinking water. At different maturation stages, the number of small, medium and large follicles were significantly reduced. With the highest dose of CrVI exposed group, the duration of estrus cycle was increased with changes in the histology of the ovary resulting in atretic follicles, cumulus cells with pyknotic nuclei and follicular cells with karyorrhexis (126). Increased post-implantation loss and decreased litter size with a high incidence of resorption sites were observed when pregnant mice were exposed to CrVI in drinking water during the entire gestation period (127). Junaid *et al.,* (1996) reported embryotoxic and fetotoxic effects of CrVI in Swiss albino mice. When high doses of CrVI (250, 500 and 750ppm) were administered through drinking water during the organogenesis period (gestation days 6-14), CrVI retarded fetal development, reduced fetal weight and litter size with an increase in fetal resorption with high doses of CrVI (128). Female mice offspring that were exposed to CrVI or CrIII experienced reduced fertility by delayed sexual maturation. CrVI reduced the number of implantations and viable fetuses whereas CrIII reduced body weight and in particular ovarian and uterine weights in female offspring (129). Our studies also exhibited similar phenotypes in CrVI exposed rats (130). However, experiments from Junaid *et al.,* (1996) (128), have used a very high amount of CrVI compared to our laboratory. We used a rat model and Junaid *et al.,* (1996) studies used a mouse model. We have used several doses of CrVI ranging from the regulatory dose of 100 ppb to 200 ppm in our studies. Our higher doses were reflective of the environmental exposure to drinking water Cr levels in the developing countries, while lower doses were relevant to Cr levels in drinking water sources in the US.

Reproductive and developmental toxicity of CrVI: Evidence from our laboratory

Research in our lab has two major goals: (1) to determine the molecular mechanisms of CrVI-induced female reproductive and developmental toxicity; and (2) to identify intervention strategies to mitigate CrVI effects.

In vivo studies

CrVI delayed puberty by disrupting ovarian development, steroidogenesis and pituitary hormone synthesis.

Rationale: When lactating women working in Cr industry or living around Cr contaminated area are exposed to Cr, the offspring were exposed to Cr through the mother's milk. This can cause several adverse health effects in the F1 progeny. Therefore, in order to check the mechanisms of Cr-induced adverse effects, the lactating dams were exposed to Cr and F1 pups were exposed to Cr through mother's milk and the analyses were performed in the F1 offspring.

Experimental Design: Lactating dams were administered with potassium dichromate (200 mg/L) in drinking water from postpartum days 1–21. Vitamin C (500 mg/L) was administered to control and CrVI-treated rats through oral gavage. The pups received CrVI during postnatal days (PND) 1–21 via the mother's milk and the effects of CrVI were studied on PND 21, PND 45 and PND 65.

Results and conclusion: Data indicated that lactational exposure to CrVI (i) delayed puberty; (ii) extended diestrous phase of the estrous cycle; (iii) On PND 21 and PND 45, CrVI decreased the number of primordial, primary, and secondary follicles in the ovaries. On PND 65, CrVI decreased the development of primordial and primary follicles without affecting the secondary and antral follicle development; (iv) CrVI also affected ovarian steroidogenesis by decreasing the levels of estradiol, testosterone, and progesterone in F1 female rats. CrVI increased the levels of FSH

without altering LH and decreased the levels of pituitary hormones, GH and PRL; (v) Vitamin C protected the ovary by mitigating or inhibiting the adverse effects of CrVI suggesting that vitamin C intake could be considered as a preventive measure to protect women from Cr-induced reproductive toxicity (130). Thus, lactational exposure to CrVI delayed puberty and impaired steroidogenesis in the ovary of F1 female offspring.

CrVI increased follicular atresia in F1 offspring through increased oxidative stress and depletion of antioxidant enzymes

Rationale: In the US and in developing countries, the usage of Cr has been increasing exponentially and the environmental contamination of Cr is one of the major threats to human health as it is not possible to remove Cr from the drinking water completely. Thus, it is imperative to develop potential intervention strategies against Cr-induced ovarian toxicity.

Experimental Design: Lactating dams were divided into the following groups: (1) control- rats received regular drinking water; (2) CrVI treatment- rats received 50 ppm CrVI, 100 ppm CrVI, and 200 ppm CrVI doses of potassium dichromate dissolved in drinking water; and (3) CrVI + Vitamin C treatment- rats received 50 ppm CrVI, 100 ppm CrVI, and 200 ppm doses of CrVI with vitamin C (500mg/kg body wt) supplementation through gavage. The lactating dams received CrVI treatment from the day of parturition to day 21 postpartum. The pups received CrVI during postnatal days (PND) 1–21 via the mother's milk and the effects of CrVI were studied on PND 21, PND 45 and PND 65.

Results and conclusion: Data indicated that (i) CrVI dose-dependently increased follicular atresia compared to control group; (ii) CrVI decreased steroidogenesis exhibited by the decreased levels of estradiol, testosterone, and progesterone in a dose-dependent manner in PND 25, 45, and 65

rats; (iii) CrVI increased oxidative stress in both ovary and plasma by increasing ROS demonstrated by increased levels of H_2O_2 and LPO in a dose-dependent manner; (iv) CrVI decreased the antioxidant enzymes (AOXs) GPx1, GR, SOD, and catalase; and increased glutathione S-transferase in both plasma and ovary; and (v) Vitamin C mitigated or inhibited the above mentioned Cr-induced toxic effects and protected the ovary. Thus lactational exposure to CrVI accelerated follicular atresia and decreased steroidogenesis by altering the ratio of ROS and AOXs in the ovary of F1 female offspring (131).

Edaravone mitigates CrVI-induced oxidative stress and depletion of antioxidant enzymes while estrogen restores antioxidant enzymes in the rat ovary in F1 offspring

Edaravone (EDA) is a potential free radical inhibitor which has been used to treat cancer and cardiac ischemia clinically. The efficacy of EDA against Cr-induced ovarian toxicity in F1 offspring was evaluated in this study.

Experimental Design: Lactating dams were divided into the following three groups: 1) control- rats received regular drinking water; 2) CrVI treatment- rats received 50 ppm CrVI in drinking water, 3) CrVI+EDA treatment- rats received 50 ppm CrVI with EDA (15 mg/kg body wt) through intra peritoneal (*i.p.)* injections. In the study, the lactating dams received CrVI in drinking water from the day of parturition to postpartum day 21. During this period, F1 female rats received respective treatments through mother's milk and the effects were studied on PND25 ovaries.

Results and conclusion: Results showed that: (i) CrVI significantly increased the percentage of atretic follicles with degenerated oocytes and granulosa cells with pyknotic nuclei; (ii) CrVI increased follicle atresia by increasing the expression of cleaved caspase-3 and decreasing the expression of BCL2 and BCL2l1 in the ovary, and EDA mitigated the CrVI-induced increase in

cleaved caspase-3 and decrease in BCL2 and BCL2l1 in the Ovary; (iii) CrVI delayed the onset of puberty and decreased estradiol, progesterone and testosterone, and EDA inhibited the effects of CrVI on those hormones; (iv) CrVI increased oxidative stress by increasing the levels of LPO and H_2O_2, and decreased activity of AOX enzymes SOD1, CAT, GPX1, and GSR in the ovary of F1 rats; and (v) EDA inhibited CrVI-induced oxidative stress and inhibited the adverse effects of CrVI on all AOX enzymes. This was the first study to demonstrate the protective effects of EDA against any toxicant in the ovary and it suggests that EDA could be a potential agent to protect women from Cr-induced reproductive toxicity (132).

Resveratrol protects the ovary against chromium-toxicity by enhancing endogenous antioxidant enzymes and inhibiting metabolic clearance of estradiol

The protective effects of resveratrol (RVT) on CrVI-induced ovarian toxicity, and estradiol turnover were determined.

Experimental Design: Lactating dams were divided into the following three groups: 1) control- rats received regular drinking water; 2) CrVI treatment- rats received 50 ppm CrVI in drinking water, 3) CrVI+RVT treatment- rats received 50 ppm CrVI with RVT (10mg/kg body wt) through oral gavage daily. In the study, the lactating dams received CrVI in drinking water from the day of parturition to postpartum day 21. During this period, F1 female rats received respective treatments through mother's milk and the effects were studied on PND25 ovaries.

Results and conclusion: Results showed that: (i) CrVI increased atresia of primordial, primary, secondary and antral follicles and RVT supplementation mitigated CrVI-induced increase in follicle atresia; (ii) CrVI increased apoptosis by upregulating cytochrome c and cleaved caspase-3, and down-regulating the key cell survival proteins BCL2, BCL-XL and HIF1α, while RVT

inhibited the CrVI effects on BCL2 and HIF1α effectively, but not on BCL-XL; (iii) CrVI significantly decreased the expression of GPX1, SOD1, SOD2, CATALASE, TXN2, and PRDX3, while RVT mitigated the effects of CrVI by upregulating AOXs; (iv) The serum levels of E2, P4, and T were significantly reduced by CrVI by downregulating key steroidogenesis proteins, StAR, 3β-HSD and p450 aromatase. RVT mitigated the effects of CrVI on the expression of StAR, and aromatase, but not on 3β-HSD; and (v) CrVI increased the metabolic clearance of E_2 and RVT restored E_2 levels by inhibiting hydroxylation, glucuronidation, and sulphation of E_2. This was the first study to report the protective effects of RVT against any toxicant in the ovary (133).

In vitro studies

Findings from our laboratory demonstrated toxic effects of Cr on the ovary and multiple mechanisms behind the adverse effects of exposure to CrVI (134-136).

CrVI increased oxidative stress and decreased steroid hormone synthesis and antioxidant machinery

Experimental design: Primary cultures of rat granulosa cells and spontaneously immortalized rat granulosa cells (SIGC) were used to study the effect of heavy metal toxicity on granulosa cells. Cells were grown to 70% confluence in DMEM-F12 supplemented with 2% DC-FBS (Dextran-charcoal coated fetal bovine serum) were divided into three treatment groups: (1) control: cells were treated with 2% DC-FBS media; (2) CrVI-12h: cells were treated with 10μM potassium dichromate for 12 h in 2% DC-FBS media; (3) CrVI-24 h: cells were treated with 10μM potassium dichromate for 24 h in 2% DC-FBS media.

Results: In SIGC, CrVI decreased the mRNA expression of StAR, SF-1, 17β-HSD-1, 17β-HSD-2, FSHR, LHR, ERα and ERβ (137). These proteins play a key role in steroid biosynthesis pathway

that regulate ovarian function. CrVI increased oxidative stress, depleted the level of endogenous antioxidants or downregulated the mRNA of antioxidants in the cells. Furthermore, CrVI increased ROS levels and decreased mRNA levels of cytosolic and mitochondrial antioxidant enzymes such as SOD1, SOD2, GR, catalase, GLRX1, GSTM1, GSTM2, GSTA4, PRDX3, TXN1, TXN2, and TXNRD2 in SIGC and primary cultures of granulosa and theca cells (138).

CrVI treatment delayed follicle development by altering cell cycle regulatory proteins

Experimental design: Primary cultures of rat granulosa cells and SIGC grown to 70% confluence in DMEM-F12 supplemented with 2% DC-FBS were divided into three treatment groups: (1) control: cells were treated in media with 2% DC-FBS; (2) CrVI-12h: cells were treated with 10μM potassium dichromate for 12 h in media with 2% DC-FBS; (3) CrVI-24 h: cells were treated with 10μM potassium dichromate for 24 h media with 2% DC-FBS.

Results: CrVI decreased cell proliferation and arrested cell cycle at the G1 phase with a decreased number of cells in S and G2-M phases. CrVI also decreased protein levels of G1-S phase regulators CDK-4, CDK-6, cyclin D2 and cyclin D3 in granulosa cells. These data suggest that granulosa cells were accumulated at the G1-phase due to down-regulation of CDK-4,-6/D-type cyclins (135). We found that CrVI also decreased cells in S-phase of the cell cycle. During the G1-S phase transition, cyclin E binds to CDK-2, resulting in hyperphosphorylation of Rb and activation of transcription factors and S-phase proteins such as thymidylate synthase and dihydrofolate reductase. Progression to S-phase is directed by the cyclin A/CDK2 complex (139). CrVI treatment down-regulated the expression of cyclin E2 and CDK-2 in granulosa cells causing a decrease in G1 to S phase progression (135).

CrVI upregulated the expression of CDK inhibitors p15, p16 and p27 in granulosa cells *in vitro*. In the mammalian ovary, p27 is a predominant CDK-inhibitor which tightly regulates primordial to primary follicle transition by negatively regulating cyclin E/CDK2 and cyclin A/CDK2 complexes. Increased primordial to primary follicle transition was observed in p27-Knockout mice leading to infertility due to exhaustion of follicle reserve (140). PCNA is expressed in the nuclear matrix of cells during all phases of the cell cycle, reaching a maximum in S and G2-phase, and its expression is required during DNA replication (141,142). In granulosa cells, PCNA is expressed from the primary follicle stage and its expression level increases during the preovulatory follicular development (143). CrVI treatment decreased PCNA in granulosa cells suggesting that the decrease in follicle number and delay/arrest in development of follicle at the secondary follicular stage caused by the CrVI (136) might be due to the reduced expression of PCNA. In G2-M phase check point, cyclin A associates with CDK1 and CDK1/cyclin B assembly is active for mitosis to occur (144). In granulosa cells, treatment of CrVI decreased cell populations in the G2-M phase by downregulating cyclin B1/CDK-1 expression. Thus, *in vitro* exposure to CrVI delayed cells from entering into G2-M phase, and its progression by downregulating the levels of cyclin A and cyclin B1, and CDK-1 (135).

CrVI treatment induced granulosa cell apoptosis by altering the sub-cellular localization of* BCL2 *family members, p53 and ERK1/2

Experimental design: Primary cultures of rat granulosa cells and SIGC were grown to 70% confluency in DMEM-F12 medium supplemented with 5% FBS. After 24 h fasting in 2% DC-FBS, cells were divided into the following treatment groups: (1) control: cells were treated with DMEM-F12 medium with 2% DC-FBS; (2) CrVI-12h: cells were treated with 10μM potassium dichromate for 12 h in DMEM-F12 medium with 2% DC-FBS; (3) CrVI-24 h: cells were treated

with 10μM potassium dichromate for 24 h in DMEM-F12 medium with 2% DC-FBS; (4) Vitamin C: cells were pre-treated with vitamin C for 2 h, then treated with DMEM-F12 medium with 2% DC-FBS; (5) Vitamin C pretreatment + CrVI-12h: cells were treated with 10μM potassium dichromate for 12 h in DMEM-F12 medium with 2% DC-FBS; (3) CrVI-24 h: cells were treated with 10μM potassium dichromate for 24 h in DMEM-F12 medium with 2% DC-FBS.

Results: Findings from our laboratory revealed that CrVI treatment induced apoptosis of granulosa cells *in vitro* through multiple mechanisms such as mitochondria-mediated intrinsic apoptosis, p53-mediated apoptosis, and ROS-mediated apoptosis (135,136). BCL2, BCL-XL, BAX, and BAD are key proteins of BCL2 family members that mediate the intrinsic apoptotic pathway. In addition, HSP70 protects the cells from undergoing apoptosis by inhibiting translocation of BAX from the cytosol to the mitochondria, cytochrome *c* release from the mitochondria into the cytosol and caspase-3 and PARP activation (145-147). We found that CrVI treatment decreased expression of BCL2, BCL-XL, HSP70 and HSP90 which are key survival anti-apoptotic proteins. On the other hand CrVI increased the translocation of pro-apoptotic proteins, BAX and BAD from cytosol to the mitochondria. This translocation increased membrane permeability of mitochondria, facilitated the cytochrome *c* release and activated caspase-3 and PARP proteins leading the granulosa cells to undergo apoptosis (136). These results suggest that CrVI attenuated anti-apoptotic pathways in order to stabilize pro-apoptotic members to execute apoptosis of granulosa cells.

DNA damage leads to apoptosis by promoting phosphorylation and subsequent stabilization of p53 (148). Phosphorylation of p53 at multiple serine residues is required for apoptosis (149). Different events and agents like H_2O_2 (150), ionization (151), UV irradiation (152) and ultimately oxidative stress (153) can induce phosphorylation of p53 at ser-15. CrVI

increased phosphorylation of p53 at ser-6, ser-9, ser-15, ser-20, ser-37, ser-46 and ser-392 and selectively translocated active p53 protein into mitochondria in granulosa cells *in vitro*. Cell death mediated by p53 requires its selective translocation into mitochondria to trigger a rapid pro-apoptotic response (154,155) and its association with antioxidants and apoptotic proteins (156-159). After translocation, the p53 protein could interact with endogenous anti-apoptotic BCL-XL and/or BCL2 protein, induce oligomerization of BAK protein, increase mitochondrial outer membrane permeabilization and result in the release of cytochrome-c (160), or interact with MnSOD and inhibit its ability to scavenge free radicals (159). AKT and ERK pathways are the major cell survival pathways and are associated with expression of anti-apoptotic BCL2 and BCL-XL proteins and phosphorylation of the pro-apoptotic BAD protein. CrVI increased the phosphorylation of ERK and JNK, and induced activation and selective translocation of ERK1/2 into nucleus and mitochondria. CrVI decreased phosphorylation of AKT, which plays a key role in cell survival. Thus, CrVI targets multiple molecular targets to cause apoptosis of the granulosa cells.

Folliculogenesis

Primordial germ cells and primordial follicle formation

Mouse primordial germ cells originate in the extra embryonic mesoderm at 7.5 days of development of the embryo (E7.5). The signals that are derived from the visceral endoderm and extra-embryonic ectoderm aid in their initial development. BMP2, BMP4, and BMP8b are the TGF family factors that are needed for primordial germ cell formation and regulation of gene expression (161-163). In mouse, primordial germ cells migrate to the genital ridge at E9.5-E11.5 (164). Between E10.5 and E13.5, primordial germ cells proliferate by the process of mitosis during which time they are called oogonia (165-167). In humans, mitosis begins at 5-week post conception and ends at 10-16 week post-conception (164). The migration, proliferation, colonization, and survival of primordial germ cells is controlled by the secretion of various factors, and their interaction with the surrounding somatic cells. In mouse, BMP2 and BMP4 are found to increase the number of primordial germ cells in culture while a reduction in the number of primordial germ cells were observed in BMP7 knockout mice (168-170). BLIMP1 and PRDM14 are critical for primordial germ cell proliferation and migration (171). In mouse, activin inhibits primordial germ cell proliferation whereas it is found to increase primordial germ cell numbers in humans (172). OCT4, NANOG, FIGLA, NANOS3, DND1, KIT and KITL are some of the factors that play important roles in the survival of primordial germ cells. Any mutation in the gene coding these factors will cause a depletion of germ cells, which leads to a defect in the primordial follicles formation (173).

Sex determination starts around the period of primordial germ cell migration and colonization to genital ridge. *Sry*, the Y-linked gene, influences the XY genital ridge to differentiate into a testis. The XX gonads develop into ovaries which seems to be the default

pathway as these gonads have no SRY (174). During mitosis, germ cells or oogonia divide and form germ cell nests connected by intercellular bridges due to incomplete cytokinesis at ~E10.5 (164,167,175,176). Most of the germ cells divide synchronously and contain 2^n germ cells in a single germ cell cluster in a nest (175,176). Nests containing a cluster of 2 or 4 cells were observed at E11.5-E12.5 whereas large nests containing clusters of 8 or 16 mitotic cells were observed at E13.5. While 8 and 16 mitotic cells were seen in largest mitotic clusters, the number cannot grow larger than 32 cells (175). The somatic cells surround the germ cell nests and this grouping of somatic cells and germ cells is called the ovigerous cords (177). The ovigerous cords are surrounded by a basal lamina (178). Following the sex determination and germ cell nest formation, mitotic divisions stop and the meiosis phase is initiated by the oogonia at E13.5 in mice and oogonia become primary oocytes (167,179,180). In humans, meiosis is initiated at 13-week post-conception (181). In the embryonic ovaries of the mouse, initiation of meiosis begins in response to retinoic acid and the expression of Stra8 (stimulated by retinoic acid gene 8), a female germ cell factor expressed just prior to entering the prophase of first meiotic division (182). Stra8 is required for premeiotic DNA replication and meiotic prophase events such as chromosome condensation, cohesion, synapsis, and recombination (183). During meiosis, oocytes proceed through leptotene, zygotene, and pachytene stages of prophase I, and become arrested at the diplotene stage, where the oocytes undergo a prolonged resting phase beginning at E17.5 with most cells reaching diplotene by PND5 (184,185). Oocytes that are located at the inner cortical and medullary region begin meiosis and grow first (167,186,187).

Around E17.5, germ cell nest breakdown occurs when the oocytes separate and the ovigerous cords surrounding the germ cell nest become fragmented with the remodeling of the basal lamina. During germ cell nest breakdown, the single oocyte become enclosed by a single

layer of flattened, crescent-shaped squamous granulosa cells and this structure, defined as primordial follicle is formed (188,189). This process is called primordial follicle assembly (167). The formation of primordial follicle following nest breakdown involves important communication between the oocyte and surrounding somatic cells. In rodents, GDF9, BMP15, FOXL2 and NOBOX were found to play an important role in this germ cell nest breakdown process. Lack of those genes, decreased expression, and reduced function of those proteins affect the timing of nest breakdown and impair the germ cell nest breakdown process (173). Throughout the germ cell nest breakdown process, substantial numbers (about two-thirds) of oocytes are lost through apoptosis (167). In the ovary, apoptosis plays a major role in follicular atresia and determines the pool of primordial follicles. Oocytes that are not surrounded by granulosa cells during the follicle assembly process undergo cell death by apoptosis. In the cortex of the ovary, oocyte death and germ cell nest breakdown begin after birth while in the medulla, they begin as early as E17.5 (190). The follicles that begin to develop first are found closer to the medullary region (191).

Progression from the primary to the secondary follicular stage

The essentiality of fertility is the establishment of the pool of primordial follicles, as the oocytes contained in them represent the absolute pool accessible during the entire reproductive life period of women (192). Thus, any alteration in this process might lead to a reduced primordial follicle pool size, resulting in POF. The primordial follicles are recruited continuously from this resting pool and begin to form primary follicle, where the oocyte begins to grow extensively surrounded by a single layer of cuboidal granulosa cells that is proliferative. In the primary stage, the oocyte is separated from the surrounding granulosa cells by the formation of a glycoprotein polymer capsule, the zona pellucida. The primary follicle becomes a secondary follicle when it is surrounded by more than one layer of granulosa cells with oocytes in mid-growth stages. Oocyte-

secreted factors recruit theca cells, and surround the outermost layer and basal lamina, and becomes theca externa and theca interna after cytodifferentiation. Also, an intricate network of capillary vessels is formed between theca externa and interna for circulating the blood around the follicle (193). In both mouse and humans, the initial growth and development of primary and secondary follicles are gonadotropin-independent as their growth occurs in the absence of hormones even though FSHR is present on the granulosa cells of those follicles (194,195).

The communication between the oocyte and surrounding somatic cells is important for the growth and development of preantral follicles. The transition from primary to secondary follicles is driven by the secretion of local intra-ovarian paracrine factors by oocytes, granulosa, and theca cells (196). Though the rate of development of follicle is dependent primarily on the oocyte, it still relies on the somatic cells for its own growth and development. The oocyte-secreted growth factor critical for the function of the somatic cells are GDF9 and BMP15, two members of the TGFβ superfamily. GDF9 is expressed by the oocytes of primary follicle and aids in the transition of the follicle to further stages (197,198). In female mice ovaries that lack *GDF9*, primordial follicles are able to form and can proceed to primary follicle formation but are not able to progress to further stages resulting in sterility (199,200). BMP15 plays an important role in stimulating the proliferation of undifferentiated granulosa cells (201). In human and mouse primordial follicles, NTF5 and BDNF, the neurotrophins expressed in primordial follicles signal through NTRK2 on the oocyte (202,203). They both play an important role in the preantral folliculogenesis, as the number of primary and secondary follicles are reduced with a compromise in the ability of follicles to grow beyond primary follicle stage when there is a concomitant loss of *NTF5* and *BDNF* (202). TATA box binding protein (TBP)-associated factor (TAF4B), is a transcription factor expressed primarily in germ cells but also present in granulosa cells, whose absence in the female mice

ovaries had reduced number of primordial and growing follicles showing its role in the follicle development process (204,205). Mice ovaries lacking *TBP2* (TATA-binding protein), another transcription factor specific to oocyte showed a reduction in secondary follicle numbers (206).

Progression from Pre-antral to Antral follicle stage

A preantral follicle is discernable from the antral follicle, also called Graafian follicle, by the presence of fluid-filled cavity called the antrum. As the follicle progresses from pre-antral stage to antral follicle stage, the antrum is formed by the coalescence of the fluid-filled spaces within the granulosa cell layers in the follicle, along with increased thecal layer vascularization, continued oocyte growth, and granulosa and thecal cell proliferation (207). The antral follicular stage is reached by most growing follicles once they enter the growing pool, and they unavoidably undergo atresia. During the peri-menstrual period, a small cohort of antral follicles are rescued from undergoing atresia by the elevated circulating FSH levels, and they continue to grow. The granulosa and theca cells continue to proliferate by mitosis along with an increase in antral volume and these follicles are referred to as tertiary follicles.

In the tertiary follicle, granulosa cell differentiates by the action of oocyte-secreted factors to form four subtypes based upon location within the follicle: corona radiata, surrounding the zona pellucida; membrana, interior to the basal lamina; cumulus oophorus, connecting the membrana and corona radiata together; and peri-antral, adjacent to the antrum. At this stage, granulosa cells, theca cells, and oocytes secrete various factors inside the follicles to ensure the successful maturation of the follicle and ovulation. Granulosa cells secrete activins and BMP-6, theca cells secrete BMP-2, BMP-4, and BMP-7 or both cells secrete TGF-beta, and oocytes secrete GDF-9 and BMP-15 (208). These factors act either alone or synergistically on selected follicles which can increase the FSH levels secreted by the pituitary, and induce the granulosa cell proliferation (193).

FSH binds to the FSHR, a G protein coupled receptor that activates the PKA pathway. In this pathway, the transcription factor CREB (cAMP Response Element Binding Protein) is phosphorylated and activated which regulates the expression of genes that are essential for the follicle development. FSH binding can also activate the PKA independent pathway where SGK1 (serum and glucocorticoid-induced kinase 1) and AKT is phosphorylated, and activated through the PI3K pathway. In granulosa cells, the PI3K pathway is also activated by IGF-1. Both IGF-1 and FSH, through the PI3K pathway regulate the expression of FOXO1 which is important for the proliferation, differentiation, and survival of granulosa cells. IGF-1 also increases FSHR levels in granulosa cells and increases FSH sensitivity (176). All these molecular events help the granulosa and theca cells to proliferate in the recruited cohort of follicles.

Preovulatory follicle development and ovulation

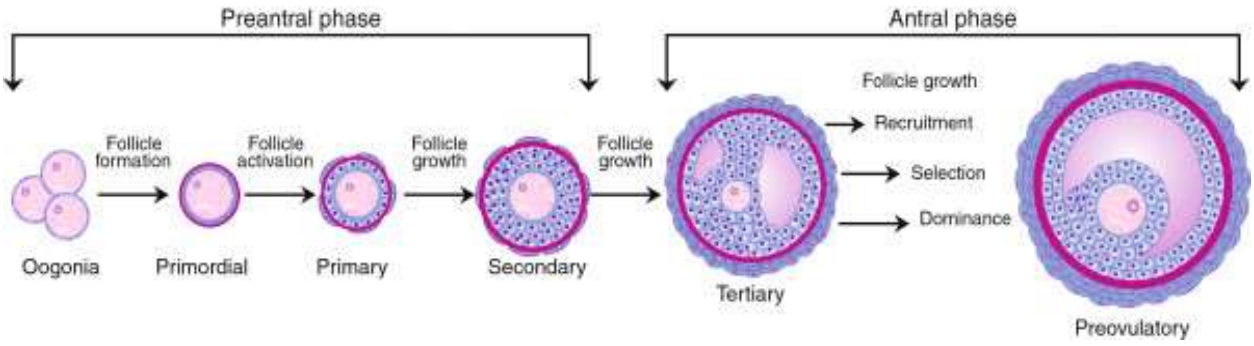

Fig. 1.1. Schematic diagram of complete follicular development. Reprinted with permission from (209).

A single dominant follicle is preferentially chosen to grow from the cohort of recruited follicles, while the subordinate follicles undergo atresia and the process is termed as follicle

selection (210-212). The follicle maturation and selection of dominant follicle is coordinated by the positive and negative feedback mechanisms in the HPG axis. It is suggested that the dominant follicle is more sensitive to FSH due to the increase in a number of the granulosa cells and FSH receptors, which further stimulate the expression of FSH and LH receptors in the granulosa cells and theca cells respectively. During the mid-follicular phase, the dominant follicle produces estrogens and inhibins which suppress the secretion of FSH from pituitary through negative feedback mechanism (213). The subordinate follicles fail to survive due to the declining levels of FSH and eventually undergo atresia (214,215).

In the late-follicular phase, the dominant follicle continues to grow with an increase in the proliferation of granulosa cells and increase in activity of aromatase, resulting in an increase in the levels of estradiol. The level of estradiol increases both in the follicle and in circulation, during which time the follicle reaches the pre-ovulatory stage. In preparation for ovulation, only one antral follicle develops each month into a pre-ovulatory follicle during the follicular phase of the menstrual cycle in 14 days. During the pre-ovulatory period, increase in response to gonadotropins and its sensitivity in the follicle mediates its growth, LH receptor expression, and over 90% production of estradiol by the granulosa cells (193). Just before the ovulation or the day before LH surge, the granulosa cells stop proliferating in the dominant pre-ovulatory follicle, its production of estradiol peaks, and stimulate the LH surge by its positive feedback at the hypothalamus and pituitary. In the pre-ovulatory follicle, increased expression of LH receptor in the granulosa cells makes it respond to LH surge. Within 24 h of the LH surge, the highly vascularized pre-ovulatory follicle responds to the LH, and the ovulation occurs by the initiation of a cascade of events leading to oocyte meiotic resumption, cumulus expansion, follicle rupture and release of the oocyte (216). Before ovulation, the oocyte in the follicle is arrested at the diplotene stage, which resume and

complete meiosis I during each month from puberty to menopause giving rise to a secondary oocyte arrested at metaphase II stage. After ovulation, these secondary oocytes will complete meiosis II if sperm penetrates fertilizing the egg. The schematic sequence of complete follicular development is shown in Fig. 1.1.

Activation of primordial follicles

Activation of the primordial follicles is a tightly controlled process and very dynamic. The process of folliculogenesis is initiated when the primordial germ cells become activated and are recruited in cohort continuously. The PI3K/AKT signaling pathway is present in oocytes from primordial and primary follicle stage, and is the major pathway required for primordial follicle activation (217,218). In oocytes, loss of PTEN leads to increased phosphorylation of AKT and FOXO3a due to increased activity of PI3K. FOXO3, a transcription factor whose activation is found to lead the cell to undergo cell cycle arrest and apoptosis. In the mouse oocytes, FOXO3 is expressed and is found to repress the activation of primordial follicles (219). Premature activation of primordial follicles and postnatal depletion of follicles occurs in *FoxO3* null mutant mice. Similarly, depletion of the primordial follicle pool is observed in mice lacking PTEN (217). mTOR signaling pathway also plays an important role in preventing the early activation of primordial follicles. It has been shown in a mouse model that TSC1 (tumor suppressor tuberous sclerosis complex 1) negatively regulates mTORC1 (mammalian target of rapamycin complex 1) and prevents the activation of primordial follicles and maintains them in a quiescent state. In oocytes, null mutation of these factors leads to early activation of primordial follicles and depletion of follicles leading to premature ovarian failure (220).

Anti-mullerian hormone (AMH), a TGFβ superfamily member expressed in granulosa cell is required to maintain a balance between the primordial follicles that stay in the resting pool and

follicles that are being activated. The recruitment of primordial follicles into the growing pool is inhibited by AMH in mouse (221,222). In *Amh* null mutant mice, primordial follicles were recruited more and the resting pool of follicles was rapidly depleted with more preantral and small antral follicles observed in the knockout compared to the wild type (223). The interaction of KIT, an oocyte-expressed receptor and its somatic cell expressed ligand, KIT ligand promotes the recruitment of theca cell, proliferation of granulosa cells and the growth of oocyte and controls the initiation of follicle growth (224). *In vitro*, it has been shown that PI3K/AKT pathway is regulated by KIT ligand in oocytes, activating AKT by increasing its phosphorylation and hence repressing the activity of FOXO3 leading to premature activation of primordial follicles (218).

Neurotrophins, the growth factors that play a role in the nervous system plays a role in regulating early folliculogenesis process. Nerve growth factor (NGF) is expressed both in the oocytes and somatic cells even before formation of the follicle plays a role in primordial follicle activation (225). It is suggested that NGF signaling is required for the primordial to primary follicle transition as the reduced population of primary and secondary follicles were observed in mice ovaries lacking *NGF* (226). Sohlh1 and Nobox, two other transcription factors expressed in the oocytes are important regulators of early oogenesis and folliculogenesis, as they are very important for the primordial follicles to progress to the primary follicle stage. In the absence of Nobox in ovaries, the majority of follicles are arrested at the primordial stage with the degeneration of oocytes (227). Similarly, in null mutant mice for Sohlh1, follicles did not progress to the primary follicle stage and the growth of primordial follicle is arrested (164). BMP4, a member of the TGFβ superfamily, also determine primordial follicle progression. In neonatal rat ovaries, *in vitro* exposure to BMP4 reduced the arrested primordial follicle number and enhanced the proportion of developing primary follicles (228). Thus, BMP4 promotes the development of primordial

follicle and its transition to the primary follicle.

Follicular dynamics

In the human, early menopause and infertility may occur due to early depletion of primordial follicles or poor stocking of the initial pool of primordial follicles (229). The decline of the non-growing, resting primordial follicle reserve due to age in human ovaries has been predicted by mathematical analyses. It predicted that at around 40 years of age menopause would occur if at birth an ovary had 35,000 non-growing follicles, but if the ovary began with 2.5 million non-growing follicles then the menopause would be delayed to 60 years (230,231). The mathematical analysis of the number of follicles leaving the resting non-growing pool shows that this number increases through childhood, peaking at 900 follicles/month at 14 years of age, then falling to 600/month at 25 years of age, and 200/month at 35 years of age (230). In mice, the loss of primordial follicles per ovary is minimal following the sharp decline of primordial follicles during the neonatal period. The primordial follicle loss occurs with an average of less than one follicle per day for up to 14 weeks and the number declines significantly up to 300 days (232-235).

It has been thought that intra-ovarian mechanisms limits the decline of the reserve of primordial follicles to conserve the stock of follicles in the early phases of postnatal life including and beyond puberty. The growing follicle pool may exert a brake in addition to inhibition by intracrine and/or paracrine factors to maintain the quiescence of the resting follicles and regulate the rate of recruitment of primordial follicles (236-239). In the postnatal mouse ovary, it has been suggested that a 'quorum-sensing' model may explain the preservation of a set number of follicles in the primordial follicle reserve which suggests that the excess primordial follicles can be eliminated *via* a BCL2 cell death mechanism but the ovary cannot add primordial follicles to an insufficient primordial follicle reserve (240,241).

Cell survival and cell death pathways

Apoptosis or programmed cell death is the major process, which determines the ultimate number of primordial follicles that are present in the reserve during the reproductive life of a female. It also influences the fertility and menopausal timing of women by regulating the oocyte number available for ovulation.

The two apoptotic pathways in mammalian cells are the *intrinsic apoptotic pathway* and *extrinsic apoptotic pathway* (242,243). Developmental cues and stress stimuli such as oxidative stress, hypoxia, heat, detachment from the extracellular matrix, DNA damage, cytokine deprivation and chemotherapy are known to activate the intrinsic apoptotic pathway (244). Whereas FAS ligand and TNF-alpha activate the extrinsic apoptotic pathway by binding to their respective cell surface death receptors (242). The pro-apoptotic and anti-apoptotic BCL2 superfamily members regulate the intrinsic apoptosis pathway (243). Based on the function and structure, the BCL2 family of apoptotic regulators is divided to three groups: i) the pro-apoptotic BH3-only proteins initiates the intrinsic apoptosis pathway by sensing cell stress and includes pathway members PUMA, NOXA, tBID, BIK, BAD, BMF, BIM, and HRK; ii) the pro-survival BCL2 like proteins include BCL2, BCL-XL, BCL-W, A1 and MCL1 which are important for cell survival by inhibiting apoptosis; and iii) the members of pro-apoptotic effector proteins that activate cell death are BAX, BAK, and BOK (245,246).

The pro-apoptotic BH3-only proteins such as PUMA, NOXA bind to the pro-survival BCL2 family proteins such as BCL2, BCL-XL and inhibit their activity thereby releasing its inhibition on the pro-apoptotic effectors BAX and BAK and activating them (246). BAX and BAK can also be activated directly by the binding of pro-apoptotic BH3-only proteins PUMA, tBID and BIM (247). In the absence of apoptotic stimulus, the pro-survival proteins prevent the

activation of BAX and BAK by sequestering those pro-apoptotic BH3-only proteins to the cytoplasm (247). BAX and BAK activation results in the destabilization of mitochondria by permeabilizing the mitochondrial outer membrane causing the release of cytochrome c. Cytochrome c release results in the formation of apoptosome, promoting the activation of initiator caspase-9 and effector caspases (caspase-3, -7, -6) resulting in apoptosis (243). In the absence of apoptotic stimulus and presence of survival cues, the pro-survival proteins such as BCL2, BCL-XL or MCL1 are activated and heterodimerize with pro-apoptotic BH3-only proteins at the mitochondria and sequesters them preventing cytochrome *c* release resulting in cell survival.

The extrinsic apoptotic pathway is activated by the binding of TNFα and FASL to their respective receptors leading to cleavage of caspase-8 and effector caspase activation and apoptosis. Caspase8 can also cleave BID and generate tBID which can engage the intrinsic apoptosis pathway (248,249). The roles of key anti-apoptotic and pro-apoptotic proteins that promote the cell survival and cell death of germ cells are discussed below.

BCL2, the pro-survival protein regulates the primordial follicle pool size at birth as it's overexpression in transgenic mice increased the number of primordial follicles at birth but the increase in number was not maintained in postnatal life (250). Also, mice lacking functional BCL2 protein showed reduced primordial follicle numbers compared to wild-type (251). Thus, BCL2 may act as an anti-apoptotic factor in the ovary which increased the primordial follicle pool size by promoting follicle survival and decreasing the germ cells that undergo apoptosis during ovary development (250).

BCL-XL, another anti-apoptotic member of the BCL2 family plays a key role in maintaining germ cell survival during gonadogenesis (252). BCL-XL hypomorphic mice showed a severe reduction in the population of primordial and primary follicles and impaired fertility. At

E13.5, the number of oocytes was reduced and by E15.5 primordial germ cells were depleted following germ cell migration indicating a role for BCL-XL in embryonic germ cell apoptosis (252).

It has been implicated that BAX is one of the key pro-apoptotic factors that initiate apoptosis in both oocytes and granulosa cells (253). *BAX* mutant mice exhibited a reduction in the primordial and primary follicle atresia due to defects in apoptosis which prolonged the reproductive lifespan of the ovary in aged mutant females (254). Mutation of the *BAX* gene increased the oocyte number, and germ cell nests contained more oocytes at E13.5, E15.5, PND4, and PND7 (255). Also, mouse oocytes that are deficient in BAX were resistant to apoptosis induced by chemotherapy, suggesting its pro-apoptotic role in the ovary (256).

Caspases are involved in regulating ovarian germ cell viability (257). Decreased germ cell death was observed in caspase-2-deficient mice with a greater number of primordial follicles compared to wild-type in the PND4 ovary (258). In both *in vivo* and *in vitro*, the absence of caspase-3 did not affect oocyte death initiated by either developmental cues or pathological insults, however, caspase-3 mutant female mice showed aberrant atretic follicles containing granulosa cells that failed to be eliminated by apoptosis (259).

PUMA-mediated apoptosis plays a key role in establishing the ovarian reserve by determining the primordial follicle number. Mice lacking *PUMA* were reported to have twice the number of primordial follicles by 15.5 to 17.5 dpc (260). In postnatal mouse oocytes and somatic cells, DNA damage repair failure triggers the intrinsic apoptosis pathway via PUMA and NOXA. Oocytes deficient in PUMA and NOXA were more resistant to DNA damage induced by γ-irradiation suggesting the key role played by them in removing the primordial follicles from the reserve that have DNA damage (234,246).

p53-miR34a-SIRT1 Signaling Network

p53

p53 is a tumor suppressor gene which is activated by DNA damage and cellular stress such as radiation, oxidative stress, hypoxia, carcinogens and chemotherapeutic drugs (261). Under normal conditions, p53 is destabilized and degraded; therefore, resting cells contain small amounts of p53. However, genotoxic stress leads to stabilization of p53 which accumulates inside cells, inducing cell cycle arrest, senescence, and apoptosis (262-265). p53 regulates cell proliferation in part by acting as a transcription factor, and either activating or suppressing a huge array of gene transcriptions (262,266). The transcriptional regulation of target genes by p53 involves the direct binding of p53 to the DNA-responsive elements present within their promoters of genes that mainly increases their expression (267). p53 also acts as a transcription factor for pro-apoptotic effector protein-encoding genes and is involved in transcription-independent cellular signaling leading directly to apoptosis (261). Apart from regulating target genes, p53 can also regulate the expression of micro RNAs (miRNA) (268).

Activation of p53

Ataxia Telangiectasia protein (ATM), the ATM-related protein (ATR), the Nejmeegen Breakage Syndrome (NBS) protein and poly(ADP-ribose)polymerase (PARP) are some of the sensors of DNA strand break induced by radiation (269). Following exposure to ionizing radiation, ATM protein can phosphorylate p53 either directly at ser15 or indirectly via CHK2 (ser20), JNK (ser37) or c-Abl (269,270). ATM activates the sequence-specific binding of p53 by activating a phosphatase that dephosphorylate p53 specifically at ser376 allowing for the binding of the 14-3-3 protein (271). ATM also stabilizes p53 by phosphorylating COP1 ubiquitin ligase leading to its

dissociation from p53 (272). In non-stressed cells, the proteins implicated in the degradation of p53 by ubiquitination are MDM2 and JNK. MDM2 binds tightly to the N-terminus of p53 leading to the ubiquitination and subsequent proteasome-mediated degradation of p53. It also blocks p53 transcriptional function by interacting with transcription activation domain of p53. Also, MDM2 promotes the nuclear export of p53 into the cytoplasm (273). $p14^{ARF}$ (ARF) is one of the mediator of oncogene-induced p53 activation by binding to Mdm2 and inhibiting it (274). DNA damage-induced kinases promote acetylation within the C-terminus of p53 and activate p53 as a transcription factor (275). Hypoxia activates p53 and stimulates apoptosis through mechanisms that involve ATR, HIF 1α (hypoxia inducible factor) and VHL (von Hippel-Lindau) (276). While HIF1α is degraded through its interaction with VHL under normal conditions, hypoxic conditions disrupts the interaction of HIF1α with VHL thereby stabilizing it. Stable HIF1α stabilizes p53 by binding to it. Also, VHL can also activate p53 by interacting with it directly and promoting the phosphorylation and acetylation of p53 (275). Thus various proteins play a role in activating p53 under stress conditions.

miR34a

miRNAs are small single-stranded non-coding RNA of about 20-24 nucleotides (277) that negatively regulate gene expression both at mRNA and protein levels through direct binding of 3'UTR of mRNAs in a sequence-specific manner and/or by silencing translation (278). miRNAs are transcribed as capped and polyadenylated primary transcripts (pri-miRNAs) by RNA polymerase II. A protein complex known as the microprocessor complex that contains Drosha ribonuclease III enzyme cleaves the primary transcripts and produce an approximately 70-nucleotide stem-loop precursor miRNA (pre-miRNA) (279). Dicer ribonuclease (Dcr-1) further cleaves the pre-miRNA to generate the mature miRNA and antisense miRNA star. The mature

miRNA is incorporated into RNA-induced silencing complex (RISC), which can cleave, degrade or suppress translation or target mRNAs depending on the complementarity between mRNA and miRNA (280). A perfect complementarity between seven consecutive nucleotides in the target mRNAs 3′ UTR and the nucleotide 2–8 (seed sequence) at the miRNA's 5′ end is required to reduce the protein levels of the target (281). On the contrary, miRNAs have the capability of activating gene expression directly or indirectly in response to different cell types and conditions and in the presence of distinct cofactors. In miRNA-mediated upregulation, miRNPs (microribonucleoproteins) act in trans in promoting their target mRNAs' expression. The mRNA expression could be activated by the direct action of miRNPs and/or could be indirectly relieved from miRNA-mediated repression by abrogating the action of repressive miRNPs (282). For example, Mmu-miR34a/34b-5p binds the 3′-UTR and upregulated translation of an alternatively cleaved and polyadenylated longer variant of β-actin mRNA without increasing mRNA levels at neuronal synapses in mouse neuronal cells (283).

p53 can regulate the expression of a set of miRNAs, including miR34 family (miR34a, miR34b, and miR34c), miR107, miR145, miR192, and miR215, contributing to the tumor suppression role of p53 (284). The miR34 family is directly regulated by p53 and it modulates cell cycle progression, senescence, and apoptosis (268,285). Ectopic miR34a acts as a tumor-suppressor gene by inducing G1 cell cycle arrest, senescence, and apoptosis (285,286). MiR34a expression is silenced in several types of cancers such as prostate and melanoma due to aberrant CpG methylation of its promoter and subsequent transcriptional silencing (287). Overexpression of miR34a promoted G1 phase cell cycle arrest and apoptosis. Conversely, the decrease of endogenous miR34 suppresses apoptosis (285). p53 can induce miR34a expression in irradiated mice and cultured fibroblast cells (285). Transcriptional activation of miR34a was found to

contribute to p53-mediated apoptosis (288). In mouse embryonic fibroblast cells deficient in p53, expression of miR34 family was correlated with p53 status. The study showed that the genes encoding miR34 family are direct transcriptional targets of p53, whose induction by DNA damage and oncogenic stress depends on p53 both *in vivo* and *in vitro*. (289). The gene encoding miR34a has a p53 binding site and p53 was shown to bind directly to p53 responsive element located upstream of the miR34 family gene (288,290). Thus, p53 acts as a transcription factor to increase miR34 family of gene expression. miR34a plays a pivotal role in a positive feedback loop that includes p53, miR34a, and SIRT1.

SIRT1

SIRTuin 1 (SIRT1) is one of the target genes of miR34a as the 3' UTR of SIRT1 has a response element for miR34a (291). SIRT1, an NAD+-dependent deacetylase, is one of the seven mammalian SIRTuins and it plays diverse roles in various physiological and pathological events, including life-span extension, neurodegeneration, age-related disorders, obesity, heart disease, inflammation, and cancer (292). Interestingly, SIRT1 was reported to improve the follicle reserve and prolong the ovarian lifespan of diet-induced obesity in female mice (293). Resveratrol, an activator of SIRT1, has an anti-aging effect and is beneficial to the cardiovascular system and diabetes and obesity (294,295). Consistently, it prolongs the ovarian lifespan and protects against age-associated infertility in rodents (296,297). SIRT1 plays a key role in protecting cells from DNA damage and oxidative stress (298,299). Apart from deacetylating histones and histone methyl-transferases, SIRT1 can also deacetylate non-histone proteins such as p53, E2F1 and NFκB (300). SIRT1 can interact with p53 and deacetylate it at Lysine-382 residue decreasing the p53-mediated transcriptional activation and hence reduces downstream target gene regulation (268). Overexpression of SIRT1 was found to represses p53-dependent cell cycle arrest and apoptosis in

response to oxidative stress and DNA damage (301,302). SIRT1 protein levels were decreased when miR34a was overexpressed in HCT116 cells and conversely, miR34a knockdown increased the protein expression of SIRT1. Thus, miR34a targets SIRT1 and suppresses it by post-transcriptional inhibition (291).

Endocrine disrupting chemicals and their effects on female reproductive system

Endocrine disrupting chemicals (EDCs) or endocrine disruptors are naturally occurring compounds or man-made synthetic chemicals or mixture of chemicals that act on the endocrine systems of humans and animals by mimicking, blocking and/or interfering in some manner with the natural cell signaling pathway of hormones in cells and produce adverse reproductive, neurological, developmental, and immune effects (303,304). These exogenous agents interfere with processes regulated by endogenous hormones. One such process is a female reproductive function where the major reproductive organ is the ovary. EDCs disrupt ovarian processes and cause adverse outcomes such as infertility, anovulation, menstrual cycle problems, endometriosis, estrogen deficiency, adverse pregnancy outcomes and premature ovarian failure (305).

BPA

(Bisphenol-A) BPA is a plasticizer and a high production volume monomer, used commonly in epoxy resins, plastics, food and drinks containers, dental sealants, and grocery receipts. BPA leaches out from food and beverage containers because of incomplete polymerization, leaching of unbound BPA and degradation of the polymers by chemicals and exposure to higher temperatures. It is estimated that around 6.6 mg/person/day of BPA is consumed by the ingestion of foods packaged in epoxy resin coated cans. Approximately, 90-99% of BPA exposure in children and adults is through ingestion from food and water.

In the developing fetal ovary, maternal exposure to BPA affects the earliest stages of oogenesis and the embryos that are produced from the BPA exposed female with the mitotic defects will be chromosomally abnormal in the adult stage. Multiple oocyte follicles (MOF) originate from improper germ cell nest breakdown. After birth, the germ cell nest breakdown is initiated by decreased levels of estrogen. BPA acts as a synthetic estrogen and prevents the proper germ cell nest breakdown after birth (306). It is also suggested that exposure of BPA to the fetus may limit the expansion of the primordial germ cells by down regulating the mitotic cell-cycle genes based on the gene ontology analysis (307). Follicle activation is confirmed by Chao *et al*., (2012) who found that ovaries exposed to BPA postnatally have significantly decreased primordial follicles but increased the primary, secondary and antral follicles (308). These might be caused by the estrogenic stimulatory effect of BPA on the early folliculogenesis and during the prepubertal stage, it caused an acceleration of folliculogenesis leading to increased follicular atresia (309). A cohort study of women undergoing infertility treatments correlated with higher BPA levels with lower antral follicle counts suggesting that ovarian failure might be accelerated by BPA exposure (305,310).

Methoxychlor

Methoxychlor (MXC) is an organochlorine pesticide used to kill insects that attack vegetables, fruits and home gardens. It is estimated that MXC and other pesticide residues are contained in 35% of agricultural commodities (311). Even though production and usage of MXC were banned in the US, human exposure occurs through importing of agricultural products containing MXC into the US from other countries. Humans are mainly exposed to MXC through food and water. MXC is highly persistent in the soil as its residues were seen even after 18 months in soil that were treated with MXC biodegrading microorganisms (312).

Inside the body, MXC is metabolized to 1,1,1-trichloro-2-(4-hydroxyphenyl)-2-(4-methoxyphenyl) ethane (MOH) and 1,1,1-trichloro-2,2-bis(4-hydroxyphenyl) ethane (HPTE) by cytochrome p450 enzymes (313). MXC and its metabolites were found to interfere with folliculogenesis. *In vivo*, treatment with MXC (100mg/kg) reduces the expression of Esr2 and increases the expression of anti-Mullerian hormone (AMH) in early antral and preantral follicles and inhibits the folliculogenesis (314). Also *in vitro* data has shown that treatment of MXC or its metabolite reduces the expression of G1-S phase cells cycle regulators such as cyclin D2 (Ccnd2) and cyclin-dependent kinase 4 (Cdk4), upregulates the expression of proapoptotic factor Bax and downregulates the expression of anti-apoptotic factor Bcl2 and inhibits the growth of isolated antral follicles (315,316). Treatment of MXC also found to inhibit ovarian steroidogenesis by inhibiting the expression of important cytochrome P450 enzymes involved in steroid hormone synthesis (317,318).

Dioxin

Dioxins comprise a group of organochlorine compounds including polychlorinated biphenyls (PCBs), polychlorinated dibenzofurans (PCDFs), and polychlorinated dibenzodioxins (PCDDs). Dioxins are formed during waste incineration and smelting and refining of metals and are used as lubricants, insulators, flame-retardants and machine and transformer fluids (319). Polybrominated diphenyl ethers (PBDE) are another group of dioxins used primarily as flame-retardants. TCDD (2,3,7,8-tetrachlorodibenzo-p-dioxin) is an environmental contaminant that is produced as a by-product of pesticide and herbicide manufacturing process, burning of municipal solid waste and in pulp and paper mills during bleaching process (320,321). Dioxins accumulate in adipose tissue due to their fat-soluble nature and contaminate the food chain. In addition, it is

also found in breastmilk, blood serum and ovarian follicular fluid (322,323). It is not readily metabolized and excreted and has a long half-life of approximately 7-11 years in human (324).

In the rat ovary, TCDD has an anti-proliferative effect by decreasing the number of antral follicles without causing an increase in atresia (325). TCDD was found to block ovulation in immature rats by reducing the number of granulosa cells in S phase and inhibiting the levels of cell cycle regulatory proteins Cdk2 and Ccnd2 (326). It also interferes with ovarian steroidogenesis due to its ability to inhibit the important steroidogenic enzymes like Hsd17b1 and Cyp19a1 (327). In isolated mouse antral follicles, TCDD exposure decreased steroid hormones like progesterone, androstenedione, testosterone, and estradiol in a dose-dependent manner (327). In Lewis rats, TCDD exposure accelerated the onset of acyclicity and caused early reproductive senescence with age (328).

Phthalate

Phthalates are plasticizers which is a synthetic chemical used as softeners of plastics. It determines the suppleness, flexibility, and elasticity of polymers such as PVC. DEHP, Di (2-ethyl hexyl phthalate), the most common plasticizer used for PVC is produced more than 2 million tons. Dibutyl phthalate (DBP), diethyl phthalate (DEP) and butyl benzyl phthalate (BBP) are used commonly in consumer products and are also produced in high volumes. It is used in products such as upholstery, infant toys, shower curtails, industrial solvents, cosmetics, blood transfusion bags, industrial paints etc. Humans are exposed to phthalate through food and skin absorption.

Phthalates have been shown to alter the development and growth of follicles and also impair steroidogenesis. In mice, studies have shown that DEHP exposure (20 μg-750 mg/kg/day) for 10 to 30 days accelerate the primordial follicle recruitment through over activation of the PI3K pathway (329). Apart from affecting folliculogenesis, phthalates also affect the health of follicles.

Increase in atretic follicle numbers and a decrease in primary and secondary follicles were observed when DEHP (600 mg/kg) was exposed to mice through oral gavage for 60 days (330). MEHP inhibits the growth of antral follicle by increasing the oxidative stress and disrupting the levels of superoxide dismutase 1 and glutathione peroxidase (331). Phthalates are also found to alter steroidogenesis. In rats, exposure to DEHP (300 and 600 mg/kg) decreased serum estradiol levels by decreasing Cyp19a1 expression (330). Serum estradiol levels were also decreased in mouse antral follicles when exposed to DEHP (10 and 100 μg/ml). In cultured mouse antral follicles, exposure to MEHP (0.1-10 μg/ml) decreased testosterone, estradiol and estrone levels by inhibiting the gene expression of Cyp17a1, Hsd17b1, and Cyp19a1 (332,333). In a cross-sectional survey using the National Health and Nutrition Examination Survey, an earlier mean age at menopause was observed in women with high levels of phthalate metabolites compared to women with low levels of phthalate metabolites suggesting that phthalate exposure causes premature ovarian failure in women (305,334).

Heavy metals

Since ancient times, heavy metals have been used by humans for various purposes, and its production and use increased exponentially after the industrial revolution (304). Metals may be divided into four groups: (a) metals that are widely spread in the human environment with greatest toxicological significance such as arsenic (As), cadmium (Cd), chromium (Cr), mercury (Hg), lead (Pb), and uranium (U), (b) essential metals required in trace quantities such as cobalt (Co), copper (Cu), iron (Fe), manganese (Mn), selenium (Se), and zinc (Zn), (c) other metals which are of biological interest such as Vanadium (V) and nickel (Ni), and (d) metals of pharmacological interest such as gallium (Ga), aluminum (Al), and lithium (Li) (304,335). The earliest EDC known

to disrupt endocrine functions in humans are the heavy metals. Following are the effects of few heavy metals on the ovary. Anthropogenic uses of heavy metals was reviewed by Banu (336) and Banu *et al*., (2018) (Encyclopedia of reproduction)

Exposure to As significantly reduces antioxidants by inducing oxidative stress and results in the production of free radicals that can cause DNA single-strand breakage. As exposure to pregnant women resulted in the increased abortion rate, preterm birth, neonatal mortality and decreased birth weight (337).

The USEPA listed Cadmium (Cd) as one of the 126 priority pollutants. Cd exposure during human pregnancy has been linked to decreased birth weights and premature birth, with the enhanced levels of Cd in the placenta. In the placenta, Cd alters human chorionic gonadotropin and zinc transfer and induced ultrastructural changes such as syncytiotrophoblastic vesiculations, stromal edema, vacuoles in Hofbauer cells and necrosis.

Copper (Cu) is an essential trace metal and is essential for normal reproduction. Cu in its unbound form is toxic and it's overexposure can cause various toxic effects, by causing redox imbalance due to its highly redox-active nature.

In women, increased iron intake is found to increase fertility in women but its overexposure is found to affect their reproductive health. Its contamination in drinking water occurs mainly through corroded pipes. The iron burden is found to be deleterious to the ovary and could predispose women to the development of ovarian cancers. The iron burden in the ovary of thalassemia major patients had an inverse correlation with AMH levels and non-transferrin bound iron. Also, a higher incidence of ovarian cancer is associated with the iron storage disease hemochromatosis through increased iron uptake.

Lead (Pb) is a ubiquitous pollutant whose atmospheric concentrations increased as a consequence of industrialization and environmental pollution. Women occupationally exposed to Pb showed an increased incidence of spontaneous abortion, decreased birth weight and minor congenital malformations in their babies, infertility, and changes in ovarian function.

High doses of mercury (Hg) in its three common forms (elemental, inorganic and methylmercury) produce adverse health effects and the most toxic form is methyl mercury. Most people are exposed to Hg through consumption of Hg-contaminated fish. Epidemiological studies indicate that occupational exposure to Hg in women resulted in abnormal menstrual cycles in terms of bleeding pattern and cycle length (338). Decreased fertility is experienced by dental assistants exposed to Hg vapor.

Exposure of humans to Mn is widespread and is known to cause DNA damage and chromosome aberrations in mammalian cells. In mammals, exposure to large amounts of Mn affect fertility and is also toxic to the embryo and fetus (339). The concentration of Mn in umbilical cord blood is directly correlated with intrauterine growth restriction in newborn children compared to newborns appropriate for gestational age (340).

Nickel is an another EDC heavy metal where the general public is exposed through consumption of contaminated drinking water, inhalation of dust, dermal contact with bath/shower water, soil, or dust, and ingestion of Ni-contaminated soil. In Northwestern Russia, women working in a metal refinery were reported to have spontaneous abortions, and the newborns suffered from congenital musculoskeletal defects, and perinatal mortality (341).

Cr disrupted ovarian function in women working in chromium industries who exhibited increased levels of Cr in their blood and urine. Those women experienced abnormal menses, infertility or increased postpartum bleeding (342). We have reported that lactational exposure to

CrIII during postnatal age extended estrous cycle, delayed follicular development, decreased the number of healthy follicles, arrested the growth or development of follicles, and increased follicular atresia in PND 21 rats. Cr also delayed pubertal onset and decreased levels of testosterone, estradiol, and progesterone in F1 rats (131). The female reproductive effect of Cr was discussed in detail in the *health effects* section (*Page no -17*). To date, there are no studies available reporting the association between CrVI and premature ovarian failure. Thus, it is important to determine whether Cr is causing premature ovarian failure and if so, the underlying mechanisms of premature ovarian failure should be determined.

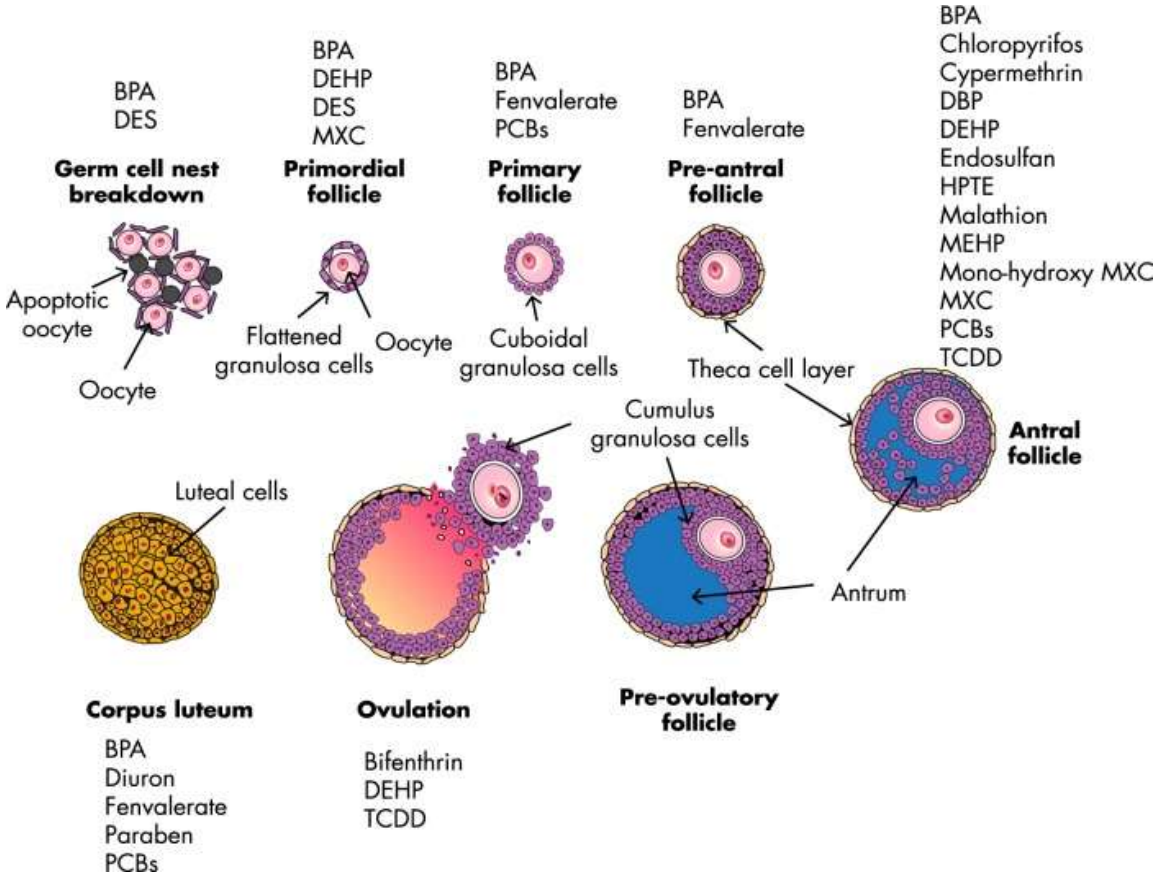

Fig. 1.2. Schematic of the normal developmental stages of ovarian follicles and some of the EDCs that adversely affect the ovary. Reprinted with permission from (305).

Premature Ovarian Failure

Premature ovarian failure (POF) is classically defined as 4-6 months of amenorrhea in women under the age of 40 years associated with the menopausal level of serum gonadotropins and hypoestrogenism and is also referred as hypergonadotropic hypogonadism (343). POF affects approximately: one in 10,000 women by age 20; one in 1,000 women by age 30; one in 100 women by age 40 (344). The two types of consequence generated by primary ovary insufficiency are premature hypoestrogenism and infertility. Premature hypoestrogenism causes the premature aging of estrogen acting tissues and untreated POF can induce a two-fold age-specific increase in mortality due to an increased incidence of osteoporosis and cardiovascular diseases, but it can be treated by hormone replacement therapy generally given until the menopausal age. The second consequence is infertility where the clinical indication is absent. Unlike premature hypoestrogenism, recovery of fertility is not possible when the POF patients reach diagnosis stage as the fertility is often compromised in the initial phases of the disease. However, the premature cessation of menses can be predicted by identifying the markers. FSH, estradiol, inhibin-B, or anti-Mullerian hormone, since these are the biomarkers commonly used to diagnose POF which is indicated by irregular menstrual cycle. Biochemically, POF is characterized by low levels of steroid hormones (estradiol and inhibin B) and high levels of gonadotropins (FSH and LH) (343).

Etiology of premature ovarian failure

The etiological causes of premature ovarian failure are highly heterogeneous and include genetic, chromosomal, metabolic, autoimmune ovary damage, viral infections, and iatrogenic factors (Radiotherapy or chemotherapy) (345). About 25% of all forms of POF are caused by iatrogenic causes and more than 50% of the cases remain idiopathic where the POF origin is still

unknown. These etiological causes can attribute to the origin of premature ovarian failure through either of the three possible mechanisms: (i) an initial primordial follicle pool decrease; (ii) an accelerated follicular atresia; or (iii) an altered primordial follicles maturation or recruitment. In most of the cases, POF occurs because of an anticipated primordial follicular pool depletion (343). POF is viewed as a complex multifactorial disease which involves several alleles contributing to its pathogenesis (346). POF can be either syndromic where the condition is part of a complex phenotype involving other tissues and organs, or non-syndromic where POF arises apparently in a woman before 40 years of age (343).

Genetic causes of premature ovarian failure

The genetic basis of premature ovarian failure is supported by the occurrence of families with several affected women (347). In as much as 5% of cases, X chromosome abnormalities account for a significant number of genetic causes of POF (345). Reduced gene dosage and non-specific chromosome effects that impair meiosis are some of the genetic mechanisms that can lead to premature ovarian failure by causing a decrease in the pool of primordial follicles, increased follicular atresia due to apoptosis or failure of follicle maturation. Broadly the genetic causes of POF can be caused by single gene or chromosome, involving the autosomes or X chromosome (345). These abnormalities range from a complete deletion of one X (Turner's syndrome or 45 X) and trisomy X to partial defects in form of deletions, isochromosomes and balanced X autosome translocations (348).

Cytogenetic and molecular analyses of women with POF carrying a balanced X-autosome translocation allowed the identification of a ''critical region'' for ovarian development and function on the long arm of the X chromosome from Xq13.3 to Xq27. This region could be split into two functionally different portions: Xq13-21 and Xq23-27 (349,350). Breakpoints in the

Xq13-21 region are responsible for balanced translocations, whereas breakpoints in the Xq23-27 region result in interstitial deletions. Heterochromatin rearrangements of the Xq13-21 region were reported to downregulate oocyte-expressed genes during oocyte and follicle maturation, indicating that X-linked POF may be an epigenetic disorder (351). Translocations that affect X chromosome structure increase apoptosis of germ cells (352), leading to POF. Direct disruption of relevant loci or a ‘‘position effect’’ caused by the rearrangements on contiguous genes can also result in POF. Transcriptional characterization of breakpoint regions in balanced translocations led to the identification of five genes interrupted by translocations (the Xpnpep2 gene in Xq25 (353), the POF1B gene in Xq21.2 (354), the DACH2 gene in Xq21.3 (354), the CHM gene in Xq21.2 (355), and the DIAPH2 gene in Xq22 (356) and classified as POF marker genes in humans. However, the mechanism by which translocations in the Xq critical region may cause POF is not clear.

Premature ovarian failure marker genes

POF1B

The *POF1B* gene is a novel evolutionary gene mapped to proximal Xq21 by FISH (357). The gene is found only in vertebrates and presents a large coiled region in the C-terminal half of the protein that shows significant homology to the myosin heavy chain rod domain as well as to the C-terminal coil of barmotin/7H6, a tight junction-associated protein (358,359). The gene is located in the critical region for normal ovarian function and it escapes X inactivation (360). The *Pof1b* gene in the mouse is found to be highly homologous to the human. When mouse and human are compared, it was found that the nucleotide sequence of the coding region is 87% identical and the aminoacid sequence is 89% identical. It is expressed at low level in the intestine, kidney and lung and absent in adult, fetal brain, spleen and liver and are barely detectable in the heart. During

mouse development, *Pof1b* mRNA was absent at E13.5, it appeared at E14.5 and was up-regulated at E15.5 of mouse development (358,361). A reciprocal translocation between chromosomes X and 3 and an additional heterozygous missense mutation in the X-linked gene *POF1B* were detected in a patient affected by premature ovarian failure (362).

The binding of POF1B to actin filaments may play an important role in the ovarian-follicle formation and the disruption of its binding to actin may have various consequences. It is speculated that due to the homology of POF1B to myosin, POF1B could play an important role in the pairing of meiotic chromosomes and its alteration like the homozygous mutations could lead to germ cell apoptosis resulting in drastic reduction in the final number of oocytes that were created during ovarian development. It is also suggested that POF1B could play a vital role in regulating germ-cell apoptosis through a role in cytoskeletal dynamics. It has been implicated that alterations in the actin cytoskeleton dynamics could lead to the release of reactive oxygen species from mitochondria resulting in germ cell apoptosis (361).

DACH2

The *dachshund/Dach* gene family encodes transcriptional cofactors that are conserved between insects and humans. In the Drosophila eye, *DAC* is a key component of the retinal determination gene network (RDGN) which governs the normal initiation of the morphogenetic furrow and eye development (363). A single dachshund gene is present in the fruitfly Drosophila melanogaster whereas, in mice, humans, and chickens, two *DACH* genes (*DACH1* and *DACH2*) have been identified (364-366). The presence of two highly conserved domains, Dachshund domain 1 (DD1) and Dachshund domain 2 (DD2) were identified by amino acid sequence comparison of DACH1, DACH2, and Dachshund proteins. The first domain, Dachshund Domain 1 (DD1), is located near the N-terminus (107aa length) and the second conserved region, DD2, is

located near the C-terminus which is 84 amino acids in length. Mouse *DACH2* and Drosophila *DACH* share 74% identity and 82% similarity for DD1 and 52% identity and 67% similarity for DD2. Mouse Dach2 encodes an additional 13 amino acids located at the C-terminus of the DD1 domain, compared to chick *DACH2* and mouse *DACH1* (367). Analogous to the expression profile of Drosophila *DACH*, mouse *DACH1* and *DACH2* are both expressed in the developing retina, limbs, and nervous system. *DACH also* plays a role in metazoan development, regulating ocular, limb, brain and gonadal development (363).

Translocation breakpoints and point mutations within *DACH2* have been documented in cases of X-linked premature ovarian failure (POF). Mutations in *DACH2* were found in patients entering amenorrhea at very variable ages, ranging from 17 to 42 years. Like *DIAPH2* and the *XPNPEP2*, the genes which were found interrupted in POF patients, the *DACH2* gene was subjected to X inactivation in POF patients. In *DACH2*, missense mutations were found in highly conserved residues and they caused (P36L, R37L, F316S) non-conservative amino acid substitutions (368). In the fruit fly, the *eya* gene was reported to have an essential role in oogenesis for the correct differentiation of somatic follicle cells into polar cells (369). In *DACH1/DACH2* double mutants, female reproductive tract development is severely disrupted. This defect was associated with the mullerian duct (370). It is suggested that due to high level of functional conservation, a complex involving DACH2 and one of the mammalian EYA and SIX genes may play an important role in the development of mammalian gonads, and alteration of the human DACH2 protein may act as a risk-factor for POF by altering the correct process of ovarian follicle differentiation (354).

DIAPH2

Formins belong to a family of conserved actin filament assembly factors that nucleate linear, unbranched filaments and remain attached to the growing barbed ends of filaments (371). The FH2 domain of formins directly nucleates actin nucleation and remains bound to the growing barbed end during elongation of the filament (processive capping) (372,373). Formins change the kinetics of filament elongation by directing the addition of profilin-actin onto barbed ends at rates much faster than onto filaments without associated formins and slow the rate of addition of G-actin without profilin onto filaments (374). Formins also protect filament barbed ends from capping proteins and depolymerization (375). Additionally, some formins can bundle or sever F-actin *in vitro* (376). Formin family proteins are located throughout the cell on both F-actin and microtubule structures, as well as on endosomes and mitochondria (377). Formins, and DRFs in particular are critical for directly regulating microtubule dynamics in migrating cells, suggesting that formins are potential mediators of actin-microtubule interplay during cell motility (378). A candidate for regulating F-actin assembly in the lamella during cell migration is the diaphanous-related formin (DRF) protein family (379). Diaphanous-related formins (DRF) contain a proline-rich FH1 domain adjacent to the FH2, which greatly accelerates actin assembly by allowing formins to efficiently recruit profilin-bound actin monomers (374). It is characterized by the presence of a C-terminal Diaphanous-autoregulatory domain (DAD), which interacts with an N-terminal Diaphanous inhibitory domain (DID) and contributes to actin nucleation (380). It is shown that auto-inhibitory DID-DAD interactions in DRFs are released by binding of RhoGTPases to an N-terminal GTPase-binding domain (GBD) (381,382). Although they act as effectors for Rho family small GTPases, the DRFs mDia1 and mDia2 have been shown to mediate assembly of F-actin in stress fibers and filopodia (383).

XPNPEP2

The *XPNPEP2* gene encodes the protein X-propyl aminopeptidase, which belongs to the family of "pita bread" metalloenzymes. It is expressed in prokaryotes and eukaryotes and hydrolyzes N-terminal Xaa-Pro bonds, where proline is the penultimate residue. Mammals have both a membrane-bound and a soluble XPNPEP2, with different tissue distributions. The membrane-bound XPNPEP2 is a heavily glycosylated glycosylphosphatidylinositol-anchored protein of 673 amino acids encoded by the *XPNPEP2* gene on human Xq25. Several biologically active polypeptides, including collagens (Cols), hormones, growth factors, and cytokines, contain N-terminal Xaa-Pro sequences and therefore are potential substrates for *XPNPEP2*. Because Cols contain a high proportion of such "triplets," *XPNPEP2* has the potential for intracellular (lysosomal) degradation of Col fibrils. In fact, proline and hydroxyproline constitute 20%-25% of the residues in Cols, and none of the lysosomal proteinases is capable of cleaving these linkages (384).

Within the ovary and follicle, the extracellular matrix (ECM), including Cols, provides structural support, organizes and connects cells, serves as a reservoir for signaling molecules and growth factors that regulate follicle growth, provides a filtration barrier, and guides cell migration (385,386). The ECM also regulates the establishment of the basement membrane, oocyte maturation, follicle atresia, steroidogenesis, and cell lineage (387-390). The ECM components of the basal membrane affect follicle development in the ovary and are important for maintaining the polarity and the degree of polarization of granulosa cells (391-393). A recent study found that Col1 is spatially and temporally expressed in immature rat ovaries and is regulated by gonadotropins, suggesting a role for Col1 in morphogenesis of follicles as well as corpus luteum formation and regression (394). Col1 is expressed in the basal lamina of follicles and participates in the

organization of the basal lamina (395). Another study using Esr2-null mice showed that Esr2 regulates Col gene expression in the ovary before puberty. Dysregulation of Esr2-mediated ECM gene expression in early postnatal life disrupts folliculogenesis and contributes to the impaired response of immature Esr2-null granulosa cells to follicle-stimulating hormone (396). To date, there are no studies available reporting the association between CrVI and premature ovarian failure. Thus, it is important to determine whether Cr is causing premature ovarian failure and if so, the underlying mechanisms in causing premature ovarian failure should be determined.

Rationale

Occupational exposure to CrVI is found among approximately half a million industrial workers in the US and several million worldwide. The health risk assessment of CrVI has largely been based on data from occupationally exposed people, although little attention has been given to reproductive and developmental effects. Women working in dichromate manufacturing industries and tanneries and living around Cr-contaminated areas have high levels of Cr in blood and urine and experience several gynecological illnesses such as premature abortion, postnatal hemorrhage, birth complications, subfertility, and infertility. Because CrVI can pass through the placental barrier, it can cause adverse effects on the developing embryos/fetuses /newborn children and impair embryonic development, implantation, fetal viability, and reproductive functions in the F1 offspring. Although CrVI is known to adversely affect reproductive health in women, the actual mechanism of reproductive toxicity is not clearly understood. Even though epidemiological studies indicate that CrVI causes infertility in women (120,397-400), there are no reports about an association between CrVI exposure and POF in women. Thus, it is imperative to identify whether CrVI causes POF, and the underlying mechanisms under CrVI-induced POF and infertility.

Central Hypothesis

The central hypothesis of the current study is that "*in utero exposure to CrVI causes premature ovarian failure in the F1 offspring*". The objectives are to (i) determine the role of CrVI in causing premature ovarian failure, and (ii) understand the underlying molecular mechanisms in F1 female offspring that were exposed to CrVI prenatally.

***Specific Aim-1*:**

Determine the effects of prenatal exposure to CrVI on premature ovarian failure in the F1 offspring.

Hypothesis:

This aim was based on the working hypothesis that "*Prenatal exposure to CrVI causes premature ovarian failure by increasing germ cell death, advancing germ cell nest breakdown and primordial follicle assembly by activating apoptotic pathways and inhibiting cell survival pathways*".

Objectives:

The objectives were to (i) determine the effects of prenatal exposure to CrVI on pregnancy rate and litter size in the F1 offspring; (ii) evaluate the role of CrVI on germ cell nest breakdown; (iii) understand the role of CrVI on primordial follicle assembly and atresia; (iv) assess the effects of CrVI on the cell survival machinery such as p-AKT, p-ERK and XIAP; and (v) explore the mechanism of p53 in CrVI-induced germ cell apoptosis, germ cell nest breakdown, and primordial follicle assembly.

Specific Aim-2:

Determine the p53-mediated mechanisms of prenatal exposure to CrVI on germ cell apoptosis, and germ cell nest breakdown, in F1 offspring.

Hypothesis:

This aim was driven by the working hypothesis that "*CrVI-induced germ cell apoptosis and advancement of germ cell nest breakdown are mediated through a p53-miR34a-SIRT1 signaling network"*.

Objectives:

The above *hypothesis* was tested by the following objectives: (i) to study the effect of CrVI on expression of acetylated p53, SIRT1 and miR-34a; (ii) to delineate the mechanism of CrVI-induced p53 activation by injecting various doses of EX-527, a SIRT1 inhibitor (SIRT-I) on both CrVI exposed and unexposed pregnant dams; (iii) to determine the effects of EX-527 on apoptosis of germ cells; and (iv) to understand the p53-mediated mechanisms by assessing the effects of SIRT1 inhibitor on the anti-apoptotic proteins BCL2, BCL-XL, pAKT and pro-apoptotic proteins BAX, cleaved Caspase-3 and PUMA.

Specific Aim-3:

Determine the mechanism of miR34a in modulating CrVI-induced germ cell apoptosis.

Hypothesis:

This aim was driven by the working hypothesis that *"miR34a increases CrVI-induced germ cell apoptosis by abrogating the association between p53 and SIRT1".*

Objectives:

The above *hypothesis* was tested by the following objectives: To determine the effects of miR34a mimetic and/or inhibitor on: (i) apoptosis of germ cells; (ii) mRNA expression of *p53, Bcl2, Bax*, *Akt* and *Sirt1* genes; (iii) protein levels of acetyl p53, SIRT1, cleaved caspase-3, BAX BCL2, and BCL-XL; and (iv) possible association/interaction between p53 and SIRT1

Specific Aim-4:

Determine the role of POF marker *Xpnpep-2* in CrVI-induced premature ovarian failure in F1 offspring.

Hypothesis:

This aim was based on the working hypothesis that "*Prenatal exposure to CrVI causes POF by targeting POF marker Xpnpep2 during fetal ovarian development*".

Objectives:

The objectives were to determine the effects of prenatal exposure to CrVI on (i) the germ cell apoptosis during fetal and postnatal ovarian development; (ii) the spatiotemporal expression of POF candidate protein aminopeptidase-2, encoded by the POF marker gene *Xpnpep-2* during ovarian development; and (iii) the targets or substrates for Xpnpep-2, namely the Cols Col1, Col3, and Col4 during GCN breakdown, primordial follicle assembly and during postnatal ovary development.

2. MATERIALS AND METHODS

In vivo dosing of the animals and experimental design

Specific aim-1

Pregnant Sprague Dawley (SD) rats of 60-70 days of age were divided into two groups: Group-1: Control (n=15) and Group-2: CrVI (n=15). Control rats received regular drinking water and diet ad libitum. Rats from the CrVI group received 25 ppm potassium dichromate in drinking water from gestational day (GD) 9.5-14.5. The first set of control (n=5) and CrVI (n=5) treated rats were euthanized on GD 20, and placentae were removed to estimate chromium levels. The second set of rats (n=5) were allowed to deliver pups. When the pups were born, ovaries were removed from pups on PND 1 for further analyses. The third set of rats (n=5) was maintained with their F1 female offspring and provided with regular drinking water and diet ad libitum until weaning on PND 22. After weaning, the F1 female pups were maintained separately and fed with regular diet and drinking water *ad libitum*. On PND 60, F1 offsprings from control (n=15) and CrVI-treated (n=15) rats were allowed to mate with normal fertility-proven male rats. The appearance of vaginal plug or presence of sperm in the vaginal lavage was considered as 0.5 day of pregnancy. Soon after the birth of F2 offspring, the pups were removed and mothers (F1) were allowed to return to the estrous cycle to be mated again. The percentage of F1 females that achieved a successful pregnancy and the number of pups/litter were calculated at 2-4, 4-6, 6-8 and 8-10 months of age.

Specific aim-2

Pregnant SD rats of 60-70 days of age were divided into eight groups: (1) *Control* (n=5) : Rats received regular drinking water and diet *ad libitum*; (2) *CrVI* (n=5) : Rats received 10 ppm of potassium dichromate in drinking water from GD 9.5 to GD 14.5; (3) *CrVI+SIRT-I-1mg* (n=5) : Rats received 10 ppm of CrVI in drinking water and 1mg of SIRT-I through intraperitoneal (IP) injection from GD 9.5 to GD 14.5; (4) *CrVI+SIRT-I-5mg* (n=5) : Rats received 10 ppm of CrVI in drinking water and 5mg of SIRT-I through IP injection from GD 9.5 to GD 14.5; (5) *CrVI+SIRT-I-50mg* (n=5) : Rats received 10 ppm of CrVI in drinking water and 50mg of SIRT-I through IP injection from GD 9.5 to GD 14.5; (6) *SIRT-I alone-1mg* (n=5) : Rats received 50mg of SIRT-I through IP injection; (7) *SIRT-I alone-5mg* (n=5): Rats received 5mg of SIRT-I through IP injection; and (8) *SIRT-I alone-50mg* (n=5): Rats received 50mg of SIRT-I through IP injection. The rats were allowed to deliver pups (F1 pups) and ovaries were removed on PND 1 for further analyses.

Specific aim-3

In vitro culture of the fetal ovary and experimental design

In vitro culture of the fetal ovary was performed based on the protocol developed and published by our laboratory (10). Timed-pregnant rats of age 60–70 days were euthanized by CO_2 asphyxiation followed by cervical dislocation on 13.5 dpc. According to the AVMA guidelines (401), the death of the dams was confirmed and the uteri were cut open quickly. The embryos were removed and immersed along with the intact amniotic sac in ice-cold physiological saline in a glass beaker until they became completely immobile. Amniotic sacs were cut open after confirming that the embryos were immobile and the embryos were decapitated using the scissors, and placed under a zoom stereo microscope. Using sterile surgical instruments, the ovaries were

removed carefully without any damage along with the mesonephros. The removed ovaries were placed carefully on top of a sterile membrane floating on the culture media in a 24-well culture plate. To prevent the ovaries from drying, a drop of the culture media was placed on top of the ovaries. Ovaries were cultured in Ham's-F-12/DMEM (1:1) media containing 1 mg/ml BSA, 1 mg/ml Albumax, 27.5 µg/ml transferrin, 5 U/ml penicillin, and 5 µg/ml streptomycin; and placed in a CO_2 incubator. E13.5 was considered as culture day (CD) 1, and ovaries were cultured for a period of 7 days and harvested on CD 9, which recapitulates PND1.

The maximum contamination level (MCL) or regulatory dose of Cr according to EPA in the drinking water is 0.1 ppm (0.1 mg/L) (11). In the current study, 0.1 ppm potassium dichromate which is the regulatory dose was used. The groups were (1) Control - Ovaries were treated with media without any treatment; (2) CrVI - Ovaries were treated with media containing 0.1 ppm CrVI; (3) CrVI+miR34a mimetics - Ovaries were treated with media containing 0.1 ppm CrVI and miR34a mimetics (100 nM); (4) CrVI+miR34a inhibitor - Ovaries were treated with media containing 0.1 ppm CrVI and miR34a inhibitor (100 nM); (5) miR34a mimetics alone - Ovaries were treated with media containing miR34a mimetics (100 nM); (6) miR34a inhibitor alone - Ovaries were treated with media containing miR34a inhibitor (100 nM); and (7) miR scramble - Ovaries were treated with media containing miR-scramble (100 nM). Media containing the respective treatments were added every 24 h from CD 2 through CD 8 (E14.5–20.5) (Fig. 2.1). The followed miRNA transfection procedure is as follows.

Transfection of miR34a mimetics/inhibitor

Ex vivo cultured ovaries were transfected with miR34a mimetics (100 nM, miRIDIAN microRNA Rat rno-miR-34a-5p - Mimic, mature miRNA Sequence -

UGGCAGUGUCUUAGCUGGUUGU, Cat. C-320335-05-0005, Dharmacon) and miR34a inhibitor (100 nM, miRIDIAN microRNA Rat rno-miR-34a-5p - Hairpin Inhibitor, mature miRNA Sequence- UGGCAGUGUCUUAGCUGGUUGU, Cat. IH-320335-06-0005, Dharmacon). The endogenous miR34a was upregulated using miRIDIAN™ miRNA mimics to study miR34a gain-of-function effects and miRIDIAN™ miRNA inhibitor was used to suppress endogenous miR34a for loss-of-function study. These miRNA mimetics and inhibitor were delivered using DharmaFECT Transfection Reagent as per manufacturer's instructions (Cat. T-2001-02, Dharmacon, Lafayette, CO). All steps of the following transfection procedure were performed in a laminar flow cell culture hood using sterile techniques. The stock (20µM) and working stock (5µM) of mimetics and inhibitor were prepared using siRNA buffer (Cat. B-002000-UB-100, Dharmacon). miR34a mimetics or inhibitor and the DharmaFECT transfection reagent were diluted in separate tubes using antibiotic (AB)/serum free media. In separate tubes, miR34a mimetics or inhibitor is diluted by adding 4µl of 5µM miR34a mimetics or inhibitor to 46µl of antibiotic (AB)/serum free media and DharmaFECT transfection reagent is diluted by adding 0.75µl of DharmaFECT transfection reagent to 49.25µl of AB/serum free media. The contents of each tube were gently mixed by pipetting carefully up and down, and incubated for 5 minutes at RT. After incubation, the contents of both tubes were added together (total volume of 100µl) and mixed well by pipetting carefully up and down and incubated for 20 minutes at RT. Finally, 100µl of AB/serum free media was added to the above-prepared mix to yield a final volume of 200µL (100nM) transfection medium. The culture medium from the well was removed and 200µL of the appropriate prepared transfection medium was added to each well carefully without disturbing the membrane containing the ovaries. The plates were incubated at 37°C in 5%

CO_2 until harvest. A drop of the transfection medium was added to the ovaries every 24 hours to prevent the ovaries from drying.

On CD 9, PND1 ovaries were removed and fixed overnight at 4°C. Next day, the tissues were removed from the fixative and transferred to 70% ethanol and embedded in paraffin blocks using the routine histological procedures. Ovaries harvested for RNA isolation were immediately transferred to RNAlater (Cat. 76104, Qiagen) and stored at -80°C.

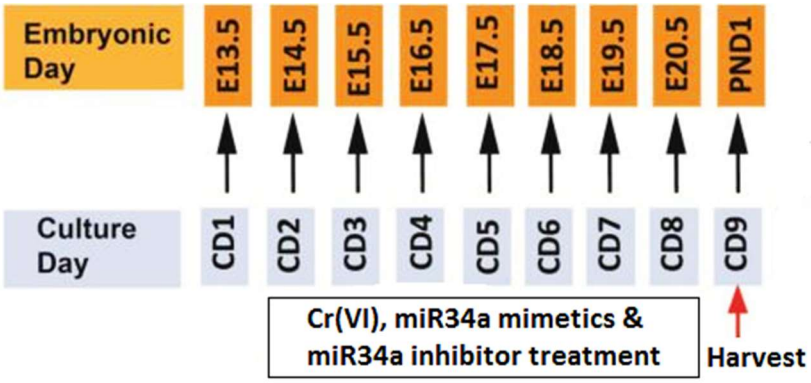

Fig. 2.1. Experimental design for treatment with CrVI (0.1 ppm), miR34a mimetic (100 nM) & inhibitor (100 nM) *ex vivo*. Embryonic/fetal ovaries were removed from normal pregnant dams on a gestational day 13.5 and cultured for 9 days. Embryonic day (E) 13.5 was considered as culture day (CD) 1, and CD 9 recapitulates PND1 as given in the schematic diagram. Media containing respective treatments were added on CD 2 and media was changed every 24h and CrVI was freshly added every day for 7 days. Ovaries were harvested on CD 9 which recapitulates PND1.

Specific aim-4

Pregnant SD rats (age, 60-70 days) were divided into two groups: control (n=25) and CrVI (n=25). Control rats received regular drinking water and diet *ad libitum*. Rats from the CrVI group received 25 ppm of potassium dichromate in drinking water from GD 9.5 to GD 14.5. The first

and second sets of control (n=5 per set) and CrVI (n=5 per set) rats were euthanized on GD 15.5 and GD 17.5, respectively. The third and fourth sets of control (n=5 per set) and CrVI (n=5 per set) rats were allowed to deliver pups (F1 pups). Ovaries from F1 pups were removed on PND 1 and PND 4 for further analyses. The fifth set of F1 pups from control (n=5) and CrVI (n=5) rats were maintained in a separate cage with their respective mothers, weaned on PND22, fed with regular drinking water and diet ad libitum, and euthanized on PND25. Blood and the ovaries were collected from these pups for further analyses.

In all the studies, animal use protocols were approved by the Animal Care and Use Committee of Texas A&M University and were in accordance with the standards established by Guiding Principles in the Use of Animals in Toxicology and Guidelines for the Care and Use of Experimental Animals by National Institute of Health.

Estimation of placental chromium

Total Cr levels in the placenta were estimated by the Trace Element Research Laboratory (TERL) core facility, College of Veterinary Medicine and Biomedical Sciences, Texas A&M University, based on the published standard protocol followed in our laboratory which is as follows (402). Placental tissue samples were digested with nitric acid (HNO_3) and hydrogen peroxide (H_2O_2) after transferring to polyethylene cryotubes. After digestion, the digestates were transferred to 15 ml polypropylene centrifuge tubes and the samples were diluted with deionized water. Digests were diluted to obtain a nitric acid concentration of 2% or less and then analyzed by ICP-MS on a Perkin Elmer DRC II instrument (PerkinElmer Life and Analytical Sciences, Shelton, CT). ^{52}Cr is analyzed in "reaction cell mode" using ammonia as a reaction gas to eliminate interferences from molecular ions. Instrument performance changes and slight differences in viscosity and surface tension between samples and standards were compensated by running

internal standards (eg, 89Y, 115In). Calibration was based on a blank and 4 standards and was verified initially by analyzing independent standards and regularly through the analytical process by analyzing a midrange standard and a blank. A blank, a spiked blank, a certified reference material, a duplicate sample, and a spiked sample were used as laboratory quality control samples to evaluate background contamination, accuracy, and precision. For each placenta, an average of Cr estimates from the 3 different regions was calculated and this average used for relating to placental function (402).

Histology

Histological processing of the ovary was performed by the Histology core lab facility, College of Veterinary Medicine & Biomedical Sciences, Texas A&M University, based on the standard protocols for paraffin-embedded sections that were cut at 5 μm thickness and stained with hematoxylin and eosin (H&E).

Analysis of oocyte numbers

Oocyte numbers were determined by counting the number of germ cells positive for the germ cell marker, Vasa, found within each optical section used for analyzing GCN breakdown and follicle development. The numbers were averaged and reported as number of oocytes per ovary in percentage.

Analysis of GCN breakdown and follicle development

For each ovary, two cores were visualized and counted. A core is a region 135 x 135 μm^2 consisting of optical sections at four different depths in the ovary, each 15-20 μm apart. Thus, for each ovary, two cores were obtained consisting of four optical sections per core for a total of eight optical sections per ovary. The number of germ cells found in the nest relative to the total number

of oocytes was determined for each ovary by analyzing each section and was reported as percent single oocytes. In order to determine whether oocytes were in nests or not, for each of the four optical sections in a core, a z-stack of images each 1 μm apart were obtained with five images above the section and five images below the section being analyzed. This allowed us to determine whether an oocyte was part of a GCN above or below the plane of focus. Follicle development was determined by counting the number of primordial and primary follicles present in relation to the total number of follicles found and reported as percent primordial and primary follicles.

TUNEL assay

Paraffin-embedded tissue sections were deparaffinized in xylene and dehydrated in a graded ethanol series: 90%, 80%, and 70% for 3-6 min followed by washing in double distilled water. Nuclei of tissue sections were stripped of proteins by incubating with protease solution (100mg of protease in 200ml of PBS) for 5 min at 37°C, and washed in double distilled water and subsequently in PBS. Endogenous peroxidase was inactivated by incubating sections with 3% H_2O_2 in methanol for 10 min at room temperature (RT) and blocked with 3% BSA in PBS for 30 min. Slides were rinsed twice in PBS followed by the addition of 50 μl of TUNEL reaction mixture to the sections followed by incubation for 60 min at 37°C in a humidified chamber in the dark. The sections were rinsed and incubated with the TUNEL detection antibody (Roche) labeled with peroxidase for 30 min at 37°C in a humidified chamber in the dark. The peroxidase was visualized with diaminobenzidine. Slides were mounted using aqueous mounting media and analyzed by light microscopy. The intensity of staining was quantified in 10 randomly selected high power fields from each experimental group, using Image-Pro Plus software (Media Cybernetics, Bethesda, MD) as described previously (131,403) according to the manufacturer's instructions.

The apoptosis index was calculated as the average percentage of TUNEL-positive germ

cells/oocytes from 20 ovaries at 400x magnification. To avoid choosing the same follicle or oocyte, we used every 12th unstained section of the ovary from PND1 and PND4 and every 40th unstained section of the ovary from PND 25 as described by Devine *et al*., (2002) (404). Only oocyte-containing follicles were counted. For E15.5 and E17.5, we used every 10th section. We employed this method to analyze ovarian sections for TUNEL, H&E, and IHC to avoid repeating the measurements on the same oocyte/follicle. Germ cells/oocytes from 20 to 35 fields were counted for E15.5, E17.5, PND1, and PND4, and those from 200 fields were counted for PND25.

Whole-mount fluorescence immunohistochemistry

Ovaries were dissected out, washed in PBS and fixed with 5.3% formaldehyde (Cat#18814, Polysciences) overnight at 4°C. The ovaries were washed for 30min in PBS+0.1% Triton-X-100 (PT) and incubated in PT+5% BSA for 1 h at RT. They were then labeled with primary antibodies for both Vasa and the somatic cell marker, Gata4; p53 and SOD2; Xpnpep2 and Col3; or Xpnpep2 and Col4 at the appropriate dilution (Table. 2.2) in PT+5% BSA by incubating overnight at 4°C. Then the ovaries were washed in PT+1% BSA for 30 min at RT, incubated in RNase A (5 µl of 20 mg/ ml RNase A in 1 ml PT+1% BSA, Cat# 12091-039, Life Technologies, Carlsbad, CA) for 30 min. Further, the tissues were incubated with fluorophore-conjugated secondary antibodies in PT+5% BSA for 4 h at RT. Then the tissues were washed 3 times in PT+1% BSA for 30 min at RT, rinsed once in PBS and mounted on a glass slide using Prolong Gold antifade reagent (Life Technologies). The slides were kept in dark overnight and images were obtained using a Zeiss Stallion Dual Detector Imaging System with Intelligent Imaging Innovations Software (Carl Zeiss, Thornwood, NY) and a Zeiss 510 Meta multiphoton/confocal microscope (Carl Zeiss) with a plan apochromat 633/1.4 NA oil objective. For the green dye, an argon laser set was used with an excitation of 488 nm and emission (collected with a band-pass filter) of 500-550 nm. For the red

dye, a helium-neon laser was used with an excitation of 543 nm and emission (collected with a long-pass filter) of 560 nm. At least eight images were collected per treatment.

Immunohistochemistry

Ovaries were fixed in 4% buffered paraformaldehyde (PFA) (6g PFA, 325mg NaOH, and 15ml 10x PBS in 100ml diethylpyrocarbonate-treated double distilled H_2O, pH 7.2) for 1 h at 4°C and processed using standard procedures (233). Paraffin sections (5 μm) were used for immunohistochemical (IHC) localization of proteins using a Vectastain Elite ABC kit (Vector Labs, Burlingame, CA) according to the manufacturer's protocols. Briefly, paraffin-embedded ovary sections were deparaffinized in xylene and dehydrated in a graded ethanol series: 100%, 95%, and 70% for 5 min followed by washing in 1xPBS. Antigen retrieval was performed by incubating with in protease solution (100mg of protease in 200ml of 1x PBS) for 5 min at 37°C, and washed three times in double distilled water and once in PBS. Endogenous peroxidase activity was removed by fixing sections in 0.3% H_2O_2 in methanol. Tissue sections were blocked in 1.5% serum of the host species where the antibody was raised for 1 h at room temperature. The tissue sections were incubated with primary antibodies as indicated in Table. 2.2 overnight at 4°C. The sections were further incubated with the secondary antibody (biotinylated IgG) for 45 min at RT. Negative controls included serum or IgG from the appropriate species related to the primary antibody at the same dilution. Digital images were captured using a Zeiss Axioplan 2 microscope with an Axiocam HR digital camera (Carl Zeiss). To determine the abundance of each protein, we included both healthy follicles and atretic follicles from the CrVI-exposed ovaries using blind and random selection criteria. The intensity of staining for each protein was quantified using Image-ProPlus 6.3 image processing and analysis software (Media Cybernetics, Inc.). In brief, six images of the ovary at 400x magnification were captured randomly without hot-spot bias in each tissue

section per animal. Integrated optical density (IOD) of immunostaining was quantified in the RGB mode. Numerical data were expressed as the least square mean ± SEM.

Immunofluorescence

Paraffin-embedded ovary sections were deparaffinized in xylene and dehydrated in a graded ethanol series: 100%, 95%, and 70% for 5 min followed by washing in 1xPBS. Antigen retrieval was performed by incubating in protease solution (100mg of protease in 200ml of 1x PBS) for 5 min at 37°C, and washed three times in double distilled water and once in PBS. Subsequently, the tissues were permeabilized by washing the sections twice for 10 minutes with 1% goat serum in PBST (PBS containing 0.4% Triton X-100) and incubated with blocking buffer (PBS containing 0.4% Triton X-100 and 5% goat serum) for 1 h at room temperature. Then the sections were incubated overnight at 4 °C with rabbit polyclonal antibody specific for p53 and SIRT1. On the following day, the sections were washed in PBST for 3 times and incubated with Alexa Fluor 488-conjugated goat anti-rabbit secondary antibody and Alexa Fluor 594-conjugated goat anti-mouse secondary antibody at 1:200 dilutions for 1 h at room temperature. The sections were washed with PBST and mounted using ProLong Gold antifade reagent with DAPI (Invitrogen, Eugene, Oregon). The slides were kept in the dark overnight at room temperature and confocal images were captured using a Zeiss 510 Meta multiphoton/confocal microscope (Carl Zeiss) with a plan apochromat 633/1.4 NA oil objective. For the green dye, an argon laser set was used with an excitation of 488 nm and emission (collected with a band-pass filter) of 500-550 nm. For the red dye, a helium-neon laser was used with an excitation of 543 nm and emission (collected with a long-pass filter) of 560 nm. At least eight images were collected per treatment.

Real-Time RT-PCR

The procedure to isolate total RNA and perform Real-Time RT-PCR was followed as previously described (10,402). Total RNA was isolated using RNeasy Micro Kit (Cat. No. 74004, Qiagen) according to manufacturer's instructions. The purity and concentration of RNA were determined spectrophotometrically by measuring the absorbance at 260/280nm and a purity of 1.8-2.0 was considered acceptable for the real-time reverse transcription (RT)-PCR analysis. The first strand cDNA was synthesized using 100ng total RNA by QuantiTect RT kit (Cat. 205311, Qiagen) according to manufacturer's instructions. Real-time PCR was performed using the Power SYBR Green master mix (Cat. 4368577, Life Technologies) according to manufacturer's instructions. cDNA (2 µl) was mixed with 10 µl master mix (dNTP mix, AmpliTaq Gold DNA polymerase, optimized buffer components, and SYBR Green I dye), sense and antisense oligonucleotide primers for respective genes and b-actin gene for internal control, with the total reaction volume, made up to 20 ml with RNase free water. The reaction cycles were as follows: PCR enzyme initial activation at 95°C for 15min; initial denaturation at 94°C for 15s, annealing at 60°C for 30s, and elongation at 72°C for 30s. All reactions were run in triplicate. The PCR amplification of all transcripts was performed on the step-one plus real-time PCR machine (Life Technologies, Carlsbad, California). The fold differences (ddCt) were calculated by normalizing the relative expression of the gene of interest with b-actin and the results expressed as fold changes. Details of the sense and antisense oligonucleotide primer sequences used for the real-time PCR analysis were given in Table. 2.1. All currently available nucleotide sequences encoding each gene analyzed in this study in the human were downloaded from the GenBank database. Primers were designed using the DNasis software, and commercially synthesized and obtained from Integrated DNA Technologies (Coralville, Iowa) (10,402).

Table. 2.1. Details of primer sequences used

S.No	Gene		Sequence
1	AKT	Forward	5'-TCAGGTTCACCCAGTGACAA-3'
		Reverse	5'-AGGGCTGTAAGGAAGGGATG-3'
2	BCL2	Forward	5'-CTGGCATCTTCTCCTTCCAG-3'
		Reverse	5'-CCTGAAGAGTTCCTCCACCA-3'
3	SIRT	Forward	5'-CCTTTCAGAACCACCAAAGCG-3'
		Reverse	5'-GCAAGGCGAGCATAAATACC-3'
4	P53	Forward	5'-AGGTTCGTGTTTGTGCCTGT-3'
		Reverse	5'-CTTCGGGTAGCTGGAGTGAG-3'
5	BAX	Forward	5'-GGAGACACCTGAGCTGACCT-3'
		Reverse	5'-GGAGGAAGTCCAGTGTCCAG-3'
6	B-ACTIN	Forward	5'-CAACCTTCTTGCAGCTCCTC-3'
		Reverse	5'-TTCTGACCCATACCCACCAT-3'

miRNA Real-Time RT-PCR

Total RNA from the PND1 ovary was isolated using mirVana miRNA isolation kit (Cat. AM1561, Invitrogen) according to manufacturer's instructions. The purity and concentration of RNA were determined spectrophotometrically by measuring the absorbance at 260/280nm and a purity of 1.8-2.0 was considered acceptable for the miRNA real-time reverse transcription (RT)-PCR analysis. Reverse transcription was performed using TaqMan® MicroRNA Reverse Transcription kit (Cat. 4366596, Applied Biosystems) according to manufacturer's instructions. Each 15µL RT reaction included 0.3 µL of dNTPs (100mM), 3µL of MultiScribe™ Reverse Transcriptase (50 U/µL), 1.5µL of Reverse Transcription buffer (10x), 0.19 µL of RNase inhibitor (20 U/µL), 1.01µL of nuclease-free water, 6 µL of RT primer (A primer pool was made by adding 10µL of 5x miR34a primer and 10µL of 5x U6 primer to 980µL of H_2O), and 3µL of RNA sample

(600ng). The RT reaction mixture was incubated for 30 min at 16°C and for 30 min at 42°C and was finally heat-inactivated for 5 min at 85°C programmed in a thermal cycler. miRNA real-time PCR of TaqMan™ microRNA Assay hsa-miR-34a-5p (Mature miRNA Sequence: UGGCAGUGUCUUAGCUGGUUGU, miRBase Accession Number: MI0000268, Assay ID: 000426, Cat. 4427975, Applied Biosystems) and TaqMan™ microRNA Control Assay U6 (NCBI Accession Number: NR_004394, Assay ID: 001973, Cat. 4427975, Applied Biosystems) was performed with TaqMan universal master mix II with UNG (Cat. 4440038, Applied Biosystems). Each 20µL qPCR reaction included 1µL of miR34a or U6 Taq Man® Small RNA Assay (20x), 1.33µL of RT reaction product, 10µL of TaqMan® Universal PCR Master Mix II with UNG (2x), and 7.67 µL of Nuclease-free water. The reaction cycles were as follows: AmpErase®UNG activity at 50°C for 2min; enzyme activation at 95°C for 10 min; and 40 PCR cycles of denaturation at 95°C for 15s, and annealing at 60°C for 60s. All reactions were run in triplicate. The PCR amplification of all transcripts was performed on the step-one plus real-time PCR machine (Life Technologies, Carlsbad, California). The fold differences (ddCt) were calculated by normalizing the relative expression of miR34a with U6 and the results were expressed as fold changes.

Cell culture and transfection

Spontaneously immortalized rat granulosa cells (SIGC) were cultured in Dulbecco modified Eagle medium/F12 (DMEM/F12, Sigma, Saint Louis, MO) containing 15 mM HEPES and supplemented with 5% fetal bovine serum (FBS, Hyclone, Logan, UT), penicillin 100 U/ml, streptomycin (100µg/ml) and amphotericin-B (2.5µg/ml) in 100mm tissue culture plates in a humidified atmosphere with 95% air, 5% CO2 at 37°C. At 70%-80% confluency, cells were used for the transfection experiment. The groups were (1) Control: Cells were treated with media without any treatment; (2) CrVI: Cells were treated with media containing 0.1 ppm CrVI; (3)

CrVI+miR34a mimetics: Cells were treated with media containing 0.1 ppm CrVI and miR34a mimetics (100nM); (4) CrVI+miR34a inhibitor: Cells were treated with media containing 0.1 ppm CrVI and miR34a inhibitor (100nM); (5) miR34a mimetics alone: Cells were treated with media containing miR34a mimetics (100nM); and (6) miR34a inhibitor alone: Cells were treated with media containing miR34a inhibitor (100nM).

The endogenous miR34a was upregulated using miRIDIAN™ microRNA Mimics (Cat. C-320335-05-0002, Dharmacon) to study miR34a gain-of-function effects and miRIDIAN™ microRNA Inhibitor (Cat. IH-320335-06-0005, Dharmacon) was used to suppress endogenous miR34a for loss-of-function studies. The mimics and inhibitors were delivered using DharmaFECT reagent as per manufacturer's instructions (Dharmacon, Lafayette, CO). Briefly, miR34a mimic or inhibitor (100nM/well) and DharmaFect-1 (1µl/well) were diluted in 50µl AB/serum-free DMEM/F12 medium separately and incubated for 5 min at room temperature. After incubation, miR34a mimic/inhibitor and DharmaFECT reagent were mixed (total volume of 100 µl) and incubated at room temperature for 20 min. Then 100µl mimic/inhibitor:DharmaFECT reagent mixture was added to each well in a total volume of 400µl/well antibiotic-free DMEM/F12 medium with 5% FBS. After 24 h, cells were harvested 24 h post-transfection for protein isolation to analyze for Immunoprecipitation and western blotting.

Protein isolation

After the CrVI treatment with or without miR34a mimetics or miR34a inhibitor, total protein from granulosa cells was isolated for immunoblotting/western blotting. Briefly, the cells were harvested using 1% Trypsin-EDTA and pelleted by centrifuging at 13, 200 rpm for 10 minutes at 4°C. The cell lysates were sonicated in sonication buffer which consisted of 20 mM Tris–HCl, 0.5 mM EDTA, 100 µM DEDTC, 1% Tween, 1mM phenylmethylsulfonyl fluoride, and

protease inhibitor cocktail tablets: complete EDTA-free (1 tablet/50 ml) and PhosStop (1 tablet/10 ml). Sonication was performed using a Microson ultrasonic cell disruptor (Microsonix Incorporated, Farmingdale, NY). After sonication, the samples were centrifuged at 13,200rpm for 15 minutes at 4°C. The supernatant was recovered and protein concentration was determined using the Bradford method and a Bio-Rad Protein Assay kit.

Immunoprecipitation

Immunoprecipitation (IP) was carried out using protocols provided by Santa Cruz Biotechnology and/or Cell Signaling Technology and as published (405). Briefly, total cell lysate (1 mg, ∼120–125 µl) was precleared by incubating with ImmunoCruz F preclearing matrix B-rabbit (50µl/ml) (Cat. SC-45057, Santa Cruz Biotechnology, Dallas, TX) for 30 min at 4°C. After incubation, matrix was pelleted by microcentrifugation at 1000rpm for 1 min at 4° C. The pellet was discarded and the precleared lysate (∼120–125 µl) was incubated with rabbit oligoclonal acetyl-p53 antibody (1µg/ml) **(**Cat. 710294, ThermoFisher scientific) overnight at 4°C with rotation. After overnight incubation, the mixture was further incubated with immunoprecipitation ImmunoCruz F IP matrix (50 µl/ml) (Cat. SC-45043, Santa Cruz Biotechnology, Dallas, TX) overnight at 4°C. Protein-antibody IP complexes were precipitated and washed three times using 500µl of IP buffer: 20mM Tris-HCl, 0.5mM EDTA, 100 µM DEDTC, 1% Tween, 1 mM phenyl methyl sulfonyl fluoride, and protease inhibitor cocktail tablets, that is, complete EDTA-free (1 tablet/50 ml) and PhosStop (1 tablet /10 ml). Finally, the protein-antibody IP complexes were resuspended in 40µl of 2× SDS sample buffer, boiled at 100°C for 5-10 min, and then resolved in 10% SDS PAGE gel. Rabbit IgG was immunoprecipitated and was used as an internal control.

Western blotting

Approximately 75-µg aliquots of total proteins were loaded in each lane and electrophoresed on 10% SDS polyacrylamide gels followed by electrotransfer onto nitrocellulose membranes (Amersham Pharmacia Biotech, Montreal, PQ, Canada). Prestained protein markers (Fisher, BP3603-1) were used as molecular weight standards for each analysis. The blots were stained with 0.5% ponceau-stain in 1% acetic acid for evaluating the quality of protein transfer. Proteins were blocked overnight at 4°C with 5% fat-free dry milk powder in PBS and 0.05% Tween-20 (PBST). The blots were incubated with SIRT1 primary antibody for 12 h at 4°C at a dilution of 1:1000 in 2% fat-free dry milk powder in PBST. The blots were washed 3 times at 10-min intervals in PBS-T and then incubated with secondary antibody (goat anti-rabbit IgG conjugated with horseradish peroxidase; Jackson Immunoresearch Laboratories, West Grove, PA) for 1 h at room temperature at a dilution of 1:10 000 in 2% fat-free dry milk powder in PBS-T. Blots were then washed 3 times at 10-min intervals in PBS-T. Chemiluminescent substrate was applied according to the manufacturer's instructions (Pierce Biotechnology). The blots were exposed to Blue X-Ray film and densitometry of autoradiograms was performed using an Alpha Imager (Alpha Innotech Corporation, San Leandro, CA).

Antibodies

Sources of antibodies, catalog numbers, dilution, host species, immunogen and homology with rat/mouse are given in Table. 2.2.

Statistical analysis

Aim 1: Effects of CrVI on various parameters in the ovary were analyzed and the results were expressed as mean±SEM. Student t-test was used to compare groups and p values less than

0.05 were considered significant. Pearson's correlation was used to derive 'R' values for colocalization between control and treatment groups.

Aim 2: All numerical data were subjected to one-way ANOVA to detect the effects of SIRT1 inhibitor (1, 5 and 50 mg/kg body weight) treatment and dose interactions, in the presence of absence of CrVI. Tukey–Kramer HSD test was used to adjust for multiple pair-wise comparisons of means. Least squares regression analysis was used to determine effects of treatment, dose and treatment × dose interactions in *in vivo* studies. We take into account the nested structure in the design. Mixed models analysis was used to account for any correlation between the results of pups from the same mother. Mixed models were used to model both fixed effects (in this case treatment) and random effects (in this case mothers and pups) (406).

Aim 3: For *ex vivo fetal whole ovarian culture* studies, least squares regression analysis was used to determine effects of treatment (Control, miR34a inhibitor, miR34a mimetic, CrVI, CrVI+ miR34a inhibitor or CrVI, CrVI+ miR34a mimetic). Each value is the mean±SEM from 8 ovaries per treatment. Similar results were obtained in three different experiments performed. Statistical analyses were performed using general linear models of Statistical Analysis System (SAS, Cary, NC) and $P < 0.05$ was considered significant.

Aim 4: Effects of CrVI on various parameters in the ovary were analyzed and the results expressed as the mean ± SEM. Student *t*-test was used to compare groups, and *P*-values of less than 0.05 were considered to be statistically significant.

Table. 2.2. Primary and secondary antibodies, company, catalog number, dilution, immunogen, dilution and application.

Antibody	Company & Cat #	Dilution	Host species	Immun-ogen	Secondary antibody	Dilution	Applica-tion
p-AKT	Cell signaling; 3787	1:50	Rabbit monoclonal	Mouse	Goat anti-rabbit	1:200	IHC
p-ERK	Cell signaling; 4370	1:100	Rabbit monoclonal	Human	Goat anti-rabbit	1:200	IHC
p53	Abcam; 131442	1:200	Rabbit polyclonal	Human	Goat anti-rabbit alexa 488 green	1:200	Whole mount
SOD-2	Sigma; S1450	2 µg/ml	Rabbit polyclonal	Human	Goat anti-rabbit	1:200	IHC
Caspase-3	Cell signaling; 9661	1:50	Rabbit polyclonal	Human	Goat anti-rabbit	1:200	IHC
BAX	Sigma; SAB 4502549	1:1000	Rabbit polyclonal	Human	Goat anti-rabbit	1:200	IHC
XIAP	Cell signaling; 2045	1:100	Rabbit monoclonal	Human	Goat anti-rabbit	1:200	IHC
p27	Cell signaling; 2552	1:500	Rabbit polyclonal	Mouse	Goat anti-rabbit	1:200	IHC
VASA	Abcam; 13840	1:100	Rabbit polyclonal	Human	Goat Anti-rabbit alexa 488 green	1:200	Whole mount
GATA-4	Santa Cruz; 25310	1:50	Mouse monoclonal	Human	Goat anti-mouse alexa 594 red	1:200	Whole mount
p53	Abcam; 131442	1:300	Rabbit polyclonal	Human	Goat anti-rabbit	1:200	IHC
p53-acetyl	Invitrogen; 710294	1:50	Rabbit polyclonal	Human	Goat anti-rabbit	1:200	IHC
SIRT1	Abcam; 110304	1:100	Mouse monoclonal	Human	Horse Anti-mouse	1:200	IHC

Table. 2.2 Continued

Antibody	Company & Cat #	Dilution	Host species	Immun-ogen	Secondary antibody	Dilution	Applica-tion
SIRT1	Cell signaling; 9475s	1:3000	Rabbit polyclonal	Human	Goat anti-rabbit	1:20,000	Western blot
PUMA	Abcam; 9643	1:500	Rabbit polyclonal	Human	Goat anti-rabbit	1:200	IHC
BCL2	Abcam; 7973	1:200	Rabbit polyclonal	Human	Goat anti-rabbit	1:200	IHC
Col-1	Abcam; AB292	1:500	Rabbit polyclonal	Human	Goat Anti-rabbit	1:200	IHC
Col-3	Sigma; C7805	1:100	Mouse monoclonal	Human	Horse Anti-mouse	1:200	IHC
Col-4	Sigma; SAB4200500	1:750	Mouse monoclonal	Human	Horse Anti-mouse	1:200	IHC
XPNPEP2	Abcam; AB97852	1:100	Rabbit polyclonal	Human	Goat Anti-rabbit	1:200	IHC
EMBP	Santa Cruz; SC-33938	1:250	Goat polyclonal	Mouse	Rabbit Anti-goat	1:200	IHC

3. PRENATAL EXPOSURE TO HEXAVALENT CHROMIUM INDUCES EARLY REPRODUCTIVE SENESCENCE BY INCREASING GERM CELL APOPTOSIS AND ADVANCING GERM CELL NEST BREAKDOWN IN THE F1 OFFSPRING*

Specific Aim-1:

Determine the effects of prenatal exposure to CrVI on premature ovarian failure in the F1 offspring.

Hypothesis:

This aim was based on the working hypothesis that **"***in utero exposure to CrVI causes premature ovarian failure by increasing germ cell death, advancing germ cell nest breakdown and primordial follicle assembly by activating apoptotic pathways and inhibiting cell survival pathways*".

Objectives:

The objectives were to (i) determine the effects of prenatal exposure to CrVI on pregnancy rate and litter size in the F1 offspring; (ii) evaluate the role of CrVI on germ cell nest breakdown; (iii) understand the role of CrVI on primordial follicle assembly and atresia; (iv) assess the effects of CrVI on the cell survival machinery such as p-AKT, p-ERK and XIAP; and (v) explore the mechanism of p53 in CrVI-induced germ cell apoptosis, germ cell nest breakdown, and primordial follicle assembly.

* Parts of this section are reprinted with permission from "Prenatal exposure to chromium induces early reproductive senescence by advancing oocyte nest breakdown and increasing primordial follicle atresia in F1 offspring". Sivakumar KK, Stanley JA, Arosh JA, Pepling ME, Burghardt RC, Banu SK. Developmental Biology. 2014. Apr; 388(1): 22-34. PMID: 24530425. Copyright-2014. doi: 10.1016/j.ydbio.2014.02.003. Epub 2014 Feb 12.

Results

Prenatal exposure to CrVI increased Cr levels in the placenta

Almost all tissues accumulate chromium (407). In order to determine if Cr passes through the placenta, we determined Cr levels in the placenta on gestational day 20. Rats were given CrVI through drinking water in order to mimic human exposure to CrVI. Gestational exposure to CrVI significantly elevated total Cr levels in the placenta (Fig. 3.1, A).

CrVI induced early reproductive senescence

Our previous studies indicated that Cr exposure through lactation increased follicular atresia. In order to determine if prenatal exposure to Cr induces reproductive failure in F1 offspring, pregnancy rates, live births and litter size in Cr-exposed F1 females for a period of 10 months were monitored. Results showed that prenatal exposure to CrVI decreased pregnancy rate (Fig. 3.1, B) and litter size (Fig. 3.1, C) in F1 offspring up to 10 months. At the end of 10 months of age, only 2% of rats became pregnant in the CrVI-treatment group. It is evident that prenatal exposure to CrVI decreased pregnancy outcome and reduced litter size in F1 offspring (Fig. 3.1, B & C).

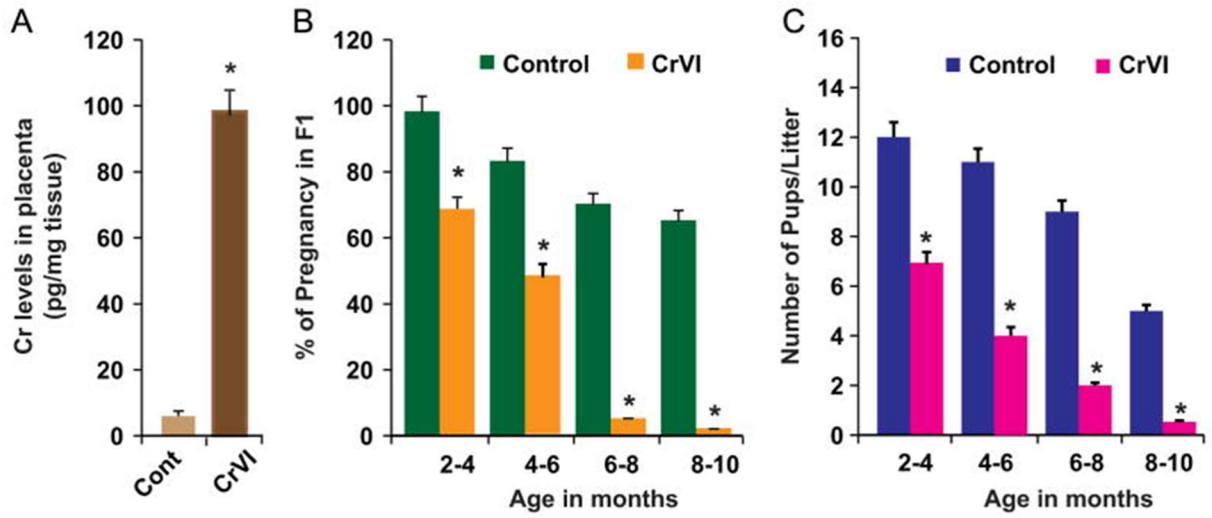

Fig. 3.1. Prenatal exposure to CrVI increased Cr accumulation in the placenta (A), and decreased pregnancy rate (B), and litter size (C) in the F1 female offspring. Pregnant mother rats (F0) received either regular drinking water (control) or CrVI (potassium dichromate 25 ppm) in drinking water from 9.5 to 14.5 days postcoitum (DPC). Developing fetuses (F1) received CrVI through placental transfer from gestational days (GD) 9.5 to 14.5. On the GD 20, one group (n=5) of control and experimental mothers were euthanized and the placentae were removed. Total Cr was estimated in the placenta. Another set of control and CrVI-treated F1 females were allowed to breed for a period of 12 months (n=15). Numbers of rats that attained pregnancy (% pregnancies) (B) and delivered live pups were recorded every month. The number of pups/litter (litter size) (C) was recorded. *control vs CrVI, p<0.05. Each value represents mean±SEM of 20 F1 rats during a period of 2 months.

CrVI accelerated oocytes/germ cells and somatic/granulosa cells apoptosis and advanced primordial follicle assembly and primary follicle transition

The number of primordial follicles within the ovary determines the life-time follicle reserve (260). Even though successful assembly of the primordial follicle is one of the most critical events and the first step in folliculogenesis, proper timing of primordial follicle assembly is strictly regulated. The timing of folliculogenesis varies from species to species; however, both genesis and survival of primordial follicles determine the reproductive life of a female (408). Effects of CrVI on germ cells apoptosis and primordial follicle assembly were determined. On E15.5 and E17.5, control ovaries were packed with rounded GCN containing healthy germ cells and few degenerating germ cells. In contrast, ovaries from CrVI-exposed F1 pups had greater numbers of degenerating germ cells with pyknotic nuclei on E15.5 and E17.5 (Fig. 3.2, A-D). On PND1, GCN from control ovaries were filled with healthy germ cells surrounded by invading somatic or pregranulosa cells, whereas CrVI treatment accelerated GCN breakdown and advanced primordial and primary follicle formation (Fig. 3.2, E & F). On PND4, control ovaries were predominantly filled with healthy primordial and few primary follicles, whereas ovaries from the CrVI exposed rats had several primary and a few secondary follicles. Interestingly, CrVI decreased healthy primordial and primary follicles and increased follicle atresia in rats exposed to CrVI in utero (Figs. 3.2, G and H).

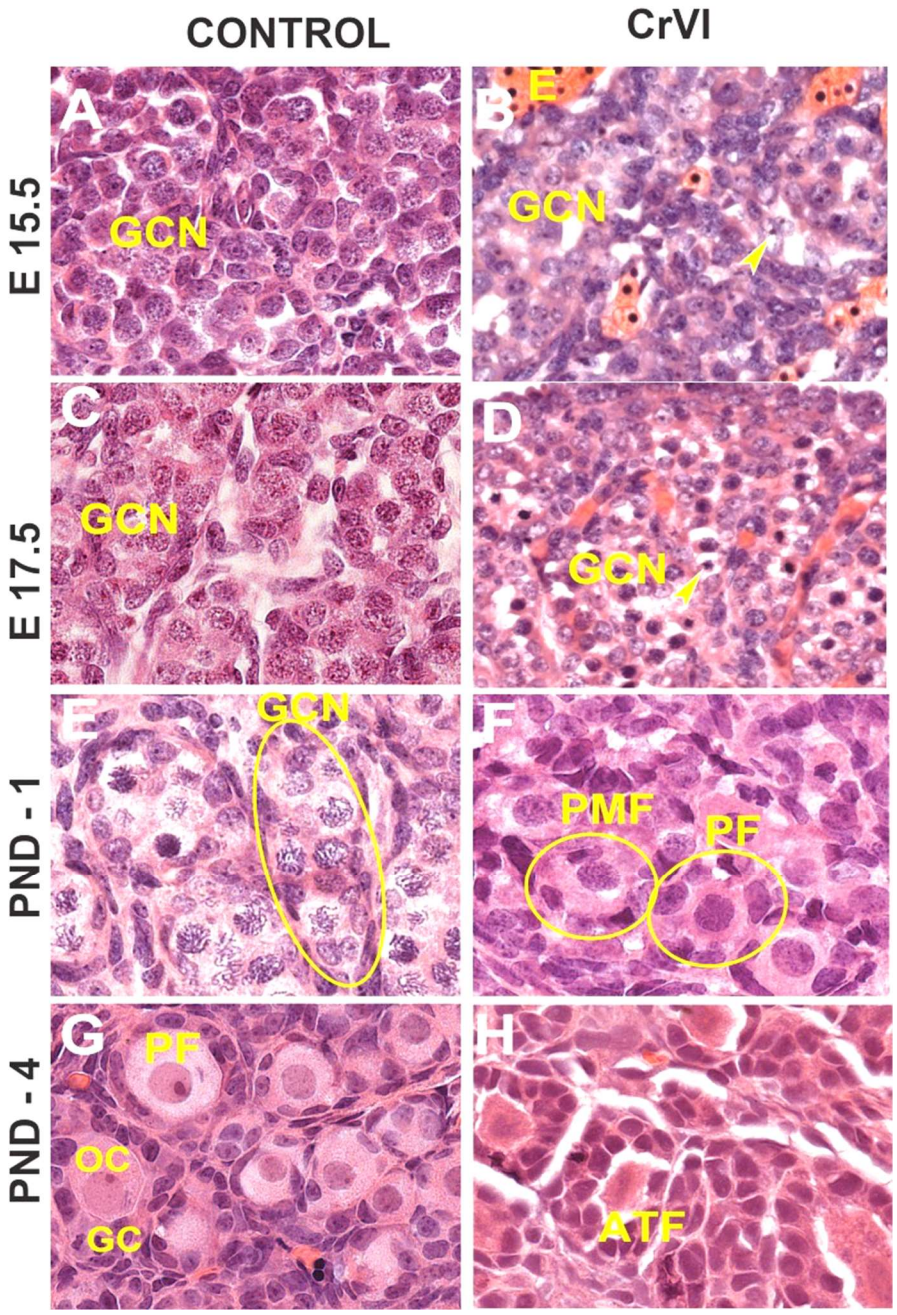

Fig. 3.2. Effects of prenatal exposure to CrVI on ovarian follicle development. Pregnant mother rats (F0; n=5) received either regular drinking water (control) or CrVI (potassium dichromate, 25 ppm; n=10) in drinking water from GD 9.5 to GD 14.5. During this period, fetuses were exposed to CrVI via transplacental transfer. On E15.5 and E17.5, ovaries from the fetuses were removed. On PND1 and PND4, ovaries were removed from F1 female pups and processed for histology (H&E). The width of field for each image is 220 or 350 µm. Arrowheads indicate pyknotic nuclei. Representative images are shown for E15.5 (A and B), E17.5 (C and D), PND1 (E and F), and PND4 (G and H). E, eosinophils; PMF, primordial follicle; PF, primary follicle; ATF, atretic follicle; OC-oocyte; GC, granulosa cells.

CrVI advanced germ cell nest breakdown

In mice, GCN breakdown begins in the medulla approximately at 17.5 dpc and in the cortex at 19.5 dpc, peaks at PND2 and 3, and continues up to PND4 with a concomitant loss of oocytes (189). Effects of CrVI on GCN breakdown were determined by co-immunolocalization of the germ cell marker, VASA, and the somatic cell marker, GATA4, in whole-mount ovaries. Control ovaries at E15.5 and E17.5 consisted of clusters of 10-29 intact and healthy germ cells within a GCN with no primordial follicles (Fig. 3.3 and 3.4, A, C, & E). In CrVI –treated rats, GCNs were broken down into smaller nests on E15.5 and E17.5 (Fig. 3.3 and 3.4, B, D, & F). In particular, penetration of the somatic cells in between the germ cells was very obvious on E15.5 and E17.5 in CrVI-exposed ovaries compared to control ovaries (Fig. 3.3 and 3.4, C & D). On PND1, control ovaries (Fig. 3.5, A, C & E) consisted of intact and healthy germ cells arranged as groups of 10-24 healthy round oocytes inside the nests with no detectable primordial follicles; whereas, few nests and mostly primordial and primary follicles or small groups of irregularly shaped oocytes were present in the ovaries from CrVI treated animals indicative of advanced germ cell nest breakdown (Fig. 3.5, B, D & F). CrVI also decreased the number of intact oocytes per section (Fig. 3.5, G), and increased the number of single oocytes (Fig. 3.5, H).

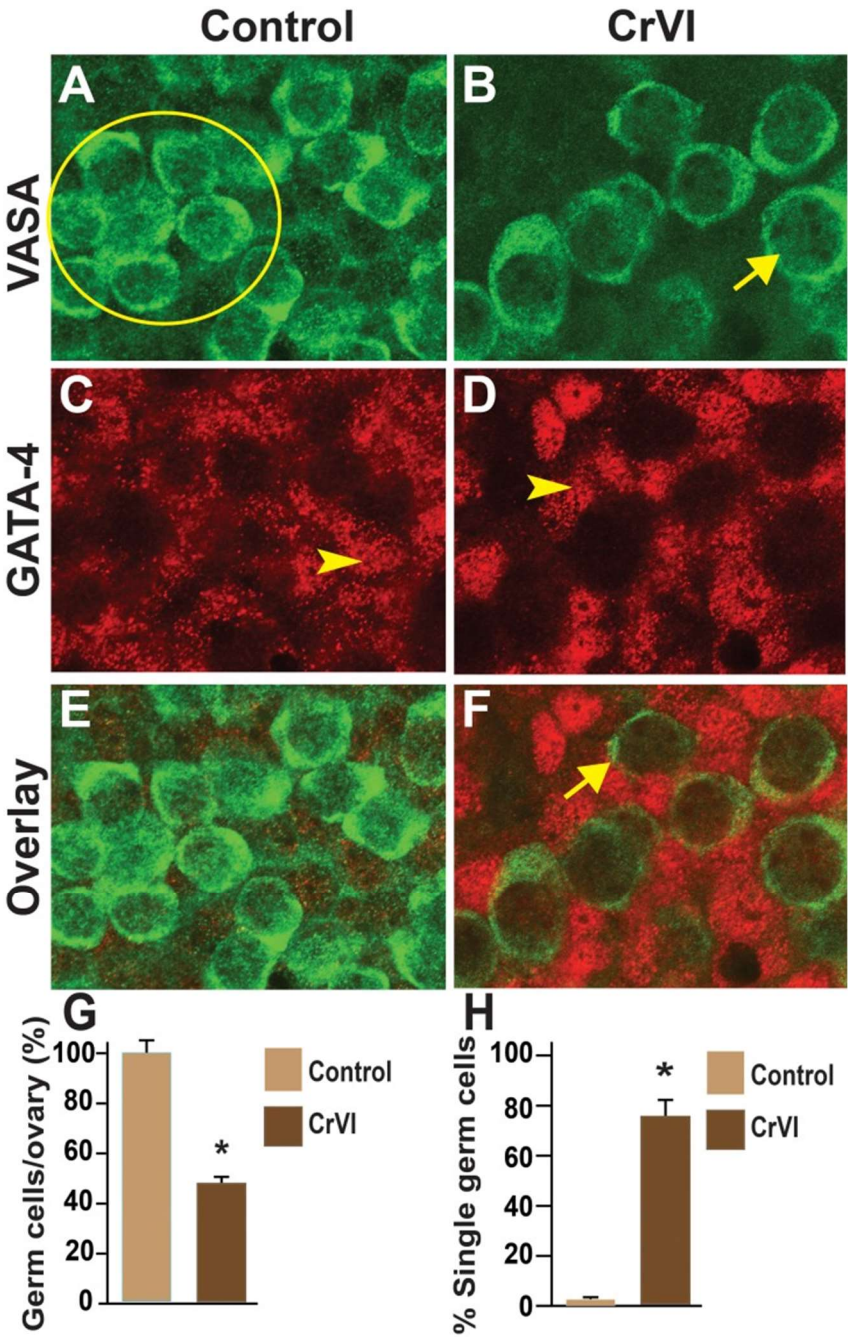

Fig. 3.3. Prenatal exposure to CrVI accelerated GCN breakdown in the fetal ovary on E15.5. Ovaries from E15.5 were processed for whole-mount double immunofluorescence assay and imaged by confocal microscopy. Germ cells were identified by VASA immunostaining (green; A and B) and somatic cells by GATA4 immunostaining (red; C and D), with overlays shown (E and F). The average number of germ cells or oocytes per ovary (G) and the percentage of single oocytes (H) are also shown. Arrows indicate germ cells; arrowheads indicate somatic cells. A circle or ellipse indicates a GCN. The width of field for each image is 115 µm. *P<0.05, control vs. CrVI.

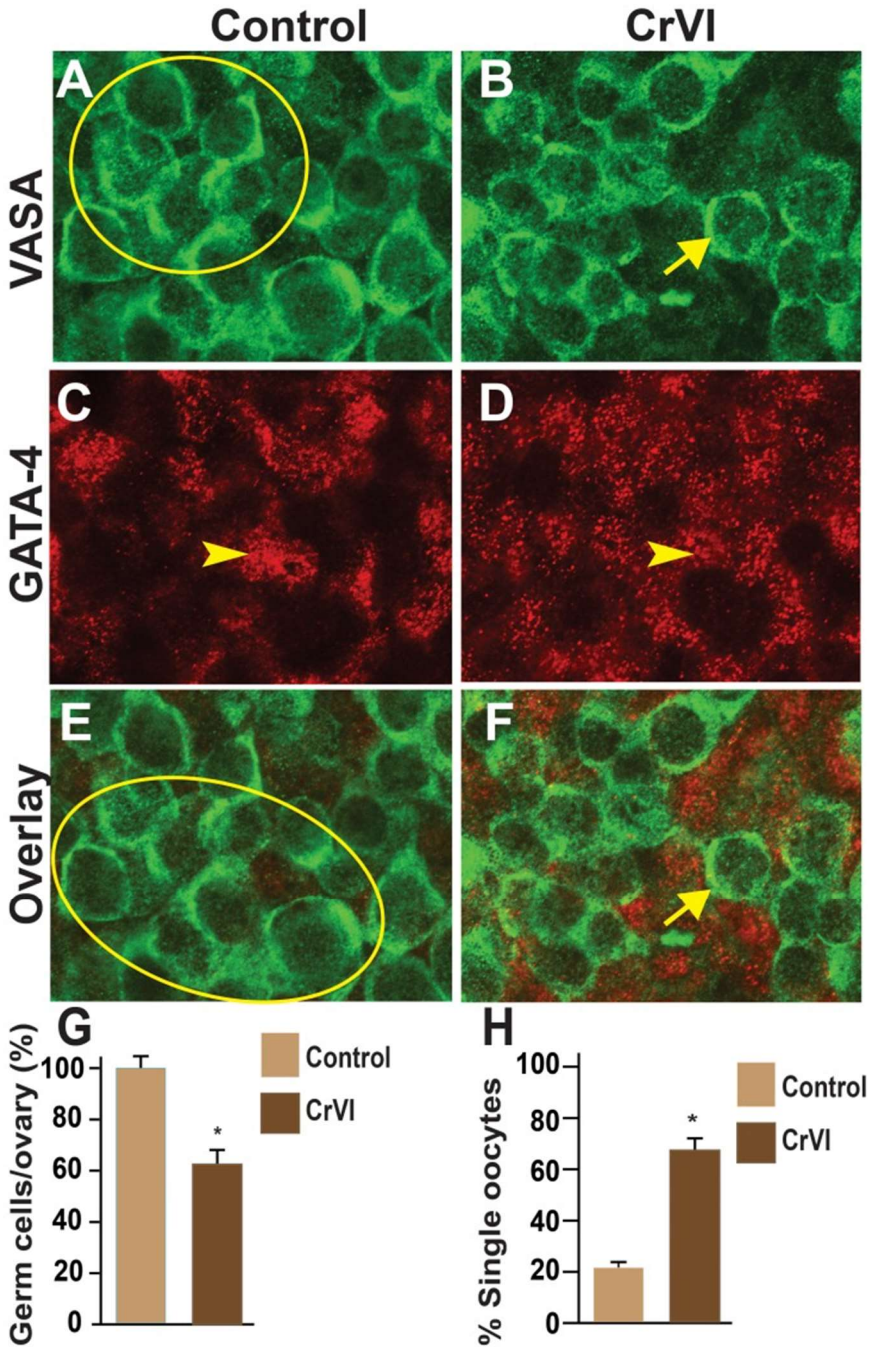

Fig. 3.4. Prenatal exposure to CrVI accelerated GCN breakdown in the fetal ovary on E17.5. Ovaries from E17.5 were processed for whole-mount double immunofluorescence assay and imaged by confocal microscopy. Germ cells were identified by Vasa immunostaining (green; A and B) and somatic cells by Gata4 immunostaining (red; C and D), with overlays shown (E and F). The average number of germ cells or oocytes per ovary (G) and the percentage of single oocytes (H) are also shown. Arrows indicate germ cells; arrowheads indicate somatic cells. A circle or ellipse indicates a GCN. The width of field for each image is 115 μm. *P<0.05, control vs. CrVI.

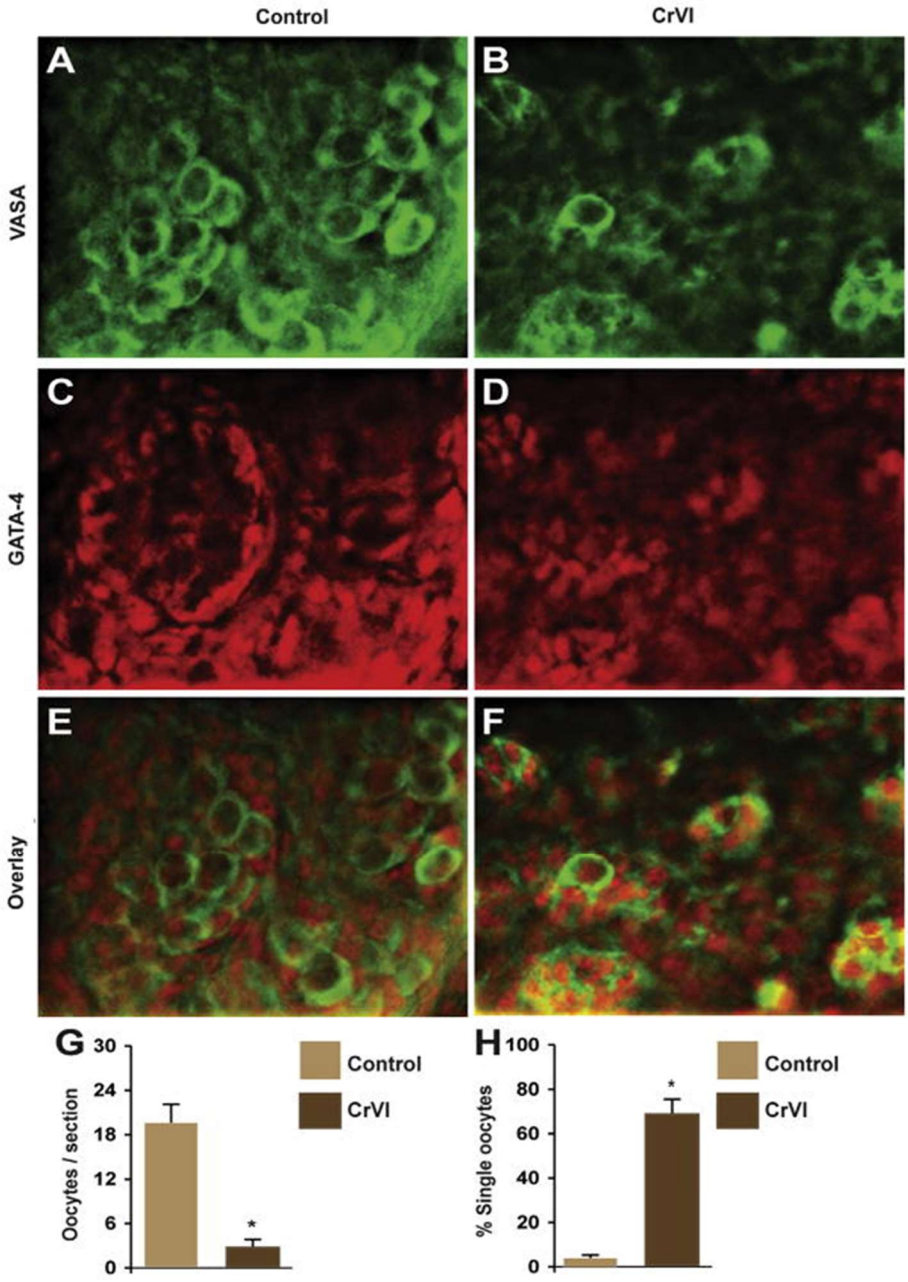

Fig. 3.5. Prenatal exposure to CrVI accelerated GCN breakdown and advanced primordial follicle assembly and primary follicle transition. On PND1, ovaries from F1 female pups were processed for whole mount double immunofluorescence assay or histology. Germ cells were identified by germ cell marker VASA (green, A and B), and somatic cells by somatic cell marker GATA-4 (red, C and D), with overlay shown in E and F. Number of germ cells or oocytes per section (G) and percentage of single oocytes (H) are shown. Every 10th section of the paraffin-embedded ovary was stained with H and E for counting primordial and primary follicles.*control vs CrVI, $p<0.05$. Each value represents mean±SEM of 10-15 ovaries of the F1 pups.

CrVI increased germ cell apoptosis

Germ cell death is one of the major events that occur during GCN breakdown and follicle formation. Approximately one-third of the primordial follicles undergo atresia within a few days after birth (409). In the current study, CrVI increased the number of TUNEL-positive germ cells on E15.5, E17.5, PND1, PND4, and PND25 compared to control (Fig. 3.7) and increased eosinophilic infiltration on E15.5 and E17.5 (Fig. 3.6). CrVI increased germ cell death. Several pyknotic nuclei were found within the GCN.

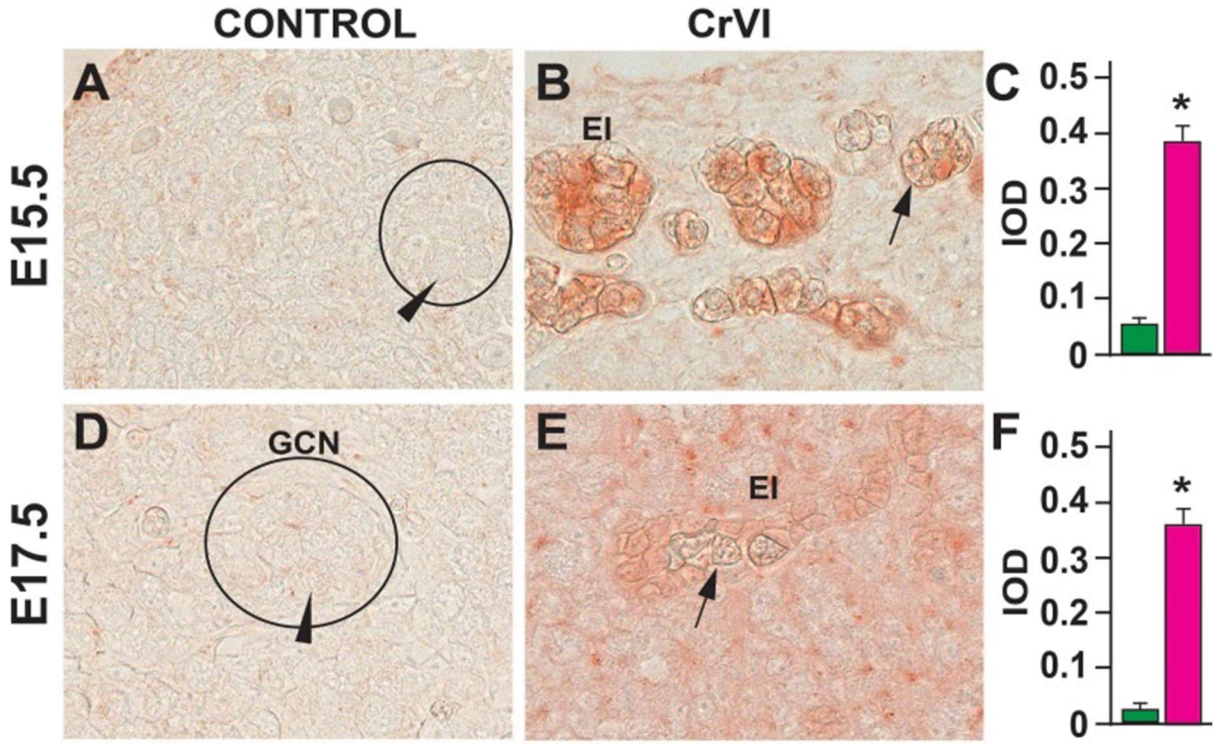

Fig. 3.6. Effects of prenatal exposure to CrVI on the expression of the eosinophilic major basic protein (EMBP) in the E15.5 (A-C) and E17.5 (D-F) ovaries. On E15.5 and E17.5, ovaries from fetuses were removed and processed for IHC. Integrated optical density (IOD) was quantified by Image ProPlus software. Each value represents the mean±SEM of 20-24 ovaries. A circle or ellipse indicates a GCN. Arrowheads indicate healthy germ cells within the nest; arrows indicate degenerating germ cells. The width of field for each image is 220 or 350 μm. EI, eosinophilic infiltration (red staining). *P< 0.05, control vs. CrVI.

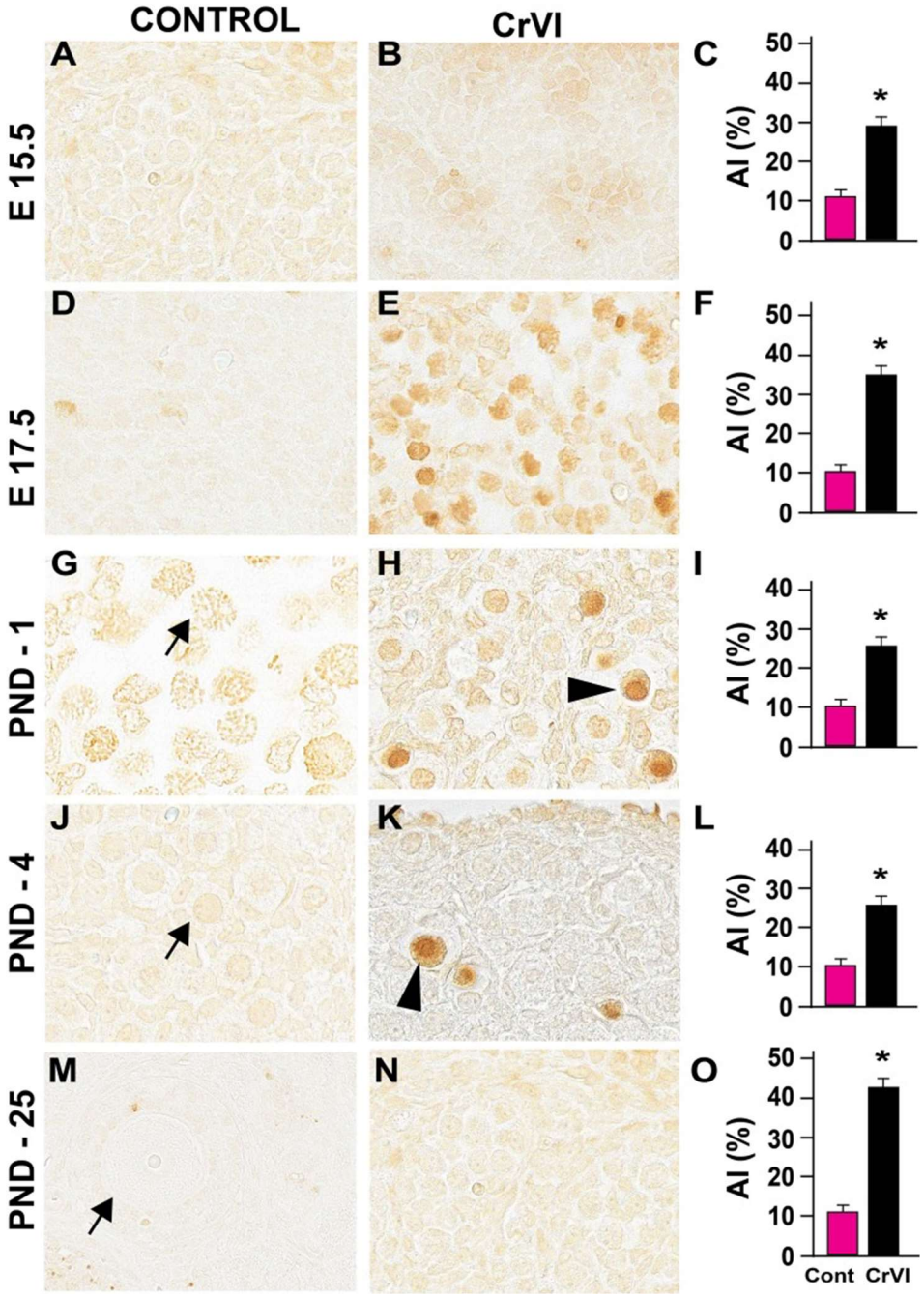

Fig. 3.7. Prenatal exposure to CrVI increased germ cell/oocyte apoptosis. The apoptosis index (AI) was calculated as the average percentage of TUNEL- positive germ cells/oocytes from 20 ovaries. Average number of TUNEL-positive cells in each control group was considered to be 10%. Each value represents the mean±SEM of TUNEL-positive germ cells/oocytes counted from 25 fields at E15.5 (A-C); from 30 to 35 fields at E17.5 (D-F), PND1 (G-I), and PND4 (J-L), and 195 fields in PND25 (M-O). The width of field for each image is 220 or 350 µm. Arrowheads indicate TUNEL-positive (apoptotic) germ cells or oocytes; arrows indicate healthy germ cells or oocytes. *P<0.05, control vs. CrVI.

CrVI down-regulated cell survival proteins p-AKT, p-ERK1/2 and XIAP and up-regulated BAX and Caspase-3

p-AKT, p-ERK1/2 and XIAP are abundantly expressed in control ovaries. Prenatal exposure to CrVI down-regulated the expression of p-AKT, p-ERK and XIAP proteins in the PND1 ovaries of F1 pups (Fig. 3.8, A-I). It is well established that the size of the primordial follicle pool is regulated by BAX (410), and BAX is a marker protein for POF (411). PND1 ovaries of control F1 pups indicated that BAX and Caspase-3 levels were very low whereas prenatal exposure to CrVI exhibited increased expression of BAX and Caspase-3 compared to control (Fig. 3.9, A-F).

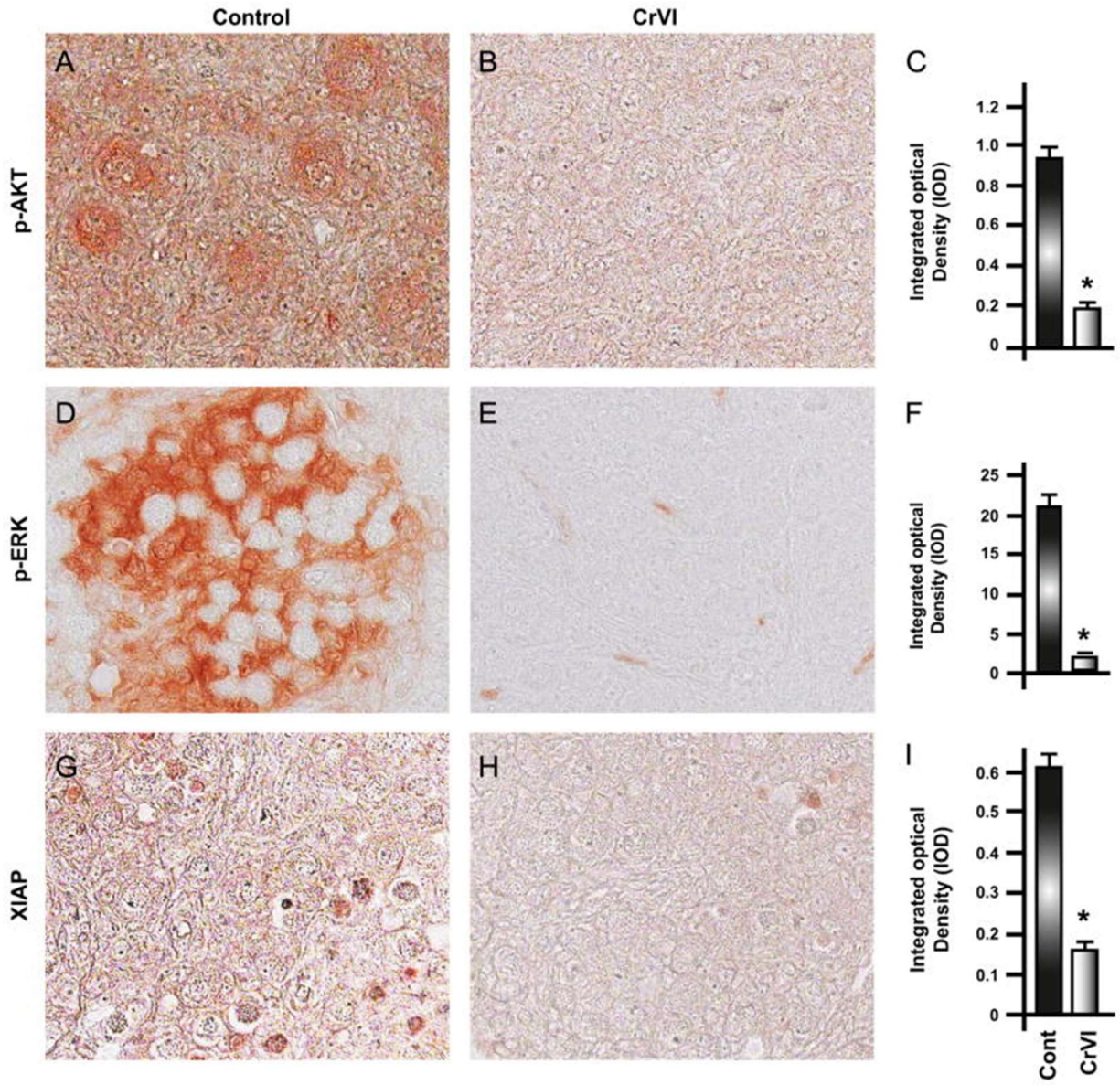

Fig. 3.8. Prenatal exposure to CrVI down regulated the expression of p-AKT, p-ERK and XIAP proteins in the PND1 ovaries of the F1 pups. On PND1, ovaries from F1 female pups were processed for immunohistochemistry. Integrated Optical Density (IOD) was quantified by Image ProPlus software. Each representative image was magnified to 400X; p-AKT (A-C), p-ERK (D-F), and XIAP (G-I). *: control vs CrVI, $p<0.05$. Each value represents mean±SEM of 10-15 ovaries of the F1 pups.

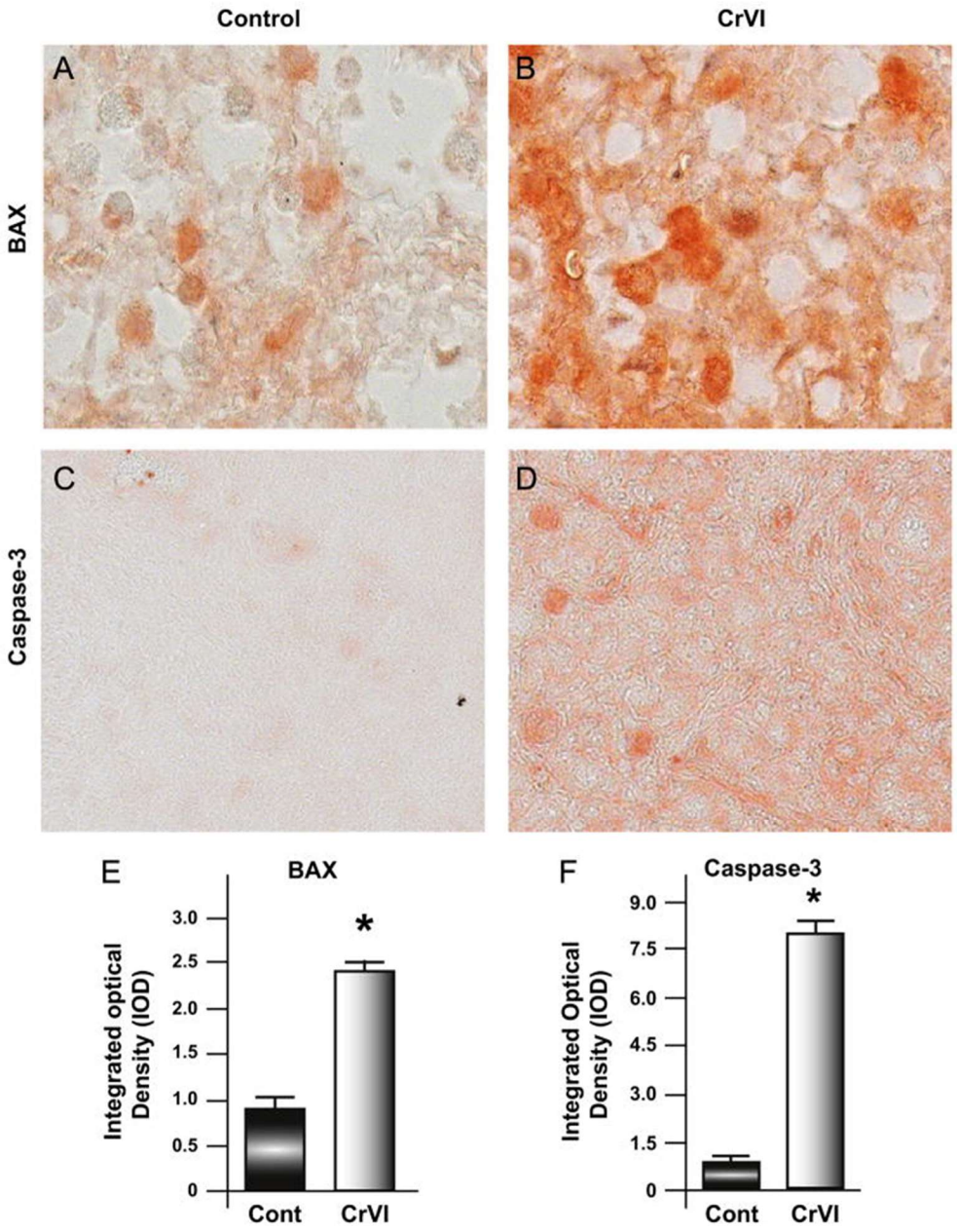

Fig. 3.9. Prenatal exposure to CrVI up-regulated the expression of BAX and cleaved-caspase-3 proteins in the PND1 ovaries of the F1 pups. On PND1, ovaries from F1 female pups were processed for immunohistochemistry. Integrated Optical Density (IOD) was quantified by Image ProPlus software. Each representative image was magnified to 400X; BAX (A, B, E) and cleaved caspase-3 (C, D, F). *: control vs CrVI, $p<0.05$. Each value represents mean±SEM of 10-15 ovaries of the F1 pups.

CrVI up-regulated p53, SOD-2, and p27

p53 is a tumor suppressor protein, and our previous findings indicated that CrVI increased granulosa cell apoptosis through a p53-mediated pathway (412). However, there are no data available on the role of p53 in GCN breakdown under normal conditions or in response to any toxicant. p27 is also a tumor suppressor and negative regulator of cell cycle progression, that activates caspase-3, and follicular atresia (413), and plays a crucial role in fetal ovary development (413,414). In order to determine the expression of p53 and p27 in GCN breakdown, both proteins were analyzed by IHC. p53 expression in control PND1 ovaries was non-detectable whereas gestational exposure to CrVI increased p53 protein expression (Fig. 3.10, A, B & G). CrVI also significantly increased p27 expression compared to control. In both control and CrVI-treated ovaries, p27 was localized in the somatic cells rather than the germ cells (Fig. 3.10, C, D and H). Previous findings indicated that p53 reduces SOD-2 activity (415). SOD-2 is expressed in the oocytes of the dormant primordial follicles (416). CrVI significantly upregulated SOD-2 (Fig. 3.10, E, F & I), compared to control (Fig. 3.10, E, F & I).

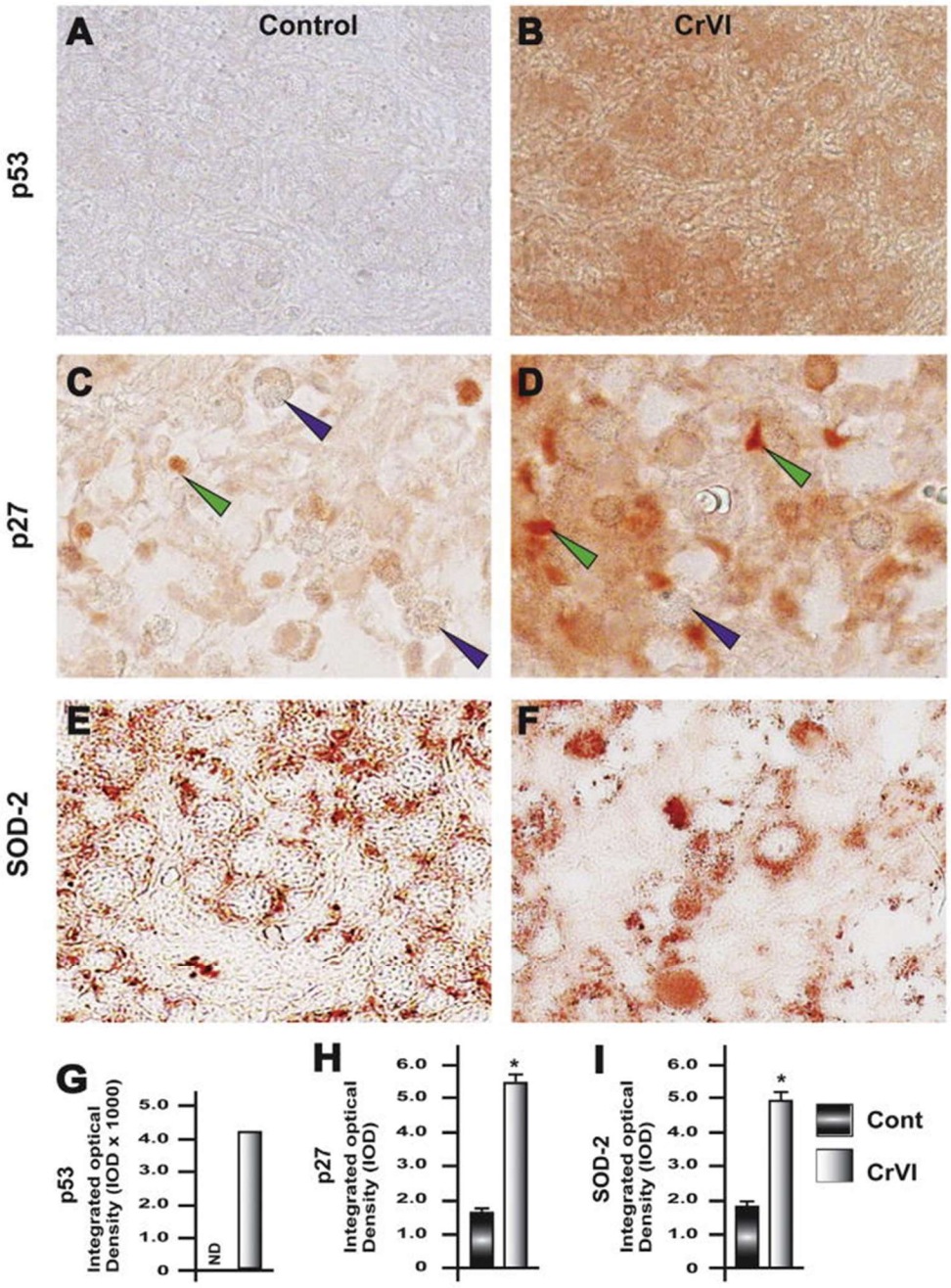

Fig. 3.10. Prenatal exposure to CrVI up-regulated the expression of p53, p27 and SOD-2 proteins in the PND1 ovaries of the F1 pups. On PND1, ovaries from F1 female pups are processed for immunohistochemistry. Integrated Optical Density (IOD) is quantified by Image ProPlus software. Each representative image is magnified to 400 ×; p53 (A, B, and G), p27 (C, D and H), and SOD-2 (E, F, and I). Green arrow heads indicate somatic cells, and purple arrow heads indicate germ cells or oocytes. *: control vs CrVI, $p<0.05$. Each value represents mean±SEM of 10-15 ovaries of the F1 pups.

CrVI increased co-localization of p53 and SOD-2 in whole mount ovaries

IHC showed increased expression of p53 and SOD-2 in CrVI-treated rats (Fig. 3.10). SOD-2 is associated with granulosa cell (131) and primordial follicle survival (417), as a protective mechanism to prevent oxidative stress (417). Therefore, we monitored co-localization of SOD-2 and p53, by evaluating the levels of expression and co-localization of both the proteins in the PND1 ovaries. In control PND1 ovaries, p53 expression was non-detectable (Fig. 3.11, A & D); and SOD-2 was abundantly expressed (Fig. 3.11, B & E). Interestingly, CrVI increased the expression levels of both p53 (Fig. 3.11, G & J), and SOD-2 (Fig. 3.11, H and K). CrVI significantly increased p53-SOD-2 co-localization compared to control (Fig. 3.11, C, F, I, L & M-P).

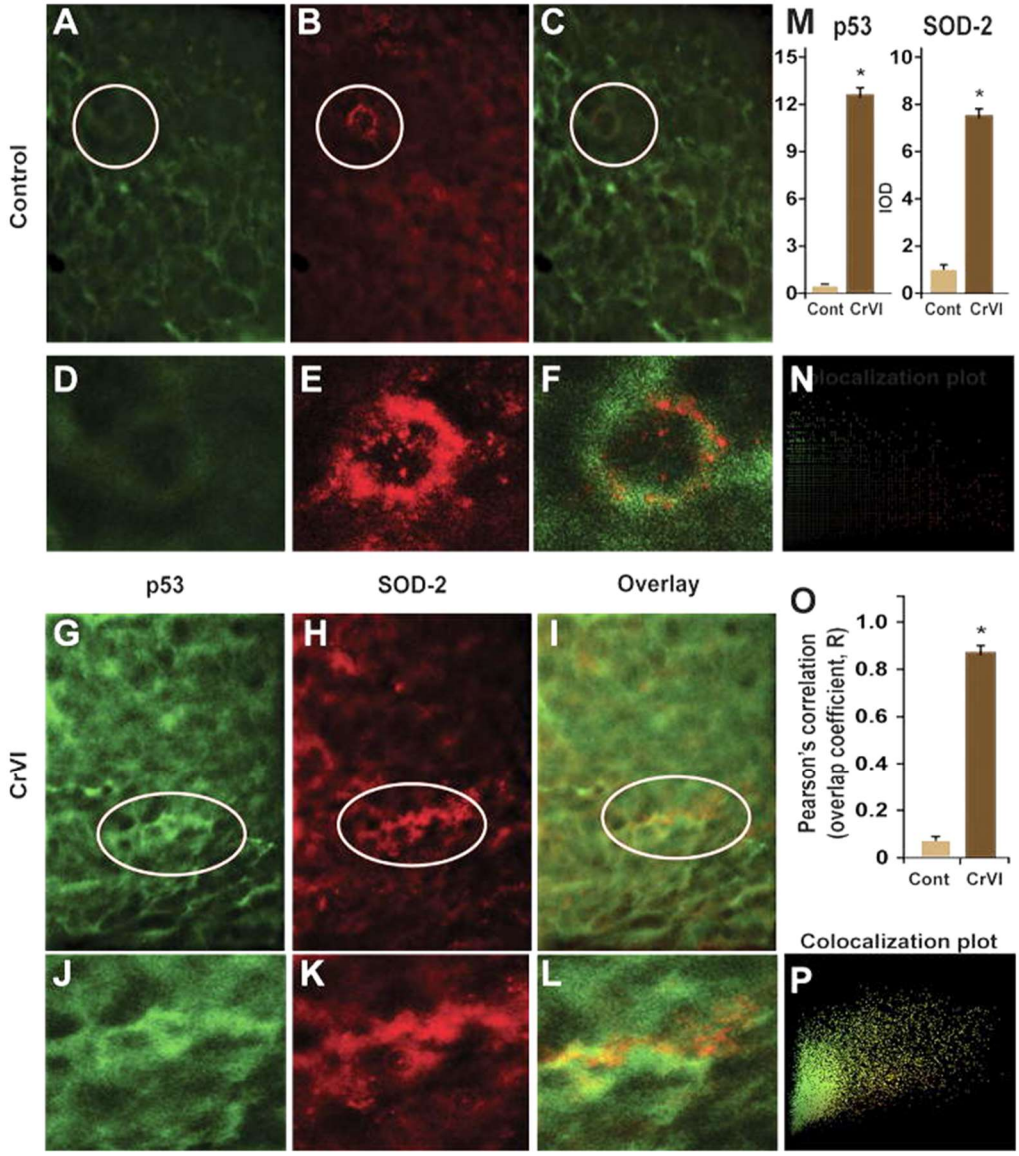

Fig. 3.11. Prenatal exposure to CrVI increased co-localization of p53 and SOD-2 proteins in the PND1 ovaries of the F1 pups. On PND1, ovaries from F1 female pups were processed for whole mount double immunofluorescence. Co-localization of p53 and SOD-2 proteins was measured by co-localization index of the p53 and SOD-2; and the degree of co-localization was measured by the "color composite" and "co-localization" functions in Image-ProPlus software. In control group, p53 expression was very minimal (green, A and D); and SOD-2 was abundantly expressed (red, B and E). CrVI increased the expression levels of both p53 (G and J), and SOD-2 (H and K). CrVI significantly increased co-localization of p53 and SOD-2 proteins compared to control (overlay, C, F, I, L and M-P). The scatter plot displays the intensity range of red and green pixels in the image (N and P). Integrated Optical Density (IOD) was quantified by Image ProPlus software. *: control vs CrVI, $p<0.05$. Each value represents mean±SEM of 10-15 ovaries of the F1 pups.

Discussion

Gestational exposure to CrVI increased total Cr levels in the placenta, indicating that Cr can traverse the placenta and increase Cr burden in the placental compartments. After crossing the placental barrier, Cr could possibly affect the fetal development and also the reproductive potential of the F1 pups in their later period of life. Reproductive outcomes such as pregnancy rate, live births and litter size were monitored for a period of 10 months in order to determine if Cr causes early reproductive senescence in Cr exposed F1 females. Interestingly, 2% of rats from CrVI-exposed group could become pregnant at the end of 10 months while ~60% of rats from the control group could become pregnant. Thus it is evident from these results that gestational exposure to CrVI induced early reproductive senescence in the F1 female rats.

The fertility rate of a female is determined by the number of primordial follicles that are present in the ovarian reserve. This is also called follicle endowment; which is the total number of oocytes available throughout the fertile lifespan for fertilization. The important developmental stage in the formation of the germline is the germ cell nest formation which is evolutionarily conserved in both vertebrates and invertebrate species (418). GCN breakdown is a prerequisite for the primordial follicle development (180). During folliculogenesis, one of the most critical events followed by GCN breakdown is the primordial follicle assembly where the primordial germ cells form primordial follicles under the influence of various secreted factors such as GDF9, BMP15, Kit-ligand, AMH, NGF, AKT1 etc. (167). In mice, germ cell nest breakdown begins at E17.5 (419) and continues up to PND4 (189). The maximum number of germ cells were observed at the time of entry of primary oocytes into meiotic prophase, after which up to two-thirds of the germ cells are lost either by autophagy or apoptosis before the ovarian reserve is established (260,420). The ultimate size of the ovarian reserve is determined by the extent of germ cell loss during that period

(260,421). POF or infertility results when there is a defect in either the timing or process of germ cell nest breakdown which can result in improper primordial follicle assembly and/or increased loss of germ cells (418). Therefore, the above period/window is a critical/vulnerable window during fetal ovarian development. Any insult or exposure to chemicals/EDCs during this period could potentially affect the entire fertility of the female offspring during the adult life. Therefore, there is a critical need to study the mechanism of GCN breakdown and germ cell death not only during the normal development of the ovary but also in response to EDCs. In order to identify the mechanism by which gestational exposure to CrVI caused early reproductive senescence, we studied the effect of CrVI on germ cell nest breakdown, primordial follicle assembly and germ cell death during the early development of the ovary.

CrVI increase germ cell apoptosis, accelerate germ cell nest breakdown, and advance the primordial follicle assembly

During oogenesis of developing rodent ovary, germ cell apoptosis occurs at all stages with two main waves: the first wave of cell death coincides with the entry of oogonia into meiosis (E13.5–15.5); and the second wave occurs between E17.5 and PND1, marking the GCN breakdown and the beginning of primordial follicle assembly (10,251,422). Results indicated that CrVI treatment accelerated germ cell nest breakdown and advanced primordial and primary follicle formation. Specifically, on E15.5 and E17.5, rounded germ cell nest containing 10-29 healthy germ cells with no primordial follicles were observed in control group, whereas CrVI treated ovaries exhibited more number of degenerating germ cells with pyknotic nuclei. Control ovaries of PND1 were filled with nests of healthy germ cells surrounded by invading somatic or pre-granulosa cells, whereas CrVI treatment group had an enormous number of primordial follicles and primary follicles indicating early germ cell nest breakdown and advanced primordial and

primary follicle formation. Control ovaries had 10-24 healthy oocytes contained in the nest within the ovigerous cords with the infrequent observation of pyknotic nuclei of germ cells and somatic cells. Whereas, >65% of CrVI treated ovaries had their nest broken down into fewer nests with disrupted ovigerous cords. On PND4, healthy primordial and few primary follicles were observed in control ovaries, whereas CrVI treated ovaries had several primary and few secondary follicles. Thus, it is very evident that prenatal exposure to CrVI adversely affected follicular development process by accelerating the GCN breakdown, and advancing primordial follicle assembly.

Germ cell death is one of the major events that occur during GCN breakdown and follicle formation (409). In the current study, CrVI increased the number of TUNEL-positive germ cells compared to control group on E15.5, E17.5, PND1, PND4, and PND25. It was also observed that most of the primordial and primary follicles were undergoing atresia. Also, eosinophilic infiltration was observed on E15.5 and E17.5. Eosinophil peroxidase has been shown to increase the ability of macrophage to phagocytize tumor cells. We suggested that increased eosinophils in CrVI-exposed ovaries might facilitate the resorption of apoptotic and/or degenerating germ cells. Also, localized eosinophilic infiltration has been linked to POF in women with eosinophilic oophoritis and eosinophilic perifolliculitis, a variant of autoimmune oophoritis (423-426).

Thus the current study documented for the first time that prenatal exposure to CrVI accelerated GCN breakdown, advanced the primordial follicle assembly and caused early reproductive senescence by increasing the germ cell and somatic cell apoptosis. In order to identify the underlying mechanisms behind germ cell death, key apoptotic and cell survival pathways were determined in the PND1 ovary of F1 offspring.

CrVI affects PI3K/AKT & MAPK signaling pathway

The PI3K-AKT signaling pathway plays a key role in critically regulating the ovarian function including survival, quiescence, and activation of primordial follicles, granulosa cell proliferation and differentiation, and meiotic oocyte maturation (427). Dysregulation of this pathway may contribute to infertility caused by impaired follicular development, intra-follicular oocyte development, and ovulation (427). AKT is the master regulator of the PI3K/AKT pathway involved in the following functions: (i) controls cell survival and growth by phosphorylating BAD, FOXO1, GSK3β, and p27; (ii) promotes cell proliferation by phosphorylating and inactivating FOXO3a to sequestrate FOXO3a in the cytoplasm; (iii) regulates cell cycle progression by indirectly stabilizing cyclin D1 and c-Myc*;* (iii) activates AKT, phosphorylates TSC2, and controls mTOR, which in turn controls translation, suppresses autophagy, regulates HIF1α, and VEGF expression (427). The MAPK/ERK signaling pathway have been implicated as key regulators of cell proliferation, differentiation, migration, senescence, and apoptosis (428). While the function of MAPK signaling is largely unknown in the early development of the ovary, recent research suggests that MAPK signaling plays an important role in primordial follicle activation through mTOR-KITL signaling (429). Results from the current study indicated that ovaries from control rats expressed p-AKT and p-ERK abundantly. Whereas CrVI decreased the expression of p-AKT and p-ERK compared to control in PND1 ovaries of F1 pups, suggesting that CrVI may have accelerated germ cell nest breakdown and increased germ cell death partly by decreasing the levels of p-AKT and p-ERK, which are critical for the growth and survival of germ cells.

CrVI disrupts germ cell survival by targeting XIAP

XIAP is also known as BIRC4 (baculoviral IAP repeat-containing protein 4) belongs to the *inhibitor of apoptosis protein family* that regulates apoptotic signaling by directly interacting with caspase targets, including caspases-3, -7 and -9 (430-432). In rats, XIAP is found to be expressed in granulosa cells, theca cells and oocytes of follicles from the preantral stage onwards (433). It has been reported that XIAP self-degrades *in vitro* in a proteasome-dependent manner in response to apoptotic stimuli by self-ubiquitination due to its ubiquitin-protein ligase activity (434). Apart from self-ubiquitination and degradation, XIAP also acts as an ubiquitin-protein ligase for caspase-3 which promotes the degradation of caspase-3 by ubiquitination, resulting in anti-apoptosis or cell survival (435). XIAP also mediates the polyubiquitination of caspase-9 (436). In the current study, CrVI decreased the expression of XIAP and increased the expression of cleaved caspase-3 in PND1 ovary suggesting a CrVI-induced down-regulation of XIAP by self-ubiquitination. On the other hand, with a decreased expression of XIAP, caspase-3 might have become more stable and functional. Thus by decreasing XIAP expression or increasing its degradation and upregulating cleaved caspase-3, CrVI might have increased or activated germ cells apoptosis.

CrVI increases germ cell apoptosis through intrinsic apoptosis pathway

BAX is a pro-apoptotic factor belonging to the family of BCL2 proteins that play a key role in regulating the size of the primordial follicle pool (254,255). It is upregulated in fetal germ cells undergoing apoptosis in the ovary and serves as a POF marker (255,437,438). Prolonged reproductive longevity was observed in BAX mutant mice due to slower depletion of the primordial follicle reserve (255). In the current study, CrVI increased BAX expression. Thus, increased BAX might have contributed to the increased germ cell apoptosis and atresia of follicles resulting in POF. A significant increase in the expression of cleaved caspase-3 that is downstream

of BAX was also observed in the ovaries of CrVI-exposed F1 rats, suggesting the caspase-3 dependent mechanism of germ cell apoptosis. On the other hand, undetected levels of cleaved caspase-3 expression in control ovaries suggests the likelihood of caspase-3-independent mechanism of germ cell apoptosis during the normal development of ovary. This data is supported by a study in mice where a similar phenomenon of caspase-3-independent mechanism was reported in the germ cell apoptosis (439). Notably, Akt-dependent phosphorylation of pro-apoptotic BAX on Ser^{184} suppresses its translocation to mitochondria (440) thereby preventing the release of cytochrome *c* from mitochondria and activation of caspases to make the cell undergo apoptosis. Thus CrVI-induced increase in germ cell apoptosis might have been partly mediated through down regulation of AKT and also by increasing the expression of BAX, leading to increased translocation to mitochondria to execute apoptosis.

In addition, CrVI increased the expression of p27 protein. p27 is a negative regulator of cell cycle progression and also a tumor suppressor protein (441). It has also been reported that caspase-9, -3, -7- PARP apoptosis pathway is suppressed in $p27^{-/-}$ ovaries leading to increased follicle survival. p27 induces follicular atresia by inhibiting Cdk2/Cdc2-cyclin A/B1 kinase activities and activating apoptotic cascade in follicles (413). Our data revealed higher expression of p27 in the ovaries of CrVI-exposed F1 offspring with predominant expression in somatic cells and not in oocytes. Thus, increased somatic cells apoptosis and disrupted paracrine communication between germ cells and somatic cells by upregulating p27 may have potentially contributed to follicle atresia.

CrVI promoted p53 translocation to the mitochondria and inhibition of SOD2 activity

p53 is a well-established homotetrameric transcription factor that plays a key role in tumor suppression *by* inducing apoptosis or cell cycle arrest by transcriptional and post-translational

mechanisms. It induces apoptosis by translocating to mitochondria and promoting changes in mitochondrial membrane potential, cytochrome c release and caspase activation (442). Oxidative stress-induced apoptosis involves phosphorylation of p53 at multiple sites of serine. Previous finding from our lab indicated that CrVI phosphorylated p53 protein at ser-9, ser-15, ser-20, ser-37, ser-46 and ser-392, and got translocated to mitochondria to induce apoptosis of granulosa cells (443). In the present study, CrVI up-regulated the expression of p53, while the levels are undetected in control ovaries. Interestingly, CrVI also upregulated the expression of SOD-2 (MnSOD-manganese superoxide dismutase) which is the mitochondrial antioxidant enzyme that detoxifies the superoxide free radical ($O_2^{\bullet -}$) generated by mitochondrial respiration (442). It has been reported that p53 localizes to the matrix of the mitochondria and physically interact with SOD-2 and increases oxidative stress by inhibiting its superoxide scavenging activity (415,442). Therefore, in the present study, we performed two-color immunofluorescence on whole mount ovaries to test whether CrVI increases p53-SOD2 colocalization. Interestingly, CrVI upregulated the expression of both p53 and SOD2 confirming the immunohistochemistry results, and also increased the co-localization of p53 and SOD-2 in PND1 ovaries. Thus, CrVI not only increased the expression of p53 and SOD-2 but also enhanced the association between p53-SOD2, enhanced translocation of p53 to mitochondria to bind with SOD2 and to inhibit ROS scavenging of SOD-2. All these events could potentially increase oxidative stress followed by germ cells apoptosis and early germ cell nest breakdown.

Taken together, as given in our working model (Fig. 3.12), CrVI is rapidly transported into the cells and reduced to CrIII. During this reduction process, a large amount of reactive oxygen species is generated, which increases oxidative stress and depletes antioxidants. In turn, CrIII either dephosphorylates or reduces the phosphorylation of p-AKT and p-ERK, decreases XIAP

and thus inhibits cell survival machinery. CrIII up-regulates caspase-3 and BAX which leads to increased apoptosis of germ cells. CrIII also increases the expression and activation of p53 and facilitates the mitochondrial transport of p53. p53 interacts with SOD-2 and arrests its scavenging of reactive oxygen species which, in turn, augments the apoptotic response in germ cells. As a result of these molecular events, the large majority of the germ cells undergo apoptosis, or prematurely assemble into primordial follicles and transit into primary follicles, thus reducing the healthy primordial follicle pool.

In summary, these studies indicate that CrVI causes early reproductive senescence by (i) increasing germ cell apoptosis through the p53/p27–BAX–caspase-3pathway; (ii) advancing germ cell nest break down and primordial follicle assembly; (iii) increasing primordial follicle transition into primary follicles; (iv) increasing follicular atresia; and (v) depleting the healthy primordial follicle pool resulting in a reduced follicular reserve.

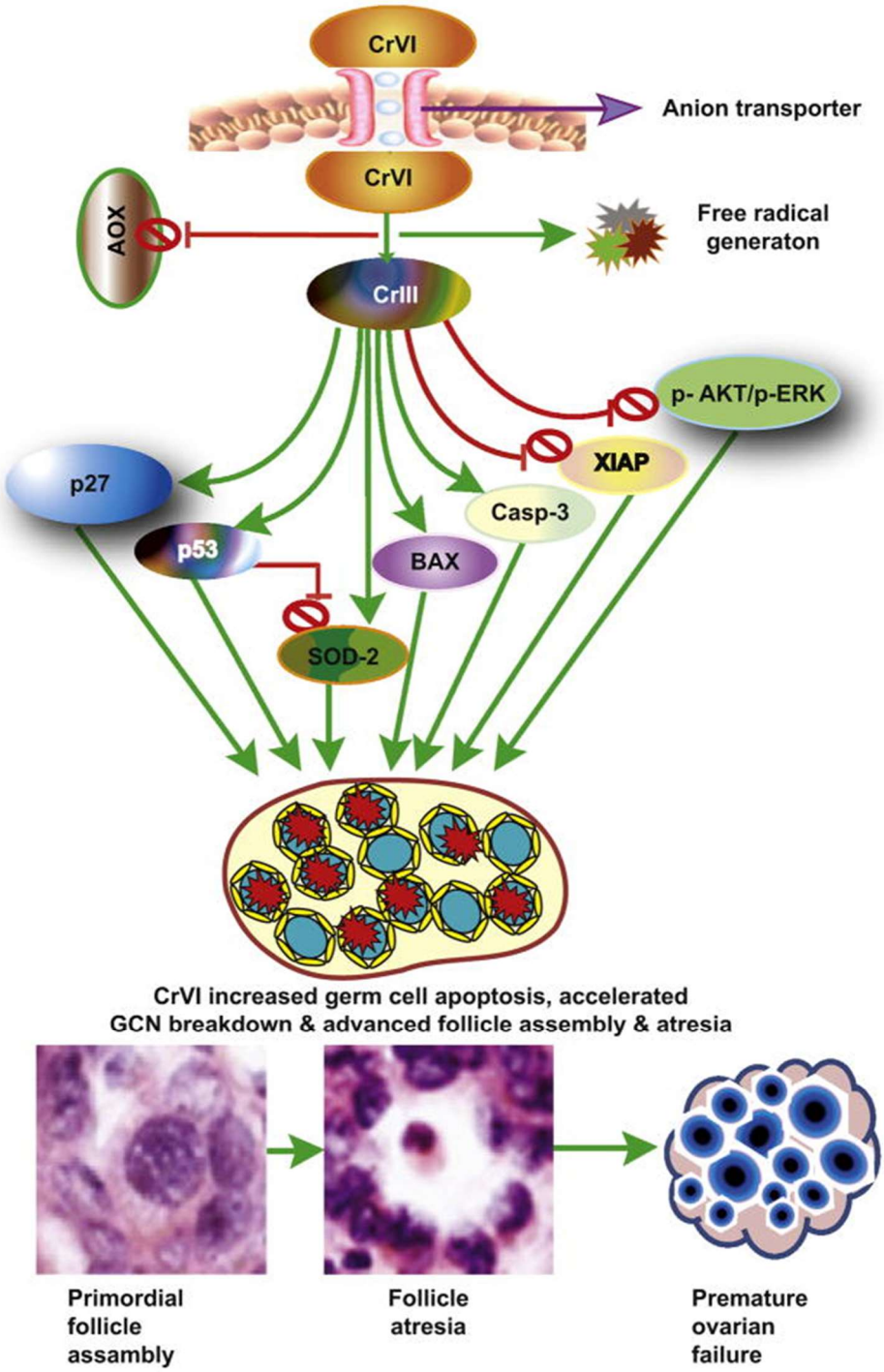

Fig. 3.12. Schematic diagram representing CrVI-induced ovotoxicity during fetal ovary development.

4. ROLE OF SIRTUIN-1 ON CRVI-INDUCED GERM CELL APOPTOSIS MEDIATED THROUGH P53 ACETYLATION

Specific Aim-2*:*

Determine the p53-mediated mechanisms on CrVI-induced germ cell apoptosis in F1 offspring.

Hypothesis:

This aim was based on the working hypothesis that "*CrVI-induced germ cell apoptosis and advancement of germ cell nest breakdown are mediated through a p53-miR34a-SIRT1 signaling network"*.

Objectives*:*

The above *hypothesis* was tested by the following objectives: (i) to study the effect of CrVI on expression of acetylated p53 (K-382), SIRT1 and miR34a; (ii) to delineate the mechanism of CrVI on p53 activation by injecting CrVI-treated pregnant rats with various doses of EX-527, a SIRT1 inhibitor; (iii) to determine the effects of EX-527 on apoptosis of germ cells; and (iv) to understand the effects of SIRT1 inhibitor on the anti-apoptotic proteins BCL2, BCL-XL, pAKT and pro-apoptotic proteins BAX, cleaved Caspase-3 and PUMA.

Results

Inhibition of SIRT1 aggravates CrVI induced germ cell apoptosis

In the current study, ovaries from PND1 pups that were exposed to CrVI showed a significant increase in the percentage of apoptotic germ cells with pyknotic nuclei compared to control group. TUNEL staining revealed that administration of SIRT1 inhibitor increased germ cell apoptosis in a dose-dependent manner (Fig. 4.1, A, D, G, J, & M). SIRT1 inhibitor also enhanced CrVI-induced germ cell apoptosis in a dose-dependent manner (Fig. 4.1, B, E, H, K, & N). The lowest dose of SIRT1 inhibitor (1mg/kg b.wt) did not have significant effects on germ cell apoptosis in either control or CrVI-treated group. However, higher doses (5 mg/kg b.wt and 50 mg/kg b.wt) significantly increased germ cell apoptosis both under normal as well as CrVI-treated groups (Fig. 4.1, N).

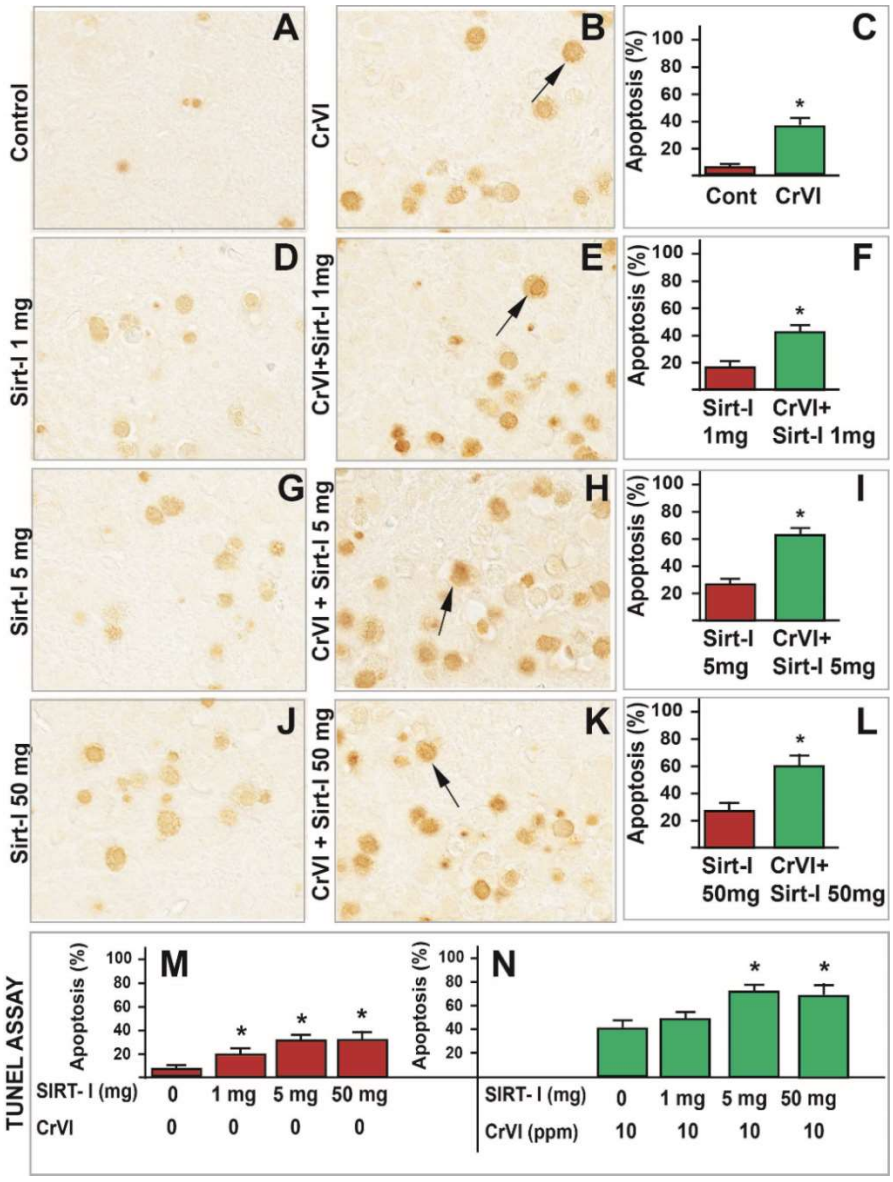

Fig. 4.1. Effect of SIRT1 inhibitor (EX-527) on CrVI-induced germ cell apoptosis. Pregnant dams were exposed to CrVI (10 ppm) through the drinking water from 9.5-14.5 dpc. CrVI exposed and unexposed dams were injected (*i.p.,)* with various doses of SIRT1 inhibitor (SIRT-I, 1.0, 5.0 and 50 mg/kg body weight). On PND1 the F1 offspring were euthanized and ovaries were processed for TUNEL assay as described under *Materials and Methods*. Representative images of ovaries are shown from control (A), CrVI (B), SIRT1-I alone 1.0 mg (D), 5.0 mg (G), and 50 mg (J) /kg body weight. Representative images from the ovaries of CrVI-treated dams: CrVI+SIRT1-I, 1.0 mg (E), 5.0 mg (H), and 50 mg (K) are shown. Histogram shows percentage of TUNEL-positive apoptotic cells (C-L). Each value is mean ±SEM of 10 ovaries from five litters. Dose response of SIRT1-I in the absence of CrVI treatment (M) and presence of CrVI treatment (N) is shown. *: control vs CrVI (C), SIRT1-I-1.0 mg vs CrVI+SIRT1-I-1.0 mg (F), SIRT1-I-5.0 mg vs CrVI+SIRT1-I-5.0 mg (I), or SIRT1-I-50 mg vs CrVI+SIRT1-I-50 mg (L). (M) Control vs SIRT1-I 1.0, 5.0 or 50 mg/kg body weight. (N) CrVI (10 ppm) vs CrVI+SIRT1-1 (1.0, 5.0 or 50 mg/kg *b.wt*). $p<0.05$. Arrows indicate apoptotic TUNEL-positive cells.

Dose-response of SIRT1 inhibitor (EX-527) on the CrVI-induced regulation of acetylated-p53

Results from Specific Aim-1 indicated that CrVI increased the expression of p53 in PND1 ovaries. Also, CrVI decreased SIRT1 expression in PND1 ovaries (Fig. 4.2, A, B, & C). It has been reported that EX-527 treatment increased acetylation of p53 (Lysine (K) 382) after DNA damage in primary human mammary epithelial cells and several cell lines (444). In order to understand if CrVI increased germ cell apoptosis by increased p53 acetylation, expression of p53 (K-382) was studied in the ovaries exposed to SIRT1 inhibitor. Results indicate that (i) SIRT1 inhibitor significantly increased acetyl-p53 (K382) expression in PND1 ovaries in a dose-dependent manner under basal condition (Fig. 4.2, A, D, G, J, & M); (ii) CrVI significantly ($p<0.05$) increased the expression of acetyl-p53 (K-382) in PND1 ovaries (Fig. 4.2, A, B, & C); and (iii) SIRT1 inhibitor attenuated CrVI-induced increase in the expression of acetyl-p53 (K-382) at the dose of 5 mg/kg b.wt and 50 mg/kg b.wt, but not 1 mg/kg b.wt (Fig. 4.2, B, E, H, K, & N).

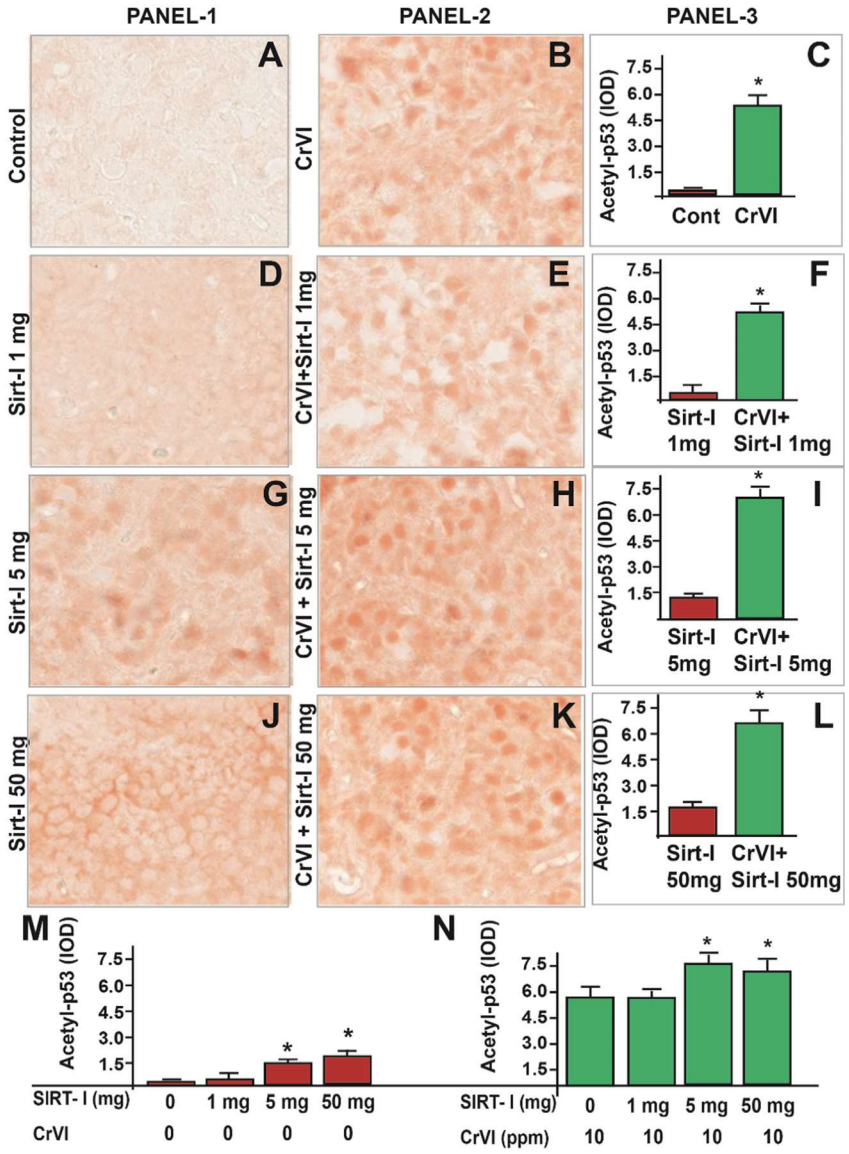

Fig. 4.2. SIRT1 inhibitor (EX-527) attenuated CrVI-induced increase in acetyl-p53 expression in the PND1 ovary. Pregnant dams were exposed to CrVI (10 ppm) through the drinking water from 9.5-14.5 dpc. CrVI exposed and unexposed dams were injected (*i.p.,)* with various doses of SIRT1 inhibitor (SIRT-I, 1.0, 5.0 and 50 mg/kg body weight). On PND1 the F1 offspring were euthanized and ovaries were processed for Immunohistochemistry as described under *Materials and Methods*. Representative images of ovaries from control (A), CrVI (B), SIRT1-I alone 1.0 mg (D), 5.0 mg (G), and 50 mg (J) /kg body weight. Representative images from the ovaries of CrVI-treated dams: CrVI+SIRT1-I, 1.0 mg (E), CrVI+SIRT1-I, 5.0 mg (H), and CrVI+SIRT1-I, 50 mg (K). Histogram shows integrated optical density (IOD) (Panel-3, C, F, I and L). Each value is mean ±SEM of 10 ovaries from five litters. Dose-response of SIRT1-I in the absence of CrVI treatment (M) and presence of CrVI treatment (N) is shown. *: control vs CrVI (C), SIRT1-I-1.0 mg vs CrVI+SIRT1-I-1.0 mg (F), SIRT1-I-5.0 mg vs CrVI+SIRT1-I-5.0 mg (I), or SIRT1-I-50 mg vs CrVI+SIRT1-I-50 mg (L). (M) Control vs SIRT1-I 1.0, 5.0 or 50 mg/kg body weight. (N) CrVI (10 ppm) vs CrVI+SIRT1-1 (1.0, 5.0 or 50 mg/kg b.wt). $p<0.05$.

CrVI and SIRT1 inhibition increases miR34a expression

It has been shown that miR34a is one of the miRNAs which can regulate the expression of SIRT1 by targeting it directly (445). Interestingly, p53 regulates the expression of miR34a and induces apoptosis, cell cycle arrest, and senescence (290). Results from *Specific Aim-1* indicate that CrVI increased the expression of acetyl-p53 (K-382) in PND1 ovaries. In order to understand if CrVI-induced acetyl-p53 (K-382) expression regulates the miR34a expression which could in turn regulate SIRT1, expression of miR34a was studied in the ovaries exposed to SIRT1 inhibitor. Results indicated that (i) CrVI significantly *($p<0.05$)* increased miR34a expression in PND1 ovaries; and (ii) treatment with SIRT1 inhibitor synergistically enhanced CrVI-induced increase in the expression of miR34a (Fig. 4.3).

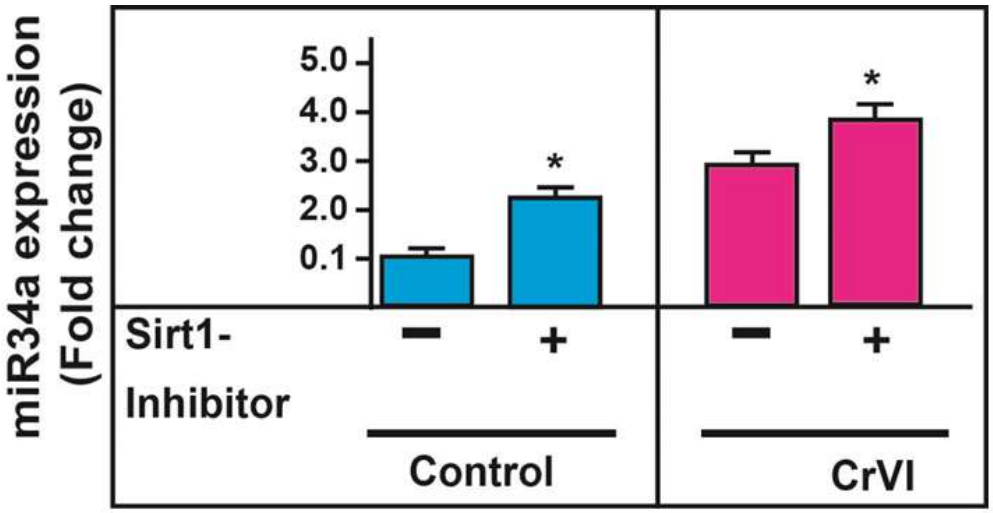

Fig. 4.3. Effect of CrVI and SIRT1 inhibitor (EX-527) on miR34a expression. Pregnant dams were exposed to CrVI (10 ppm) through the drinking water from 9.5-14.5 dpc. CrVI exposed and unexposed dams were injected (*i.p.,)* with 50 mg/kg body weight SIRT1 inhibitor. On PND1 the F1 offspring were euthanized and ovaries were processed for RNA isolation and real-time PCR of miR34a was performed as described under *Materials and Methods*. Histogram shows the fold change normalized to the internal control U6. Each value is mean ±SEM of 3 replicates. *: Control vs SIRT1-I-50 mg/kg body weight, CrVI (10 ppm) vs CrVI+SIRT1-1-50 mg/kg *b.wt*. $p<0.05$.

Dose-response of SIRT1 inhibitor (EX-527) on the CrVI-induced regulation of* BCL*2

BCL2 is an important cell survival protein that prevents apoptosis by directly binding and inhibiting the pro-apoptotic BAX and BAK (446). Over expression of BCL*2* in the oocytes increased the size of the primordial follicle pool at birth in mice (250). In order to understand if BCL2 is regulated through SIRT1, BCL2 expression was studied in the ovaries exposed to the SIRT1 inhibitor. Results indicate that (i) BCL2 is abundantly expressed in the control ovaries of PND1 pups (Fig. 4.4, A); (ii) CrVI significantly ($p<0.05$) decreased the expression of BCL2 compared to control (Fig. 4.4, A, B, & C); (iii) SIRT1 inhibitor decreased the expression of BCL2 in a dose-dependent manner in PND1 ovaries (Fig. 4.4, A, D, G, J, & M); (iv) SIRT1 inhibitor attenuated CrVI-induced decrease in the expression of BCL2 at the dose of 5 mg/kg b.wt and 50 mg/kg b.wt significantly ($p<0.05$), but not 1 mg/kg b.wt (Fig. 4.4, B, E, H, K, & N).

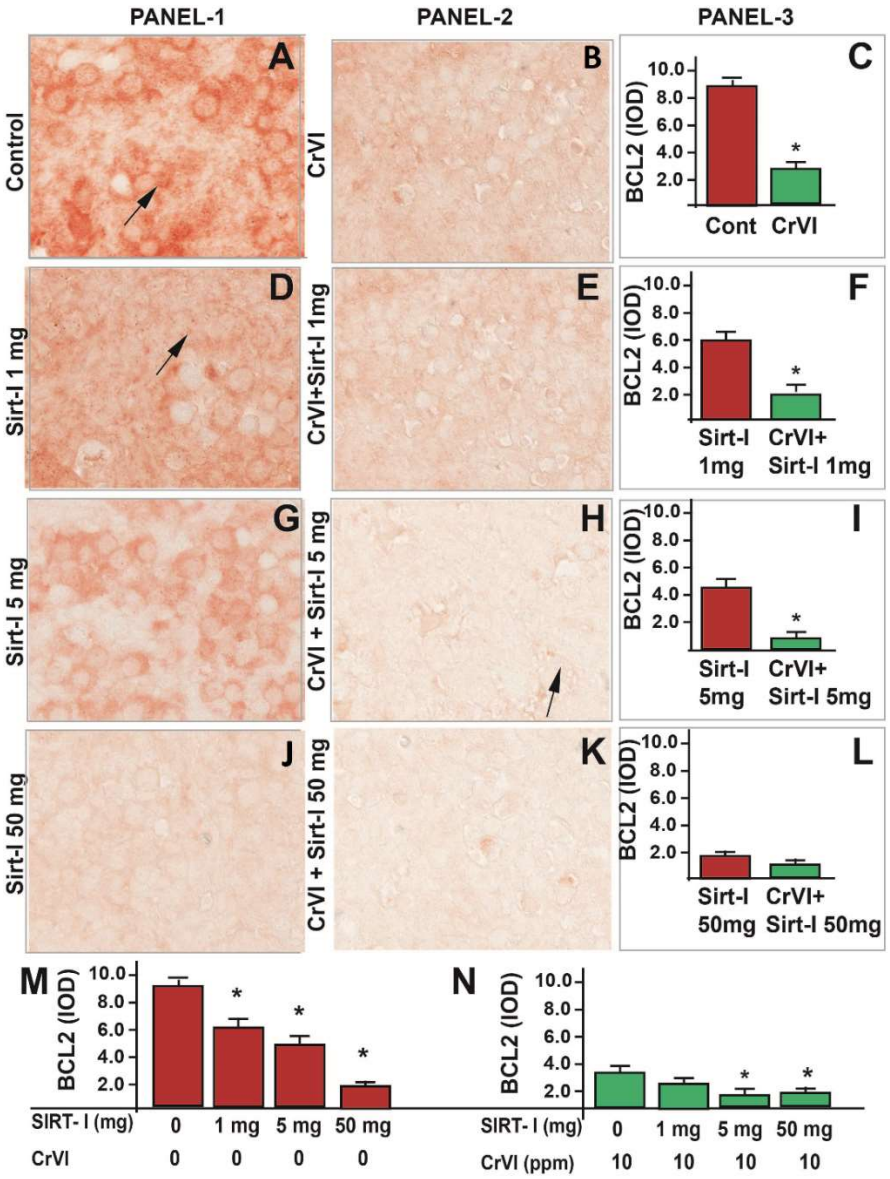

Fig. 4.4. SIRT1 inhibitor (EX-527) attenuated CrVI-induced decrease in BCL2 expression in the PND1 ovary. Pregnant dams were exposed to CrVI (10 ppm) through the drinking water from 9.5-14.5 dpc. CrVI exposed and unexposed dams were injected (*i.p.,)* with various doses of SIRT1 inhibitor (SIRT-I, 1.0, 5.0 and 50 mg/kg body weight). On PND1 the F1 offspring were euthanized and ovaries were processed for Immunohistochemistry as described under *Materials and Methods*. Representative images of ovaries from control (A), CrVI (B), SIRT1-I alone 1.0 mg (D), 5.0 mg (G), and 50 mg (J) /kg body weight. Representative images from the ovaries of CrVI-treated dams: CrVI+SIRT1-I, 1.0 mg (E), CrVI+SIRT1-I, 5.0 mg (H), and CrVI+SIRT1-I, 50 mg (K). Histogram shows integrated optical density (IOD) (Panel-3, C, F, I and L). Each value is mean ±SEM of 10 ovaries from five litters. Dose-response of SIRT1-I in the absence of CrVI treatment (M) and presence of CrVI treatment (N) is shown. *: control vs CrVI (C), SIRT1-I-1.0 mg vs CrVI+SIRT1-I-1.0 mg (F), or SIRT1-I-5.0 mg vs CrVI+SIRT1-I-5.0 mg (I). (M) Control vs SIRT1-I 1.0, 5.0 or 50 mg/kg b.wt. (N) CrVI (10 ppm) vs CrVI+SIRT1-1 (1.0, 5.0 or 50 mg/kg b.wt). $p<0.05$.

Dose-response of SIRT1 inhibitor (EX-527) on the CrVI-induced regulation of* BCL-*XL

BCL-XL is an anti-apoptotic protein that plays a key role in determining germ cell fate in early gonadal development (447). Mice deficient in BCL-XL showed a decrease in number of primordial follicles compared to wild type (252). In order to understand if BCL-XL is regulated through SIRT1, BCL-XL expression was studied in the ovaries exposed to SIRT1 inhibitor. Results indicate that (i) BCL-XL is abundantly expressed in the primordial germ cells of control ovaries of PND1 pups (Fig. 4.5, A); (ii) CrVI significantly ($p<0.05$) decreased the expression of BCL-XL compared to control (Fig. 4.5, A, B, & C); (iii) SIRT1 inhibitor decreased the expression of BCL-XL in a dose-dependent manner in PND1 ovaries (Fig. 4.5, A, D, G, J, & M); (iv) SIRT1 inhibitor attenuated CrVI-induced decrease in the expression of BCL-XL at the dose of 50 mg/kg b.wt significantly ($p<0.05$), but not 1 mg/kg b.wt and 5 mg/kg b.wt (Fig. 4.5, B, E, H, K, & N).

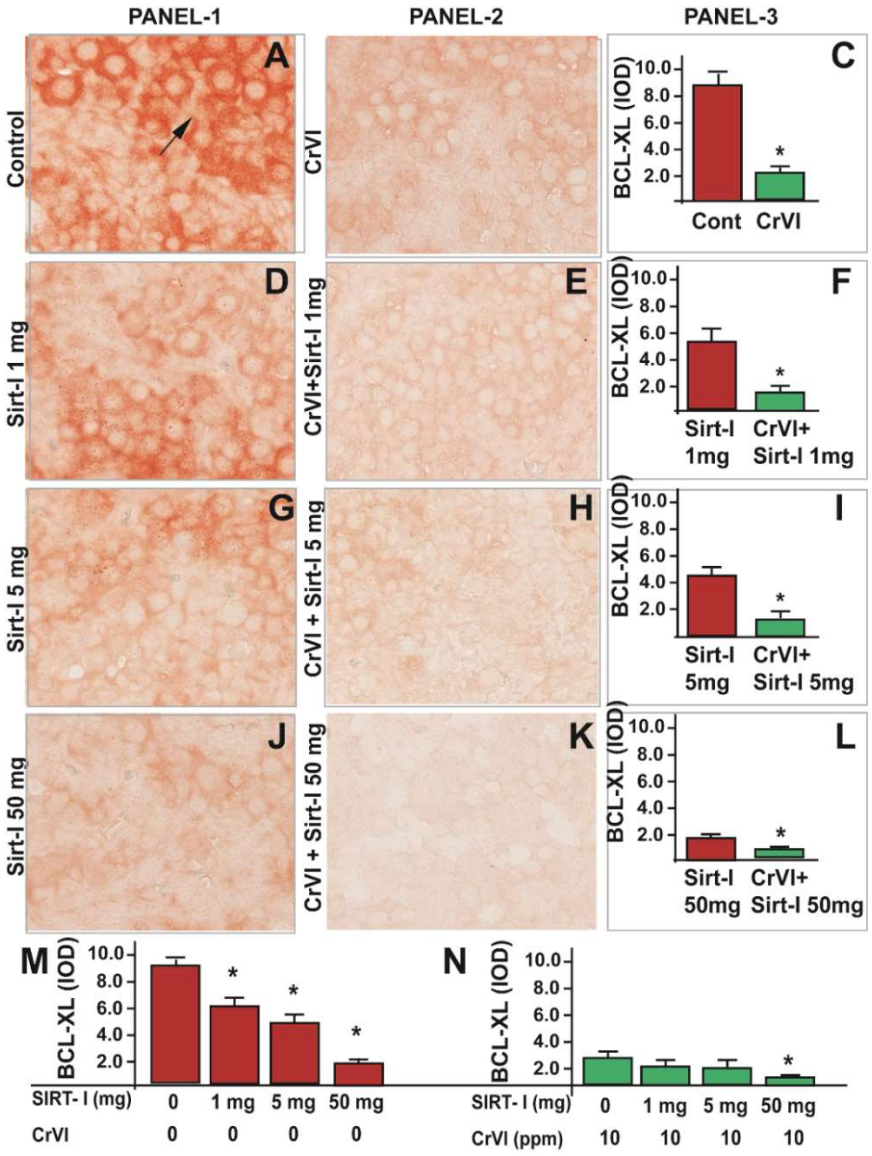

Fig. 4.5. SIRT1 inhibitor (EX-527) attenuated CrVI-induced decrease in BCL-XL expression in the PND1 ovary. Pregnant dams were exposed to CrVI (10 ppm) through the drinking water from 9.5-14.5 dpc. CrVI exposed and unexposed dams were injected (*i.p.,)* with various doses of SIRT1 inhibitor (SIRT-I, 1.0, 5.0 and 50 mg/kg body weight). On PND1 the F1 offspring were euthanized and ovaries were processed for Immunohistochemistry as described under *Materials and Methods*. Representative images of ovaries from control (A), CrVI (B), SIRT1-I alone 1.0 mg (D), 5.0 mg (G), and 50 mg (J) /kg body weight. Representative images from the ovaries of CrVI-treated dams: CrVI+SIRT1-I, 1.0 mg (E), CrVI+SIRT1-I, 5.0 mg (H), and CrVI+SIRT1-I, 50 mg (K). Histogram shows integrated optical density (IOD) (Panel-3, C, F, I and L). Each value is mean ±SEM of 10 ovaries from five litters. Dose-response of SIRT1-I in the absence of CrVI treatment (M) and presence of CrVI treatment (N) is shown. *: control vs CrVI (C), SIRT1-I-1.0 mg vs CrVI+SIRT1-I-1.0 mg (F), or SIRT1-I-5.0 mg vs CrVI+SIRT1-I-5.0 mg (I). (M) Control vs SIRT1-I 1.0, 5.0 or 50 mg/kg b.wt. (N) CrVI (10 ppm) vs CrVI+SIRT1-1 (1.0, 5.0 or 50 mg/kg b.wt). $p<0.05$. Arrow indicates healthy germ cells in the nest expressing BCL-XL.

Dose-response of SIRT1 inhibitor (EX-527) on the CrVI-induced regulation of pAKT

PI3K/AKT pathway is very important for the survival, dormancy, and activation of the primordial follicle and any disruption of AKT pathway could lead to infertility (427). AKT is the critical regulator of cell survival and proliferation (448). Results from *Specific Aim-1* indicated that CrVI decreased pAKT expression in postnatal ovaries (Fig. 3.5, A, B, & C). In order to understand if AKT is regulated through SIRT1, AKT expression was studied in the ovaries exposed to the SIRT1 inhibitor. Results indicate that (i) SIRT1 inhibitor decreased pAKT expression in PND1 ovaries in a dose-dependent manner (Fig. 4.6, A, D, G, J, & M); (ii) CrVI significantly ($p<0.05$) decreased pAKT (Fig. 4.6, A, B, & C); and (iii) SIRT1 inhibitor attenuated CrVI-induced decrease in the expression of pAKT at all three doses (1 mg/kg b.wt, 5 mg/kg b.wt, and 50 mg/kg b.wt) (Fig. 4.6, B, E, H, K, & N).

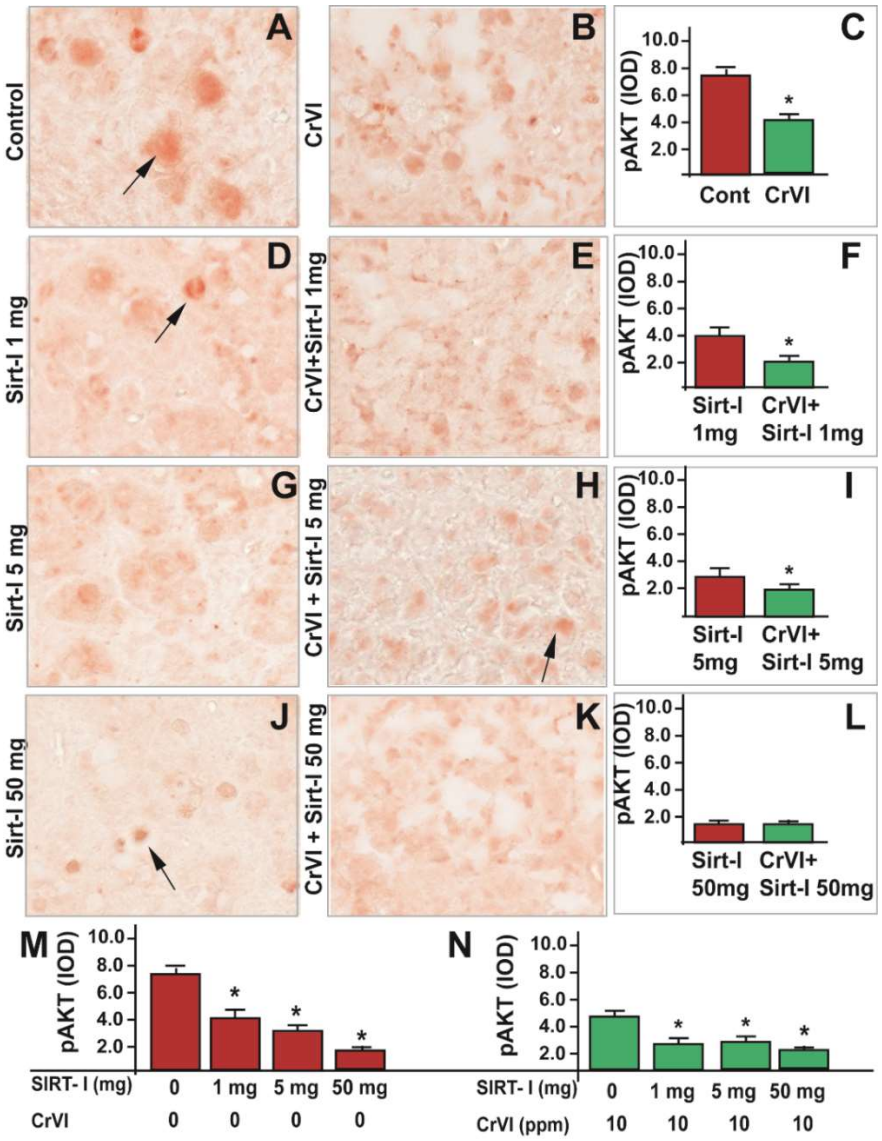

Fig. 4.6. SIRT1 inhibitor (EX-527) attenuated CrVI-induced decrease in pAKT expression in the PND1 ovary. Pregnant dams were exposed to CrVI (10 ppm) through the drinking water from 9.5-14.5 dpc. CrVI exposed and unexposed dams were injected (*i.p.,)* with various doses of SIRT1 inhibitor (SIRT-I, 1.0, 5.0 and 50 mg/kg body weight). On PND1 the F1 offspring were euthanized and ovaries were processed for Immunohistochemistry as described under *Materials and Methods*. Representative images of ovaries from control (A), CrVI (B), SIRT1-I alone 1.0 mg (D), 5.0 mg (G), and 50 mg (J) /kg body weight. Representative images from the ovaries of CrVI-treated dams: CrVI+SIRT1-I, 1.0 mg (E), CrVI+SIRT1-I, 5.0 mg (H), and CrVI+SIRT1-I, 50 mg (K). Histogram shows integrated optical density (IOD) (Panel-3, C, F, I and L). Each value is mean ±SEM of 10 ovaries from five litters. Dose-response of SIRT1-I in the absence of CrVI treatment (M) and presence of CrVI treatment (N) is shown. *: control vs CrVI (C), SIRT1-I-1.0 mg vs CrVI+SIRT1-I-1.0 mg (F), SIRT1-I-5.0 mg vs CrVI+SIRT1-I-5.0 mg (I), or SIRT1-I-50 mg vs CrVI+SIRT1-I-50 mg (L). (M) Control vs SIRT1-I 1.0, 5.0 or 50 mg/kg body weight. (N) CrVI (10 ppm) vs CrVI+SIRT1-1 (1.0, 5.0 or 50 mg/kg b.wt). $p<0.05$. Arrows indicate oocytes expressing pAKT.

Dose response of SIRT1 inhibitor (EX-527) on CrVI-induced regulation of p53 upregulated modulator of apoptosis (PUMA)

Results from *Specific Aim-1* indicate that CrVI increased the expression of p53 in PND1 ovaries. PUMA (p53 upregulated modulator of apoptosis) is the direct target of p53, and a critical regulator of germ cell death during ovarian development. PUMA-mediated cell death limits the primordial follicle number established in the initial ovarian reserve (421). In order to understand if PUMA is regulated through SIRT1, expression of PUMA was studied in the ovaries exposed to SIRT1 inhibitor. Results indicated that (i) SIRT1 inhibitor significantly increased the expression of PUMA in PND1 ovaries at the dose of 5 mg/kg b.wt and 50 mg/kg b.wt, but not 1mg (Fig. 4.7, A, D, G, J, & M); (ii) CrVI significantly ($p<0.05$) increased the expression of PUMA (Fig. 4.7, A, B, & C); and (iii) SIRT1 inhibitor attenuated CrVI-induced increase in the expression of PUMA in a dose dependent manner (Fig. 4.7, B, E, H, K, & N).

.

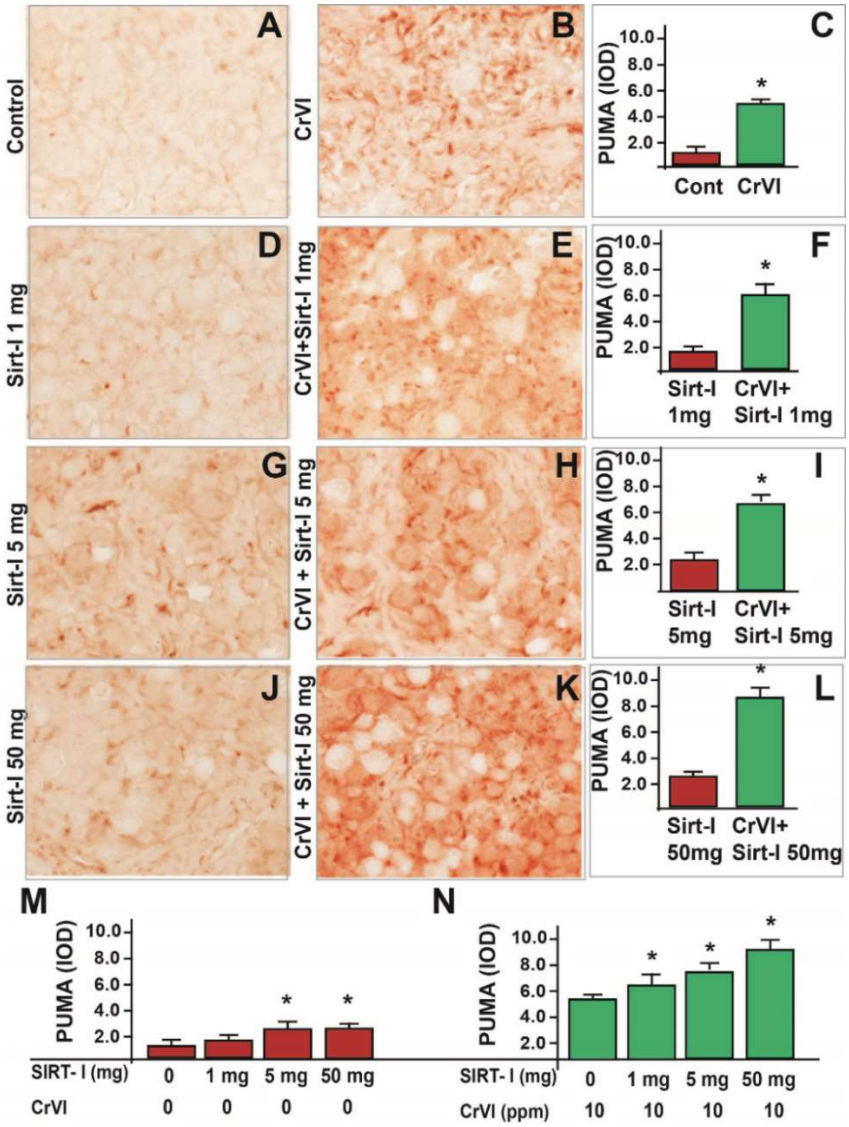

Fig. 4.7. SIRT1 inhibitor (EX-527) attenuated CrVI-induced increase in PUMA expression in the PND1 ovary. Pregnant dams were exposed to CrVI (10 ppm) through the drinking water from 9.5-14.5 dpc. CrVI exposed and unexposed dams were injected (*i.p.,)* with various doses of SIRT1 inhibitor (SIRT-I, 1.0, 5.0 and 50 mg/kg body weight). On PND1 the F1 offspring were euthanized and ovaries were processed for Immunohistochemistry as described under *Materials and Methods*. Representative images of ovaries from control (A), CrVI (B), SIRT1-I alone 1.0 mg (D), 5.0 mg (G), and 50 mg (J) /kg body weight. Representative images from the ovaries of CrVI-treated dams: CrVI+SIRT1-I, 1.0 mg (E), CrVI+SIRT1-I, 5.0 mg (H), and CrVI+SIRT1-I, 50 mg (K). Histogram shows integrated optical density (IOD) (Panel-3, C, F, I and L). Each value is mean ±SEM of 10 ovaries from five litters. Dose-response of SIRT1-I in the absence of CrVI treatment (M) and presence of CrVI treatment (N) is shown. *: control vs CrVI (C), SIRT1-I-1.0 mg vs CrVI+SIRT1-I-1.0 mg (F), SIRT1-I-5.0 mg vs CrVI+SIRT1-I-5.0 mg (I), or SIRT1-I-50 mg vs CrVI+SIRT1-I-50 mg (L). (M) Control vs SIRT1-I 1.0, 5.0 or 50 mg/kg body weight. (N) CrVI (10 ppm) vs CrVI+SIRT1-1 (1.0, 5.0 or 50 mg/kg b.wt). $p<0.05$. Arrow indicates healthy follicle (D) and follicle undergoing apoptosis (H).

Dose response of SIRT1 inhibitor (EX-527) on the CrVI-induced regulation of BAX

BAX regulates the primordial germ cell survival and apoptosis in mice (252). BAX mutant mice exhibited three times larger follicle pool when compared to wild-type (254). In order to understand if BAX is regulated through SIRT1, BAX expression was studied in the ovaries exposed to the SIRT1 inhibitor. Results indicate that (i) SIRT1 inhibitor significantly increased BAX expression in PND1 ovaries at the dose of 5 mg/kg b.wt and 50 mg/kg b.wt, but not 1 mg/kg b.wt (Fig. 4.8, A, D, G, J, & M); (ii) CrVI significantly ($p<0.05$) increased the expression of BAX (Fig. 4.8, A, B, & C); and (iii) SIRT1 inhibitor attenuated CrVI-induced increase in the expression of BAX at the dose of 5 mg/kg b.wt and 50 mg/kg b.wt, but not 1 mg/kg b.wt (Fig. 4.8, B, E, H, K, & N).

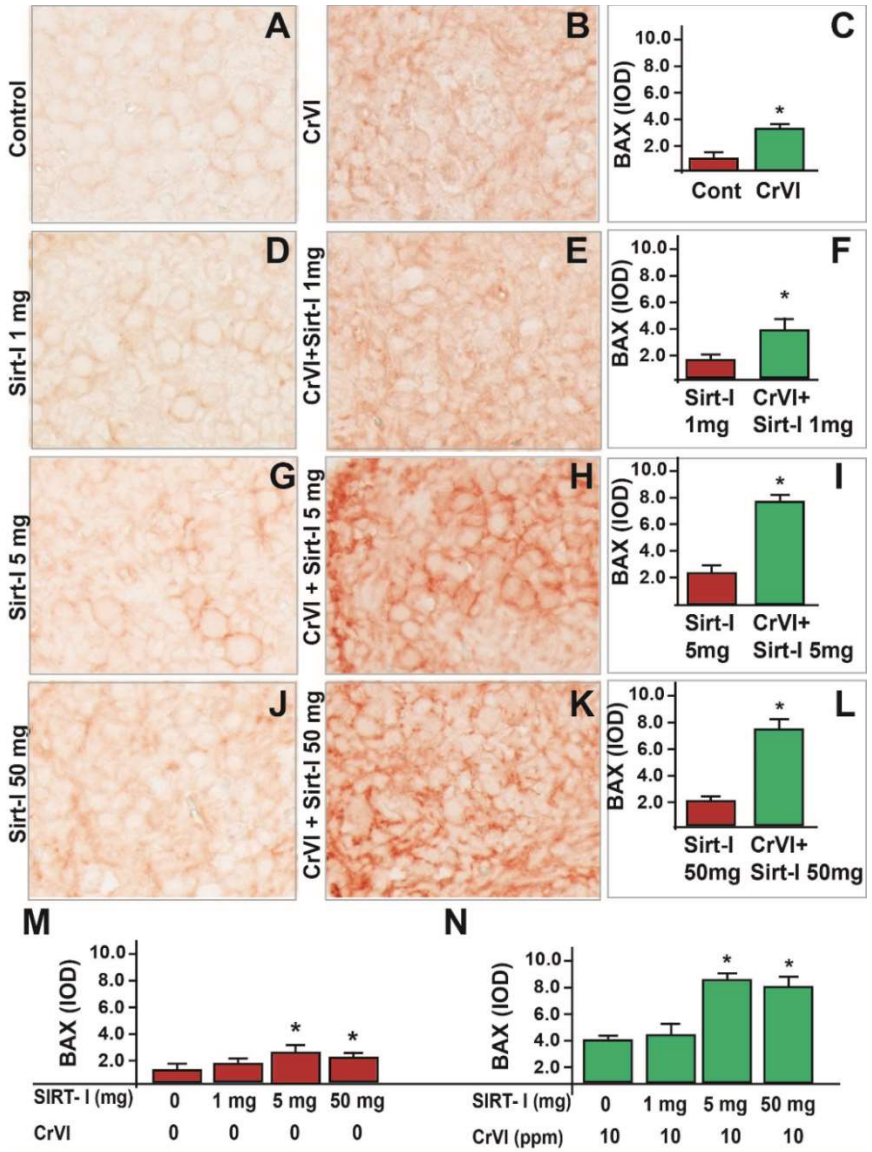

Fig. 4.8. SIRT1 inhibitor (EX-527) attenuates CrVI-induced increase in BAX expression in the PND1 ovary. Pregnant dams were exposed to CrVI (10 ppm) through the drinking water from 9.5-14.5 dpc. CrVI exposed and unexposed dams were injected (*i.p.,)* with various doses of SIRT1 inhibitor (SIRT-I, 1.0, 5.0 and 50 mg/kg body weight). On PND1 the F1 offspring were euthanized and ovaries were processed for Immunohistochemistry as described under *Materials and Methods*. Representative images of ovaries from control (A), CrVI (B), SIRT1-I alone 1.0 mg (D), 5.0 mg (G), and 50 mg (J) /kg body weight. Representative images from the ovaries of CrVI-treated dams: CrVI+SIRT1-I, 1.0 mg (E), CrVI+SIRT1-I, 5.0 mg (H), and CrVI+SIRT1-I, 50 mg (K). Histogram shows integrated optical density (IOD) (Panel-3, C, F, I and L). Each value is mean ±SEM of 10 ovaries from five litters. Dose-response of SIRT1-I in the absence of CrVI treatment (M) and presence of CrVI treatment (N) is shown. *: control vs CrVI (C), SIRT1-I-1.0 mg vs CrVI+SIRT1-I-1.0 mg (F), SIRT1-I-5.0 mg vs CrVI+SIRT1-I-5.0 mg (I), or SIRT1-I-50 mg vs CrVI+SIRT1-I-50 mg (L). (M) Control vs SIRT1-I 1.0, 5.0 or 50 mg/kg body weight. (N) CrVI (10 ppm) vs CrVI+SIRT1-1 (1.0, 5.0 or 50 mg/kg b.wt). $p<0.05$.

Dose response of SIRT1 inhibitor (EX-527) on CrVI-induced regulation of cleaved caspase-3

Results from Specific Aim-1 indicated that CrVI increased cleaved caspase-3 expression in PND1 ovaries. In order to understand if caspase-dependent germ cell apoptosis is regulated through SIRT1, cleaved caspase-3 expression was studied in the ovaries exposed to the SIRT1 inhibitor. Results indicate that (i) SIRT1 inhibitor significantly increased cleaved caspase-3 expression in PND1 ovaries at the dose of 5 mg/kg b.wt and 50 mg/kg b.wt, but not 1 mg/kg b.wt (Fig. 4.9, A, D, G, J, & M); (ii) CrVI significantly ($p<0.05$) increased the expression of cleaved caspase-3 (Fig. 4.9, A, B, & C); and (iii) SIRT1 inhibitor attenuated CrVI-induced increase in the expression of cleaved-caspase-3 at the dose of 5 mg/kg b.wt and 50 mg/kg b.wt, but not 1 mg/kg b.wt (Fig. 4.9, B, E, H, K, & N).

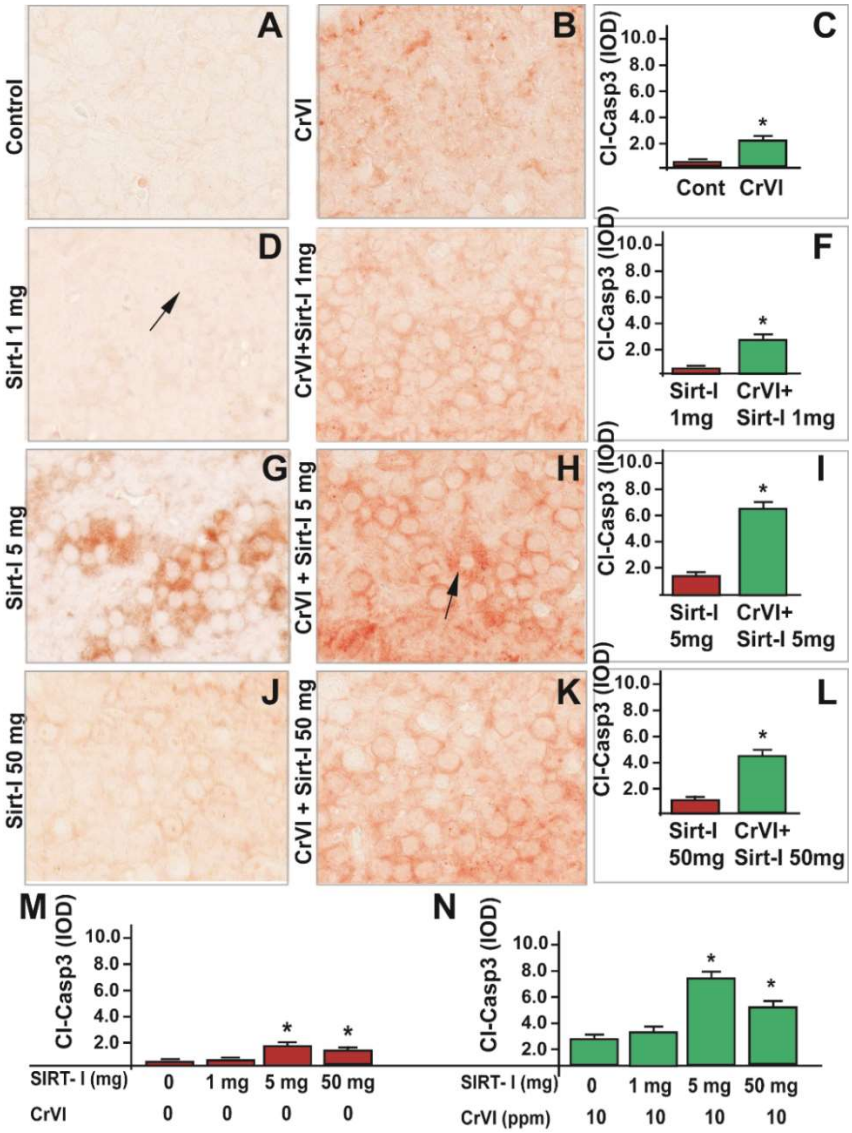

Fig. 4.9. SIRT1 inhibitor (EX-527) attenuated CrVI-induced increase in cleaved-Caspase-3 expression in the PND1 ovary. Pregnant dams were exposed to CrVI (10 ppm) through the drinking water from 9.5-14.5 dpc. CrVI exposed and unexposed dams were injected (*i.p.,)* with various doses of SIRT1 inhibitor (SIRT-I, 1.0, 5.0 and 50 mg/kg body weight). On PND1 the F1 offspring were euthanized and ovaries were processed for Immunohistochemistry as described under *Materials and Methods*. Representative images of ovaries from control (A), CrVI (B), SIRT1-I alone 1.0 mg (D), 5.0 mg (G), and 50 mg (J) /kg body weight. Representative images from the ovaries of CrVI-treated dams: CrVI+SIRT1-I, 1.0 mg (E), CrVI+SIRT1-I, 5.0 mg (H), and CrVI+SIRT1-I, 50 mg (K). Histogram shows integrated optical density (IOD) (Panel-3, C, F, I and L). Each value is mean ±SEM of 10 ovaries from five litters. Dose response of SIRT1-I in the absence of CrVI treatment (M) and presence of CrVI treatment (N) is shown. *: control vs CrVI (C), SIRT1-I-1.0 mg vs CrVI+SIRT1-I-1.0 mg (F), SIRT1-I-5.0 mg vs CrVI+SIRT1-I-5.0 mg (I), or SIRT1-I-50 mg vs CrVI+SIRT1-I-50 mg (L). (M) Control vs SIRT1-I 1.0, 5.0 or 50 mg/kg body weight. (N) CrVI (10 ppm) vs CrVI+SIRT1-1 (1.0, 5.0 or 50 mg/kg b.wt). $p<0.05$. Arrow indicate healthy follicle (D) and follicle undergoing apoptosis (H).

Discussion

CrVI Stabilizes p53 by increasing its acetylation

Results from Specific Aim-1 indicated that gestational exposure to CrVI caused POF by increasing germ cell apoptosis during fetal ovarian development in F1 offspring. Germ cell apoptosis in F1 fetuses was mediated through p53 pathway. Strikingly, CrVI increased the translocation of p53 to mitochondria where it binds to the SOD2 antioxidant enzyme and decreased its activity. When cells are exposed to oxidative stress, toxicants, stress, DNA damage and hypoxia signals, p53 protein is stabilized, activated and transported into the nucleus and induces cell growth arrest, senescence or apoptosis (268,449). Our results indicated that CrVI increased the expression of total-p53 in PND 1 ovaries of F1 pups. Cellular stress can cause several changes in p53 both at the level of transcription and post-translational modification. CBP/p300, a histone acetyl-transferase (HAT), acts as a coactivator of p53 and potentiates its transcriptional activity as well as biological function *in vivo* by specifically acetylating p53 in the C-terminal regulatory domain at multiple lysine residues (Lys-370, Lys-371, Lys-372, Lys-381, Lys-382) (450,451).

Stress can also cause post-translational modifications in p53 such as ubiquitination, phosphorylation, and acetylation (450). Mdm2 is one of the key negative regulators of p53. Mdm2 inhibits p53 by ubiquitination followed by proteasome degradation (452). However, acetylation of p53 on the C-terminal domain abrogates its ubiquitination by Mdm2 stabilizing the p53 protein under physiological conditions (450). Thus acetylation of p53 plays a critical role in stabilizing p53 to exert its anti-proliferative effects, growth arrest, apoptosis, and cell senescence, in response to stress signals (268). Interestingly, results from the current study indicated that gestational exposure to CrVI stabilized p53 by increasing its acetylation, resulting in germ cell apoptosis.

Activation of p53 by CrVI induced regulation of SIRT1

It is evident from the above studies that CrVI acetylates p53 in causing germ cell apoptosis. Therefore, current study further explored the mechanism behind CrVI-induced p53 acetylation. Silent information regulator or SIRTuin 1 (SIRT1) is a highly conserved nicotinamide adenine dinucleotide (NAD)+-dependent protein deacetylase that participates in several cellular functions such as cell cycle, response to DNA damage, metabolism, apoptosis, and autophagy in response to oxidative and genotoxic stress (268,453). SIRT1 protects and mediates the survival of cells from cellular oxidative stress and DNA damage through the inhibition of apoptosis. Upon activation, SIRT1 deacetylates histones and histone methyl-transferases. SIRT1 also deacetylates a variety of non-histone target proteins and one of which is the tumor suppressor p53. SIRT1 physically interacts with p53 and deacetylates p53 at Lys-382 in an NAD^+- dependent manner, resulting in inhibition of p53-mediated apoptosis due to decreased p53-mediated transcriptional activation of target proteins (268,453). Our data indicated that CrVI decreased the expression of SIRT1, therefore, SIRT1's ability to deacetylate p53 was minimized. As a result, p53 might have been stabilized and remained in an active form to induce germ cell apoptosis through its downstream signaling cascade under CrVI treatment.

To delineate the mechanism of CrVI-induced p53 activation, both CrVI exposed and unexposed pregnant dams were injected (*i.p.,)* with various doses of EX-527, a SIRT1 inhibitor (1, 5 and 50 mg/kg body weight). EX-527 binds deep in the catalytic cleft of SIRT1, occupies the nicotinamide site and displaces the NAD^+ nicotinamide, forcing the cofactor into an extended conformation by contacting the ribose of NAD^+ which sterically prevents substrate binding, namely the p53, thus inhibiting the deacetylation function of SIRT1 (454,455). Results indicate that (i) CrVI dose-dependently decreased SIRT1 expression in the F1 ovaries on PND1; (ii)

Inhibition of SIRT1 in normal rats increased germ cell apoptosis, with the maximum effect with 5 or 50 mg/kg body weight; (iii) SIRT1 attenuated CrVI-induced germ cell apoptosis; and (iv) SIRT1 inhibition increased p53 acetylation in a dose-dependent manner, facilitating increased germ cell apoptosis. All the above results indicated that CrVI might potentially stabilize p53 by increasing its acetyl form by down regulating SIRT1 expression. Interestingly, p53 acetylation could have increased its half-life and its ability to transactivate p53-responsive target genes by preventing it from undergoing ubiquitination mediated proteasomal degradation.

Regulation of p53-miR34a-SIRT1 pathway by CrVI

While SIRT1 expression is controlled at multiple levels by transcriptional and post-translational mechanisms under physiological and pathological conditions, it has been shown that miRNAs can regulate the expression of SIRT1 by targeting it directly (445). Some of the miRNAs that can directly regulate SIRT1 are miR34a, miR-181a, miR-9, miR-146, miR-143, miR-132, miR-34c, and miR-217. Interestingly, miR34a directly increases p53 gene expression and represses SIRT1 gene expression (445). Moreover, p53 increases miR34a (268) and inhibits SIRT1 expression through a miR34a-binding site within the 3′ UTR of SIRT1. This regulatory network between miR34a-p53-SIRT1 lead to an increase in p53-downstream candidates p21 and PUMA, transcriptional targets of p53 that regulate the cell cycle and apoptosis (291).

miR34a is found to repress not only the SIRT1 expression but also its activity by targeting NAMPT, the rate-limiting enzyme of the NAD^+ salvage pathway (445). In osteosarcoma cells, miR34a overexpression was found to inhibit cell viability, migration, invasion and promote cell apoptosis by downregulating SIRT1 and deactivating p38/ERK/AKT and Wnt-ß-catenin signaling pathways (456). The BCL2 family of intracellular proteins governs the intrinsic apoptotic pathway where BCL2, one of the pro-survival proteins, prevents cytochrome c release from the

mitochondria and inhibits apoptosis (457). BCL2 has been identified as a direct target of miR34a as its overexpression was found to suppress BCL2 and inactivated the PI3K/AKT pathway in cervical cancer cells (285,458,459). Interestingly, ovaries from CrVI-exposed F1 offspring exhibited an increased expression of miR34a compared to the control group. On the other hand, CrVI downregulated the expression of pAKT, as well as BCL2, the key players in cell survival. Taken together, current data suggest that (i) CrVI-induced decrease in SIRT1 could be partly due to the inhibition of SIRT1 by miR34a, in order to stabilize p53 to activate apoptosis of germ cells; (ii) CrVI-induced upregulation of miR34a may have decreased the expression of AKT and BCL2, thereby inhibiting cell survival pathway mediated through PI3K/AKT.

CrVI increased germ cell apoptosis through p53-mediated mechanisms

During UV-induced apoptosis, PUMA promotes the translocation of BAX by interacting with BAX directly (460). Current data clearly shows a significant increase in PUMA. Early studies from our laboratory showed that CrVI altered the selective sub-cellular translocation of phosphorylated p53 from cytosol into mitochondria (443). Our data indicate that CrVI increased the expression of PUMA as well as BAX in PND1 ovaries suggesting that the p53-mediated transcriptional activation of PUMA could have promoted the translocation of BAX to mitochondria to initiate germ cell apoptosis. However, our future studies will confirm CrVI-induced selective translocation of BAX from cytosol to mitochondria. It has been demonstrated that p53 deficient mice exhibited an increase in BCL2 and decrease in BAX, a pro-apoptotic protein that disrupts mitochondrial membrane potential and causes apoptosis by releasing cytochrome *c* and activating caspases (461). Our data indicated that CrVI decreased the expression of anti-apoptotic proteins BCL2 and BCL-XL, and increased the expression of pro-apoptotic proteins BAX and cleaved caspase-3 in the F1 ovaries compared to control. Thus CrVI

downregulated anti-apoptotic proteins, upregulated pro-apoptotic proteins, increased the translocation of p53 to mitochondria forming complexes with BCL2 and BCL-XL proteins thereby increasing the permeabilization of the outer mitochondrial membrane. Thus, impaired mitochondrial membrane integrity leads to cytochrome *c* release, and activation of caspase-3, inducing germ cell apoptosis through a p53-mediated transcription independent mechanism. Thus, CrVI might have increased germ cell apoptosis by both p53-mediated transcription-dependent and independent mechanisms.

Gene encoding miR34a is a direct transcriptional target of p53 and the expression of miR34a was increased by p53 in response to genotoxic stress. Also, miR34a is a pro-apoptotic transcriptional target of p53 as miR34a inactivation was found to compromise p53-dependent apoptosis (288). Cellular stress due to arsenic exposure or folate deprivation was shown to upregulate miR34a (462). Taken together our data indicate that CrVI increased p53 expression, which increases the expression of miR34a that targets and downregulates the levels of SIRT1. Down-regulation of SIRT1 in turn increases the expression and activity of p53. The resulted increase of p53 increases the synthesis and activation of miR34a.

In summary, the results indicate that CrVI increased germ cell apoptosis and accelerated the GCN breakdown through the p53-miR34a-SIRT1 network (Fig. 4.9). These novel findings for the first time indicate clear evidence for the key roles played by p53 in CrVI induced germ cell apoptosis through the p53-miR34a-SIRT1 regulatory network which may lead to premature depletion of follicles resulting in early reproductive senescence or POF.

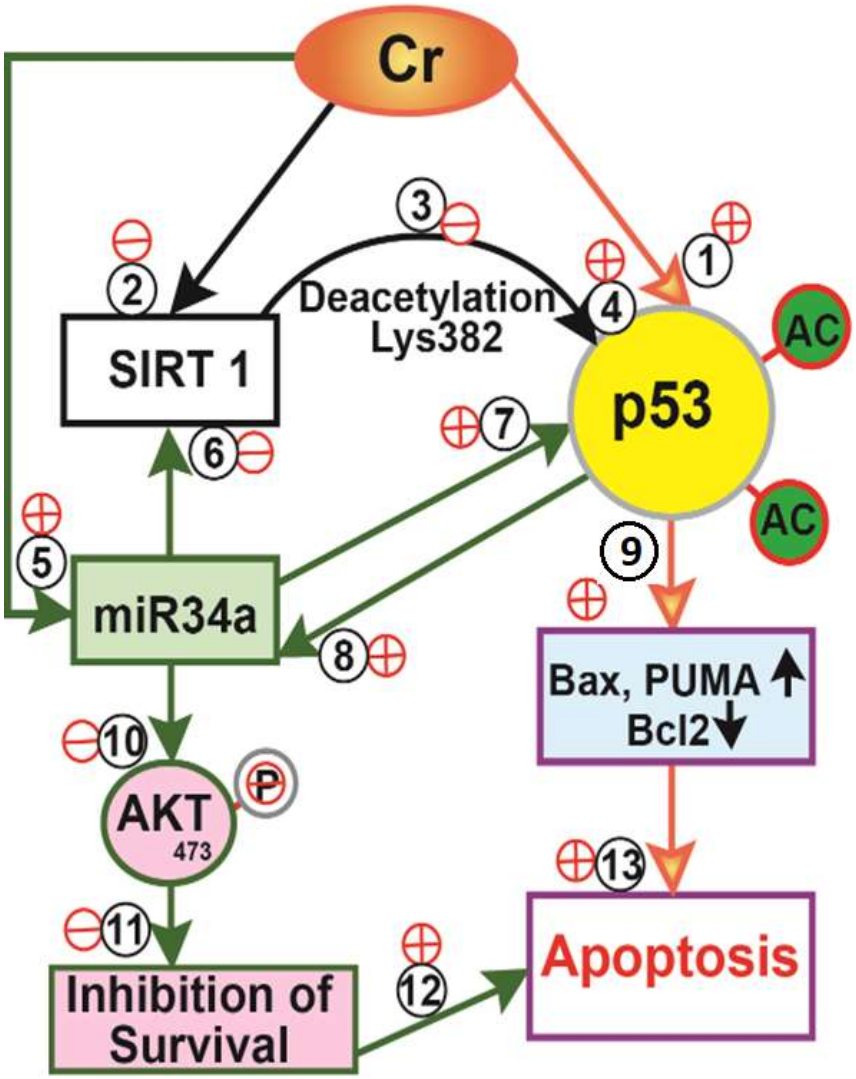

Fig. 4.10. Schematic diagram of p53-SIRT1-mi34a signaling network on CrVI-induced germ cell apoptosis:

The results of the *Specific Aim-2* are summarized as follows. CrVI increases the expression, activation and stabilization of p53 and by increasing acetylation of-p53 (1).CrVI decreases the expression and activity of the SIRT1 protein (2). Decreased levels and activity of SIRT1 failed to deacetylate p53 at Lys382 (3), resulting in increased acetylated p53 (K-382) levels and its activation (4). CrVI increases the miR34a expression (5), which decreased the expression of SIRT1 (6). Increase in miR34a also increases the expression and activation of p53 (7). In turn, activated p53 increases the expression of miR34a (8). Increase in P53 activation decreases the expression of BCL2, BCL-XL and increases the expression of Bax and PUMA (9). Increase in miR34a expression decreases the phosphorylation of AKT at Ser-473 (10). Decrease in phosphorylation of AKT inhibits the cell survival machinery (11), resulting in increased apoptosis (13).

5. CHROMIUM ACTIVATES P53-SIRT1-miR34A SIGNALING NETWORK TO INDUCE GERM CELL APOPTOSIS DURING FETAL OVARIAN DEVELOPMENT

Specific Aim-3:

Determine the mechanism of miR34a in modulating CrVI-induced germ cell apoptosis.

Hypothesis*:*

This aim was driven by the working hypothesis that *"miR34a increases CrVI-induced germ cell apoptosis by abrogating the association between p53 and SIRT1".*

Objectives:

The above *hypothesis* was tested by the following objectives: To determine the effects of miR34a mimetic and/or inhibitor on: (i) apoptosis of germ cells; (ii) mRNA expression of *p53, Bcl2, Bax*, *Akt* and *Sirt1* genes; (iii) protein levels of acetyl p53, SIRT1, cleaved caspase-3, BAX BCL2, and BCL-XL; and (iv) association/interaction between p53 and SIRT1.

Results from the above studies indicated a clear role for miR34a in CrVI-induced apoptosis of germ cells. In order to further delineate the mechanism of miR34a in CrVI-induced germ cell apoptosis, we transfected the fetal whole ovaries with miR34a mimetic and/or inhibitor *ex vivo*, and treated the ovaries with CrVI, and determined machinery that mediates cell survival and apoptosis at the mRNA and protein levels.

Results

Effects of miR34a mimetic or inhibitor on CrVI-induced germ cell apoptosis

Results indicate that *ex vivo* cultured ovaries on CD9 (which recapitulated PND1) that were exposed to CrVI showed a significant increase in the percentage of apoptotic germ cells with pyknotic nuclei compared to the control group (Fig. 5.1, A & B). TUNEL staining revealed that transfection with miR34a mimetic increased germ cell apoptosis both in the presence or absence of CrVI (Fig. 5.1, C & D). Transfection with miR34a inhibitor alone did not have any effect on germ cell apoptosis, whereas ovaries transfected with miR34a inhibitor mitigated the CrVI-induced increase in germ cell apoptosis (Fig. 5.1, E & F).

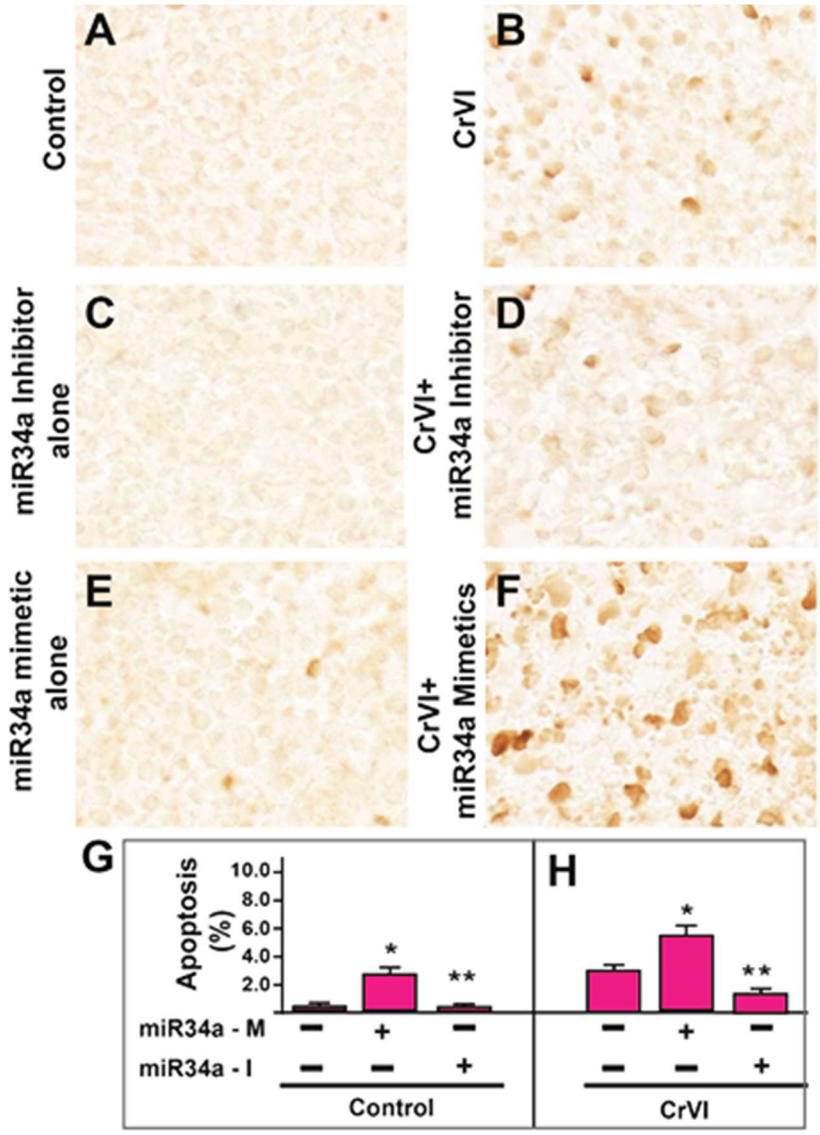

Fig. 5.1. Effects of miR34a mimetic or inhibitor on CrVI-induced germ cell apoptosis in cultured fetal whole ovaries. Fetal ovaries from E13.5 were cultured for 8 days ex vivo and treated with or without CrVI (0.1 ppm) from culture day (CD)2 to CD8. Ovaries treated with and without CrVI (0.1 ppm) were transfected with miR34a mimetic (100 nM) and miR34a inhibitor (100 nM) from CD2 to CD8, and harvested on CD9 (which recapitulated PND1). Ovaries were harvested and processed for TUNEL assay as described under *Materials and Methods*. Representative images of the ovaries are control (A), CrVI (B), miR34a mimetic alone (C), CrVI+miR34a mimetic (D), miR34a inhibitor alone (E), and CrVI+miR34a inhibitor (F). Histogram shows TUNEL positive apoptotic cell percentage (G & H). Each value represents mean ± SEM of 10 ovaries. *: Control vs miR34a mimetic alone (G); or * CrVI vs CrVI+ miR34a mimetic (H); ** miR34a mimetic alone vs miR34a inhibitor alone (G); or CrVI+miR34a mimetic vs CrVI + miR34a inhibitor (H). $p<0.05$.

Effect of miR34a mimetic on mRNA expression of key cell survival and cell death pathway proteins

Results indicate that (i) Transfection with miR34a mimetic downregulated the mRNA expression of cell survival proteins *AKT, BCL2* and *SIRT1* significantly ($p<0.05$) compared to control ovaries; and (ii) miR34a mimetic significantly ($p<0.05$) upregulated the mRNA expression of *p53* and anti-apoptotic *BAX* compared to control ovaries (Fig. 5.2).

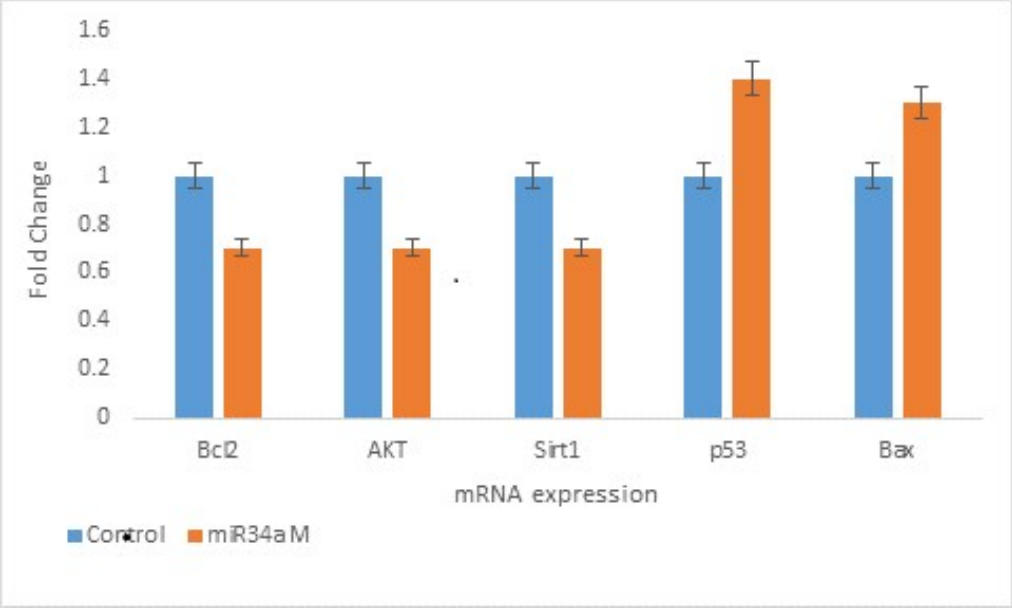

Fig. 5.2. Effect of miR34a mimetic on mRNA expression of key cell survival and cell death pathway proteins in fetal ovaries. Fetal ovaries from E13.5 were cultured for 8 days ex vivo and transfected with miR34a mimetic (100nM) from CD2 to CD8, and harvested on CD9 (which recapitulated PND1). Ovaries from culture were harvested and processed for RNA isolation and real-time PCR was performed as described under *Materials and Methods*. Histogram shows the fold change normalized to the internal control U6. Each value is mean ±SEM of 3 replicates. *: Control vs miR34a mimetic.

Effects of miR34a mimetic or inhibitor on CrVI-induced increase in acetyl-p53 (K-382) expression

To understand the possible regulatory role of miR34a on acetylated p53, we studied the expression of acetyl-p53 in the ovaries transfected with miR34a mimetic or miR34a inhibitor. Results indicated that (i) CrVI significantly ($p<0.05$) increased the expression of acetyl-p53 compared to control group in fetal ovaries on CD9 (Fig. 5.3, A & B); (ii) Transfection with miR34a mimetic significantly ($p<0.05$) increased acetyl-p53 expression both in the presence or absence of CrVI (Fig. 5.3, C & D); (iii) Transfection with miR34a inhibitor mitigated CrVI-induced increase in acetyl-p53 expression, whereas, miR34a inhibitor alone did not have any effect on acetyl-p53 expression (Fig. 5.3, E & F).

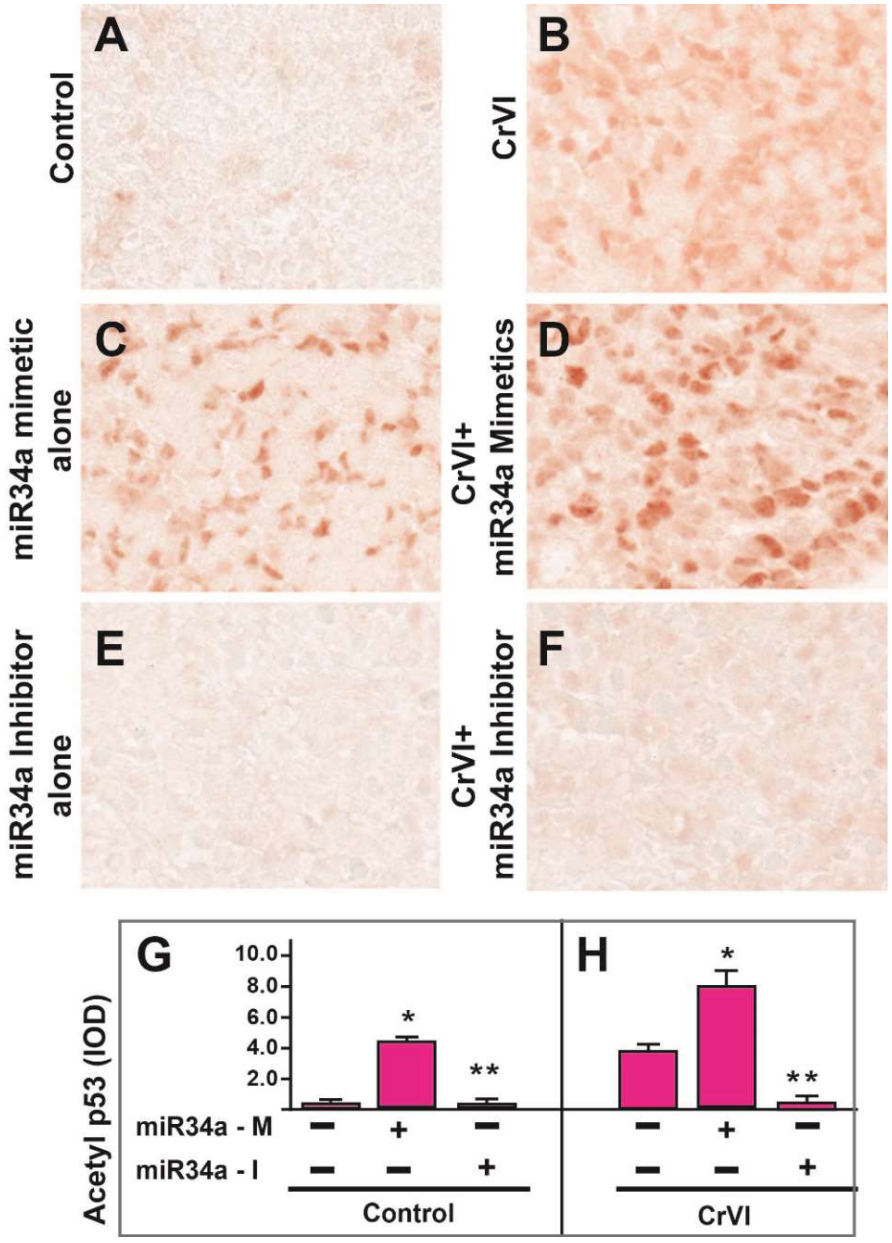

Fig. 5.3. Effects of miR34a mimetic or inhibitor on CrVI-induced increase in acetyl-p53 expression in cultured fetal whole ovaries. Fetal ovaries from E13.5 were cultured for 8 days ex vivo and treated with or without CrVI (0.1 ppm) from culture day (CD)2 to CD8. Ovaries treated with and without CrVI (0.1 ppm) were transfected with miR34a mimetic (100 nM) and miR34a inhibitor (100 nM) from CD2 to CD8, and harvested on CD9 (which recapitulated PND1). Representative images of the ovaries are control (A), CrVI (B), miR34a mimetic alone (C), CrVI+miR34a mimetic (D), miR34a inhibitor alone (E), and CrVI+miR34a inhibitor (F). Histogram shows integrated optical density (IOD) quantified using Image ProPlus software (G & H). Each value represents mean ± SEM of 10 ovaries. *: Control vs miR34a mimetic alone (G); or * CrVI vs CrVI+ miR34a mimetic alone (H); ** miR34a mimetic alone vs miR34a inhibitor alone (G); or CrVI+miR34a mimetic vs CrVI + miR34a inhibitor (H). $p<0.05$.

Effects of miR34a mimetic or inhibitor on CrVI-induced decrease in SIRT1 expression

In order to understand if SIRT1 is regulated through miR34a, SIRT1 expression was studied in the ovaries transfected with miR34a mimetic and miR34a inhibitor. Results indicate that (i) CrVI significantly ($p<0.05$) decreased the expression of SIRT1 compared to control group in cultured fetal ovaries on CD9 (Fig. 5.4, A & B); (ii) Transfection with miR34a mimetic significantly ($p<0.05$) decreased SIRT1 expression both in the presence or absence of CrVI (Fig. 5.4, C & D); and (iii) Transfection with miR34a inhibitor mitigated CrVI-induced decrease in SIRT1 expression (Fig.5.4, E & F).

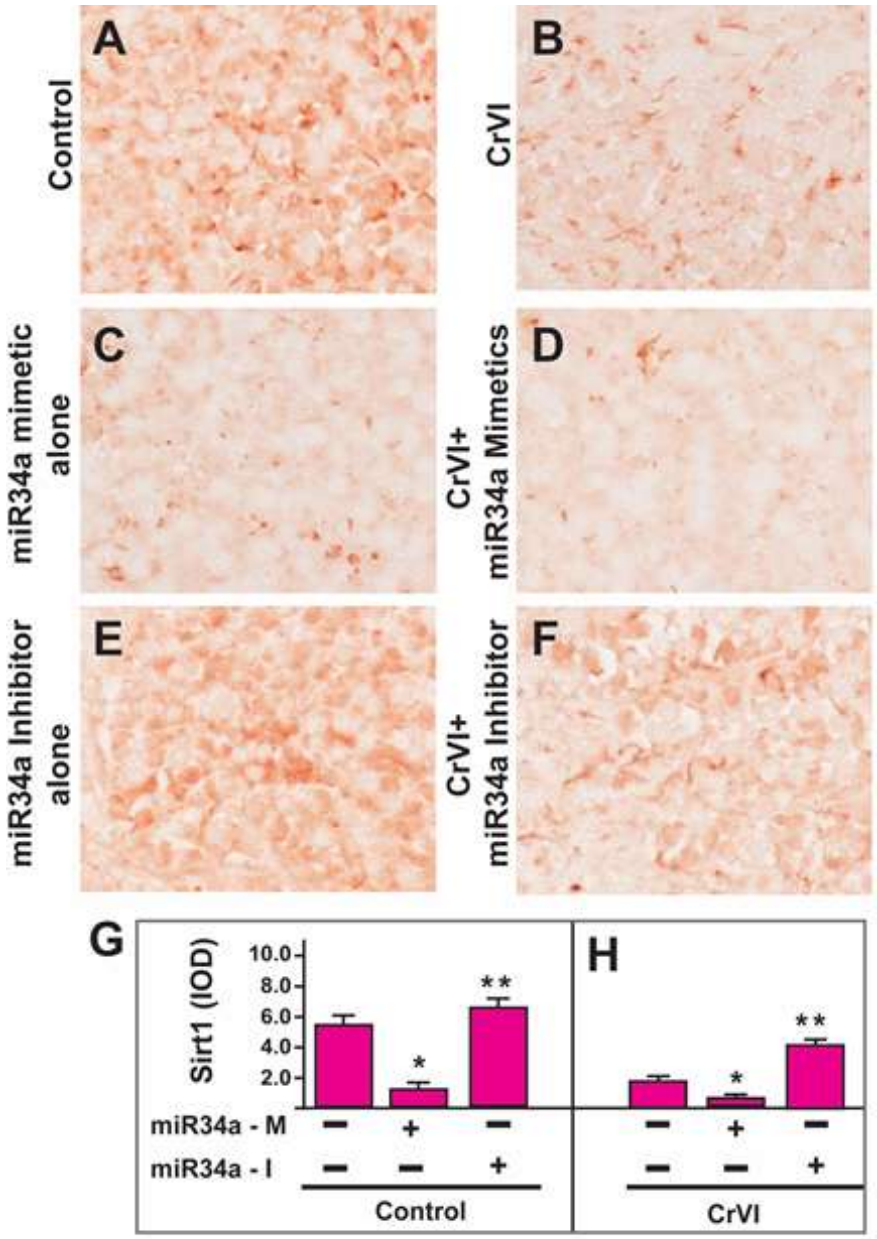

Fig. 5.4. Effects of miR34a mimetic or inhibitor on CrVI-induced decrease in SIRT1 expression in cultured fetal whole ovaries. Fetal ovaries from E13.5 were cultured for 8 days ex vivo and treated with or without CrVI (0.1 ppm) from culture day (CD)2 to CD8. Ovaries treated with and without CrVI (0.1 ppm) were transfected with miR34a mimetic (100 nM) and miR34a inhibitor (100 nM) from CD2 to CD8, and harvested on CD9 (which recapitulated PND1). Representative images of the ovaries are control (A), CrVI (B), miR34a mimetic alone (C), CrVI+miR34a mimetic (D), miR34a inhibitor alone (E), and CrVI+miR34a inhibitor (F). Histogram shows integrated optical density (IOD) quantified using Image ProPlus software (G & H). Each value represents mean ± SEM of 10 ovaries. *: Control vs miR34a mimetic alone (G); or * CrVI vs CrVI+ miR34a mimetic (H); ** miR34a mimetic vs miR34a inhibitor (G); or CrVI+miR34a mimetic vs CrVI + miR34a inhibitor (H). $p<0.05$.

Effects of miR34a mimetic or inhibitor on the ratio of p53 & SIRT1

Data from IHC showed increased expression of acetyl-p53 and decreased expression of SIRT1 in CrVI-treated ovaries (Fig. 5.3 and 5.4). As mentioned earlier, SIRT1 mediates cell survival by physically interacting with p53 and deacetylating at Lys-382 residue resulting in a decrease in the p53-mediated transcriptional activation (268). Also, it has been reported that SIRT1 inhibition increased acetylation of p53 at Lysine-382 after DNA damage in primary human mammary epithelial cells (444). Therefore, colocalization of p53 and SIRT1 was studied by double immunofluorescence in cultured fetal ovaries on CD9. Results indicate that (i) CrVI significantly ($p<0.05$) increased the ratio of p53:SIRT1 compared to control group (Fig. 5.5, A ,D, G, J, M, & N); (ii) Transfection with miR34a mimetic significantly ($p<0.05$) increased the ratio of p53:SIRT1 both in the presence or absence of CrVI (Fig. 5.5, B, E, H, K, M, & D); and (iii) Transfection with miR34a inhibitor alone mitigated CrVI-induced increase in p53:SIRT1 ratio compared to control (Fig. 5.5, C, F, I, L, M, & N).

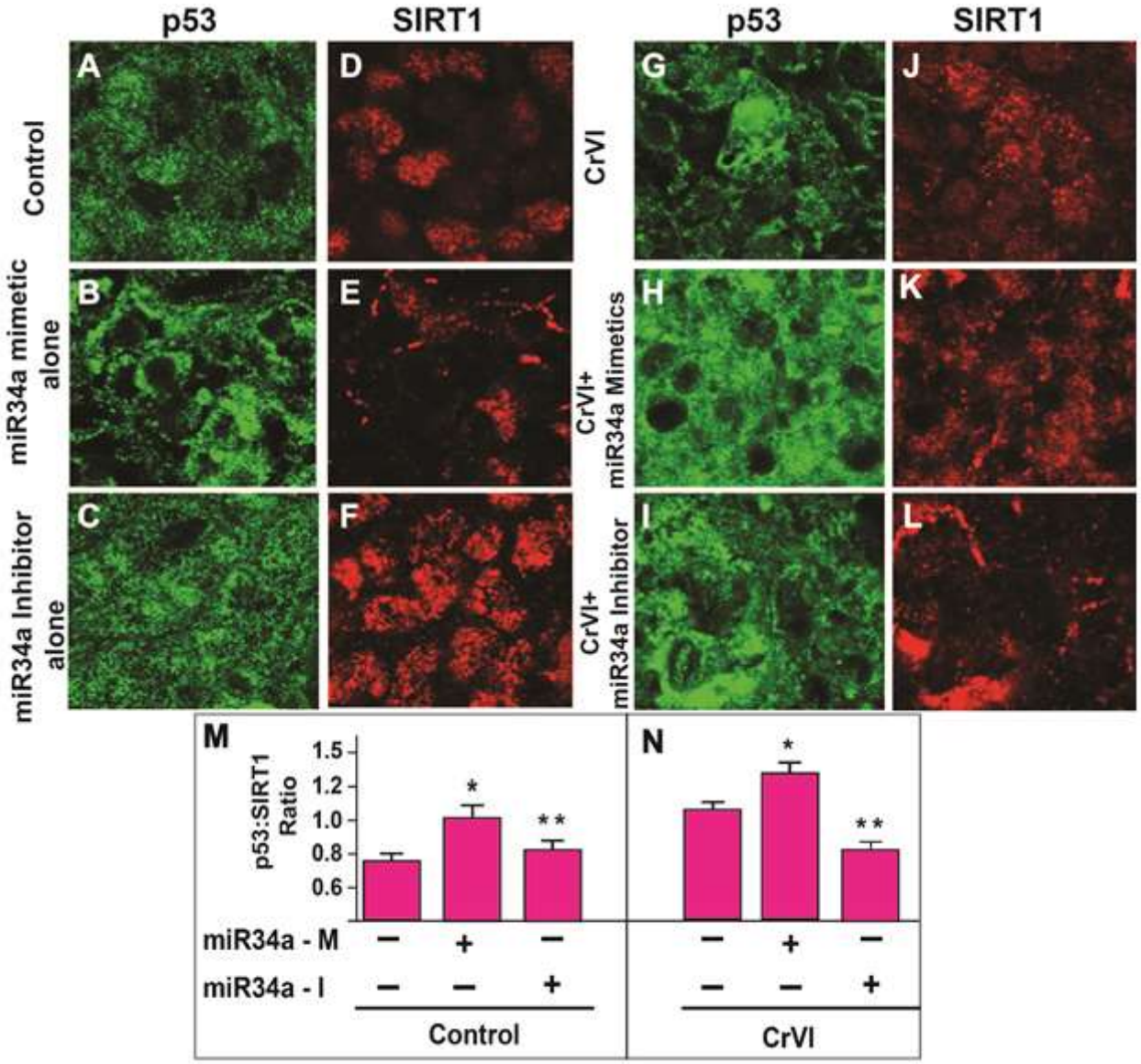

Fig. 5.5. Effects of miR34a mimetic or inhibitor on the ratio of p53 and SIRT1 in cultured fetal whole ovaries. Fetal ovaries from E13.5 were cultured for 8 days ex vivo and treated with or without CrVI (0.1 ppm) from culture day (CD)2 to CD8. Ovaries treated with and without CrVI (0.1 ppm) were transfected with miR34a mimetic (100 nM) and miR34a inhibitor (100 nM) from CD2 to CD8, and harvested on CD9 (which recapitulated PND1). Representative images of the p53 expression in the ovaries of control (A), miR34a mimetic alone (B), miR34a inhibitor alone (C), CrVI (G), CrVI+miR34a mimetic (H) and CrVI+miR34a inhibitor (I). Representative images of the SIRT1 expression in the ovaries of control (D), miR34a mimetic alone (E), miR34a inhibitor alone (F), CrVI (J), CrVI+miR34a mimetic (K) and CrVI+miR34a inhibitor (L). Histogram shows the ratio between p53 and SIRT1 based on integrated optical density (IOD) quantified using Image ProPlus software (M & N). Each value represents mean ± SEM of 10 ovaries. *: Control vs miR34a mimetic alone (M); or * CrVI vs CrVI+ miR34a mimetic (N); ** miR34a mimetic vs miR34a inhibitor (M); or CrVI+miR34a mimetic vs CrVI + miR34a inhibitor (N). $p<0.05$.

Effect of CrVI and miR34a on the interaction between p53 and SIRT1

IHC showed increased expression of acetyl-p53 and decreased expression of SIRT1 in CrVI-treated ovaries (Fig. 5.3 and 5.4). SIRT1 physically interacts with p53 and deacetylates its Lys-382 residue resulting in a decrease in the p53-mediated transcriptional activation (268). In order to validate the interaction between SIRT1and p53 and to understand the role of miR34a in regulating the SIRT1-p53 interaction, spontaneously immortalized rat granulosa cells (SIGC) were transfected with miR34a mimetic or miR34a inhibitor, and treated with or without CrVI and immunoprecipitation (IP) was performed with acetyl-p53 (K-382) antibody, and western blot was performed with SIRT1 antibody. Results from the immunoblot analysis indicate that (i) SIRT1 interacts with p53 in the control group; (ii) CrVI significantly ($p<0.05$) decreased the interaction between SIRT1 and p53 proteins compared to control; (iii) Transfection with miR34a mimetic significantly ($p<0.05$) decreased the interaction between SIRT1 and p53 both in the presence or absence of CrVI (Fig. 5.6).

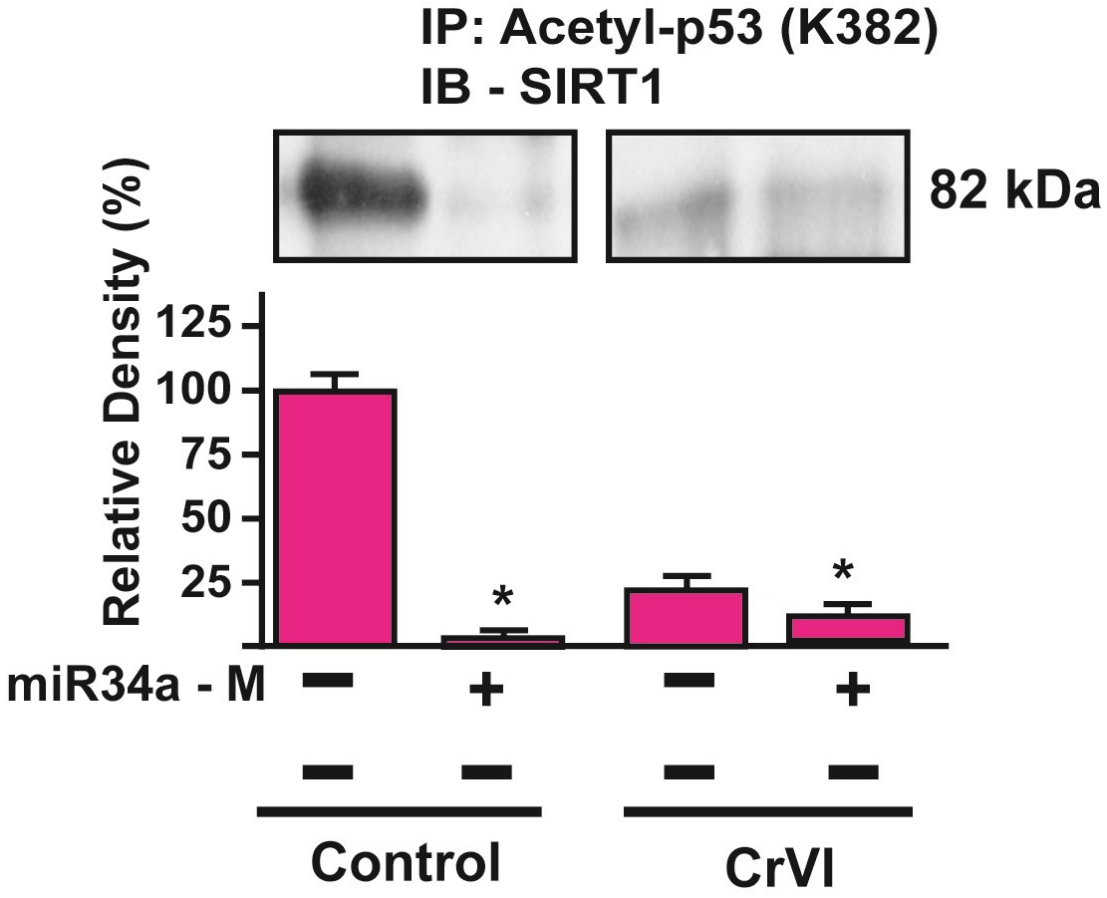

Fig. 5.6. Effect of miR34a mimetic and CrVI on p53-SIRT1 interaction. SIGC cells were cultured in DMEM-F12 with 5% fetal bovine serum (FBS) with antibiotics and antimycotics. At 70–80% confluency, cells treated with or without CrVI (0.1 ppm) were transfected with miR34a mimetic (100 nM). Cells were harvested 24 h post-transfection to isolate protein for Immunoprecipitation (with acetyl p53 (K-382 antibody) and western blotting (with SIRT1 antibody) as described under *Materials and Methods*. The blots were exposed to Blue X-Ray film and densitometry of autoradiograms was performed using an Alpha Imager (Alpha Innotech Corporation, San Leandro, CA). Histogram shows integrated optical density (IOD) relative to control. *: Control vs miR34a mimetic alone; or * CrVI vs CrVI+ miR34a mimetic. $p<0.05$.

Effect of miR34a mimetic or inhibitor on interaction between p53 and SIRT1

Data from IHC showed that CrVI increased expression of acetyl-p53 and decreased expression of SIRT1 in CrVI-treated ovaries (Fig. 5.3 and 5.4). SIRT1 physically interacts with p53 and deacetylates Lys-382 residue resulting in a decrease in the p53-mediated transcriptional activation (268). Transcriptional activation of miR34a was found to contribute to p53-mediated apoptosis and miR34a was also found to target SIRT1 in colon cancer cells (288,291). Therefore, in order to understand whether miR34a affects the physical interaction between p53 and SIRT, we monitored co-localization of p53 and SIRT in the cultured fetal whole ovaries treated with and without CrVI and transfected with miR34a mimetic or inhibitor. Results indicate that (i) SIRT1 interacts with p53 in the control group (Fig. 5.7, A, B & C); (ii) CrVI significantly ($p<0.05$) decreased the interaction between SIRT1 and p53 proteins compared to control (Fig. 5.7, J, K & L); (iii) Transfection with miR34a mimetic significantly ($p<0.05$) decreased the interaction between SIRT1 and p53 both in the presence or absence of CrVI (Fig. 5.7, D, E, F, M, N & O); and (iv) Transfection with miR34a inhibitor mitigated the CrVI-induced decrease in interaction between SIRT1 and p53 (Fig. 5.7, G, H, I, P, Q & R).

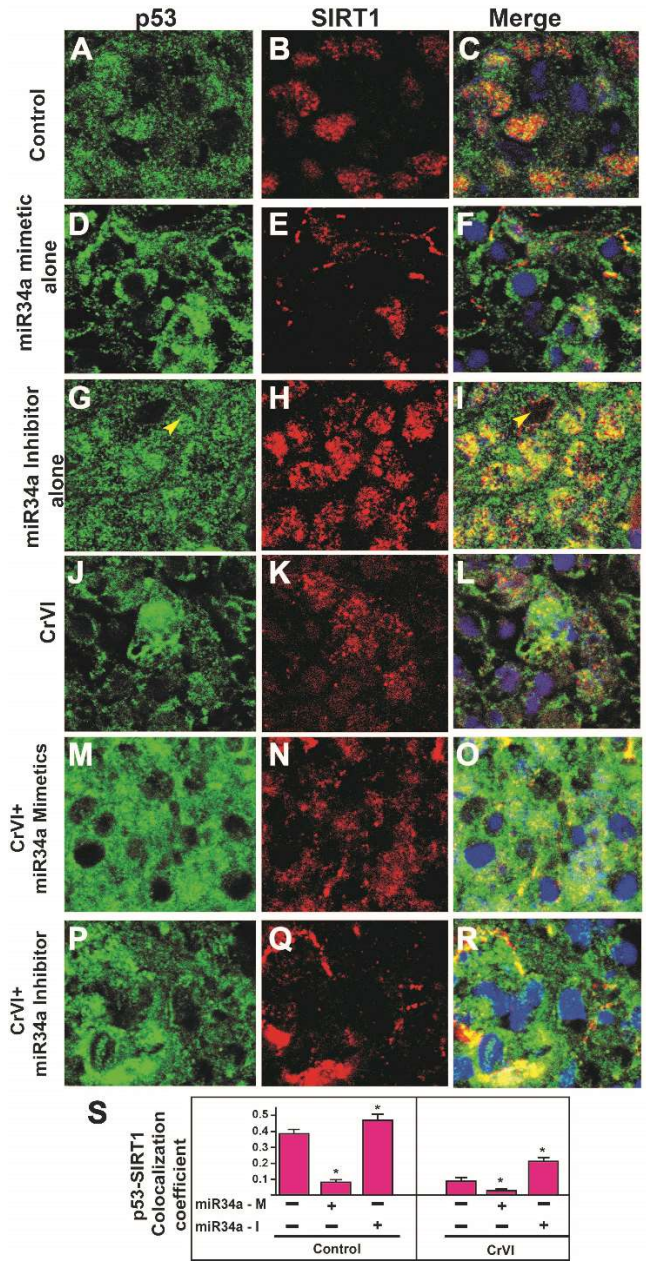

Fig. 5.7. Effect of miR34a mimetic or inhibitor on interaction between p53 and SIRT1 in cultured fetal whole ovaries. Fetal ovaries from E13.5 were cultured for 8 days *ex vivo* and treated with or without CrVI (0.1 ppm) from culture day (CD)2 to CD8. Ovaries were transfected with miR34a mimetic (100 nM) and miR34a inhibitor (100 nM) on E13.5. Twenty four h post-transfection ovaries were treated with or without CrVI (0.1 ppm) from CD2 to CD8, and harvested on CD9 (which recapitulated PND1). Harvested ovaries were fixed in 4% buffered paraformaldehyde and processed for Immunofluorescence as described under *Materials and Methods*. Representative images of p53 (Green), SIRT1 (Red), and merge: Control (A, B & C), miR34a mimetic alone (D, E & F), miR34a inhibitor alone (G, H & I), CrVI (J, K & L), CrVI+miR34a mimetic (M, N & O), and CrVI+miR34a inhibitor (P, Q & R). Degree of colocalization of p53 and SIRT1 proteins was measured by pearson's correlation coefficient using Image ProPlus software. Histogram shows p53-SIRT1 colocalization coefficient (S). *: Control vs miR34a mimetic alone (M); or * CrVI vs CrVI+ miR34a mimetic (N); ** miR34a mimetic vs miR34a inhibitor (M); or CrVI+miR34a mimetic vs CrVI + miR34a inhibitor (N), $p<0.05$. Each value represents mean±SEM of 10 ovaries.

Effects of miR34a mimetic or inhibitor on CrVI-induced increase in cleaved caspase-3 expression

In order to understand if cleaved caspase-3 is regulated through miR34a, cleaved caspase-3 expression was studied in the ovaries transfected with miR34a mimetic or miR34a inhibitor. Results indicated that (i) CrVI significantly ($p<0.05$) increased the expression of cleaved caspase-3 compared to control group in cultured fetal ovaries on CD9 (Fig. 5.8, A & B); (ii) Transfection with miR34a mimetic significantly ($p<0.05$) increased cleaved caspase-3 expression both in the presence or absence of CrVI (Fig. 5.8, C & D); and (iii) Transfection with miR34a inhibitor mitigated CrVI-induced increase in cleaved caspase-3, whereas, miR34a inhibitor alone did not have any effect on caspase-3 expression (Fig. 5.8, E & F).

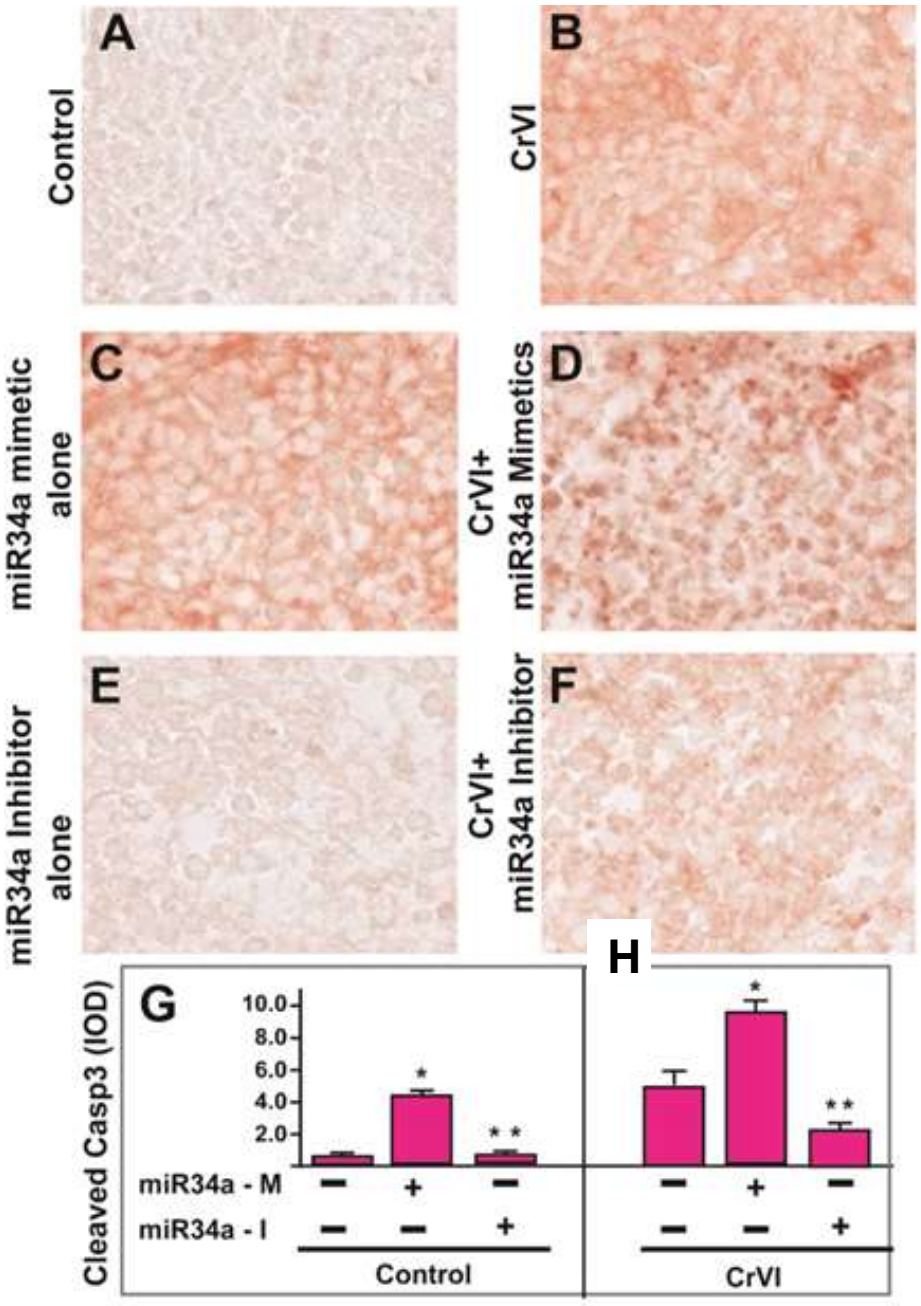

Fig. 5.8. Effects of miR34a mimetic or inhibitor on CrVI-induced increase in cleaved caspase-3 expression in cultured fetal whole ovaries. Fetal ovaries from E13.5 were transfected with miR34a mimetic (100 nM) or miR34a inhibitor (100 nM) from CD2 to CD8, treated with or without CrVI (0.1 ppm) from culture day (CD)2 to CD8, and harvested on CD9 (which recapitulated PND1). Representative images of the ovaries are control (A), CrVI (B), miR34a mimetic alone (C), CrVI+miR34a mimetic (D), miR34a inhibitor alone (E), and CrVI+miR34a inhibitor (F). Histogram shows integrated optical density (IOD) quantified using Image ProPlus software (G & H). Each value represents mean ± SEM of 10 ovaries. *: Control vs miR34a mimetic alone (G); or * CrVI vs CrVI+ miR34a mimetic alone (H); ** miR34a mimetic vs miR34a inhibitor (G); or CrVI+miR34a mimetic vs CrVI + miR34a inhibitor (H). $p<0.05$.

Effects of miR34a mimetic or inhibitor on CrVI-induced increase in BAX expression

BAX expression in the ovaries transfected with miR34a mimetic or miR34a inhibitor was studied in order to understand the possible regulatory role of miR34a on BAX. Results indicate that (i) CrVI significantly ($p<0.05$) increased the expression of BAX compared to control group in cultured fetal ovaries on CD9 (Fig. 5.9, A & B); (ii) Transfection with miR34a mimetic significantly ($p<0.05$) increased BAX expression both in the presence or absence of CrVI (Fig. 5.9, C & D); (iii) Transfection with miR34a inhibitor mitigated CrVI-induced increase in BAX expression (Fig. 5.9, E & F).

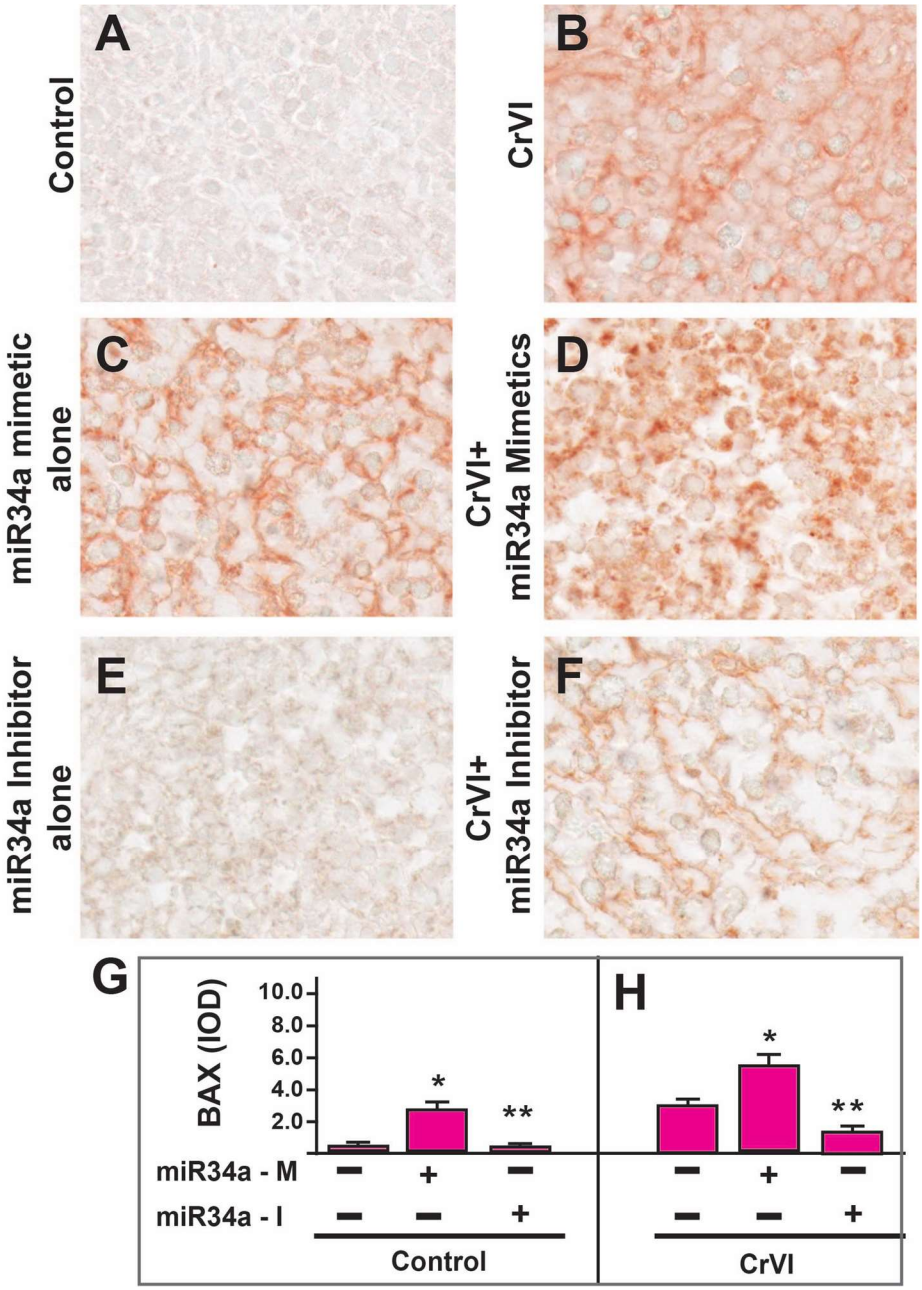

Fig. 5.9. Effects of miR34a mimetic or inhibitor on CrVI-induced increase in BAX expression in cultured fetal whole ovaries. Fetal ovaries from E13.5 were transfected with miR34a mimetic (100 nM) or miR34a inhibitor (100 nM) from CD2 to CD8, treated with or without CrVI (0.1 ppm) from culture day (CD)2 to CD8, and harvested on CD9 (which recapitulated PND1). Representative images of the ovaries are control (A), CrVI (B), miR34a mimetic alone (C), CrVI+miR34a mimetic (D), miR34a inhibitor alone (E), and CrVI+miR34a inhibitor (F). Histogram shows integrated optical density (IOD) quantified using Image ProPlus software (G & H). Each value represents mean ± SEM of 10 ovaries. *: Control vs miR34a mimetic alone (G); or * CrVI vs CrVI+ miR34a mimetic alone (H); ** miR34a mimetic vs miR34a inhibitor (G); or CrVI+miR34a mimetic vs CrVI + miR34a inhibitor (H). $p<0.05$.

Effects of miR34a mimetic or inhibitor on CrVI-induced decrease in BCL2 expression

In order to understand if BCL2 is regulated through miR34a, BCL2 expression was studied in the ovaries transfected with miR34a mimetic or miR34a inhibitor. Results indicate that (i) CrVI significantly ($p<0.05$) decreased the expression of BCL2 compared to control group in cultured fetal ovaries on CD9 (Fig. 5.10, A & B); (ii) Transfection with miR34a mimetic significantly ($p<0.05$) decreased BCL2 expression both in the presence or absence of CrVI (Fig. 5.10, C & D); (iii) Transfection with miR34a inhibitor attenuated CrVI-induced decrease in BCL2 expression, whereas, miR34a inhibitor alone did not have any effect on BCL2 expression (Fig. 5.10, E & F).

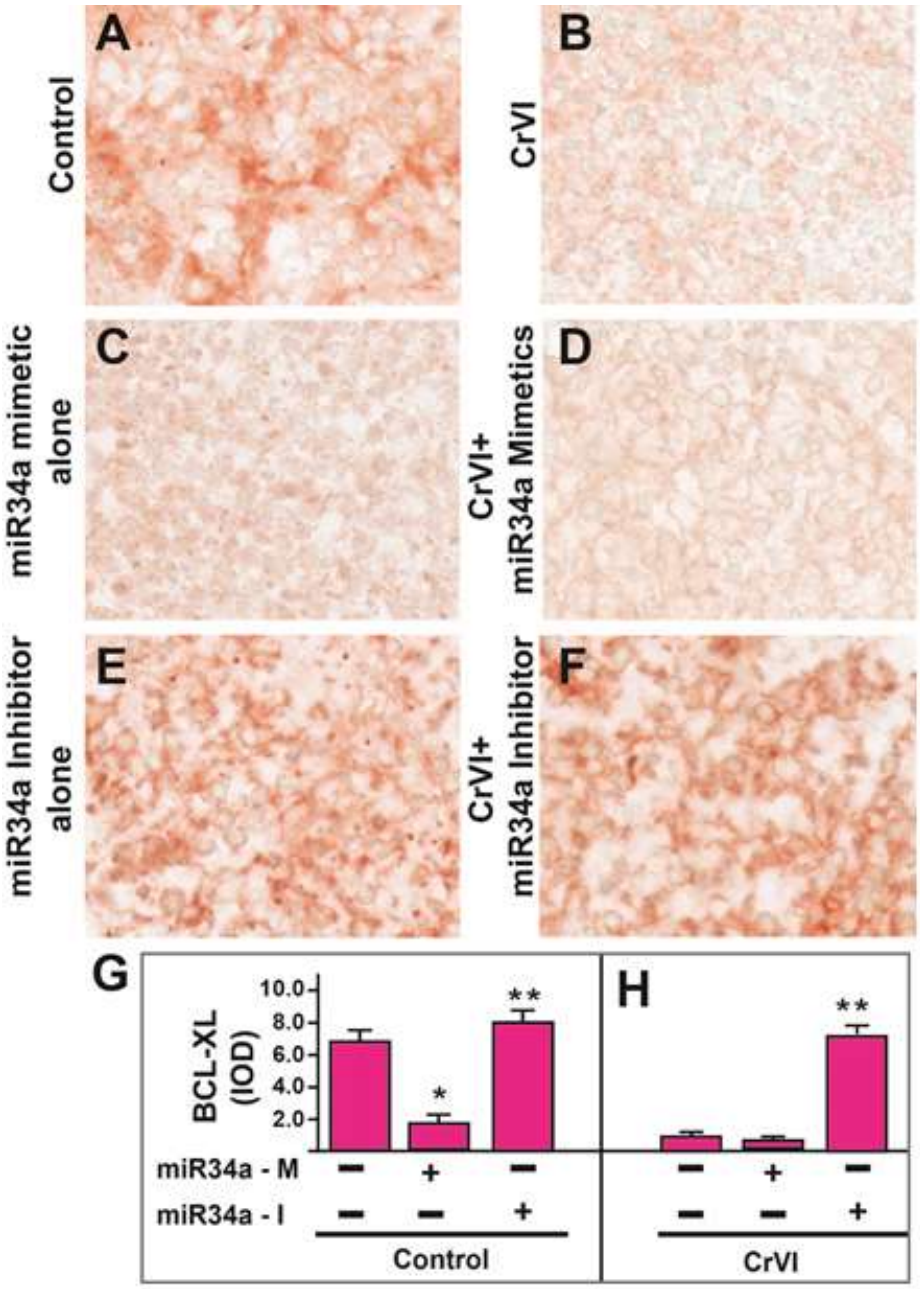

Fig. 5.10. Effects of miR34a mimetic or inhibitor on CrVI-induced decrease in BCL2 expression in cultured fetal whole ovaries. Fetal ovaries from E13.5 were transfected with miR34a mimetic (100 nM) or miR34a inhibitor (100 nM) from CD2 to CD8, treated with or without CrVI (0.1 ppm) from culture day (CD)2 to CD8, and harvested on CD9 (which recapitulated PND1). Representative images of the ovaries are control (A), CrVI (B), miR34a mimetic alone (C), CrVI+miR34a mimetic (D), miR34a inhibitor alone (E), and CrVI+miR34a inhibitor (F). Histogram shows integrated optical density (IOD) quantified using Image ProPlus software (G & H). Each value represents mean ± SEM of 10 ovaries. *: Control vs miR34a mimetic alone (G); or *: CrVI vs CrVI+ miR34a mimetic alone (H); **: miR34a mimetic vs miR34a inhibitor (G); or CrVI+miR34a mimetic vs CrVI + miR34a inhibitor (H). $p<0.05$.

Effects of miR34a mimetic or inhibitor on CrVI-induced decrease in BCL-XL expression

In order to understand if BCL-XL is regulated through miR34a, BCL-XL expression was studied in the ovaries transfected with miR34a mimetic or miR34a inhibitor. Results indicate that (i) CrVI significantly ($p<0.05$) decreased the expression of BCL-XL compared to control group in cultured fetal ovaries on CD9 (Fig. 5.11, A & B); (ii) Transfection with miR34a mimetic significantly ($p<0.05$) decreased BCL-XL expression both in the presence or absence of CrVI (Fig. 5.11, C & D); (iii) Transfection with miR34a inhibitor alone attenuated CrVI-induced decrease in BCL-XL expression (Fig. 5.11, E & F).

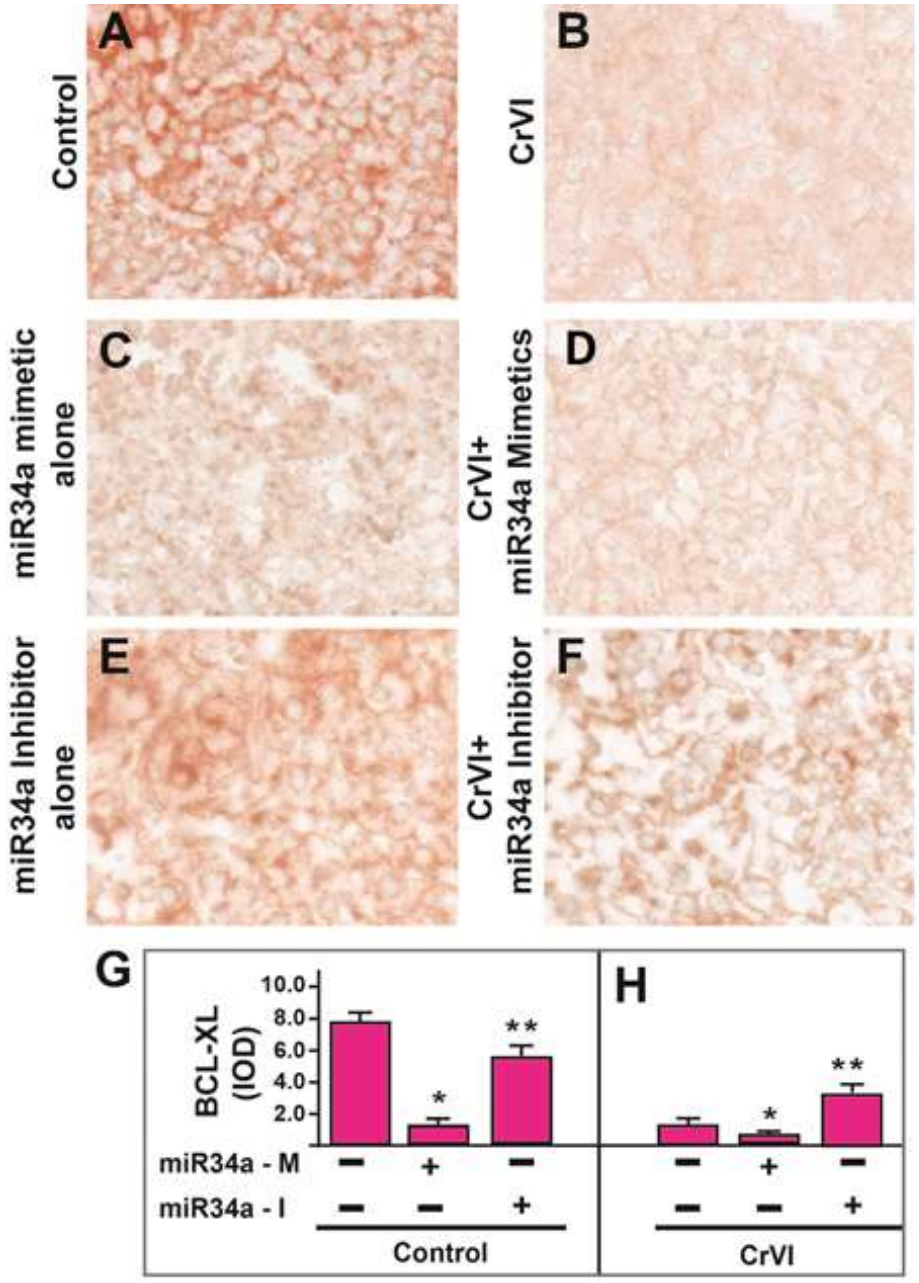

Fig. 5.11. Effects of miR34a mimetic or inhibitor on CrVI-induced decrease in BCL-XL expression in cultured fetal whole ovaries. Fetal ovaries from E13.5 were transfected with miR34a mimetic (100 nM) or miR34a inhibitor (100 nM) from CD2 to CD8, treated with or without CrVI (0.1 ppm) from culture day (CD)2 to CD8, and harvested on CD9 (which recapitulated PND1). Representative images of the ovaries are control (A), CrVI (B), miR34a mimetic alone (C), CrVI+miR34a mimetic (D), miR34a inhibitor alone (E), and CrVI+miR34a inhibitor (F). Histogram shows integrated optical density (IOD) quantified using Image ProPlus software (G & H). Each value represents mean ± SEM of 10 ovaries. *: Control vs miR34a mimetic alone (G); or *: CrVI vs CrVI+ miR34a mimetic alone (H); **: miR34a mimetic vs miR34a inhibitor (G); or CrVI+miR34a mimetic vs CrVI + miR34a inhibitor (H). $p<0.05$.

Discussion

Results from *Specific Aim-3* indicate that CrVI activates p53-SIRT1-miR34a signaling network to induce germ cell apoptosis by increasing the expression of p53 and miR34a, and decreasing the SIRT1 expression. It is evident that SIRT1 directly interacts with p53 protein to deacetylate and inactivate p53 in cancer cells (463). However, the role of CrVI in modulating p53-SIRT1 interaction is unknown. In order to investigate the effect of CrVI on p53-SIRT1 interaction, fetal whole ovaries were cultured *ex vivo* and transfected with miR34a mimetic or inhibitor with or without CrVI. Results indicated that transfection with miR34a mimetic: (i) increased apoptosis of germ cells, (ii) increased mRNA expression of *p53 and Bax,* and decreased *Bcl2, AKT, and SIRT1*; (ii) increased protein expression of acetyl-p53 (K-382), cleaved caspase-3, BAX and decreased SIRT1, BCL2 and BCL-XL expression; (iii) decreased interaction between p53 and SIRT1 proteins compared to control; and (iv) miR34a mimetic attenuated the effects of CrVI on the above parameters. In turn miR34a inhibitor: (v) protected germ cells from CrVI-induced apoptosis; (vi) increased protein expression of SIRT1, BCL2 and BCL-XL and decreased expression of acetyl-p53, cleaved caspase-3 and BAX, (vii) increased interaction between p53 and SIRT1 proteins compared to control; and (viii) miR34a inhibitor mitigated or inhibited adverse effects of CrVI on germ cells survival.

Results indicate that transfection with miR34a mimetic decreased SIRT1 expression both in the presence or absence of CrVI and transfection with miR34a inhibitor mitigated CrVI-induced decrease in SIRT1 expression. It has been reported that SIRT1 is one of the targets of miR34a as the 3'UTR of SIRT1 has a response element for miR34a (291). Overexpression of miR34a decreased the SIRT1 protein levels in HCT116 cells and conversely, miR34a knockdown increased the SIRT1 protein expression. Thus miR34a targets SIRT1 and suppresses it by post-

transcriptional inhibition (291). Results indicate that transfection with miR34a mimetic increased acetyl-p53 expression both in the presence or absence of CrVI suggesting that CrVI-induced increase in the expression of miR34a could have targeted SIRT1 and decreased its expression by binding to the 3'UTR response elements in SIRT1. Since the function of SIRT1 is to deacetylate p53 at Lysine-382, the miR34a caused decrease in the expression of SIRT1 could have decreased the deacetylation function of SIRT1 thereby leading to increased levels of acetylated p53. It has been reported that AKT enhances the ubiquitination-promoting function of MDM2 by phosphorylation of Ser186 resulting in the reduction of p53 protein (464). Our data indicate that miR34a mimetic decreased the expression of pAKT both in the presence or absence of CrVI, suggesting that CrVI could have increased the half-life of p53 by reducing MDM2 mediated ubiquitination and proteasomal degradation of p53 by decreasing the phosphorylation of MDM2 by AKT.

Acetylated form of p53 is an active form which activates the transcription of the p53-target genes. It has been reported that PUMA is one of the target for activation by p53 (465). The function of PUMA is to bind to the anti-apoptotic BCL2 and mediate p53-induced cell death through the cytochrome c/Apaf-1-dependent pathway (465). Our data indicate that CrVI and SIRT1 inhibition increased the expression of PUMA, suggesting that miR34a could have mediated germ cell death through activation of PUMA by increasing the expression of acetyl-p53. Also, transfection with miR34a mimetic significantly decreased the expression of BCL2 and BCL-XL both in the presence and absence of CrVI. This suggests that activation and binding of PUMA to pro-survival BCL2 could have released the inhibition of BCL2 on the pro-apoptotic effectors BAX and BAK resulting in their activation (246). It has been reported that PUMA promotes BAX translocation by both directly interacting with BAX and by binding to BCL-XL during UV-induced apoptosis (460).

Data indicate that miR34a increased the expression of BAX and cl.capase-3 both in the presence and absence of CrVI. Thus CrVI-increased levels of PUMA could have interacted directly with BAX and promoted its translocation to mitochondria or PUMA could have activated BAX indirectly by relieving BAX from BCL2/BCL-XL inhibition and promoted its translocation to mitochondria resulting in the permeabilization of mitochondrial outer membrane and change in membrane potential. This change in mitochondria membrane potential could have released the cytochrome c and activated caspase-3 ultimately leading the germ cell to undergo apoptosis.

Findings from the literature clearly indicate that inhibition of SIRT1 induces growth arrest and apoptosis in a variety of cancer cells (466,467). Furthermore, p53 is a target for SIRT1; SIRT1 binds and deacetylates p53 resulting in its inactivation (292). In turn, activated p53 can induce the expression of miR34a which in turn targets and suppresses SIRT1 (268). p53-null mice have increased levels of SIRT1 and several p53-null tumor cell lines show SIRT1 overexpression (468). In line with the literature, our results clearly demonstrate that p53 and miR34a partner with each other to negatively regulate SIRT1 and induce germ cell apoptosis. Inhibition of miR34a ameliorates CrVI-induced germ cell apoptosis, and restore cell survival proteins such as AKT, BCL2 and BCL-XL against the adverse effects of CrVI. Thus, data from the *Specific Aim-3* clearly demonstrated that targeting miR34a could emerge as a potential therapeutic strategy to protect the ovaries from CrVI-induced toxic effects.

p53, Xpnpep2, and POF

Our data indicate that CrVI increases germ cell apoptosis and accelerates germ cell nest breakdown by upregulating p53. Since CrVI accelerated the germ cell apoptosis and accelerated germ cell nest breakdown and primordial follicle assembly by upregulating p53 which ultimately led to early reproductive senescence in adult female rats, we ventured to identify the mechanism

by which CrVI causes POF through p53. It has been reported that *Tripterygium* glycosides, a component extracted from the Chinese herb *Tripterygium wilfordii* Hook. f. induce POF in rats by inducing apoptosis and necrosis in rat ovarian tissues by inducing the p53 activation (469).

Upon cytogenetic and molecular analyses of women with POF, transcriptional characterization of breakpoint regions in balanced translocations led to the identification of five genes interrupted by translocations, the Xpnpep2 gene in Xq25 (353), the POF1B gene in Xq21.2 (354), the DACH2 gene in Xq21.3 (354), the CHM gene in Xq21.2 (355), and the DIAPH2 gene in Xq22 (356) and classified as POF marker genes in humans. Translocations that affect X chromosome structure increase apoptosis of germ cells (352), leading to POF.

It has been reported that forced expression of ectopic p53 in dermal fibroblasts repressed Col gene expression, whereas the absence of cellular p53 was found to be associated with the significantly enhanced transcriptional activity of the Type I Col gene (*COL1A2*) and Col synthesis by repressing TGFβ pathway (470). Interestingly, Col is one of the main substrates for the translated product of POF candidate protein gene Xpnpep2 which encodes the protein X-propyl aminopeptidase belonging to the family of ‘‘pita bread’’ metalloenzymes. It is expressed in prokaryotes and eukaryotes and hydrolyzes N-terminal Xaa-Pro bonds, where proline is the penultimate residue (471). The membrane-bound Xpnpep2 is a heavily glycosylated glycosylphosphatidylinositol-anchored protein of 673 amino acids encoded by the Xpnpep2 gene on human Xq25 (472). Apart from cols several biologically active polypeptides, including hormones, growth factors, and cytokines, contain N- terminal Xaa-Pro sequences and therefore are potential substrates for Xpnpep2.

Substrates of Xpnpep2

Because Cols contain a high proportion of such “triplets”, Xpnpep2 has the potential for intracellular (lysosomal) degradation of Col fibrils (473-475). In fact, proline and hydroxyproline constitute 20%-25% of the residues in Cols (476), and none of the lysosomal proteinases is capable of cleaving these linkages (474). Within the ovary and follicle, the extracellular matrix (ECM), including Cols, provides structural support, organizes and connects cells, serves as a reservoir for signaling molecules and growth factors that regulate follicle growth, provides a filtration barrier, and guides cell migration [28, 29]. The ECM also regulates the establishment of the basement membrane, oocyte maturation, follicle atresia, steroidogenesis, and cell lineage (387-390). The ECM components of the basal membrane affect follicle development in the ovary and are important for maintaining the polarity and the degree of polarization of granulosa cells (391-393). A recent study found that Col1 is spatially and temporally expressed in immature rat ovaries and is regulated by gonadotropins, suggesting a role for Col1 in morphogenesis of follicles as well as corpus luteum formation and regression (394). Col1 is expressed in the basal lamina of follicles and participates in the organization of the basal lamina (395). Thus, Cols are important in maintaining the histoarchitecture of the ovary and maintaining the microenvironment of the follicles and is imperative to identify the role played by Xpnpep2, the POF candidate gene whose main substrate is Col in the CrVI caused POF condition.

It has been also reported that peptidase D (PEPD), an enzyme that hydrolyzes dipeptides with proline or hydroxyproline at the carboxy terminus binds and suppresses nuclear and cytoplasmic p53 under normal conditions. It binds to the proline-rich domain in p53, which inhibits nuclear p53 phosphorylation and MDM2-mediated mitochondrial translocation of cytoplasmic and nuclear p53 (477). PEPD is expressed ubiquitously and is also important for Col metabolism

(478,479). The function of Xpnpep2 is similar to PEPD except that Xpnpep2 hydrolyzes peptides with proline or hydroxyproline in N-terminus while PEPD hydrolyzes PEPD in C-terminus. It is also reported that melatonin, the hormone secreted by pineal gland protects from POF by reducing oxidative stress and apoptotic damage via activation of SIRT1 signaling in a receptor-dependent manner (480). It is well known that SIRT1 deacetylates p53 and protects the cell from undergoing apoptosis while our data indicate that CrVI increased germ cell apoptosis by downregulating SIRT1 and upregulating p53. Thus the functional relation of Xpnpep2 with PEPD and its effects on p53, along with the connection between p53 and POF through SIRT1 and in turn the connection of Xpnpep2 to POF as a candidate gene logically directed us to explore and identify the role played by Xpnpep2 during normal ovary development and during CrVI exposure leading to POF in the following *Specific Aim-4*.

6. IDENTIFYING A NOVEL ROLE FOR X-PROLYL AMINOPEPTIDASE (XPNPEP)2 IN CRVI-INDUCED ADVERSE EFFECTS ON GERM CELL NEST BREAKDOWN AND FOLLICLE DEVELOPMENT IN RATS*

Specific Aim-4:

Determine the role of POF marker *Xpnpep-2* in CrVI-induced premature ovarian failure in F1 offspring.

Hypothesis*:*

This aim was based on the working hypothesis that "*Prenatal exposure to CrVI causes POF by targeting POF marker Xpnpep2 during fetal ovarian development*".

Objectives:

The objectives were to determine the effects of prenatal exposure to CrVI on (i) the germ cell apoptosis during fetal and postnatal ovarian development; (ii) the spatiotemporal expression of POF candidate protein aminopeptidase-2, encoded by the POF marker gene *Xpnpep-2* during ovarian development; and (iii) the targets or substrates for Xpnpep-2, namely the Cols Col1, Col3, and Col4 during GCN breakdown, primordial follicle assembly and during postnatal ovary development.

* Parts of this section are reprinted with permission from "Identifying a novel role for X-prolyl aminopeptidase (Xpnpep) 2 in CrVI-induced adverse effects on germ cell nest breakdown and follicle development in rats". Banu SK, Stanley JA, Sivakumar KK, Arosh JA, Mouneimne RB, Burghardt RC. Biology of Reproduction. 2015. Mar;92(3):67. PMID: 25568306. Copyright-2015. doi: 10.1095/biolreprod.114.125708. Epub 2015 Jan 7.

Results

Expression of Xpnpep2 and collagen distribution on the E15.5 ovary

The *Xpnpep2* gene is one of the marker genes for POF in women (481,482) and is involved in the hydrolysis of Cols (474). We recently showed that gestational exposure to CrVI induced POF in F1 rats (483). To understand the role of Xpnpep2 in regulating the distribution of Cols during GCN breakdown and ovarian development, we determined the distribution of Xpnpep2, Col1, Col3, and Col4 in the ovaries on E15.5, E17.5, PND1, PND4, and PND25.

On E15.5, the expression of Xpnpep2 was greater in the ovaries of CrVI-treated animals compared to control (Fig. 6.1, A-C). In the control ovaries, Col1 was highly expressed, with the Col1 bundles thicker along the ovigerous cords surrounding the GCN, and minimally expressed inside the GCN and between the germ cells (Fig. 6.1, D-F). CrVI significantly decreased the expression of Col1, and because the GCN had broken down to smaller nests, the penetration of Col1 within the nests and a few single oocytes was very obvious. In control ovaries on E15.5, Col3 and Col4 were distributed along the ovigerous cords (borders surrounding the GCN). CrVI down-regulated the expression of Col1, Col3, and Col4 (Fig. 6.1, D-L).

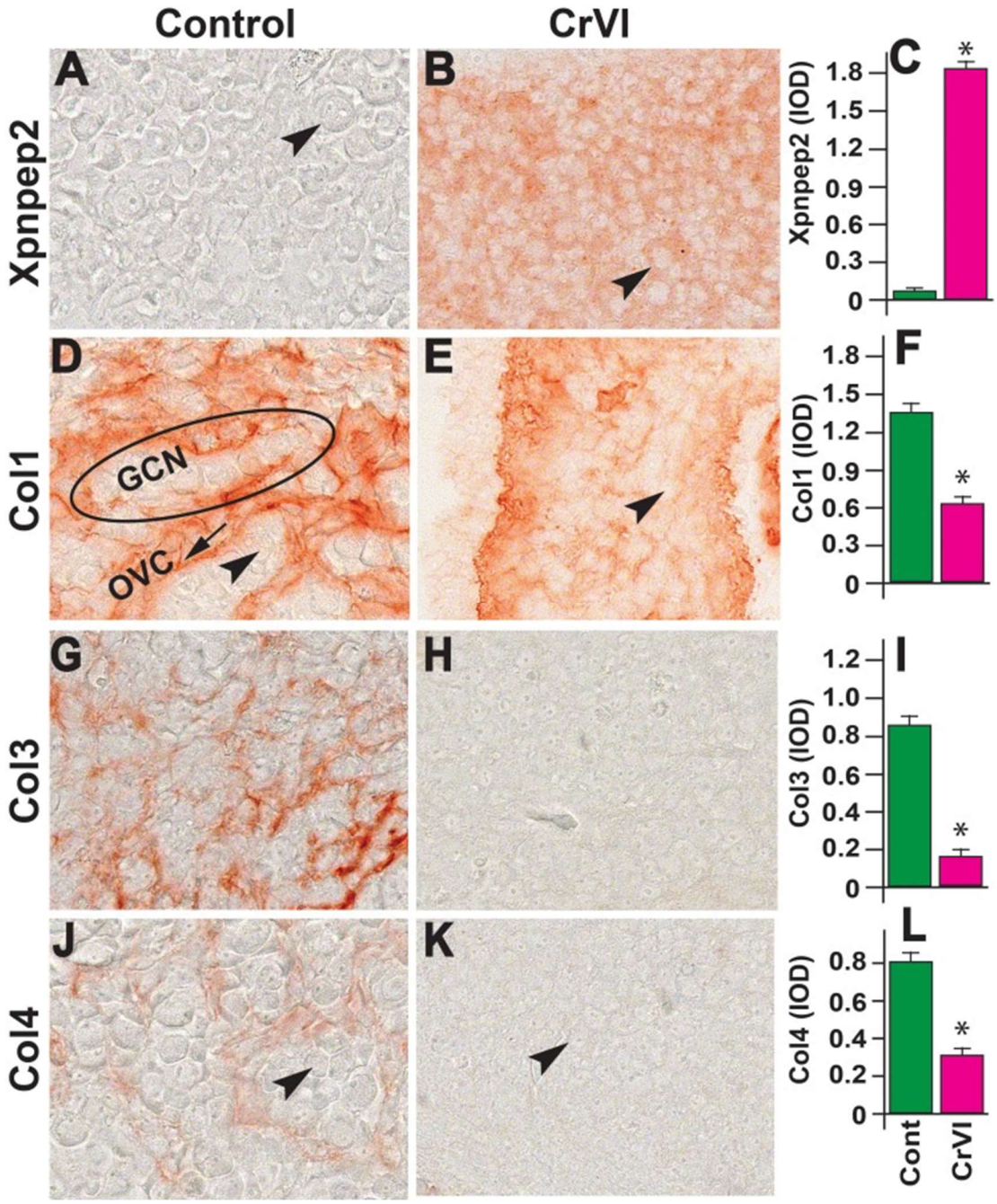

Fig. 6.1. Effects of prenatal exposure to CrVI on the expression of Xpnpep2 (A-C), Col1 (D-F), Col3 (G-I), and Col4 (J-L) proteins in the E15.5 ovaries. Ovaries from E15.5 fetuses were processed for IHC, and the integrated optical density (IOD) of staining was quantified using Image ProPlus software. The width of field for each image is 220 or 350μm. Arrowheads indicate germ cells. The ellipse indicates a GCN; an arrow indicates ovigerous cord (OVC). Each value represents the mean 6 SEM of 20-24 ovaries. *P<0.05, control vs. CrVI.

Expression of Xpnpep2 and collagen distribution on E17.5 ovary

On E17.5, ovaries from both control and CrVI groups had high expression of Xpnpep2, although expression was significantly greater in the CrVI group (Fig. 6.2, A-C). Col1 was expressed in both control and CrVI groups, whereas Col1 was significantly decreased in the CrVI group (Fig. 6.2, D-F). In the control group, Col1 was distributed at the periphery of the GCN along the ovigerous cords. In the CrVI group, Col1 was distributed around the smaller and disrupted nests of germ cells, with an increased thickness of Col bundles. Col3 and Col4 expression were very low, being sporadic and homogeneous in both control and CrVI-exposed ovaries, with a slight increase in the ovarian surface epithelium (OSE) in the control ovaries.

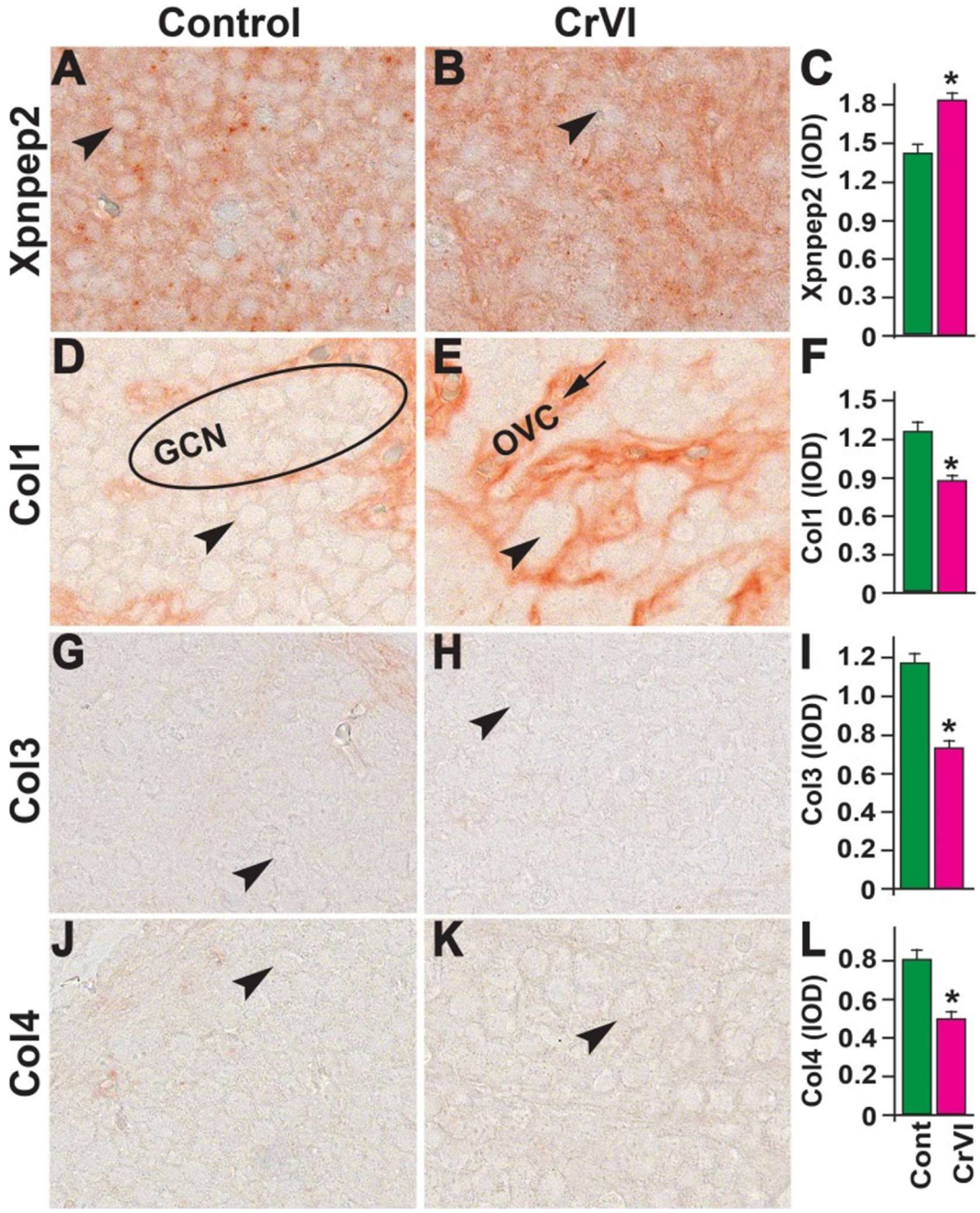

Fig. 6.2. Effects of prenatal exposure to CrVI on the expression of Xpnpep2 (A-C), Col1 (D-F), Col3 (G-I), and Col4 (J-L) proteins in the E17.5 ovaries. Ovaries from E17.5 fetuses were processed for IHC and the integrated optical density (IOD) of staining was quantified using Image ProPlus software. The width of field for each image is 220 or 350 µm. Arrowheads indicate germ cells. The ellipse indicates a GCN; an arrow indicates ovigerous cord (OVC). Each value represents the mean 6 SEM of 20-24 ovaries. *P<0.05, control vs. CrVI.

Expression of Xpnpep2 and collagen distribution on PND1 ovary

On PND1, CrVI significantly decreased ovarian Xpnpep2 levels compared to control (Fig. 6.3, A-C). Xpnpep2 was localized primarily within the oocytes compared to surrounding stroma and/or somatic cells. Accompanying the decreased Xpnpep2 levels in CrVI-treated animals, the expression of Col1, Col3, and Col4 was significantly increased compared to control animals (Fig. 6.3, D-L). The elevated Col1, Col3, and Col4 levels were predominantly localized around follicular basal lamina (Fig. 6.3, E, H, & K).

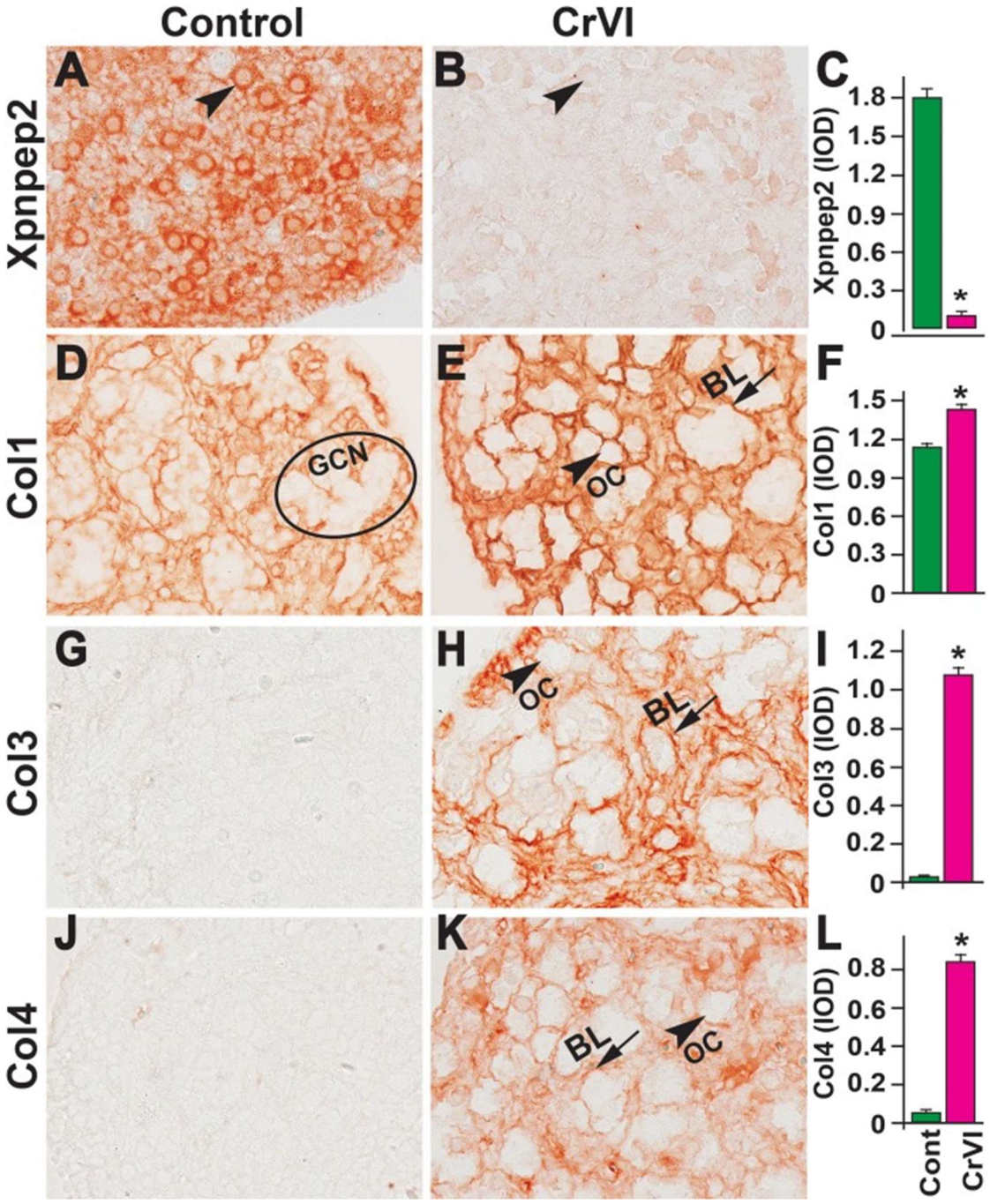

Fig. 6.3. Effects of prenatal exposure to CrVI on the expression of Xpnpep2 (A-C), Col1 (D-F), Col3 (G-I), and Col4 (J-L) proteins in the PND1 ovaries. Ovaries from PND1 pups (F1) were processed for IHC and the integrated optical density (IOD) of staining was quantified using Image ProPlus software. The width of field for each image is 220 or 350 µm. Arrowheads indicate germ cells or oocytes (OC); arrows indicate ovigerous cord basal lamina (BL) of the follicles. The ellipse indicates a GCN. Each value represents the mean 6 SEM of 15-18 ovaries. *P<0.05, control vs. CrVI.

Expression of Xpnpep2 and collagen distribution on PND4 ovary

On PND4, Xpnpep2 was highly expressed in the oocytes and moderately expressed in granulosa cells of control ovaries. In the CrVI group, Xpnpep2 was expressed only in the oocytes and at a very low level (Fig. 6.4, A-C), and the expression of Col1, Col3, and Col4 was elevated compared to control. Col1, Col3, and Col4 were distributed in the follicular basal lamina, stroma, and interstitium in both the control and CrVI groups (Fig. 6.4, D-L).

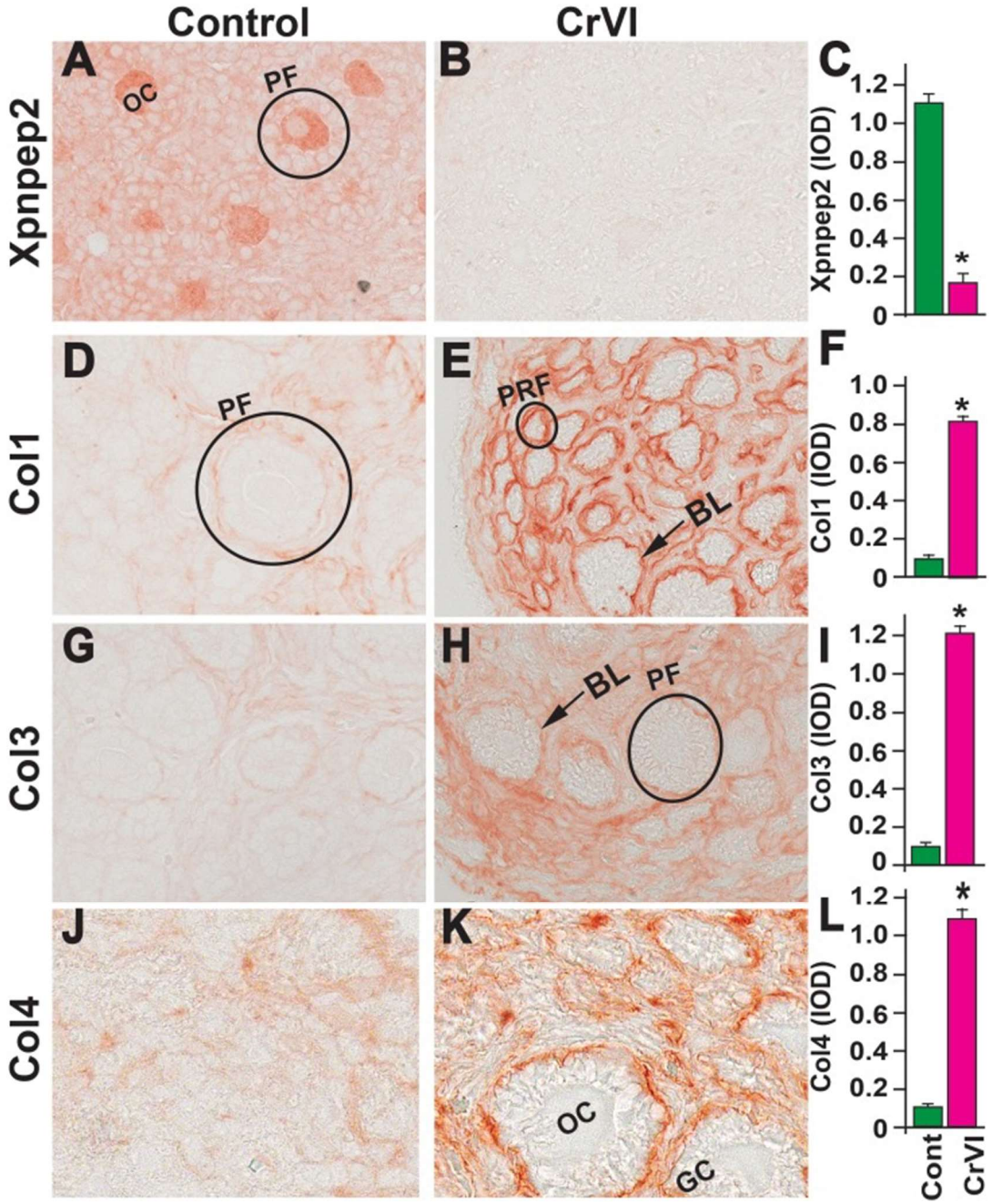

Fig. 6.4. Effects of prenatal exposure to CrVI on the expression of Xpnpep2 (A-C), Col1 (D-F), Col3 (G-I), and Col4 (J-L) proteins in the PND4 ovaries. Ovaries from PND4 pups (F1) were processed for IHC and the integrated optical density (IOD) of staining was quantified using Image ProPlus software. The width of field for each image is 220 or 350 µm. Each value represents the mean 6 SEM of 20-24 ovaries. Arrows indicate basal lamina (BL) of the follicle. A circle or ellipse indicates a primordial follicle (PRM) or primary follicle (PF). OC, oocyte; GC, granulosa cell. *P<0.05, control vs. CrVI.

Expression of Xpnpep2 and collagen distribution on PND25 ovary

On PND25, Xpnpep2 remained highly expressed in the oocytes and granulosa cells of control ovaries and barely detectable in CrVI-exposed ovaries (Fig. 6.5, A-C). In the control ovaries, Col1 was highly expressed in the follicular basal lamina, stroma, and theca/interstitial cells and in the OSE (Fig. 6.5, D). In the CrVI-treated animals, Col1 expression was elevated in the granulosa cells, follicular fluid, follicular basal lamina, stroma, and interstitium (Fig. 6.5, E). In both the control and CrVI groups, Col3 and Col4 were expressed around the oocytes, within the granulosa cells, and around the antrum and follicular basal membrane (Fig. 6.5, G-L); however, CrVI up-regulated Col3 and Col4 and increased their expression within the oocyte, follicular fluid, follicular basal lamina, and theca interstitium (Fig. 6.5, H & K).

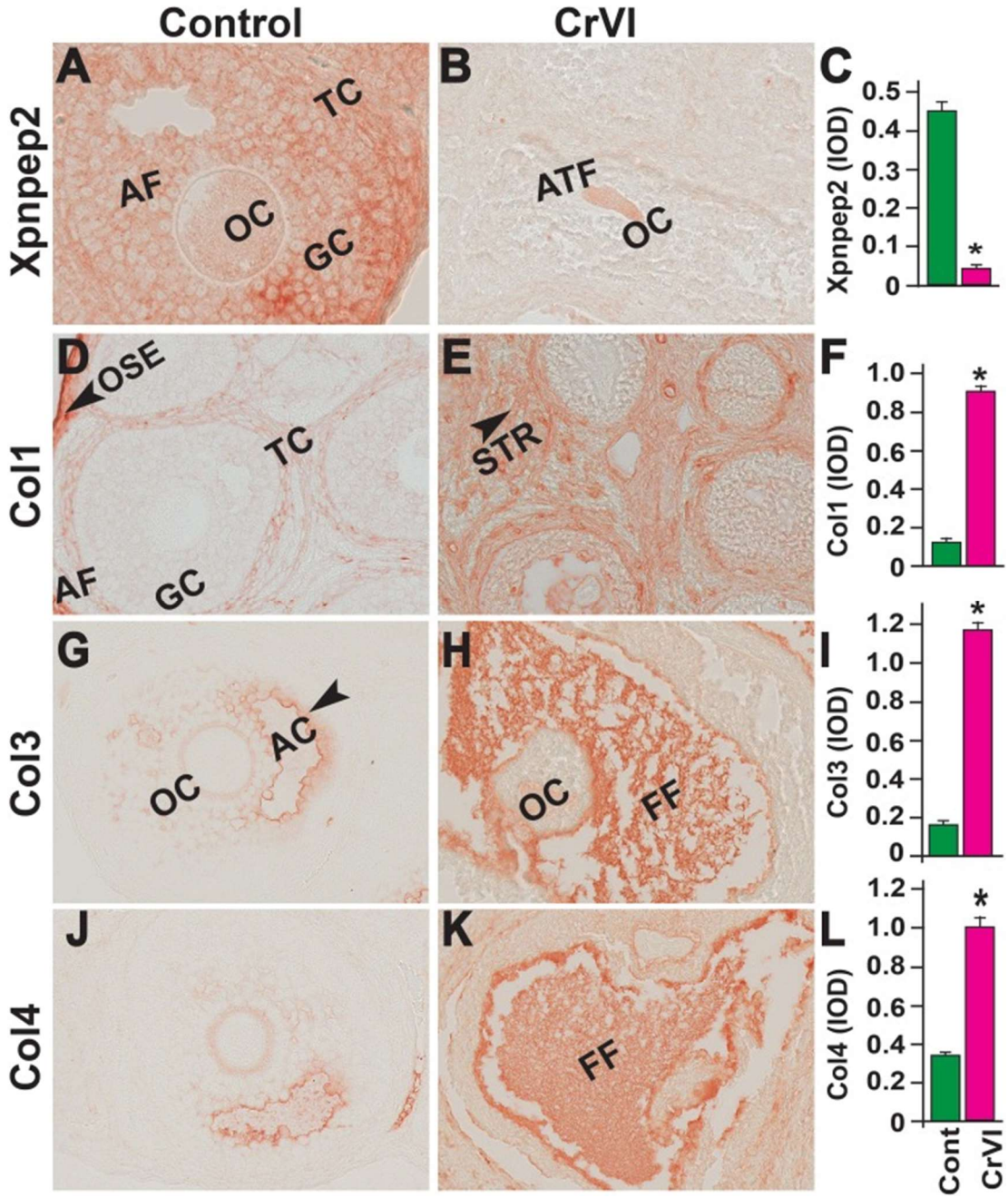

Fig. 6.5. Effects of prenatal exposure to CrVI on the expression of Xpnpep2 (A-C), Col1 (D-F), Col3 (G-I), and Col4 (J-L) proteins in the PND25 ovaries. Ovaries from PND25 pups (F1) were processed for IHC and the integrated optical density (IOD) of staining was quantified using Image ProPlus software. The width of field for each image is 220 or 350 µm. Each value represents the mean 6 SEM of 20-24 ovaries. OC, oocyte; GC, granulosa cells; TC, theca cells; ATF, atretic follicle; STR, stroma; AC, antral cavity; FF, follicular fluid. *P<0.05, control vs. CrVI.

Xpnpep2 is colocalized with Col3 and Col4 in fetal ovaries

Data from the IHC showed a significant negative correlation between the expressions of Xpnpep2 and Col1, Col3, and Col4. To confirm the colocalization of Xpnpep2 and Cols, we performed whole-mount double immunofluorescence labeling of Xpnpep2 with Col3 and Col4 on E17.5. Xpnpep2 was colocalized with Col3 (Fig. 6.6, A-F) and Col4 (Fig. 6.7, A-F) in both control and CrVI groups around the germ cells, GCN, and along the ovigerous cords. However, CrVI significantly increased colocalization of Xpnpep2 with Col3 (Fig. 6.6, G) and Col4 (Fig. 6.7, G).

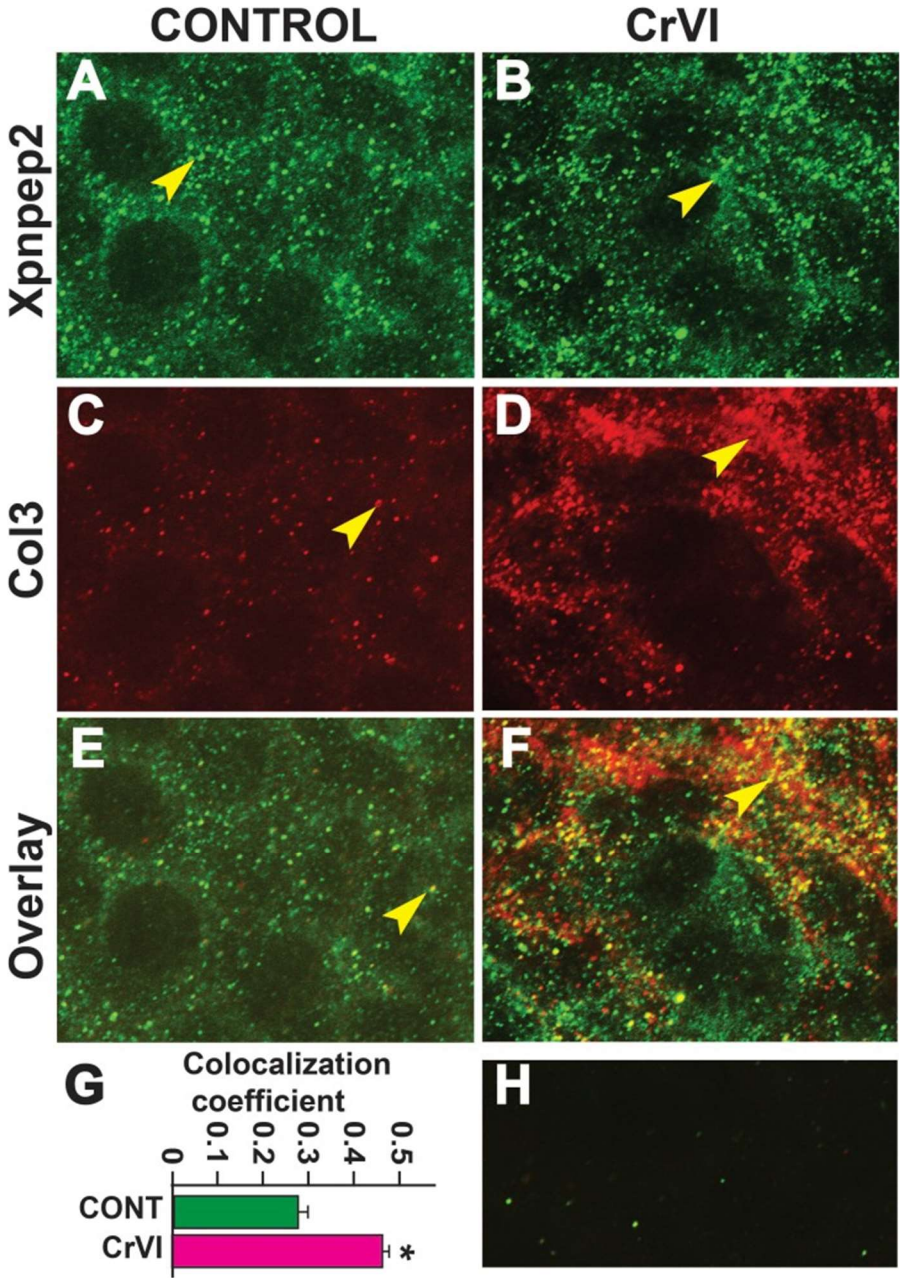

Fig. 6.6. Effects of prenatal exposure to CrVI on colocalization of Xpnpep2 and Col3 proteins in the E17.5 ovaries. On E17.5, ovaries from fetuses were processed for whole-mount double immunofluorescence assay. Colocalization of Xpnpep2 and Col3 proteins was evaluated by confocal microscopy. CrVI significantly increased colocalization of Xpnpep2 and Col3 proteins compared to control (overlay; E and F). Width of the images was 115 µm. Arrowheads indicate localization of Xpnpep2 (A and B), localization of Col3 (C and D), and colocalization of Xpnpep2 and Col4 (E and F) in a GCN. Histogram of colocalization coefficient (G), and negative control (H) are shown. *P<0.05, control vs. CrVI.

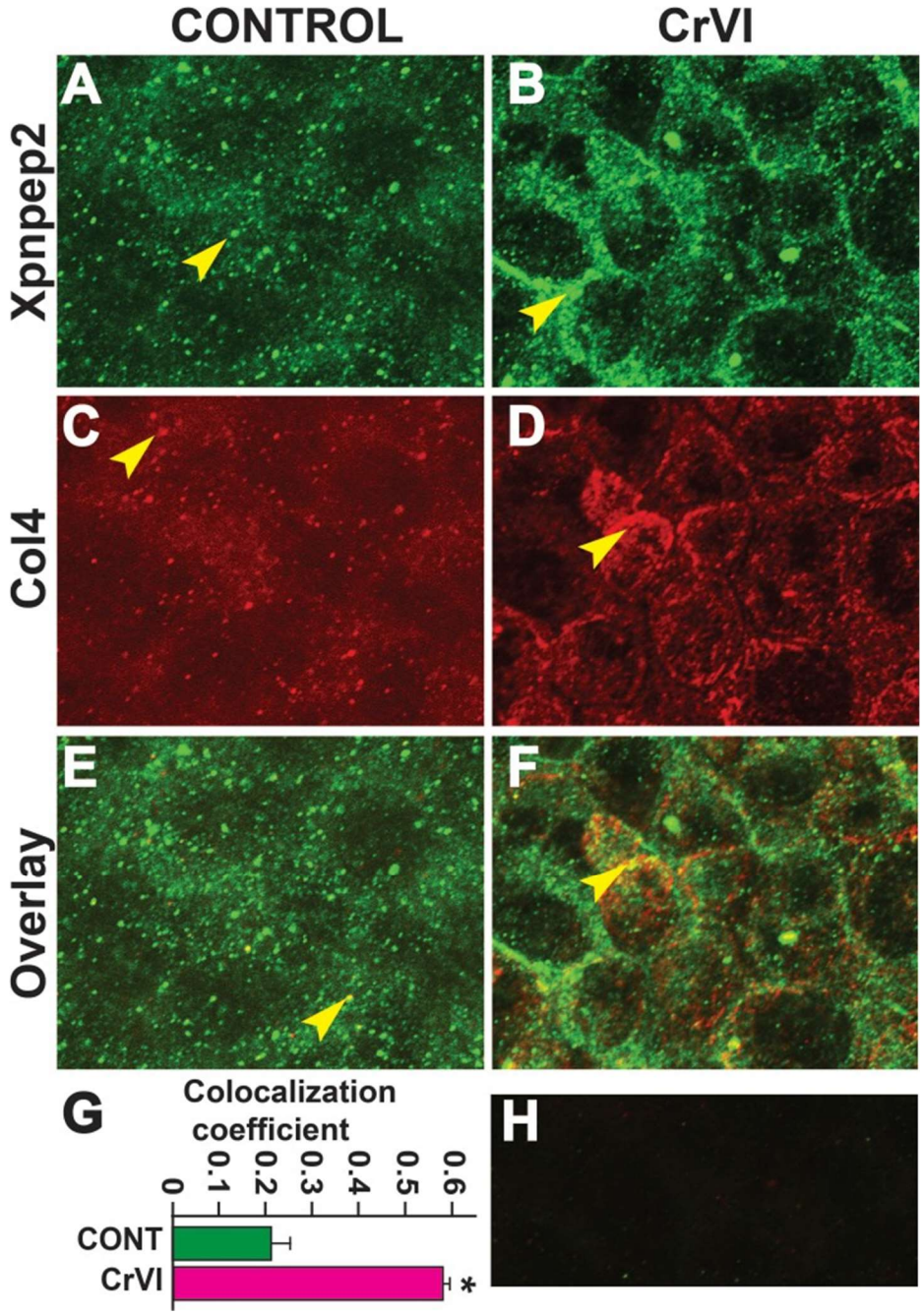

Fig. 6.7. Effects of prenatal exposure to CrVI on colocalization of Xpnpep2 and Col4 proteins in the E17.5 ovaries. On E17.5, ovaries from fetuses were processed for whole-mount double immunofluorescence assay. Colocalization of Xpnpep2 and Col4 proteins was evaluated by confocal microscopy. CrVI significantly increased colocalization of Xpnpep2 and Col4 proteins compared to control (overlay; E and F). The width of field for images was 115μm. Arrowheads indicate localization of Xpnpep2 (A and B), localization of Col4 (C and D), and colocalization of Xpnpep2 and Col4 (E and F) in a GCN. Histogram of colocalization coefficient (G) and negative control (H) are shown. *P<0.05, control vs. CrVI.

Discussion

Xpnpep2 and its potential targets

Xpnpep2, the gene that encodes the protein X-propyl aminopeptidase belonging to the family of "pita bread" metalloenzymes are one of the marker genes for POF in women and it hydrolyzes N-terminal Xaa-Pro bonds, where proline is the penultimate residue (356,471). Some of the potential targets of Xpnpep2 are collagens (Cols), hormones, growth factors, and cytokines as they contain N terminal Xaa-Pro sequences. Xpnpep2 has the potential for intracellular (lysosomal) degradation of Col fibrils as they contain a high proportion of such 'triplets' (474-476). In the ovary, the normal follicle development and oocyte maturation are relying on the intracellular communication among the various cell types and the stroma which is highly dependent on the follicular architecture (484). The extracellular matrix (ECM) is composed of a variety of molecules, which can include collagens, laminin, fibronectin, proteoglycans, and polysaccharides (485).

Within the ovary and follicle, the ECM including Cols provides structural support, provides a filtration barrier, organizes and connects cells, serves as a signaling molecule and growth factor reservoir, and guides cell migration (388,486). There are a number of different compartments and ECM in ovary follicles. These include the follicular basal lamina, follicular fluid, zona pellicuda, membrana granulosa, cumulus, and either theca interna and theca externa in larger antral follicles, or the stroma in the smaller primordial and preantral follicles (487). While the matrices of follicles have each been studied to varying degrees, the specific role of ECM in germ cell nest breakdown or early development of the follicles is not known yet. Since Xpnpep2 is a POF candidate gene and hydrolyzes cols, we ventured to understand the role of Xpnpep2 in regulating the distribution

of Cols during GCN breakdown and ovarian development by determining the distribution of Xpnpep2, Col1, Col3, and Col4 in the ovaries on E15.5, E17.5, PND1, PND4, and PND25.

Spatiotemporal expression of Xpnpep2 and Col distribution during GCN breakdown

Our data for the first time showed that Xpnpep2 is involved in germ cell nest breakdown under normal physiological conditions and that CrVI advances and accelerates GCN breakdown by up-regulating Xpnpep2 and decreasing the distribution of Col1, Col3, and Col4 in the fetal ovary on E15.5 and E17.5. During germ cell nest breakdown, a negative correlation in the levels of Xpnpep2 and Cols were observed suggesting that Xpnpep2 may be a direct regulator of Cols during nest breakdown. To confirm this, we colocalized Xpnpep2 with Col3 and Col4 in the E15.5 and E17.5 whole mount ovaries. Results indicated that in both E15.5 and E17.5, Xpnpep2 was co-localized with Col3 and Col4 along the ovigerous cords, within the germ cell nest, and around the germ cells in both control and CrVI groups. Both control and CrVI groups had lower levels of Col3 and Col4, and their co-localization with Xpnpep-2 was stronger on E17.5, a time point when the germ cell nest breakdown just began in control group, whereas CrVI group had already reached its peak level. It is suggested that hydrolysis or degradation of Col3 and Col4 may facilitate germ cell nest breakdown. These results indicate that CrVI advanced germ cell nest breakdown by upregulating Xpnpep2 and whether under normal physiological conditions or CrVI exposure, Xpnpep2 may facilitate germ cell nest breakdown by regulating the hydrolysis of Cols.

Spatiotemporal expression of Xpnpep2 and Col distribution during postnatal ovary development

To investigate whether Xpnpep2 play a role during postnatal ovarian development, we studied the expression of the Xpnpep2 protein in the ovaries at PND1, PND4, and PND25 under normal physiological conditions and following gestational exposure to CrVI. Results indicated an

interesting spatio-temporal pattern of Xpnpep2 expression during primordial follicle assembly and primary follicle transition. Xpnpep2 expression was increased from E17.5 to PND1, a window where germ cell nest breakdown peaks and its expression declined on PND4 and PND25. Whereas, CrVI down-regulated Xpnpep2 on PND1, PND4, and PND25, when an increased follicle atresia was observed compared to control. In all studied age groups, we observed a negative correlation of expression of Col1, Col3, and Col4 with Xpnpep2 expression.

CrVI increased follicular atresia by targeting Xpnpep2

The ECM sequesters and provides a repository for cytokines, enzymes, and growth factors and contributes significantly to establishing stage-specific follicle microenvironments that allow or restrict access of growth factors and hormones to the follicle (484,488). Hence the ECM components have to be degraded or hydrolyzed to release these active molecules necessary for the follicle development or else the developing follicle will be deprived of the growth factors and will eventually undergo atresia. Analyzing these data together, increased col accumulation due to decreased Xpnpep2 expression during the postnatal ovary development suggest that increased Cols may have altered the histoarchitecture of the ovary and microenvironment of the follicles, thus preventing intercellular communication and/or paracrine signaling by inhibiting the release and distribution of active growth factors required for the survival and growth of the follicle. This could be the reason for the observation of an increased number of atretic follicles in CrVI exposed groups during fetal and postnatal ovary development.

In summary, results of S*pecific Aim-4* indicate that Xpnpep2 may play a critical role during germ cell nest breakdown and primordial follicle assembly by regulating the distribution of Cols during normal development of the ovary. During germ cell nest breakdown, CrVI up-regulates Xpnpep2 and decreases Col distribution, and during primordial follicle assembly, CrVI down-

regulates Xpnpep2 and up-regulates Col in a spatiotemporal pattern. And CrVI increases accumulation of Cols by decreasing expression of Xpnpep2 that eventually leads to an increase in follicle atresia in F1 offspring. These novel findings suggest, to our knowledge for the first time that disruption of the Xpnpep2 gene in women with POF may result in abnormal accumulation of Cols, follicle atresia, and early reproductive senescence or infertility.

7. SUMMARY AND CONCLUSIONS

1. Prenatal exposure to CrVI significantly elevated total Cr levels and increased its accumulation in the placenta when SD rats were administered with 25ppm CrVI, a dose relevant to human/environmental exposure through drinking water in order to mimic human exposure to CrVI.
2. CrVI decreased pregnancy outcome and reduced litter size, and induced early reproductive senescence in F1 offspring.
3. CrVI accelerated oocytes/germ cells and somatic/granulosa cells apoptosis on E15.5, E17.5, PND 1, PND 4, and PND 25 ovaries.
4. CrVI upregulated the expression of the pro-apoptotic p53, p27, BAX, and cleaved-caspase-3, along with SOD-2. CrVI increased co-localization of p53 and SOD-2 proteins, and p53 inhibited the antioxidant function of the SOD-2. CrVI also downregulated the expression of p-AKT, p-ERK, and XIAP thus reduced the pro-survival pathways in the PND-1 ovaries of F1 pups. As a result of these events, CrVI accelerated germ cell and somatic cell apoptosis, advanced germ cell nest breakdown, primordial follicle assembly, and enhanced primordial to primary follicle transition, culminating in increased follicular atresia.
5. CrVI increased germ cells apoptosis and accelerated germ cell best breakdown by mediating a positive loop of the p53-miR34a-SIRT1 regulatory network by increasing the expression and activation of p53, increasing miR34a expression and decreasing SIRT1 expression. p53 and miR34a partner with each other to negatively regulate SIRT1 and induced germ cell apoptosis by down-regulating the cell survival anti-apoptotic factors and upregulating the pro-apoptotic factors.

6. Xpnpep2, a POF marker gene may play a critical role during germ cell nest breakdown and primordial follicle assembly by regulating the distribution of Cols during normal development of the ovary. CrVI up-regulates Xpnpep2 and decreases Col distribution during germ cell nest breakdown and CrVI down-regulates Xpnpep2 and up-regulates Col during primordial follicle assembly. CrVI induces decreased expression of Xpnpep2 and increased accumulation of Cols that eventually leads to an increase in follicle atresia.

   All these adverse effects of CrVI ultimately resulted in early reproductive senescence/POF in the F1 rat offspring.

The contribution of this dissertation to society is significant as the results and outcomes of this research work can be translated to clinics by developing intervention strategies, which may help to treat the reproductive health problems faced by the women who were affected by CrVI exposure either directly or indirectly.

REFERENCES

1. Zhitkovich A. Chromium in drinking water: sources, metabolism, and cancer risks. Chemical research in toxicology 2011; 24:1617-1629
2. Wilbur S, Abadin H, Fay M, Yu D, Tencza B, Ingerman L, Klotzbach J, James S. Agency for Toxic Substances and Disease Registry (ATSDR) Toxicological Profiles. Toxicological Profile for Chromium. Atlanta (GA): Agency for Toxic Substances and Disease Registry (US); 2012:419.
3. WHO. Chromium in Drinking-water. Guidelines for drinking-water quality. Vol 2. 2 ed. Geneva: World Health Organization; 1996: http://www.who.int/iris/handle/10665/38551.
4. Anderson RA. Chromium as an Essential Nutrient for Humans. Regulatory Toxicology and Pharmacology 1997; 26:S35-S41
5. Pechova A, Pavlata L. Chromium as an essential nutrient: a review. Veterinarni Medicina 2007; 52:1-18
6. Cerulli J, Grabe DW, Gauthier I, Malone M, McGoldrick MD. Chromium picolinate toxicity. Annals of pharmacotherapy 1998; 32:428-431
7. Crawford V, Scheckenbach R, Preuss HG. Effects of niacin-bound chromium supplementation on body composition in overweight African-American women. Diabetes, obesity & metabolism 1999; 1:331-337
8. Cefalu WT, Hu FB. Role of chromium in human health and in diabetes. Diabetes care 2004; 27:2741-2751
9. Offenbacher EG, Pi-Sunyer FX. Beneficial effect of chromium-rich yeast on glucose tolerance and blood lipids in elderly subjects. Diabetes 1980; 29:919-925
10. Stanley JA, Arosh JA, Burghardt RC, Banu SK. A fetal whole ovarian culture model for the evaluation of CrVI-induced developmental toxicity during germ cell nest breakdown. Toxicology and applied pharmacology 2015; 289:58-69
11. USEPA. National primary drinking water regulations. 2009(EPA-816-F-09–004):1-6. https://www.nrc.gov/docs/ML1307/ML13078A040.pdf.
12. Tchounwou PB, Yedjou CG, Patlolla AK, Sutton DJ. Heavy Metals Toxicity and the Environment. EXS 2012; 101:133-164
13. Junaid M, Hashmi MZ, Malik RN, Pei D-S. Toxicity and oxidative stress induced by chromium in workers exposed from different occupational settings around the globe: A review. Environmental Science and Pollution Research 2016; 23:20151-20167
14. Kirpnick-Sobol Z, Reliene R, Schiestl RH. Carcinogenic Cr (VI) and the nutritional supplement Cr (III) induce DNA deletions in yeast and mice. Cancer research 2006; 66:3480-3484
15. Annangi B, Bonassi S, Marcos R, Hernández A. Biomonitoring of humans exposed to arsenic, chromium, nickel, vanadium, and complex mixtures of metals by using the micronucleus test in lymphocytes. Mutation Research/Reviews in Mutation Research 2016; 770:140-161
16. Barceloux DG. Chromium. J Toxicol Clin Toxicol 1999; 37:173-192
17. Nriagu JO, Pacyna JM. Quantitative assessment of worldwide contamination of air, water and soils by trace metals. nature 1988; 333:134-139

18. Armienta-Hernandez A, Rodriguez-Castillo R. Environmental exposure to chromium compounds in the valley of Leon, Mexico. Environmental Health Perspectives 1995; 103:47-51
19. Dubey C, Sahoo B, Nayak N. Chromium (VI) in waters in parts of Sukinda chromite valley and health hazards, Orissa, India. Bulletin of environmental contamination and toxicology 2001; 67:541-548
20. Zhang JD, Li XL. Chromium pollution of soil and water in Jinzhou. Zhonghua Yu Fang Yi Xue Za Zhi 1987; 21:262-264
21. Banchhor Alka PM, Pandey Piyush kant. A review of hexavalent chromium contamination in India. Research Journal of Chemical Sciences 2017; 7:39-44
22. Rangasamy S, Purushothaman G, Alagirisamy B, Santiago M. Chromium contamination in soil and groundwater due to tannery wastes disposals at Vellore district of Tamil Nadu. International Journal of Environmental Sciences 2015; 6:114
23. USGS. Mineral commodity summaries 2018. US Geological Survey 2018:1-200. https://doi.org/10.3133/70194932.
24. Sutton R. Chromium-6 in U.S. Tap Water. Washington, DC2010.
25. Coleman R. UPDATE: 'Erin Brockovich' Carcinogen in 250 Million Americans' Drinking Water 2017; https://www.ewg.org/enviroblog/2017/08/update-erin-brockovich-carcinogen-250-million-americans-drinking-water#.WylUt6LErG-. Accessed 06/19/2018, 2018.
26. Jin Y, Liu Z, Liu F, Ye Y, Peng T, Fu Z. Embryonic exposure to cadmium (II) and chromium (VI) induce behavioral alterations, oxidative stress and immunotoxicity in zebrafish (Danio rerio). Neurotoxicology and Teratology 2015; 48:9-17
27. Basu D, Blackburn K, Harris B, Neal M, Stoss F. Health Assessment Document for Chromium. Final Report. 1984;
28. Association AWW. Chromium in drinking water: a technical information primer. March; 2013.
29. Stout MD, Herbert RA, Kissling GE, Collins BJ, Travlos GS, Witt KL, Melnick RL, Abdo KM, Malarkey DE, Hooth MJ. Hexavalent Chromium Is Carcinogenic to F344/N Rats and B6C3F1 Mice after Chronic Oral Exposure. Environmental Health Perspectives 2009; 117:716-722
30. Malott V. West County Road 112 ground water plume. EPA Region 6 2014:1-7
31. CalEPA. Chromium-6 Drinking Water MCL. California Environmental Protection Agency 2017; https://www.waterboards.ca.gov/drinking_water/certlic/drinkingwater/Chromium6.html.
32. GarcÍa E, Cabrera C, Lorenzo ML, LÓpez MC, SÁnchez J. Estimation of chromium bioavailability from the diet by an in vitro method. Food Additives & Contaminants 2001; 18:601-606
33. Kerger BD, Richter R, Chute S, Dodge D, Overman S, Liang J, Finley B, Paustenbach D. Refined exposure assessment for ingestion of tapwater contaminated with hexavalent chromium: consideration of exogenous and endogenous reducing agents. Journal of exposure analysis and environmental epidemiology 1996; 6:163-179
34. Sun H, Brocato J, Costa M. Oral chromium exposure and toxicity. Current environmental health reports 2015; 2:295-303

35. DiSilvestro RA, Dy E. Comparison of acute absorption of commercially available chromium supplements. Journal of Trace Elements in Medicine and Biology 2007; 21:120-124
36. Sullivan M, Miller B, Goebel J. Gastrointestinal absorption of metals (51Cr, 65Zn, 95mTc, 109Cd, 113Sn, 147Pm, and 238Pu) by rats and swine. Environmental research 1984; 35:439-453
37. Schroeder HA, Balassa JJ, Tipton IH. Abnormal trace metals in man—chromium. Journal of chronic diseases 1962; 15:941-964
38. Maruyama J. The health effect of mice given oral administration of trivalent and hexavalent chromium over long-term. Acta Scholae Medicinalis Universitatis in Gifu 1982; 31:24-46
39. MacKenzie R, Byerrum R, Decker C, Hoppert C, Langham R. Chronic Toxi-city Studies. II. Hexavalent and Trivalent Chromium administered in Drinking Water to Rats. Arch Indust Health 1958; 18:232-234
40. Kargacin B, Squibb KS, Cosentino S, Zhitkovich A, Costa M. Comparison of the uptake and distribution of chromate in rats and mice. Biological trace element research 1993; 36:307
41. Collins BJ, Stout MD, Levine KE, Kissling GE, Melnick RL, Fennell TR, Walden R, Abdo K, Pritchard JB, Fernando RA. Exposure to hexavalent chromium resulted in significantly higher tissue chromium burden compared with trivalent chromium following similar oral doses to male F344/N rats and female B6C3F1 mice. Toxicological Sciences 2010; 118:368-379
42. De Flora S, Camoirano A, Bagnasco M, Bennicelli C, Corbett G, Kerger B. Estimates of the chromium (VI) reducing capacity in human body compartments as a mechanism for attenuating its potential toxicity and carcinogenicity. Carcinogenesis 1997; 18:531-537
43. Samitz M. Ascorbic acid in the prevention and treatment of toxic effects from chromates. Acta dermato-venereologica 1970; 50:59
44. De Flora S. Threshold mechanisms and site specificity in chromium (VI) carcinogenesis. Carcinogenesis 2000; 21:533-541
45. Pellerin C, Booker SM. Reflections on hexavalent chromium: health hazards of an industrial heavyweight. Environmental health perspectives 2000; 108:A402
46. Valko M, Morris H, Cronin MT. Metals, toxicity and oxidative stress. Current medicinal chemistry 2005; 12:1161-1208
47. Valko M, Rhodes CJ, Moncol J, Izakovic M, Mazur M. Free radicals, metals and antioxidants in oxidative stress-induced cancer. Chem Biol Interact 2006; 160:1-40
48. Gruber J, Jennette K. Metabolism of the carcinogen chromate by rat liver microsomes. Biochemical and biophysical research communications 1978; 82:700-706
49. Hoch-Ligeti C, Bourne G. Changes in the concentration and histological distribution of the ascorbic acid in ovaries, adrenals and livers of rats during oestrous cycles. British Journal of Experimental Pathology 1948; 29:400-407
50. Deane HW. Histochemical observations on the ovary and oviduct of the albino rat during the estrous cycle. Developmental Dynamics 1952; 91:363-413
51. Standeven AM, Wetterhahn KE. Is there a role for reactive oxygen species in the mechanism of chromium (VI) carcinogenesis? Chemical research in toxicology 1991; 4:616-625

52. Brooks B, O'Brien TJ, Ceryak S, Wise JP, Wise SS, Wise JP, DeFabo E, Patierno SR. Excision repair is required for genotoxin-induced mutagenesis in mammalian cells. Carcinogenesis 2008; 29:1064-1069
53. Lee J-C, Son Y-O, Pratheeshkumar P, Shi X. Oxidative stress and metal carcinogenesis. Free Radical Biology and Medicine 2012; 53:742-757
54. Wise SS, Holmes AL, Wise JP, Sr. Hexavalent chromium-induced DNA damage and repair mechanisms. Rev Environ Health 2008; 23:39-57
55. Jennette KW. Microsomal reduction of the carcinogen chromate produces chromium (V). Journal of the American Chemical Society 1982; 104:874-875
56. Guthtie BE. The nutritional role of chromium. In: Langård S, ed. Biological and Environmental Aspects of Chromium: Elsevier; 1982:117-148.
57. Langård S. Biological and environmental aspects of chromium. Vol 5: Elsevier.
58. Netherlands HCot. Chromium VI compounds. Evaluation of the effects on reproduction, recommendation for classification. . The Hague: Health Council of the Netherlands 2016; publication no. 2016/04.
59. Wang S, Shi X. Molecular mechanisms of metal toxicity and carcinogenesis. Molecular Mechanisms of Metal Toxicity and Carcinogenesis: Springer; 2001:3-9.
60. Leonard SS, Bower JJ, Shi X. Metal-induced toxicity, carcinogenesis, mechanisms and cellular responses. Molecular and cellular biochemistry 2004; 255:3-10
61. Shi X, Dalal N. The role of superoxide radical in chromium (VI)-generated hydroxyl radical: the Cr (VI) Haber-Weiss cycle. Archives of biochemistry and biophysics 1992; 292:323-327
62. Benov L. How superoxide radical damages the cell. Protoplasma 2001; 217:33-36
63. Ding M, Shi X. Molecular mechanisms of Cr (VI)-induced carcinogenesis. Molecular and cellular biochemistry 2002; 234:293-300
64. Wang X, Son Y-O, Chang Q, Sun L, Hitron JA, Budhraja A, Zhang Z, Ke Z, Chen F, Luo J. NADPH oxidase activation is required in reactive oxygen species generation and cell transformation induced by hexavalent chromium. Toxicological Sciences 2011; 123:399-410
65. Son Y-O, Hitron JA, Wang X, Chang Q, Pan J, Zhang Z, Liu J, Wang S, Lee J-C, Shi X. Cr (VI) induces mitochondrial-mediated and caspase-dependent apoptosis through reactive oxygen species-mediated p53 activation in JB6 Cl41 cells. Toxicology and applied pharmacology 2010; 245:226-235
66. Droge W. Free radicals in the physiological control of cell function. Physiological reviews 2002; 82:47-95
67. Cadet J, Douki T, Ravanat J-L. Oxidatively generated damage to the guanine moiety of DNA: mechanistic aspects and formation in cells. Accounts of chemical research 2008; 41:1075-1083
68. Cadet J, Douki T, Ravanat J-L. Oxidatively generated base damage to cellular DNA. Free Radical Biology and Medicine 2010; 49:9-21
69. Dizdaroglu M, Kirkali G, Jaruga P. Formamidopyrimidines in DNA: mechanisms of formation, repair, and biological effects. Free Radical Biology and Medicine 2008; 45:1610-1621

70. Matés JM, Sánchez-Jiménez FM. Role of reactive oxygen species in apoptosis: implications for cancer therapy. The international journal of biochemistry & cell biology 2000; 32:157-170
71. Son Y-O, Jang Y-S, Heo J-S, Chung W-T, Choi K-C, Lee J-C. Apoptosis-inducing factor plays a critical role in caspase-independent, pyknotic cell death in hydrogen peroxide-exposed cells. Apoptosis 2009; 14:796-808
72. Son YO, Kook SH, Jang YS, Shi X, Lee JC. Critical role of poly (ADP-ribose) polymerase-1 in modulating the mode of cell death caused by continuous oxidative stress. Journal of cellular biochemistry 2009; 108:989-997
73. Broedbaek K, Weimann A, Stovgaard ES, Poulsen HE. Urinary 8-oxo-7, 8-dihydro-2′-deoxyguanosine as a biomarker in type 2 diabetes. Free Radical Biology and Medicine 2011; 51:1473-1479
74. Calderón-Garcidueñas L, Wen-Wang L, Zhang Y-J, Rodriguez-Alcaraz A, Osnaya N, Villarreal-Calderón A, Santella RM. 8-hydroxy-2'-deoxyguanosine, a major mutagenic oxidative DNA lesion, and DNA strand breaks in nasal respiratory epithelium of children exposed to urban pollution. Environmental health perspectives 1999; 107:469
75. Demple B, Harrison L. Repair of oxidative damage to DNA: enzymology and biology. Annual review of biochemistry 1994; 63:915-948
76. Ha L, Ceryak S, Patierno SR. Generation of S phase-dependent DNA double-strand breaks by Cr (VI) exposure: involvement of ATM in Cr (VI) induction of γ-H2AX. Carcinogenesis 2004; 25:2265-2274
77. Holmes AL, Wise SS, Sandwick SJ, Wise JP. The clastogenic effects of chronic exposure to particulate and soluble Cr (VI) in human lung cells. Mutation Research/Genetic Toxicology and Environmental Mutagenesis 2006; 610:8-13
78. Wise SS, Holmes AL, Wise JP. Particulate and soluble hexavalent chromium are cytotoxic and genotoxic to human lung epithelial cells. Mutation Research/Genetic Toxicology and Environmental Mutagenesis 2006; 610:2-7
79. Wise SS, Holmes AL, Xie H, Thompson WD, Wise JP. Chronic exposure to particulate chromate induces spindle assembly checkpoint bypass in human lung cells. Chemical research in toxicology 2006; 19:1492-1498
80. Yao H, Guo L, Jiang B-H, Luo J, Shi X. Oxidative stress and chromium (VI) carcinogenesis. Journal of Environmental Pathology, Toxicology and Oncology 2008; 27
81. Rao MV, Chawla SL, Sharma SR. Protective role of vitamin E on nickel and/or chromium induced oxidative stress in the mouse ovary. Food Chem Toxicol 2009; 47:1368-1371
82. Pritchard DE, Singh J, Carlisle DL, Patierno SR. Cyclosporin A inhibits chromium(VI)-induced apoptosis and mitochondrial cytochrome c release and restores clonogenic survival in CHO cells. Carcinogenesis 2000; 21:2027-2033
83. Sutton R. Chromium-6 in U.S. Tap Water. CA, USA: Environmental Working Group; 2010:1-22.
84. Grevatt PC. Toxicological review of trivalent chromium. www epa gov/IRIS/toxreviews/0028-tr pdf 1998;
85. Fresquez MR, Pappas RS, Watson CH. Establishment of Toxic Metal Reference Range in Tobacco from US Cigarettes. Journal of Analytical Toxicology 2013; 37:298-304

86. Smith C, Livingston S, Doolittle D. An international literature survey of "IARC Group I carcinogens" reported in mainstream cigarette smoke. Food and Chemical Toxicology 1997; 35:1107-1130
87. Bodaghpour S, Joo N, Ahmadi S. A review on the existence of chrome in cementand environmental remedies to control its effects. International Journal of Geology 2012; 2
88. Barceloux DG, Barceloux D. Chromium. Journal of Toxicology: Clinical Toxicology 1999; 37:173-194
89. Khan FH, Ambreen K, Fatima G, Kumar S. Assessment of health risks with reference to oxidative stress and DNA damage in chromium exposed population. Science of the total environment 2012; 430:68-74
90. Zhang M, Chen Z, Chen Q, Zou H, Lou J, He J. Investigating DNA damage in tannery workers occupationally exposed to trivalent chromium using comet assay. Mutation Research/Genetic Toxicology and Environmental Mutagenesis 2008; 654:45-51
91. Junaid M, Hashmi MZ, Malik RN. Evaluating levels and health risk of heavy metals in exposed workers from surgical instrument manufacturing industries of Sialkot, Pakistan. Environmental Science and Pollution Research 2016; 23:18010-18026
92. Weiss T, Pesch B, Lotz A, Gutwinski E, Van Gelder R, Punkenburg E, Kendzia B, Gawrych K, Lehnert M, Heinze E. Levels and predictors of airborne and internal exposure to chromium and nickel among welders—results of the WELDOX study. International journal of hygiene and environmental health 2013; 216:175-183
93. Gil F, Hernández AF, Márquez C, Femia P, Olmedo P, López-Guarnido O, Pla A. Biomonitorization of cadmium, chromium, manganese, nickel and lead in whole blood, urine, axillary hair and saliva in an occupationally exposed population. Science of the total environment 2011; 409:1172-1180
94. CarexCanada. Chromium (Hexavalent) occupational estimates in Canada. https://wwwcarexcanadaca/en/chromium_(hexavalent)/occupational_estimate/ 2017.
95. Beaumont JJ, Sedman RM, Reynolds SD, Sherman CD, Li LH, Howd RA, Sandy MS, Zeise L, Alexeeff GV. Cancer mortality in a Chinese population exposed to hexavalent chromium in drinking water. Epidemiology (Cambridge, Mass) 2008; 19:12-23
96. Zhang J, Li X. Chromium pollution of soil and water in Jinzhou. Zhonghua yu fang yi xue za zhi [Chinese journal of preventive medicine] 1987; 21:262-264
97. Linos A, Petralias A, Christophi CA, Christoforidou E, Kouroutou P, Stoltidis M, Veloudaki A, Tzala E, Makris KC, Karagas MR. Oral ingestion of hexavalent chromium through drinking water and cancer mortality in an industrial area of Greece-An ecological study. Environmental Health 2011; 10:50
98. Sharma P, Bihari V, Agarwal SK, Verma V, Kesavachandran CN, Pangtey BS, Mathur N, Singh KP, Srivastava M, Goel SK. Groundwater Contaminated with Hexavalent Chromium [Cr (VI)]: A Health Survey and Clinical Examination of Community Inhabitants (Kanpur, India). PLOS ONE 2012; 7:e47877
99. Junaid M, Hashmi MZ, Malik RN. Evaluating levels and health risk of heavy metals in exposed workers from surgical instrument manufacturing industries of Sialkot, Pakistan. Environmental science and pollution research international 2016; 23:18010-18026
100. Fristedt B, Lindqvist B, SCHÜTZ A, ÖVRUM P. Survival in a case of acute oral chromic acid poisoning with acute renal failure treated by haemodialysis. Journal of Internal Medicine 1965; 177:153-159

101. Program NT. NTP technical report on the toxicity studies of sodium dichromate dihydrate (CAS No. 7789-12-0) administered in drinking water to male and female F344/N rats and B6C3F1 mice and male BALB/c and am3-C57BL/6 mice. Toxic Rep Ser 2007; 72:1-74
102. Clochesy J. Chromium ingestion: a case report. Journal of emergency nursing: JEN: official publication of the Emergency Department Nurses Association 1984; 10:281-282
103. Ellis EN, Brouhard BH, Lynch RE, Dawson EB, Tisdell R, Nichols MM, Ramirez F. Effects of hemodialysis and dimercaprol in acute dichromate poisoning. Journal of Toxicology: Clinical Toxicology 1982; 19:249-258
104. Loubières Y, Lassence Ad, Bernier M, Vieillard-Baron A, Schmitt J-M, Page B, Jardin F. Acute, fatal, oral chromic acid poisoning. Journal of Toxicology: Clinical Toxicology 1999; 37:333-336
105. Kumar A, Rana S. Enzymological effects of hexavalent chromium in the rat kidney. International journal of tissue reactions 1984; 6:135-139
106. Soudani N, Troudi A, Bouaziz H, Amara IB, Boudawara T, Zeghal N. Cardioprotective effects of selenium on chromium (VI)-induced toxicity in female rats. Ecotoxicology and environmental safety 2011; 74:513-520
107. Sharma B, Singhal P, Chugh K. Intravascular haemolysis and acute renal failure following potassium dichromate poisoning. Postgraduate medical journal 1978; 54:414-415
108. Kaaber K, Veien N. The significance of chromate ingestion in patients allergic to chromate. Acta dermato-venereologica 1977; 57:321-323
109. Goitre M, Bedeleo P, Cane D. Chromium dermatitis and oral administration of the metal. Contact Dermatitis 1982; 8:208-209
110. Salama A, Hegazy R, Hassan A. Intranasal Chromium Induces Acute Brain and Lung Injuries in Rats: Assessment of Different Potential Hazardous Effects of Environmental and Occupational Exposure to Chromium and Introduction of a Novel Pharmacological and Toxicological Animal Model. PLoS One 2016; 11:e0168688
111. Singh P, Chowdhuri DK. Environmental Presence of Hexavalent but Not Trivalent Chromium Causes Neurotoxicity in Exposed Drosophila melanogaster. Molecular neurobiology 2017; 54:3368-3387
112. Jensen TK, Bonde JP, Joffe M. The influence of occupational exposure on male reproductive function. Occupational Medicine 2006; 56:544-553
113. Pizent A, Tariba B, Živković T. Reproductive toxicity of metals in men. Archives of Industrial Hygiene and Toxicology 2012; 63:35-46
114. Li H, Chen Q, Li S, Yao W, Li L, Shi X, Wang L, Castranova V, Vallyathan V, Ernst E. Effect of Cr (VI) exposure on sperm quality: human and animal studies. The Annals of occupational hygiene 2001; 45:505-511
115. Danadevi K, Rozati R, Reddy P, Grover P. Semen quality of Indian welders occupationally exposed to nickel and chromium. Reproductive toxicology 2003; 17:451-456
116. Marouani N, Tebourbi O, Mahjoub S, Yacoubi MT, Sakly M, Benkhalifa M, Rhouma KB. Effects of hexavalent chromium on reproductive functions of male adult rats. Reproductive biology 2012; 12:119-133
117. Subramanian S, Rajendiran G, Sekhar P, Gowri C, Govindarajulu P, Aruldhas MM. Reproductive toxicity of chromium in adult bonnet monkeys (Macaca radiata Geoffrey). Reversible oxidative stress in the semen. Toxicology and Applied Pharmacology 2006; 215:237-249

118. Aruldhas MM, Subramanian S, Sekhar P, Hasan GC, Govindarajulu P, Akbarsha M. Microcanalization in the epididymis to overcome ductal obstruction caused by chronic exposure to chromium–a study in the mature bonnet monkey (Macaca radiata Geoffroy). Reproduction 2004; 128:127-137
119. Quansah R, Jaakkola JJ. Paternal and maternal exposure to welding fumes and metal dusts or fumes and adverse pregnancy outcomes. International archives of occupational and environmental health 2009; 82:529-537
120. Remy LL, Byers V, Clay T. Reproductive outcomes after non-occupational exposure to hexavalent chromium, Willits California, 1983-2014. Environmental Health 2017; 16:18
121. Teklay A. Physiological effect of chromium exposure: A review. Int J Food Sci Nutr Diet S 2016; 7:1-11
122. Pan X, Hu J, Xia W, Zhang B, Liu W, Zhang C, Yang J, Hu C, Zhou A, Chen Z. Prenatal chromium exposure and risk of preterm birth: a cohort study in Hubei, China. Scientific Reports 2017; 7:3048
123. Banu SK, Stanley JA, Taylor RJ, Sivakumar KK, Arosh JA, Zeng L, Pennathur S, Padmanabhan V. Sexually Dimorphic Impact of Chromium Accumulation on Human Placental Oxidative Stress and Apoptosis. Toxicological Sciences 2017:In Press
124. Barreau B, Underwood M, Hoshiko S. Evaluation of Exposures to Contaminants from the Former Abex/Remco Hydraulics Facility, Willits, Mendocino County, California. CERCLIS No. CAD000097287. Department of Department of Health Services under Cooperative Agreement with the US Department of Health and Human Services Agency for Toxic Substances and Disease Registry; 2006:1-124.
125. Remy LL, Byers V, Clay T. Reproductive outcomes after non-occupational exposure to hexavalent chromium, Willits California, 1983-2014. Environmental Health 2017; 16:1-15
126. Murthy RC, Junaid M, Saxena DK. Ovarian dysfunction in mice following chromium (VI) exposure. Toxicology letters 1996; 89:147-154
127. Trivedi B, Saxena DK, Murthy RC, Chandra SV. Embryotoxicity and fetotoxicity of orally administered hexavalent chromium in mice. Reproductive Toxicology 1989; 3:275-278
128. Junaid M, Murthy RC, Saxena DK. Embryotoxicity of orally administered chromium in mice: exposure during the period of organogenesis. Toxicology letters 1996; 84:143-148
129. Al-Hamood M, Elbetieha A, Bataineh H. Sexual maturation and fertility of male and female mice exposed prenatally and postnatally to trivalent and hexavalent chromium compounds. Reproduction, fertility and development 1998; 10:179-184
130. Banu SK, Samuel JB, Arosh JA, Burghardt RC, Aruldhas MM. Lactational exposure to hexavalent chromium delays puberty by impairing ovarian development, steroidogenesis and pituitary hormone synthesis in developing Wistar rats. Toxicology and applied pharmacology 2008; 232:180-189
131. Stanley JA, Sivakumar KK, Nithy TK, Arosh JA, Hoyer PB, Burghardt RC, Banu SK. Postnatal exposure to chromium through mother's milk accelerates follicular atresia in F1 offspring through increased oxidative stress and depletion of antioxidant enzymes. Free radical biology & medicine 2013; 61C:179-196
132. Stanley JA, Sivakumar KK, Arosh JA, Burghardt RC, Banu SK. Edaravone Mitigates Hexavalent Chromium-Induced Oxidative Stress and Depletion of Antioxidant Enzymes while Estrogen Restores Antioxidant Enzymes in the Rat Ovary in F1 Offspring. Biol Reprod 2014; 91:12

133. Banu SK, Stanley JA, Sivakumar KK, Arosh JA, Burghardt RC. Resveratrol protects the ovary against chromium-toxicity by enhancing endogenous antioxidant enzymes and inhibiting metabolic clearance of estradiol. Toxicology and applied pharmacology 2016; 303:65-78
134. Banu SK, Samuel JB, Arosh JA, Burghardt RC, Aruldhas MM. Lactational exposure to hexavalent chromium delays puberty by impairing ovarian development, steroidogenesis and pituitary hormone synthesis in developing Wistar rats. Toxicol Appl Pharmacol 2008; 232:180-189
135. Stanley JA, Lee J, Nithy TK, Arosh JA, Burghardt RC, Banu SK. Chromium-VI arrests cell cycle and decreases granulosa cell proliferation by down-regulating cyclin-dependent kinases (CDK) and cyclins and up-regulating CDK-inhibitors. Reprod Toxicol 2011; 32:112-123
136. Banu SK, Stanley JA, Lee J, Stephen SD, Arosh JA, Hoyer PB, Burghardt RC. Hexavalent chromium-induced apoptosis of granulosa cells involves selective sub-cellular translocation of Bcl-2 members, ERK1/2 and p53. Toxicol Appl Pharmacol 2011; 251:253-266
137. Stanley JA, Lee J, Nithy TK, Arosh JA, Burghardt RC, Banu SK. Chromium-VI arrests cell cycle and decreases granulosa cell proliferation by down-regulating cyclin-dependent kinases (CDK) and cyclins and up-regulating CDK-Inhibitors. Reproductive toxicology (Elmsford, NY) 2011; 32:112-123
138. Stanley JA, Sivakumar KK, Nithy TK, Arosh JA, Hoyer PB, Burghardt RC, Banu SK. Postnatal exposure to hexavalent chromium through mother's milk accelerates follicular atresia in F1 offspring through increased oxidative stress and depletion of antioxidant enzymes. Free Rad Biol Med 2012;
139. Malumbres M. Physiological relevance of cell cycle kinases. Physiol Rev 2011; 91:973-1007
140. Edson MA, Nagaraja AK, Matzuk MM. The mammalian ovary from genesis to revelation. Endocrine reviews 2009; 30:624–712
141. Jaskulski D, deRiel JK, Mercer WE, Calabretta B, Baserga R. Inhibition of cellular proliferation by antisense oligodeoxynucleotides to PCNA cyclin. Science 1988; 240:1544-1546
142. Casasco A, Calligaro A, Casasco E, Marchetti C, Poggi P, Casasco M. An immunocytochemical method for studying embryo cytokinetics. Basic Appl Histochem 1988; 32:293-296
143. Oktay K, Schenken RS, Nelson JF. Proliferating cell nuclear antigen marks the initiation of follicular growth in the rat. Biology of reproduction 1995; 53:295-301
144. Pomerening JR. Positive-feedback loops in cell cycle progression. FEBS Lett 2009; 583:3388-3396
145. Stankiewicz AR, Lachapelle G, Foo CP, Radicioni SM, Mosser DD. Hsp70 inhibits heat-induced apoptosis upstream of mitochondria by preventing Bax translocation. J Biol Chem 2005; 280:38729–38739
146. Bivik C, Rosdahl I, Ollinger K. Hsp70 protects against UVB induced apoptosis by preventing release of cathepsins and cytochrome c in human melanocytes. Carcinogenesis 2007; 28:537–544

147. Joly AL, Wettstein G, Mignot G, Ghiringhelli F, Garrido C. Dual role of heat shock proteins as regulators of apoptosis and innate immunity. J Innate Immun 2010; 2:238-247
148. Meek DW, Anderson CW. Posttranslational modification of p53: cooperative integrators of function. Cold Spring Harb Perspect Biol 2009; 1:a000950
149. Kurihara A, Nagoshi H, Yabuki M, Okuyama R, Obinata M, Ikawa S. Ser46 phosphorylation of p53 is not always sufficient to induce apoptosis: multiple mechanisms of regulation of p53-dependent apoptosis. Genes Cells 2007; 12:853–861
150. Verschoor ML, Wilson LA, Singh G. Mechanisms associated with mitochondrial-generated reactive oxygen species in cancer. Canadian journal of physiology and pharmacology 2010; 88:204–219
151. Sluss HK, Gannon H, Coles AH, Shen Q, Eischen CM, Jones SN. Phosphorylation of p53 serine 18 upregulates apoptosis to suppress Myc-induced tumorigenesis. Mol Cancer Res 2010; 8:216–222
152. Milne DM, Campbell LE, Campbell DG, Meek DW. p53 is phosphorylated in vitro and in vivo by an ultraviolet radiation-induced protein kinase characteristic of the c-Jun kinase, JNK1. J Biol Chem 1995; 270:5511–5518
153. Long X, Goldenthal MJ, Marin-Garcia J. Oxidative stress enhances phosphorylation of p53 in neonatal rat cardiomyocytes. Mol Cell Biochem 2007; 303:167–174
154. Erster S, Moll UM. Stress-induced p53 runs a direct mitochondrial death program: its role in physiologic and pathophysiologic stress responses in vivo. Cell Cycle 2004; 3:1492–1495
155. Zhao Y, Chaiswing L, Velez JM, Batinic-Haberle I, Colburn NH, Oberley TD, St Clair DK. p53 translocation to mitochondria precedes its nuclear translocation and targets mitochondrial oxidative defense protein-manganese superoxide dismutase. Cancer Res 2005; 65:3745–3750
156. Pani G, Colavitti R, Bedogni B, Fusco S, Ferraro D, Borrello S, Galeotti T. Mitochondrial superoxide dismutase: a promising target for new anticancer therapies. Curr Med Chem 2004; 11:1299–1308
157. Siu PM, Wang Y, Alway SE. Apoptotic signaling induced by H2O2-mediated oxidative stress in differentiated C2C12 myotubes. Life sciences 2009; 84:468-481
158. Galluzzi L, Morselli E, Kepp O, Vitale I, Pinti M, Kroemer G. Mitochondrial liaisons of p53. Antioxid Redox Signal 2011; 15:1691-1714
159. Holley AK, Dhar SK, St Clair DK. Manganese superoxide dismutase versus p53: the mitochondrial center. Ann NY Acad Sci 2010; 1201:72-78
160. Mihara M, Erster S, Zaika A, Petrenko O, Chittenden T, Pancoska P, Moll UM. p53 has a direct apoptogenic role at the mitochondria. Mol Cell 2003; 11:577–590
161. Lawson K, Hage W. Clonal analysis of the origin of primordial germ cells in the mouse. Germline development 1994; 165:68-84
162. Ying Y, Liu X-M, Marble A, Lawson KA, Zhao G-Q. Requirement of Bmp8b for the generation of primordial germ cells in the mouse. Molecular endocrinology 2000; 14:1053-1063
163. Ying Y, Zhao G-Q. Cooperation of Endoderm-Derived BMP2 and Extraembryonic Ectoderm-Derived BMP4 in Primordial Germ Cell Generation in the Mouse. Developmental Biology 2001; 232:484-492

164. Pangas SA, Choi Y, Ballow DJ, Zhao Y, Westphal H, Matzuk MM, Rajkovic A. Oogenesis requires germ cell-specific transcriptional regulators Sohlh1 and Lhx8. Proceedings of the National Academy of Sciences 2006; 103:8090-8095
165. Monk M, McLaren A. X-chromosome activity in foetal germ cells of the mouse. Development 1981; 63:75-84
166. Gondos B. Intercellular bridges and mammalian germ cell differentiation. Differentiation 1973; 1:177-182
167. Pepling ME. Follicular assembly: mechanisms of action. Reproduction 2012; 143:139-149
168. Pesce M, Gioia Klinger F, De Felici M. Derivation in culture of primordial germ cells from cells of the mouse epiblast: phenotypic induction and growth control by Bmp4 signalling. Mechanisms of Development 2002; 112:15-24
169. Puglisi R, Montanari M, Chiarella P, Stefanini M, Boitani C. Regulatory role of BMP2 and BMP7 in spermatogonia and Sertoli cell proliferation in the immature mouse. European journal of endocrinology 2004; 151:511-520
170. Ross A, Munger S, Capel B. Bmp7 regulates germ cell proliferation in mouse fetal gonads. Sexual Development 2007; 1:127-137
171. Jagarlamudi K, Rajkovic A. Oogenesis: transcriptional regulators and mouse models. Molecular and cellular endocrinology 2012; 356:31-39
172. Da Silva SM, Bayne R, Cambray N, Hartley P, McNeilly A, Anderson R. Expression of activin subunits and receptors in the developing human ovary: activin A promotes germ cell survival and proliferation before primordial follicle formation. Developmental biology 2004; 266:334-345
173. Sánchez F, Smitz J. Molecular control of oogenesis. Biochimica et Biophysica Acta (BBA) - Molecular Basis of Disease 2012; 1822:1896-1912
174. Bowles J, Koopman P. Sex determination in mammalian germ cells: extrinsic versus intrinsic factors. Reproduction 2010; 139:943-958
175. Pepling ME, Spradling AC. Female mouse germ cells form synchronously dividing cysts. Development 1998; 125:3323-3328
176. Edson MA, Nagaraja AK, Matzuk MM. The Mammalian Ovary from Genesis to Revelation. Endocrine Reviews 2009; 30:624-712
177. Byskov AG. Differentiation of mammalian embryonic gonad. Physiological reviews 1986; 66:71-117
178. Mazaud S, Guyot R, Guigon CJ, Coudouel N, Le Magueresse-Battistoni B, Magre S. Basal membrane remodeling during follicle histogenesis in the rat ovary: contribution of proteinases of the MMP and PA families. Developmental biology 2005; 277:403-416
179. Ginsburg M, Snow M, McLAREN A. Primordial germ cells in the mouse embryo during gastrulation. Development 1990; 110:521-528
180. Pepling ME. From primordial germ cell to primordial follicle: mammalian female germ cell development. Genesis 2006; 44:622-632
181. Wang C, Zhou B, Xia G. Mechanisms controlling germline cyst breakdown and primordial follicle formation. Cellular and Molecular Life Sciences 2017; 74:2547-2566
182. Zhou Q, Li Y, Nie R, Friel P, Mitchell D, Evanoff RM, Pouchnik D, Banasik B, McCarrey JR, Small C. Expression of stimulated by retinoic acid gene 8 (Stra8) and maturation of murine gonocytes and spermatogonia induced by retinoic acid in vitro. Biology of reproduction 2008; 78:537-545

183. Baltus AE, Menke DB, Hu Y-C, Goodheart ML, Carpenter AE, de Rooij DG, Page DC. In germ cells of mouse embryonic ovaries, the decision to enter meiosis precedes premeiotic DNA replication. Nature genetics 2006; 38:1430
184. Hunt PA, Hassold TJ. Human female meiosis: what makes a good egg go bad? Trends in Genetics 2008; 24:86-93
185. Borum K. Oogenesis in the mouse: a study of the meiotic prophase. Experimental cell research 1961; 24:495-507
186. Nandedkar T, Dharma S, Modi D, Dsouza S. Differential gene expression in transition of primordial to preantral follicles in mouse ovary. Society of Reproduction and Fertility supplement 2007; 63:57-67
187. Peters H. Effect of radiation in early life on morphology and reproductive function of mouse ovary. Advances in reproductive physiology 1969; 4:149-
188. Karavan JR, Pepling ME. Effects of estrogenic compounds on neonatal oocyte development. Reproductive Toxicology 2012; 34:51-56
189. Pepling ME, Spradling AC. Mouse Ovarian Germ Cell Cysts Undergo Programmed Breakdown to Form Primordial Follicles. Developmental Biology 2001; 234:339-351
190. Pepling ME, Sundman EA, Patterson NL, Gephardt GW, Medico L, Wilson KI. Differences in oocyte development and estradiol sensitivity among mouse strains. Reproduction 2010; 139:349-357
191. Hirshfield AN, DeSanti AM. Patterns of ovarian cell proliferation in rats during the embryonic period and the first three weeks postpartum. Biology of reproduction 1995; 53:1208-1221
192. Maheshwari A, Fowler P. Primordial follicular assembly in humans–revisited. Zygote 2008; 16:285-296
193. Li H, Chian R-C. Follicular Development and Oocyte Growth. Development of In Vitro Maturation for Human Oocytes: Springer; 2017:37-57.
194. O'shaughnessy P, Dudley K, Rajapaksha W. Expression of follicle stimulating hormone-receptor mRNA during gonadal development. Molecular and cellular endocrinology 1996; 125:169-175
195. Fortune J, Eppig J. Effects of gonadotropins on steroid secretion by infantile and juvenile mouse ovaries in vitro. Endocrinology 1979; 105:760-768
196. Kol S, Adashi EY. Intraovarian factors regulating ovarian function. Current Opinion in Obstetrics and Gynecology 1995; 7:209-213
197. Elvin JA, Clark AT, Wang P, Wolfman NM, Matzuk MM. Paracrine actions of growth differentiation factor-9 in the mammalian ovary. Molecular endocrinology (Baltimore, Md) 1999; 13:1035-1048
198. McGrath SA, Esquela AF, Lee SJ. Oocyte-specific expression of growth/differentiation factor-9. Molecular endocrinology (Baltimore, Md) 1995; 9:131-136
199. Hayashi M, McGee E, Min G, Klein C, Rose UM, Duin Mv, Hsueh AJ. Recombinant growth differentiation factor-9 (GDF-9) enhances growth and differentiation of cultured early ovarian follicles. Endocrinology 1999; 140:1236-1244
200. Nilsson EE, Skinner MK. Growth and differentiation factor-9 stimulates progression of early primary but not primordial rat ovarian follicle development. Biology of reproduction 2002; 67:1018-1024

201. Otsuka F, Yao Z, Lee T-h, Yamamoto S, Erickson GF, Shimasaki S. Bone morphogenetic protein-15 identification of target cells and biological functions. Journal of Biological Chemistry 2000; 275:39523-39528
202. Paredes A, Romero C, Dissen GA, DeChiara TM, Reichardt L, Cornea A, Ojeda SR, Xu B. TrkB receptors are required for follicular growth and oocyte survival in the mammalian ovary. Dev Biol 2004; 267:430-449
203. Anderson RA, Robinson LL, Brooks J, Spears N. Neurotropins and their receptors are expressed in the human fetal ovary. The Journal of clinical endocrinology and metabolism 2002; 87:890-897
204. Falender AE, Shimada M, Lo YK, Richards JS. TAF4b, a TBP associated factor, is required for oocyte development and function. Developmental biology 2005; 288:405-419
205. Voronina E, Lovasco LA, Gyuris A, Baumgartner RA, Parlow AF, Freiman RN. Ovarian granulosa cell survival and proliferation requires the gonad-selective TFIID subunit TAF4b. Developmental biology 2007; 303:715-726
206. Gazdag E, Santenard A, Ziegler-Birling C, Altobelli G, Poch O, Tora L, Torres-Padilla M-E. TBP2 is essential for germ cell development by regulating transcription and chromatin condensation in the oocyte. Genes & development 2009; 23:2210-2223
207. Oktem O, Urman B. Understanding follicle growth in vivo. Human reproduction 2010; 25:2944-2954
208. Knight PG, Glister C. TGF-β superfamily members and ovarian follicle development. Reproduction 2006; 132:191-206
209. Araújo VR, Gastal MO, Figueiredo JR, Gastal EL. In vitro culture of bovine preantral follicles: a review. Reproductive Biology and Endocrinology : RB&E 2014; 12:78
210. Richards J, Fitzpatrick S, Clemens J, Morris J, Alliston T, Sirois J. Ovarian cell differentiation: a cascade of multiple hormones, cellular signals, and regulated genes. Recent progress in hormone research 1995; 50:223
211. Fair T. Follicular oocyte growth and acquisition of developmental competence. Animal reproduction science 2003; 78:203-216
212. Ginther O, Beg M, Bergfelt D, Donadeu F, Kot K. Follicle selection in monovular species. Biology of reproduction 2001; 65:638-647
213. Gougeon A. Regulation of ovarian follicular development in primates: facts and hypotheses. Endocrine reviews 1996; 17:121-155
214. Fortune J. The early stages of follicular development: activation of primordial follicles and growth of preantral follicles. Animal reproduction science 2003; 78:135-163
215. Webb R, Garnsworthy PC, Gong JG, Armstrong DG. Control of follicular growth: local interactions and nutritional influences. Journal of animal science 2004; 82 E-Suppl:E63-74
216. Sánchez F, Smitz J. Molecular control of oogenesis. Biochimica et Biophysica Acta (BBA)-Molecular Basis of Disease 2012; 1822:1896-1912
217. Reddy P, Liu L, Adhikari D, Jagarlamudi K, Rajareddy S, Shen Y, Du C, Tang W, Hämäläinen T, Peng SL. Oocyte-specific deletion of Pten causes premature activation of the primordial follicle pool. Science 2008; 319:611-613
218. Reddy P, Shen L, Ren C, Boman K, Lundin E, Ottander U, Lindgren P, Liu Y-x, Sun Q-y, Liu K. Activation of Akt (PKB) and suppression of FKHRL1 in mouse and rat oocytes by

stem cell factor during follicular activation and development. Developmental biology 2005; 281:160-170
219. Liu K, Rajareddy S, Liu L, Jagarlamudi K, Boman K, Selstam G, Reddy P. Control of mammalian oocyte growth and early follicular development by the oocyte PI3 kinase pathway: New roles for an old timer. Developmental Biology 2006; 299:1-11
220. Adhikari D, Zheng W, Shen Y, Gorre N, Hämäläinen T, Cooney AJ, Huhtaniemi I, Lan Z-J, Liu K. Tsc/mTORC1 signaling in oocytes governs the quiescence and activation of primordial follicles. Human Molecular Genetics 2010; 19:397-410
221. Durlinger AL, Gruijters MJ, Kramer P, Karels B, Ingraham HA, Nachtigal MW, Uilenbroek JTJ, Grootegoed JA, Themmen AP. Anti-Mullerian hormone inhibits initiation of primordial follicle growth in the mouse ovary. Endocrinology 2002; 143:1076-1084
222. Durlinger A, Visser JA, Themmen A. Regulation of ovarian function: the role of anti-Mullerian hormone. Reproduction 2002; 124:601-609
223. Fortune JE. The early stages of follicular development: activation of primordial follicles and growth of preantral follicles. Animal Reproduction Science 2003; 78:135-163
224. Nilsson EE, Skinner MK. Kit ligand and basic fibroblast growth factor interactions in the induction of ovarian primordial to primary follicle transition. Molecular and Cellular Endocrinology 2004; 214:19-25
225. Dissen GA, Garcia-Rudaz C, Ojeda SR. Role of neurotrophic factors in early ovarian development. Paper presented at: Seminars in reproductive medicine2009
226. Dissen GA, Romero C, Hirshfield AN, Ojeda SR. Nerve growth factor is required for early follicular development in the mammalian ovary. Endocrinology 2001; 142:2078-2086
227. Rajkovic A, Pangas SA, Ballow D, Suzumori N, Matzuk MM. NOBOX deficiency disrupts early folliculogenesis and oocyte-specific gene expression. Science 2004; 305:1157-1159
228. Nilsson EE, Skinner MK. Bone morphogenetic protein-4 acts as an ovarian follicle survival factor and promotes primordial follicle development. Biology of reproduction 2003; 69:1265-1272
229. Nelson SM. Biomarkers of ovarian response: current and future applications. Fertility and sterility 2013; 99:963-969
230. Kelsey TW, Wallace WHB. Ovarian volume correlates strongly with the number of nongrowing follicles in the human ovary. Obstetrics and gynecology international 2012; 2012
231. Wallace WHB, Kelsey TW. Human ovarian reserve from conception to the menopause. PloS one 2010; 5:e8772
232. Kerr JB, Brogan L, Myers M, Hutt KJ, Mladenovska T, Ricardo S, Hamza K, Scott C, Strasser A, Findlay JK. The primordial follicle reserve is not renewed after chemical or γ-irradiation mediated depletion. Reproduction 2012:REP-11-0430
233. Kerr JB, Duckett R, Myers M, Britt KL, Mladenovska T, Findlay JK. Quantification of healthy follicles in the neonatal and adult mouse ovary: evidence for maintenance of primordial follicle supply. Reproduction 2006; 132:95-109
234. Kerr JB, Hutt KJ, Michalak EM, Cook M, Vandenberg CJ, Liew SH, Bouillet P, Mills A, Scott CL, Findlay JK. DNA damage-induced primordial follicle oocyte apoptosis and loss of fertility require TAp63-mediated induction of Puma and Noxa. Molecular cell 2012; 48:343-352

235. Rodrigues P, Limback D, McGinnis LK, Plancha CE, Albertini DF. Multiple mechanisms of germ cell loss in the perinatal mouse ovary. Reproduction 2009; 137:709-720
236. Barnett K, Schilling C, Greenfeld C, Tomic D, Flaws J. Ovarian follicle development and transgenic mouse models. Human reproduction update 2006; 12:537-555
237. Monget P, Bobe J, Gougeon A, Fabre S, Monniaux D, Dalbies-Tran R. The ovarian reserve in mammals: a functional and evolutionary perspective. Molecular and cellular endocrinology 2012; 356:2-12
238. Moniruzzaman M, Miyano T. Growth of primordial oocytes in neonatal and adult mammals. Journal of Reproduction and Development 2010; 56:559-566
239. Reddy P, Zheng W, Liu K. Mechanisms maintaining the dormancy and survival of mammalian primordial follicles. Trends in Endocrinology & Metabolism 2010; 21:96-103
240. Bristol-Gould SK, Kreeger PK, Selkirk CG, Kilen SM, Mayo KE, Shea LD, Woodruff TK. Fate of the initial follicle pool: empirical and mathematical evidence supporting its sufficiency for adult fertility. Developmental biology 2006; 298:149-154
241. Tingen C, Kim A, Woodruff TK. The primordial pool of follicles and nest breakdown in mammalian ovaries. Mol Hum Reprod 2009; 15:795-803
242. Elmore S. Apoptosis: A Review of Programmed Cell Death. Toxicologic pathology 2007; 35:495-516
243. Happo L, Strasser A, Cory S. BH3-only proteins in apoptosis at a glance. J cell sci 2012; 125:1081-1087
244. Youle RJ, Strasser A. The BCL-2 protein family: opposing activities that mediate cell death. Nature reviews Molecular cell biology 2008; 9:47
245. Czabotar PE, Lessene G, Strasser A, Adams JM. Control of apoptosis by the BCL-2 protein family: implications for physiology and therapy. Nature reviews Molecular cell biology 2014; 15:49
246. Hutt KJ. The role of BH3-only proteins in apoptosis within the ovary. Reproduction 2015; 149:R81-R89
247. Westphal D, Dewson G, Czabotar PE, Kluck RM. Molecular biology of Bax and Bak activation and action. Biochimica et Biophysica Acta (BBA) - Molecular Cell Research 2011; 1813:521-531
248. Kaufmann T, Jost PJ, Pellegrini M, Puthalakath H, Gugasyan R, Gerondakis S, Cretney E, Smyth MJ, Silke J, Hakem R. Fatal hepatitis mediated by tumor necrosis factor TNFα requires caspase-8 and involves the BH3-only proteins Bid and Bim. Immunity 2009; 30:56-66
249. Strasser A, O'Connor L, Dixit VM. Apoptosis signaling. Annual review of biochemistry 2000; 69:217-245
250. Flaws JA, Hirshfield AN, Hewitt JA, Babus JK, Furth PA. Effect of bcl-2 on the primordial follicle endowment in the mouse ovary. Biol Reprod 2001; 64:1153-1159
251. Ratts VS, Flaws JA, Kolp R, Sorenson CM, Tilly JL. Ablation of bcl-2 gene expression decreases the numbers of oocytes and primordial follicles established in the post-natal female mouse gonad. Endocrinology 1995; 136:3665-3668
252. Rucker III EB, Dierisseau P, Wagner K-U, Garrett L, Wynshaw-Boris A, Flaws JA, Hennighausen L. Bcl-x and Bax regulate mouse primordial germ cell survival and apoptosis during embryogenesis. Molecular Endocrinology 2000; 14:1038-1052

253. Kim M-R, Tilly JL. Current concepts in Bcl-2 family member regulation of female germ cell development and survival. Biochimica et Biophysica Acta (BBA)-Molecular Cell Research 2004; 1644:205-210
254. Perez G, Robles R, Knudson C, Flaws J, Korsmeyer S, Tilly J. Prolongation of ovarian lifespan into advanced chronological age by Bax-deficiency. Nature genetics 1999; 21:200-203
255. Greenfeld CR, Babus JK, Furth PA, Marion S, Hoyer PB, Flaws JA. BAX is involved in regulating follicular growth, but is dispensable for follicle atresia in adult mouse ovaries. Reproduction 2007; 133:107-116
256. Perez GI, Robles R, Knudson CM, Flaws JA, Korsmeyer SJ, Tilly JL. Prolongation of ovarian lifespan into advanced chronological age by Bax-deficiency. Nature genetics 1999; 21:200
257. Johnson AL, Bridgham JT. Caspase-mediated apoptosis in the vertebrate ovary. Reproduction 2002; 124:19-27
258. Bergeron L, Perez GI, Macdonald G, Shi L, Sun Y, Jurisicova A, Varmuza S, Latham KE, Flaws JA, Salter JC. Defects in regulation of apoptosis in caspase-2-deficient mice. Genes & development 1998; 12:1304-1314
259. Matikainen T, Perez GI, Zheng TS, Kluzak TR, Rueda BR, Flavell RA, Tilly JL. Caspase-3 Gene Knockout Defines Cell Lineage Specificity for Programmed Cell Death Signaling in the Ovary*. Endocrinology 2001; 142:2468-2480
260. Findlay JK, Hutt KJ, Hickey M, Anderson RA. How Is the Number of Primordial Follicles in the Ovarian Reserve Established? Biol Reprod 2015; 93:111
261. Pflaum J, Schlosser S, Müller M. p53 Family and Cellular Stress Responses in Cancer. Frontiers in Oncology 2014; 4:285
262. Pucci B, Kasten M, Giordano A. Cell Cycle and Apoptosis. Neoplasia (New York, NY) 2000; 2:291-299
263. Fridman JS, Lowe SW. Control of apoptosis by p53. Oncogene 2003; 22:9030
264. Rufini A, Tucci P, Celardo I, Melino G. Senescence and aging: the critical roles of p53. Oncogene 2013; 32:5129-5143
265. Oren M. Decision making by p53: life, death and cancer. Cell death and differentiation 2003; 10:431
266. Fischer M. Census and evaluation of p53 target genes. Oncogene 2017; 36:3943
267. Marcel V, Catez F, Diaz JJ. p53, a translational regulator: contribution to its tumour-suppressor activity. Oncogene 2015; 34:5513
268. Yamakuchi M, Lowenstein CJ. MiR-34, SIRT1 and p53: the feedback loop. Cell cycle (Georgetown, Tex) 2009; 8:712-715
269. Ljungman M. Dial 9-1-1 for p53: Mechanisms of p53 Activation by Cellular Stress. Neoplasia (New York, NY) 2000; 2:208-225
270. Caspari T. Checkpoints: how to activate p53. Current biology 2000; 10:R315-R317
271. Waterman MJ, Stavridi ES, Waterman JL, Halazonetis TD. ATM-dependent activation of p53 involves dephosphorylation and association with 14-3-3 proteins. Nat Genet 1998; 19:175-178
272. Dornan D, Shimizu H, Mah A, Dudhela T, Eby M, O'rourke K, Seshagiri S, Dixit VM. ATM engages autodegradation of the E3 ubiquitin ligase COP1 after DNA damage. Science 2006; 313:1122-1126

273. McCarthy A, Lain S. Upstream Targets in the p53 Pathway. In: Hainaut P, Magali Olivier, and Klas G. Wiman, ed. P53 in the clinics Springer Science & Business Media; 2012:209-229.
274. Sherr CJ. Divorcing ARF and p53: an unsettled case. Nature Reviews Cancer 2006; 6:663
275. Horn HF, Vousden KH. Coping with stress: multiple ways to activate p53. Oncogene 2007; 26:1306
276. Hammond EM, Giaccia AJ. The role of p53 in hypoxia-induced apoptosis. Biochemical and biophysical research communications 2005; 331:718-725
277. Kaikkonen MU, Lam MTY, Glass CK. Non-coding RNAs as regulators of gene expression and epigenetics. Cardiovascular Research 2011; 90:430-440
278. Oliveto S, Mancino M, Manfrini N, Biffo S. Role of microRNAs in translation regulation and cancer. World Journal of Biological Chemistry 2017; 8:45-56
279. Felekkis K, Touvana E, Stefanou C, Deltas C. microRNAs: a newly described class of encoded molecules that play a role in health and disease. Hippokratia 2010; 14:236-240
280. Virant-Klun I, St, #xe5, hlberg A, Kubista M, Skutella T. MicroRNAs: From Female Fertility, Germ Cells, and Stem Cells to Cancer in Humans. Stem Cells International 2016; 2016:17
281. Soifer HS, Rossi JJ, Sætrom P. MicroRNAs in Disease and Potential Therapeutic Applications. Molecular Therapy 2007; 15:2070-2079
282. Valinezhad Orang A, Safaralizadeh R, Kazemzadeh-Bavili M. Mechanisms of miRNA-Mediated Gene Regulation from Common Downregulation to mRNA-Specific Upregulation. International Journal of Genomics 2014; 2014:15
283. Ghosh T, Soni K, Scaria V, Halimani M, Bhattacharjee C, Pillai B. MicroRNA-mediated up-regulation of an alternatively polyadenylated variant of the mouse cytoplasmic β-actin gene. Nucleic Acids Research 2008; 36:6318-6332
284. Feng Z, Zhang C, Wu R, Hu W. Tumor suppressor p53 meets microRNAs. Journal of Molecular Cell Biology 2011; 3:44-50
285. Bommer GT, Gerin I, Feng Y, Kaczorowski AJ, Kuick R, Love RE, Zhai Y, Giordano TJ, Qin ZS, Moore BB. p53-mediated activation of miRNA34 candidate tumor-suppressor genes. Current biology 2007; 17:1298-1307
286. Li XJ, Ren ZJ, Tang JH. MicroRNA-34a: a potential therapeutic target in human cancer. Cell Death &Amp; Disease 2014; 5:e1327
287. Lodygin D, Tarasov V, Epanchintsev A, Berking C, Knyazeva T, Körner H, Knyazev P, Diebold J, Hermeking H. Inactivation of miR-34a by aberrant CpG methylation in multiple types of cancer. Cell cycle (Georgetown, Tex) 2008; 7:2591-2600
288. Raver-Shapira N, Marciano E, Meiri E, Spector Y, Rosenfeld N, Moskovits N, Bentwich Z, Oren M. Transcriptional activation of miR-34a contributes to p53-mediated apoptosis. Molecular cell 2007; 26:731-743
289. He L, He X, Lim LP, De Stanchina E, Xuan Z, Liang Y, Xue W, Zender L, Magnus J, Ridzon D. A microRNA component of the p53 tumour suppressor network. Nature 2007; 447:1130
290. Chang T-C, Wentzel EA, Kent OA, Ramachandran K, Mullendore M, Lee Kwang H, Feldmann G, Yamakuchi M, Ferlito M, Lowenstein CJ, Arking Dan E, Beer MA, Maitra A, Mendell JT. Transactivation of miR-34a by p53 Broadly Influences Gene Expression and Promotes Apoptosis. Molecular Cell 2007; 26:745-752

291. Yamakuchi M, Ferlito M, Lowenstein CJ. miR-34a repression of SIRT1 regulates apoptosis. Proceedings of the National Academy of Sciences 2008; 105:13421
292. Lin Z, Fang D. The Roles of SIRT1 in Cancer. Genes & Cancer 2013; 4:97-104
293. Zhou X-L, Xu J-J, Ni Y-H, Chen X-C, Zhang H-X, Zhang X-M, Liu W-J, Luo L-L, Fu Y-C. SIRT1 activator (SRT1720) improves the follicle reserve and prolongs the ovarian lifespan of diet-induced obesity in female mice via activating SIRT1 and suppressing mTOR signaling. Journal of ovarian research 2014; 7:97
294. Das M, Das DK. Resveratrol and cardiovascular health. Molecular aspects of medicine 2010; 31:503-512
295. Szkudelska K, Szkudelski T. Resveratrol, obesity and diabetes. European journal of pharmacology 2010; 635:1-8
296. Chen Z-G, Luo L-L, Xu J-J, Zhuang X-L, Kong X-X, Fu Y-C. Effects of plant polyphenols on ovarian follicular reserve in aging rats. Biochemistry and Cell Biology 2010; 88:737-745
297. Liu M, Yin Y, Ye X, Zeng M, Zhao Q, Keefe DL, Liu L. Resveratrol protects against age-associated infertility in mice. Human reproduction 2013; 28:707-717
298. Jang J, Huh YJ, Cho H-J, Lee B, Park J, Hwang D-Y, Kim D-W. SIRT1 Enhances the Survival of Human Embryonic Stem Cells by Promoting DNA Repair. Stem Cell Reports 2017; 9:629-641
299. Salminen A, Kaarniranta K, Kauppinen A. Crosstalk between Oxidative Stress and SIRT1: Impact on the Aging Process. International Journal of Molecular Sciences 2013; 14:3834-3859
300. Yuan F, Liu L, Lei Y, Tang P. p53 inhibits the upregulation of sirtuin 1 expression induced by c-Myc. Oncology Letters 2017; 14:4396-4402
301. Luo J, Nikolaev AY, Imai S, Chen D, Su F, Shiloh A, Guarente L, Gu W. Negative control of p53 by Sir2alpha promotes cell survival under stress. Cell 2001; 107:137-148
302. Vaziri H, Dessain SK, Ng Eaton E, Imai SI, Frye RA, Pandita TK, Guarente L, Weinberg RA. hSIR2(SIRT1) functions as an NAD-dependent p53 deacetylase. Cell 2001; 107:149-159
303. Andrew DAC, Edward AR, GuilletteJr FOJ. Endocrine disrupting contaminants and hormone dynamics: Lessons from wild life. In: GuilletteJr LJ, Crain A, eds. Environmental endocrine disruptors: An evolutionary perspective. New York: Taylor & Francis; 2010:1-21.
304. Banu SK. Heavy Metals and the Ovary. Ovarian Toxicology, Second Edition: CRC Press; 2013:191-228.
305. Gore AC, Chappell VA, Fenton SE, Flaws JA, Nadal A, Prins GS, Toppari J, Zoeller RT. EDC-2: The Endocrine Society's Second Scientific Statement on Endocrine-Disrupting Chemicals. Endocrine Reviews 2015; 36:E1-E150
306. Hunt PA, Lawson C, Gieske M, Murdoch B, Smith H, Marre A, Hassold T, VandeVoort CA. Bisphenol A alters early oogenesis and follicle formation in the fetal ovary of the rhesus monkey. Proceedings of the National Academy of Sciences 2012; 109:17525-17530
307. Lawson C, Gieske M, Murdoch B, Ye P, Li Y, Hassold T, Hunt PA. Gene Expression in the Fetal Mouse Ovary Is Altered by Exposure to Low Doses of Bisphenol A. Biology of Reproduction 2011; 84:79-86

308. Chao H-H, Zhang X-F, Chen B, Pan B, Zhang L-J, Li L, Sun X-F, Shi Q-H, Shen W. Bisphenol A exposure modifies methylation of imprinted genes in mouse oocytes via the estrogen receptor signaling pathway. Histochemistry and cell biology 2012; 137:249-259
309. Rivera OE, Varayoud J, Rodríguez HA, Muñoz-de-Toro M, Luque EH. Neonatal exposure to bisphenol A or diethylstilbestrol alters the ovarian follicular dynamics in the lamb. Reproductive Toxicology 2011; 32:304-312
310. Souter I, Smith KW, Dimitriadis I, Ehrlich S, Williams PL, Calafat AM, Hauser R. The association of bisphenol-A urinary concentrations with antral follicle counts and other measures of ovarian reserve in women undergoing infertility treatments. Reprod Toxicol 2013; 42:224-231
311. Krol WJ, Arsenault TL, Pylypiw HM, Incorvia Mattina MJ. Reduction of pesticide residues on produce by rinsing. Journal of agricultural and food chemistry 2000; 48:4666-4670
312. Golovleva L, Polyakova A, Pertsova R, Finkelshtein Z. The fate of methoxychlor in soils and transformation by soil microorganisms. Journal of Environmental Science & Health Part B 1984; 19:523-538
313. Stresser DM, Kupfer D. Human Cytochrome P450–Catalyzed Conversion of the Proestrogenic Pesticide Methoxychlor Into an Estrogen: Role of CYP2C19 and CYP1A2 inO-Demethylation. Drug Metabolism and disposition 1998; 26:868-874
314. Uzumcu M, Kuhn PE, Marano JE, Armenti AE, Passantino L. Early postnatal methoxychlor exposure inhibits folliculogenesis and stimulates anti-Mullerian hormone production in the rat ovary. Journal of endocrinology 2006; 191:549-558
315. Gupta RK, Meachum S, Hernández-Ochoa I, Peretz J, Yao HH, Flaws JA. Methoxychlor inhibits growth of antral follicles by altering cell cycle regulators. Toxicology and applied pharmacology 2009; 240:1-7
316. Miller KP, Gupta RK, Greenfeld CR, Babus JK, Flaws JA. Methoxychlor directly affects ovarian antral follicle growth and atresia through Bcl-2-and Bax-mediated pathways. Toxicological Sciences 2005; 88:213-221
317. Basavarajappa MS, Craig ZR, Hernández-Ochoa I, Paulose T, Leslie TC, Flaws JA. Methoxychlor reduces estradiol levels by altering steroidogenesis and metabolism in mouse antral follicles in vitro. Toxicology and applied pharmacology 2011; 253:161-169
318. Zachow R, Uzumcu M. The methoxychlor metabolite, 2, 2-bis-(p-hydroxyphenyl)-1, 1, 1-trichloroethane, inhibits steroidogenesis in rat ovarian granulosa cells in vitro. Reproductive Toxicology 2006; 22:659-665
319. Virtanen HE, Koskenniemi JJ, Sundqvist E, Main KM, Kiviranta H, Tuomisto JT, Tuomisto J, Viluksela M, Vartiainen T, Skakkebaek NE, Toppari J. Associations between congenital cryptorchidism in newborn boys and levels of dioxins and PCBs in placenta. International journal of andrology 2012; 35:283-293
320. Hites RA. Dioxins: an overview and history. ACS Publications; 2010.
321. Tuppurainen K, Asikainen A, Ruokojärvi P, Ruuskanen J. Perspectives on the formation of polychlorinated dibenzo-p-dioxins and dibenzofurans during municipal solid waste (MSW) incineration and other combustion processes. Accounts of chemical research 2003; 36:652-658
322. Humblet O, Sergeyev O, Altshul L, Korrick SA, Williams PL, Emond C, Birnbaum LS, Burns JS, Lee MM, Revich B. Temporal trends in serum concentrations of polychlorinated

dioxins, furans, and PCBs among adult women living in Chapaevsk, Russia: a longitudinal study from 2000 to 2009. Environmental Health 2011; 10:62
323. Ulaszewska MM, Zuccato E, Davoli E. PCDD/Fs and dioxin-like PCBs in human milk and estimation of infants' daily intake: a review. Chemosphere 2011; 83:774-782
324. Mukerjee D. Health Impact of Polychlorinated Dibenzo-p-dioxins: A Critical Review. Journal of the Air & Waste Management Association 1998; 48:157-165
325. Heimler I, Trewin AL, Chaffin CL, Rawlins RG, Hutz RJ. Modulation of ovarian follicle maturation and effects on apoptotic cell death in Holtzman rats exposed to 2, 3, 7, 8-tetrachlorodibenzo-p-dioxin (TCDD) in utero and lactationally. Reproductive toxicology 1998; 12:69-73
326. Jung N-K, Park J-Y, Park J-H, Kim S-Y, Park J-K, Chang W-K, Lee H-C, Kim S-W, Chun S-Y. Attenuation of cell cycle progression by 2, 3, 7, 8-tetrachlorodibenzo-p-dioxin eliciting ovulatory blockade in gonadotropin-primed immature rats. Endocrine journal 2010; 57:863-871
327. Karman BN, Basavarajappa MS, Hannon P, Flaws JA. Dioxin exposure reduces the steroidogenic capacity of mouse antral follicles mainly at the level of HSD17B1 without altering atresia. Toxicology and applied pharmacology 2012; 264:1-12
328. Jablonska O, Shi Z, Valdez KE, Ting AY, Petroff BK. Temporal and anatomical sensitivities to the aryl hydrocarbon receptor agonist 2,3,7,8-tetrachlorodibenzo-p-dioxin leading to premature acyclicity with age in rats. International journal of andrology 2010; 33:405-412
329. Hannon PR, Peretz J, Flaws JA. Daily exposure to Di (2-ethylhexyl) phthalate alters estrous cyclicity and accelerates primordial follicle recruitment potentially via dysregulation of the phosphatidylinositol 3-kinase signaling pathway in adult mice. Biology of reproduction 2014; 90:136, 131-111
330. Xu C, Chen J-A, Qiu Z, Zhao Q, Luo J, Yang L, Zeng H, Huang Y, Zhang L, Cao J. Ovotoxicity and PPAR-mediated aromatase downregulation in female Sprague–Dawley rats following combined oral exposure to benzo [a] pyrene and di-(2-ethylhexyl) phthalate. Toxicology letters 2010; 199:323-332
331. Wang W, Craig ZR, Basavarajappa MS, Hafner KS, Flaws JA. Mono-(2-ethylhexyl) phthalate induces oxidative stress and inhibits growth of mouse ovarian antral follicles. Biology of reproduction 2012; 87:152, 151-110
332. Hannon PR, Brannick KE, Wang W, Flaws JA. Mono (2-ethylhexyl) phthalate accelerates early folliculogenesis and inhibits steroidogenesis in cultured mouse whole ovaries and antral follicles. Biology of reproduction 2015; 92:120, 121-111
333. Hannon PR, Brannick KE, Wang W, Gupta RK, Flaws JA. Di (2-ethylhexyl) phthalate inhibits antral follicle growth, induces atresia, and inhibits steroid hormone production in cultured mouse antral follicles. Toxicology and applied pharmacology 2015; 284:42-53
334. Grindler NM, Allsworth JE, Macones GA, Kannan K, Roehl KA, Cooper AR. Persistent organic pollutants and early menopause in U.S. women. PLoS One 2015; 10:e0116057
335. Domingo JL. Metal-induced developmental toxicity in mammals: a review. J Toxicol Environ Health 1994; 42:123-141
336. Banu SK. Ovarian toxicology. Second ed: CRC Press.
337. Liao K-W, Chang C-H, Tsai M-S, Chien L-C, Chung M-Y, Mao IF, Tsai Y-A, Chen M-L. Associations between urinary total arsenic levels, fetal development, and neonatal birth

outcomes: A cohort study in Taiwan. Science of The Total Environment 2018; 612:1373-1379
338. Rodriguez-Villamizar LA, Jaimes DC, Manquian-Tejos A, Sanchez LH. Human mercury exposure and irregular menstrual cycles in relation to artisanal gold mining in Colombia. Biomedica : revista del Instituto Nacional de Salud 2015; 35:38-45
339. Colomina MT, Domingo JL, Llobet JM, Corbella J. Effect of day of exposure on the developmental toxicity of manganese in mice. Veterinary and Human Toxicology 1996; 38:7-9
340. Vigeh M, Yokoyama K, Ramezanzadeh F, Dahaghin M, Fakhriazad E, Seyedaghamiri Z, Araki S. Blood manganese concentrations and intrauterine growth restriction. Reproductive toxicology 2008; 25:219-223
341. Vaktskjold A, Talykova L, Chashchin V, Odland JØ, Nieboer E. Spontaneous abortions among nickel-exposed female refinery workers. International Journal of Environmental Health Research 2008; 18:99-115
342. Makarov Y, Shimtova LA. Occupational conditions and gynecological illness in workers engaged in the production of chromium compounds. Environ Health Perspect 1978; 24:1-128
343. Persani L, Rossetti R, Cacciatore C. Genes involved in human premature ovarian failure. Journal of molecular endocrinology 2010; 45:257-279
344. Coulam CB, Adamson SC, Annegers JF. Incidence of premature ovarian failure. Obstet Gynecol 1986; 67:604-606
345. Goswami D, Conway GS. Premature ovarian failure. Human reproduction update 2005; 11:391-410
346. Toniolo D. X-linked premature ovarian failure: a complex disease. Current opinion in genetics & development 2006; 16:293-300
347. Bretherick KL, Hanna CW, Currie LM, Fluker MR, Hammond GL, Robinson WP. Estrogen receptor α gene polymorphisms are associated with idiopathic premature ovarian failure. Fertility and sterility 2008; 89:318-324
348. Zinn AR. The X chromosome and the ovary. Journal of the Society for Gynecologic Investigation 2001; 8:S34-S36
349. Rizzolio F, Sala C, Alboresi S, Bione S, Gilli S, Goegan M, Pramparo T, Zuffardi O, Toniolo D. Epigenetic control of the critical region for premature ovarian failure on autosomal genes translocated to the X chromosome: a hypothesis. Human genetics 2007; 121:441-450
350. Therman E, Laxova R, Susman B. The critical region on the human Xq. Human genetics 1990; 85:455-461
351. Rizzolio F, Pramparo T, Sala C, Zuffardi O, De Santis L, Rabellotti E, Calzi F, Fusi F, Bellazzi R, Toniolo D. Epigenetic analysis of the critical region I for premature ovarian failure: demonstration of a highly heterochromatic domain on the long arm of the mammalian X chromosome. Journal of medical genetics 2009; 46:585-592
352. Schlessinger D, Herrera L, Crisponi L, Mumm S, Percesepe A, Pellegrini M, Pilia G, Forabosco A. Genes and translocations involved in POF. American Journal of Medical Genetics Part A 2002; 111:328-333

353. Prueitt RL, Ross JL, Zinn AR. Physical mapping of nine Xq translocation breakpoints and identification of XPNPEP2 as a premature ovarian failure candidate gene. Cytogenetics and cell genetics 2000; 89:44-50
354. Bione S, Rizzolio F, Sala C, Ricotti R, Goegan M, Manzini M, Battaglia R, Marozzi A, Vegetti W, Dalpra L. Mutation analysis of two candidate genes for premature ovarian failure, DACH2 and POF1B. Human reproduction 2004; 19:2759-2766
355. Bokhoven Hv, Hurk JAvd, Bogerd L, Philippe C, Gilgenkrantz S, Jong Pd, Ropers H-H, Cremers FP. Cloning and characterization of the human choroideremia gene. Human molecular genetics 1994; 3:1041-1046
356. Bione S, Sala C, Manzini C, Arrigo G, Zuffardi O, Banfi S, Borsani G, Jonveaux P, Philippe C, Zuccotti M. A human homologue of the Drosophila melanogaster diaphanous gene is disrupted in a patient with premature ovarian failure: evidence for conserved function in oogenesis and implications for human sterility. The American Journal of Human Genetics 1998; 62:533-541
357. Bione S, Toniolo D. X chromosome genes and premature ovarian failure. Paper presented at: Seminars in reproductive medicine2000
358. Rizzolio F, Bione S, Villa A, Berti E, Cassetti A, Bulfone A, Tribioli C, Toniolo D. Spatial and temporal expression of POF1B, a gene expressed in epithelia. Gene expression patterns 2007; 7:529-534
359. Lacombe A, Lee H, Zahed L, Choucair M, Muller J-M, Nelson SF, Salameh W, Vilain E. Disruption of POF1B binding to nonmuscle actin filaments is associated with premature ovarian failure. The American Journal of Human Genetics 2006; 79:113-119
360. Padovano V, Lucibello I, Alari V, Della Mina P, Crespi A, Ferrari I, Recagni M, Lattuada D, Righi M, Toniolo D, Villa A, Pietrini G. The POF1B candidate gene for premature ovarian failure regulates epithelial polarity. J Cell Sci 2011; 124:3356-3368
361. Lacombe A, Lee H, Zahed L, Choucair M, Muller JM, Nelson SF, Salameh W, Vilain E. Disruption of POF1B binding to nonmuscle actin filaments is associated with premature ovarian failure. Am J Hum Genet 2006; 79:113-119
362. Ledig S, Preisler-Adams S, Morlot S, Liehr T, Wieacker P. Premature ovarian failure caused by a heterozygous missense mutation in POF1B and a reciprocal translocation 46,X,t(X;3)(q21.1;q21.3). Sexual development : genetics, molecular biology, evolution, endocrinology, embryology, and pathology of sex determination and differentiation 2015; 9:86-90
363. Mardon G, Solomon NM, Rubin GM. dachshund encodes a nuclear protein required for normal eye and leg development in Drosophila. Development 1994; 120:3473-3486
364. Ayres JA, Shum L, Akarsu AN, Dashner R, Takahashi K, Ikura T, Slavkin HC, Nuckolls GH. DACH: genomic characterization, evaluation as a candidate for postaxial polydactyly type A2, and developmental expression pattern of the mouse homologue. Genomics 2001; 77:18-26
365. Davis RJ, Shen W, Heanue TA, Mardon G. Mouse Dach, a homologue of Drosophila dachshund, is expressed in the developing retina, brain and limbs. Development genes and evolution 1999; 209:526-536
366. Davis RJ, Shen W, Sandler YI, Heanue TA, Mardon G. Characterization of mouse Dach2, a homologue of Drosophiladachshund. Mechanisms of development 2001; 102:169-179

367. Davis RJ, Shen W, Sandler YI, Heanue TA, Mardon G. Characterization of mouse Dach2, a homologue of Drosophila dachshund. Mechanisms of Development 2001; 102:169-179
368. Davis RJ, Pesah YI, Harding M, Paylor R, Mardon G. Mouse Dach2 mutants do not exhibit gross defects in eye development or brain function. Genesis 2006; 44:84-92
369. Bai J, Montell D. Eyes absent, a key repressor of polar cell fate during Drosophila oogenesis. Development 2002; 129:5377-5388
370. Davis RJ, Harding M, Moayedi Y, Mardon G. Mouse Dach1 and Dach2 are redundantly required for Müllerian duct development. Genesis 2008; 46:205-213
371. Breitsprecher D, Goode BL. Formins at a glance. J Cell Sci 2013; 126:1-7
372. Kovar DR, Pollard TD. Insertional assembly of actin filament barbed ends in association with formins produces piconewton forces. Proceedings of the National Academy of Sciences of the United States of America 2004; 101:14725-14730
373. Moseley JB, Sagot I, Manning AL, Xu Y, Eck MJ, Pellman D, Goode BL. A conserved mechanism for Bni1-and mDia1-induced actin assembly and dual regulation of Bni1 by Bud6 and profilin. Molecular biology of the cell 2004; 15:896-907
374. Kovar DR, Harris ES, Mahaffy R, Higgs HN, Pollard TD. Control of the assembly of ATP- and ADP-actin by formins and profilin. Cell 2006; 124:423-435
375. Harris ES, Higgs HN. Biochemical analysis of mammalian formin effects on actin dynamics. Methods in enzymology 2006; 406:190-214
376. Michelot A, Guérin C, Huang S, Ingouff M, Richard S, Rodiuc N, Staiger CJ, Blanchoin L. The formin homology 1 domain modulates the actin nucleation and bundling activity of Arabidopsis FORMIN1. The Plant Cell 2005; 17:2296-2313
377. Wallar BJ, DeWard AD, Resau JH, Alberts AS. RhoB and the mammalian Diaphanous-related formin mDia2 in endosome trafficking. Experimental cell research 2007; 313:560-571
378. Wen Y, Eng CH, Schmoranzer J, Cabrera-Poch N, Morris EJ, Chen M, Wallar BJ, Alberts AS, Gundersen GG. EB1 and APC bind to mDia to stabilize microtubules downstream of Rho and promote cell migration. Nature cell biology 2004; 6:820
379. Pruyne D, Evangelista M, Yang C, Bi E, Zigmond S, Bretscher A, Boone C. Role of formins in actin assembly: nucleation and barbed-end association. Science 2002; 297:612-615
380. Gould CJ, Maiti S, Michelot A, Graziano BR, Blanchoin L, Goode BL. The formin DAD domain plays dual roles in autoinhibition and actin nucleation. Current biology 2011; 21:384-390
381. Sagot I, Rodal AA, Moseley J, Goode BL, Pellman D. An actin nucleation mechanism mediated by Bni1 and profilin. Nature cell biology 2002; 4:626
382. Watanabe N, Kato T, Fujita A, Ishizaki T, Narumiya S. Cooperation between mDia1 and ROCK in Rho-induced actin reorganization. Nature cell biology 1999; 1:136
383. Hotulainen P, Lappalainen P. Stress fibers are generated by two distinct actin assembly mechanisms in motile cells. The Journal of cell biology 2006; 173:383-394
384. Banu SK, Stanley JA, Sivakumar KK, Arosh JA, Barhoumi R, Burghardt RC. Identifying a novel role for X-prolyl aminopeptidase (Xpnpep) 2 in CrVI-induced adverse effects on germ cell nest breakdown and follicle development in rats. Biology of reproduction 2015; 92:67, 61-18

385. Nakano K, Naito I, Momota R, Sado Y, Hasegawa H, Ninomiya Y, Ohtsuka A. The distribution of type IV collagen α chains in the mouse ovary and its correlation with follicular development. Archives of histology and cytology 2007; 70:243-253
386. Berkholtz CB, Lai BE, Woodruff TK, Shea LD. Distribution of extracellular matrix proteins type I collagen, type IV collagen, fibronectin, and laminin in mouse folliculogenesis. Histochemistry and cell biology 2006; 126:583-592
387. Aharoni D, Meiri I, Atzmon R, Vlodavsky I, Amsterdam A. Differential effect of components of the extracellular matrix on differentiation and apoptosis. Current Biology 1997; 7:43-51
388. Berkholtz CB, Lai BE, Woodruff TK, Shea LD. Distribution of extracellular matrix proteins type I collagen, type IV collagen, fibronectin, and laminin in mouse folliculogenesis. Histochem Cell Biol 2006; 126:583-592
389. Oktay K, Karlikaya G, Akman O, Ojakian GK, Oktay M. Interaction of extracellular matrix and activin-A in the initiation of follicle growth in the mouse ovary. Biology of reproduction 2000; 63:457-461
390. Rodgers R, Irving-Rodgers H, Lavranos T, Irvine C, Krupa M. Roles of extracellular matrix in follicular development. Journal of reproduction and fertility Supplement 1999; 54:343-352
391. Irving-Rodgers H, Catanzariti K, Aspden W, D'Occhio M, Rodgers R. Remodeling of extracellular matrix at ovulation of the bovine ovarian follicle. Molecular reproduction and development 2006; 73:1292-1302
392. Irving-Rodgers HF, Rodgers RJ. Extracellular matrix of the developing ovarian follicle. Paper presented at: Seminars in reproductive medicine2006
393. Rodgers R, Rodgers HI. Extracellular matrix of the bovine ovarian membrana granulosa. Molecular and cellular endocrinology 2002; 191:57-64
394. Bagavandoss P. Temporal expression of tenascin-C and type I collagen in response to gonadotropins in the immature rat ovary. Acta histochemica 2014; 116:1125-1133
395. Woodruff TK, Shea LD. The role of the extracellular matrix in ovarian follicle development. Reproductive sciences 2007; 14:6-10
396. Zalewski A, Cecchini EL, Deroo BJ. Expression of extracellular matrix components is disrupted in the immature and adult estrogen receptor β-null mouse ovary. PloS one 2012; 7:e29937
397. Greene LE, Riederer AM, Marcus M, Lkhasuren O. Associations of fertility and pregnancy outcomes with leather tannery work in Mongolia: a pilot study. Int J Occup Environ Health 2010; 16:60-68
398. Hemminki K, Kyyronen P, Niemi ML, Koskinen K, Sallmen M, Vainio H. Spontaneous abortions in an industrialized community in Finland. American journal of public health 1983; 73:32-37
399. Hemminki K, Niemi ML, Koskinen K, Vainio H. Spontaneous abortions among women employed in the metal industry in Finland. International archives of occupational and environmental health 1980; 47:53-60
400. Quansah R, Jaakkola JJ. Paternal and maternal exposure to welding fumes and metal dusts or fumes and adverse pregnancy outcomes. International archives of occupational and environmental health 2009; 82:529-537

401. Steven L, Wendy U, Raymond A, Samuel C, Douglas C, Temple G. AVMA guidelines for the euthanasia of animals: 2013 edition. Schaumburg (IL): American Veterinary Medical Association 2013:46-50
402. Banu SK, Stanley JA, Taylor RJ, Sivakumar KK, Arosh JA, Zeng L, Pennathur S, Padmanabhan V. Sexually Dimorphic Impact of Chromium Accumulation on Human Placental Oxidative Stress and Apoptosis. Toxicological sciences : an official journal of the Society of Toxicology 2018; 161:375-387
403. Banu SK, Lee J, Speights VOJ, Starzinski-Powitz A, Arosh JA. Selective inhibition of prostaglandin E2 receptors EP2 and EP4 induces apoptosis of human endometriotic cells through suppression of ERK1/2, AKT, NFkappaB, and beta-catenin pathways and activation of intrinsic apoptotic mechanisms. Mol Endocrinol 2009; 23:1291-1305
404. Devine PJ, Sipes IG, Skinner MK, Hoyer PB. Characterization of a rat in vitro ovarian culture system to study the ovarian toxicant 4-vinylcyclohexene diepoxide. Toxicology and applied pharmacology 2002; 184:107-115
405. Lee J, Banu SK, Burghardt RC, Starzinski-Powitz A, Arosh JA. Selective Inhibition of Prostaglandin E2 Receptors EP2 and EP4 Inhibits Adhesion of Human Endometriotic Epithelial and Stromal Cells Through Suppression of Integrin-Mediated Mechanisms. Biology of Reproduction 2013; 88:77-77
406. Kratzer DD, Littell RC. Appropriate statistical methods to compare dose responses of methionine sources. Poult Sci 2006; 85:947-954
407. Collins BJ, Stout MD, Levine KE, Kissling GE, Melnick RL, Fennell TR, Walden R, Abdo K, Pritchard JB, Fernando RA, Burka LT, Hooth MJ. Exposure to hexavalent chromium resulted in significantly higher tissue chromium burden compared with trivalent chromium following similar oral doses to male F344/N rats and female B6C3F1 mice. Toxicol Sci 2010; 118:368-379
408. Greep RO. The Ovary: A Correlation of Structure and Function in Mammals. Hannah Peters , Kenneth P. McNatty. The Quarterly Review of Biology 1981; 56:201-201
409. Takagi K, Yamada T, Miki Y, Umegaki T, Nishimura M, Sasaki J. Histological observation of the development of follicles and follicular atresia in immature rat ovaries. Acta medica Okayama 2007; 61:283-298
410. Perez GI, Robles R, Knudson CM, Flaws JA, Korsmeyer SJ, Tilly JL. Prolongation of ovarian lifespan into advanced chronological age by Bax-deficiency. Nat Genet 1999; 21:200-203
411. Matikainen T, Perez GI, Jurisicova A, Pru JK, Schlezinger JJ, Ryu H-Y, Laine J, Sakai T, Korsmeyer SJ, Casper RF, Sherr DH, Tilly JL. Aromatic hydrocarbon receptor-driven Bax gene expression is required for premature ovarian failure caused by biohazardous environmental chemicals. Nat Genet 2001; 28:355-360
412. Banu SK, Stanley JA, Lee J, Stephen SD, Arosh JA, Hoyer PB, Burghardt RC. Hexavalent chromium-induced apoptosis of granulosa cells involves selective sub-cellular translocation of Bcl-2 members, ERK1/2 and p53. Toxicol Appl Pharmacol 2011;
413. Rajareddy S, Reddy P, Du C, Liu L, Jagarlamudi K, Tang W, Shen Y, Berthet C, Peng SL, Kaldis P, Liu K. p27kip1 (Cyclin-Dependent Kinase Inhibitor 1B) Controls Ovarian Development by Suppressing Follicle Endowment and Activation and Promoting Follicle Atresia in Mice. Molecular Endocrinology 2007; 21:2189-2202

414. Nagahama H, Hatakeyama S, Nakayama K, Nagata M, Tomita K, Nakayama K. Spatial and temporal expression patterns of the cyclin-dependent kinase (CDK) inhibitors p27Kip1 and p57Kip2 during mouse development. Anatomy and embryology 2001; 203:77-87
415. Zhao Y, Chaiswing L, Velez JM, Batinic-Haberle I, Colburn NH, Oberley TD, Clair DKS. p53 translocation to mitochondria precedes its nuclear translocation and targets mitochondrial oxidative defense protein-manganese superoxide dismutase. Cancer research 2005; 65:3745-3750
416. El Mouatassim S, Guerin P, Menezo Y. Expression of genes encoding antioxidant enzymes in human and mouse oocytes during the final stages of maturation. Mol Hum Reprod 1999; 5:720-725
417. Matzuk MM, Dionne L, Guo Q, Kumar TR, Lebovitz RM. Ovarian function in superoxide dismutase 1 and 2 knockout mice. Endocrinology 1998; 139:4008-4011
418. Tingen C, Kim A, Woodruff TK. The primordial pool of follicles and nest breakdown in mammalian ovaries. MHR: Basic science of reproductive medicine 2009; 15:795-803
419. Pepling ME, Sundman EA, Patterson NL, Gephardt GW, Medico L, Jr., Wilson KI. Differences in oocyte development and estradiol sensitivity among mouse strains. Reproduction 2010; 139:349-357
420. Sun Y-C, Sun X-F, Dyce PW, Shen W, Chen H. The role of germ cell loss during primordial follicle assembly: a review of current advances. International Journal of Biological Sciences 2017; 13:449-457
421. Myers M, Morgan FH, Liew SH, Zerafa N, Gamage TU, Sarraj M, Cook M, Kapic I, Sutherland A, Scott CL, Strasser A, Findlay JK, Kerr JB, Hutt KJ. PUMA regulates germ cell loss and primordial follicle endowment in mice. Reproduction 2014; 148:211-219
422. Coucouvanis EC, Sherwood SW, Carswell-Crumpton C, Spack EG, Jones PP. Evidence That the Mechanism of Prenatal Germ Cell Death in the Mouse Is Apoptosis. Experimental Cell Research 1993; 209:238-247
423. Page K, Pagidas K, Derosa MC, Quddus MR. Eosinophilic perifolliculitis presenting as a painful cystic ovarian mass in a woman with fibromyalgia: a case report. The Journal of reproductive medicine 2006; 51:141-144
424. Butterfield JH, Kephart GM, Frankson J. Eosinophilic oophoritis: association with positive Strongyloides stercoralis serology and clinical response to ivermectin. Journal of pediatric and adolescent gynecology 2006; 19:329-332
425. Khan F, Naab T. Eosinophilic Perifolliculitis, a Rare Cause of Painful Unilateral Cystic Ovarian Mass. American Journal of Clinical Pathology 2016; 146:265-265
426. Luborsky JL, Tung KSK. CHAPTER 61 - Oophoritis A2 - Rose, Noel R. In: Mackay IR, ed. The Autoimmune Diseases (Fourth Edition). St. Louis: Academic Press; 2006:849-859.
427. Makker A, Goel MM, Mahdi AA. PI3K/PTEN/Akt and TSC/mTOR signaling pathways, ovarian dysfunction, and infertility: an update. Journal of molecular endocrinology 2014; 53:R103-R118
428. Sun Y, Liu WZ, Liu T, Feng X, Yang N, Zhou HF. Signaling pathway of MAPK/ERK in cell proliferation, differentiation, migration, senescence and apoptosis. Journal of receptor and signal transduction research 2015; 35:600-604
429. Zhao Y, Zhang Y, Li J, Zheng N, Xu X, Yang J, Xia G, Zhang M. MAPK3/1 participates in the activation of primordial follicles through mTORC1-KITL signaling. Journal of cellular physiology 2018; 233:226-237

430. Phillipps HR, Hurst PR. XIAP: a potential determinant of ovarian follicular fate. Reproduction 2012; 144:165-176
431. Scott FL, Denault JB, Riedl SJ, Shin H, Renatus M, Salvesen GS. XIAP inhibits caspase-3 and -7 using two binding sites: evolutionarily conserved mechanism of IAPs. Embo j 2005; 24:645-655
432. Shiozaki EN, Chai J, Rigotti DJ, Riedl SJ, Li P, Srinivasula SM, Alnemri ES, Fairman R, Shi Y. Mechanism of XIAP-Mediated Inhibition of Caspase-9. Molecular Cell 2003; 11:519-527
433. Li J, Kim J-M, Liston P, Li M, Miyazaki T, Mackenzie AE, Korneluk RG, Tsang BK. Expression of inhibitor of apoptosis proteins (IAPs) in rat granulosa cells during ovarian follicular development and atresia. Endocrinology 1998; 139:1321-1328
434. Yang Y, Fang S, Jensen JP, Weissman AM, Ashwell JD. Ubiquitin protein ligase activity of IAPs and their degradation in proteasomes in response to apoptotic stimuli. Science 2000; 288:874-877
435. Suzuki Y, Nakabayashi Y, Takahashi R. Ubiquitin-protein ligase activity of X-linked inhibitor of apoptosis protein promotes proteasomal degradation of caspase-3 and enhances its anti-apoptotic effect in Fas-induced cell death. Proc Natl Acad Sci U S A 2001; 98:8662-8667
436. Morizane Y, Honda R, Fukami K, Yasuda H. X-linked inhibitor of apoptosis functions as ubiquitin ligase toward mature caspase-9 and cytosolic Smac/DIABLO. Journal of biochemistry 2005; 137:125-132
437. Matikainen T, Perez GI, Jurisicova A, Pru JK, Schlezinger JJ, Ryu H-Y, Laine J, Sakai T, Korsmeyer SJ, Casper RF. Aromatic hydrocarbon receptor-driven Bax gene expression is required for premature ovarian failure caused by biohazardous environmental chemicals. Nature genetics 2001; 28:355
438. Felici MD, Carlo AD, Pesce M, Iona S, Farrace MG, Piacentini M. Bcl-2 and Bax regulation of apoptosis in germ cells during prenatal oogenesis in the mouse embryo. Cell death and differentiation 1999; 6:908-915
439. Tingen CM, Bristol-Gould SK, Kiesewetter SE, Wellington JT, Shea L, Woodruff TK. Prepubertal primordial follicle loss in mice is not due to classical apoptotic pathways. Biology of Reproduction 2009; 81:16-25
440. Cecconi S, Mauro A, Cellini V, Patacchiola F. The role of Akt signalling in the mammalian ovary. International Journal of Developmental Biology 2013; 56:809-817
441. Kaldis P. Another piece of the p27Kip1 puzzle. Cell 2007; 128:241-244
442. Candas D, Li JJ. MnSOD in Oxidative Stress Response-Potential Regulation via Mitochondrial Protein Influx. Antioxidants & Redox Signaling 2014; 20:1599-1617
443. Banu SK, Stanley JA, Lee J, Stephen SD, Arosh JA, Hoyer PB, Burghardt RC. Hexavalent chromium-induced apoptosis of granulosa cells involves selective sub-cellular translocation of Bcl-2 members, ERK1/2 and p53. Toxicology and applied pharmacology 2011; 251:253-266
444. Solomon JM, Pasupuleti R, Xu L, McDonagh T, Curtis R, DiStefano PS, Huber LJ. Inhibition of SIRT1 catalytic activity increases p53 acetylation but does not alter cell survival following DNA damage. Molecular and cellular biology 2006; 26:28-38
445. Choi S-E, Kemper JK. Regulation of SIRT1 by MicroRNAs. Molecules and Cells 2013; 36:385-392

446. Chipuk JE, Green DR. How do BCL-2 proteins induce mitochondrial outer membrane permeabilization? Trends in cell biology 2008; 18:157-164
447. Vaskivuo TE, Tapanainen JS. Apoptosis in the human ovary. Reproductive biomedicine online 2003; 6:24-35
448. Song G, Ouyang G, Bao S. The activation of Akt/PKB signaling pathway and cell survival. Journal of cellular and molecular medicine 2005; 9:59-71
449. Giaccia AJ, Kastan MB. The complexity of p53 modulation: emerging patterns from divergent signals. Genes Dev 1998; 12:2973-2983
450. Li M, Luo J, Brooks CL, Gu W. Acetylation of p53 inhibits its ubiquitination by Mdm2. Journal of Biological Chemistry 2002; 277:50607-50611
451. Gu W, Roeder RG. Activation of p53 sequence-specific DNA binding by acetylation of the p53 C-terminal domain. Cell 1997; 90:595-606
452. Haupt S, Berger M, Goldberg Z, Haupt Y. Apoptosis - the p53 network. Journal of cell science 2003; 116:4077-4085
453. Yamakuchi M. MicroRNA Regulation of SIRT1. Frontiers in physiology 2012; 3:68
454. Zhao X, Allison D, Condon B, Zhang F, Gheyi T, Zhang A, Ashok S, Russell M, MacEwan I, Qian Y, Jamison JA, Luz JG. The 2.5 Å Crystal Structure of the SIRT1 Catalytic Domain Bound to Nicotinamide Adenine Dinucleotide (NAD+) and an Indole (EX527 Analogue) Reveals a Novel Mechanism of Histone Deacetylase Inhibition. Journal of medicinal chemistry 2013; 56:963-969
455. Gertz M, Fischer F, Nguyen GT, Lakshminarasimhan M, Schutkowski M, Weyand M, Steegborn C. Ex-527 inhibits Sirtuins by exploiting their unique NAD+-dependent deacetylation mechanism. Proc Natl Acad Sci U S A 2013; 110:E2772-2781
456. Jia D, Niu Y, Li D, Liu Z. LncRNA C2dat1 Promotes Cell Proliferation, Migration, and Invasion by Targeting MiR-34a-5p in Osteosarcoma Cells. Oncology research 2017;
457. Cory S, Adams JM. The Bcl2 family: regulators of the cellular life-or-death switch. Nature reviews Cancer 2002; 2:647-656
458. Rokavec M, Li H, Jiang L, Hermeking H. The p53/miR-34 axis in development and disease. Journal of Molecular Cell Biology 2014; 6:214-230
459. Wang X, Xie Y, Wang J. Overexpression of MicroRNA-34a-5p Inhibits Proliferation and Promotes Apoptosis of Human Cervical Cancer Cells by Downregulation of Bcl-2. Oncology research 2017;
460. Zhang Y, Xing D, Liu L. PUMA Promotes Bax Translocation by Both Directly Interacting with Bax and by Competitive Binding to Bcl-X(L) during UV-induced Apoptosis. Molecular Biology of the Cell 2009; 20:3077-3087
461. Miyashita T, Krajewski S, Krajewska M, Wang HG, Lin HK, Liebermann DA, Hoffman B, Reed JC. Tumor suppressor p53 is a regulator of bcl-2 and bax gene expression in vitro and in vivo. Oncogene 1994; 9:1799-1805
462. Marsit CJ, Eddy K, Kelsey KT. MicroRNA responses to cellular stress. Cancer research 2006; 66:10843-10848
463. Deng C-X. SIRT1, Is It a Tumor Promoter or Tumor Suppressor? International Journal of Biological Sciences 2009; 5:147-152
464. Ogawara Y, Kishishita S, Obata T, Isazawa Y, Suzuki T, Tanaka K, Masuyama N, Gotoh Y. Akt enhances Mdm2-mediated ubiquitination and degradation of p53. J Biol Chem 2002; 277:21843-21850

465. Nakano K, Vousden KH. PUMA, a novel proapoptotic gene, is induced by p53. Mol Cell 2001; 7:683-694
466. Kalle AM, Mallika A, Badiger J, Alinakhi, Talukdar P, Sachchidanand. Inhibition of SIRT1 by a small molecule induces apoptosis in breast cancer cells. Biochem Biophys Res Commun 2010; 401:13-19
467. Zhang Y, Cai X, Chai N, Gu Y, Zhang S, Ding M, Cao H, Sha S, Yin J, Li M, Wu K, Nie Y. SIRT1 Is Reduced in Gastric Adenocarcinoma and Acts as a Potential Tumor Suppressor in Gastric Cancer. Gastrointestinal Tumors 2015; 2:109-123
468. Brooks CL, Gu W. How does SIRT1 affect metabolism, senescence and cancer? Nature reviews Cancer 2009; 9:123-128
469. Liu T, Zhang L, Wang S, Chen C, Zheng J. Tripterygium glycosides induce premature ovarian failure in rats by promoting p53 phosphorylation and activating the serine/threonine kinase 11-p53-p21 signaling pathway. Experimental and therapeutic medicine 2015; 10:12-18
470. Ghosh AK, Bhattacharyya S, Varga J. The tumor suppressor p53 abrogates Smad-dependent collagen gene induction in mesenchymal cells. Journal of Biological Chemistry 2004; 279:47455-47463
471. Venema RC, Ju H, Zou R, Venema VJ, Ryan JW. Cloning and tissue distribution of human membrane-bound aminopeptidase P. Biochimica et biophysica acta 1997; 1354:45-48
472. Sprinkle T, Stone A, Venema RC, Denslow N, Caldwell C, Ryan J. Assignment of the membrane-bound human aminopeptidase P gene (XPNPEP2) to chromosome Xq25. Genomics 1998; 50:114-116
473. Fietzek PP, Kühn K. The primary structure of collagen. International review of connective tissue research. Vol 7: Elsevier; 1976:1-60.
474. McDonald JK, Hoisington AR, Eisenhauer DA. Partial purification and characterization of an ovarian tripeptidyl peptidase: A lysosomal exopeptidase that sequentially releases collagen-related (Gly-Pro-X) triplets. Biochemical and Biophysical Research Communications 1985; 126:63-71
475. Molinaro G, Boileau G, Adam A. Aminopeptidase P and Vasoactive Peptides. In: Hooper N, Lendeckel U, eds. Aminopeptidases in Biology and Disease. Vol 2: Springer US; 2004:251-269.
476. Fietzek PP, Kühn K. The Primary Structure of Collagen. In: David A H, D.S J, eds. International Review of Connective Tissue Research. Vol Volume 7: Elsevier; 1976:1-60.
477. Yang L, Li Y, Bhattacharya A, Zhang Y. PEPD is a pivotal regulator of p53 tumor suppressor. Nature Communications 2017; 8:2052
478. Myara I, Charpentier C, Lemonnier A. Prolidase and prolidase deficiency. Life sciences 1984; 34:1985-1998
479. Lupi A, Della Torre S, Campari E, Tenni R, Cetta G, Rossi A, Forlino A. Human recombinant prolidase from eukaryotic and prokaryotic sources. The FEBS journal 2006; 273:5466-5478
480. Ma M, Chen X-Y, Li B, Li X-T. Melatonin protects premature ovarian insufficiency induced by tripterygium glycosides: role of SIRT1. American Journal of Translational Research 2017; 9:1580-1602

481. Prueitt R, Ross J, Zinn A. Physical mapping of nine Xq translocation breakpoints and identification of XPNPEP2 as a premature ovarian failure candidate gene. Cytogenetic and Genome Research 2000; 89:44-50
482. Prueitt RL, Chen H, Barnes RI, Zinn AR. Most X;autosome translocations associated with premature ovarian failure do not interrupt X-linked genes. Cytogenetic and Genome Research 2002; 97:32-38
483. Sivakumar KK, Stanley JA, Arosh JA, Pepling ME, Burghardt RC, Banu SK. Prenatal exposure to chromium induces early reproductive senescence by increasing germ cell apoptosis and advancing germ cell cyst breakdown in the F1 offspring. Developmental biology 2014; 388:22-34
484. Woodruff TK, Shea LD. The Role of the Extracellular Matrix in Ovarian Follicle Development. Reproductive sciences (Thousand Oaks, Calif) 2007; 14:6-10
485. Berkholtz CB, Shea LD, Woodruff TK. Extracellular Matrix Functions in Follicle Maturation. Seminars in reproductive medicine 2006; 24:262-269
486. Nakano K, Naito I, Momota R, Sado Y, Hasegawa H, Ninomiya Y, Ohtsuka A. The distribution of type IV collagen alpha chains in the mouse ovary and its correlation with follicular development. Archives of histology and cytology 2007; 70:243-253
487. Rodgers RJ, Irving-Rodgers HF, van Wezel IL. Extracellular matrix in ovarian follicles. Molecular and Cellular Endocrinology 2000; 163:73-79
488. Macri L, Silverstein D, Clark RA. Growth factor binding to the pericellular matrix and its importance in tissue engineering. Advanced drug delivery reviews 2007; 59:1366-1381

APPENDIX

PUBLICATIONS DURING Ph.D. PROGRAM

1. Stanley JA, **Sivakumar KK**, Nithy TK, Arosh JA, Hoyer PB, Burghardt RC, Banu SK. Postnatal exposure to chromium through mother's milk accelerates follicular atresia in F1 offspring through increased oxidative stress and depletion of antioxidant enzymes. **Free radical biology & medicine** 2013; 61C:179-196

2. Stanley JA, **Sivakumar KK**, Arosh JA, Burghardt RC, Banu SK. Edaravone Mitigates Hexavalent Chromium-Induced Oxidative Stress and Depletion of Antioxidant Enzymes while Estrogen Restores Antioxidant Enzymes in the Rat Ovary in F1 Offspring. **Biology of Reproduction** 2014; 91:12

3. **Sivakumar KK**, Stanley JA, Arosh JA, Pepling ME, Burghardt RC, Banu SK. Prenatal exposure to chromium induces early reproductive senescence by increasing germ cell apoptosis and advancing germ cell cyst breakdown in the F1 offspring. **Developmental biology** 2014; 388:22-34

4. Banu SK, Stanley JA, **Sivakumar KK**, Arosh JA, Barhoumi R, Burghardt RC. Identifying a novel role for X-prolyl aminopeptidase (Xpnpep) 2 in CrVI-induced adverse effects on germ cell nest breakdown and follicle development in rats. **Biology of reproduction** 2015; 92:67, 61-18

5. Banu SK, Stanley JA, **Sivakumar KK**, Arosh JA, Burghardt RC. Resveratrol protects the ovary against chromium-toxicity by enhancing endogenous antioxidant enzymes and inhibiting metabolic clearance of estradiol. **Toxicology and applied pharmacology** 2016; 303:65-78

6. Banu SK, Stanley JA, **Sivakumar KK**, Arosh JA, Taylor RJ, Burghardt RC. Chromium VI - Induced developmental toxicity of placenta is mediated through spatiotemporal dysregulation of cell survival and apoptotic proteins. **Reproductive Toxicology** 2017; 68:171-190

7. Banu SK, Stanley JA, **Sivakumar KK**, Taylor RJ, Arosh JA, Burghardt RC. Editor's Highlight: Exposure to CrVI during Early Pregnancy Increases Oxidative Stress and Disrupts the Expression of Antioxidant Proteins in Placental Compartments. **Toxicological sciences** 2017; 155:497-511

8. Banu SK, Stanley JA, Taylor RJ, **Sivakumar KK**, Arosh JA, Zeng L, Pennathur S, Padmanabhan V. Sexually Dimorphic Impact of Chromium Accumulation on Human Placental Oxidative Stress and Apoptosis. **Toxicological sciences** 2018; 161:375-387

9. **Sivakumar KK**, Stanley JA, Arosh JA, Burghardt RC, Banu SK. Inhibition of Sirtuin 1 attenuates CrVI-induced germ cell apoptosis during ovarian development through the activation of p53-acetylation. **Toxicology & Applied Pharmacology** 2018; In preparation